PLATELET-CANCER CELL INTERACTIONS INDUCE PAI-1 EXPRESSION IN AN OVARIAN CANCER CELL LINE MODEL: IMPLICATIONS FOR THE METASTASIS OF EPITHELIAL OVARIAN CANCER

By

Tanya Elizabeth Kelly

M.S. University of Southern Maine, 2015

A.S. Southern Maine Community College, 2012

B.A. Brandeis University, 1996

A THESIS

Submitted in Fulfillment of the

Requirements for the Degree of

Doctor of Philosophy

(in Histopathology and Morbid Anatomy)

Trinity College Dublin

The University of Dublin

March 2021

Advisors:

Sharon O'Toole, Ph.D. Senior Research Fellow

Professor John J. O'Leary, Professor Consultant, Histopathology

Professor Consultant, Molecular Medicine Ireland

LIBRARY RIGHTS STATEMENT

In presenting this thesis in fulfillment of the requirements for an advanced degree at Trinity College Dublin, The University of Dublin, I agree that the library shall make it freely available for inspection. I further agree that permission for "fair use" copying of this thesis for scholarly purposes may be granted by the Librarian. It is understood that any copying or publication of this thesis for financial gain shall not be allowed without my written permission.

Signature:

Date:

PLATELET-CANCER CELL INTERACTIONS INDUCE PAI-1 EXPRESSION IN AN OVARIAN CANCER CELL LINE MODEL: IMPLICATIONS FOR THE METASTASIS OF EPITHELIAL OVARIAN CANCER

By Tanya Elizabeth Kelly

Thesis Advisors: Dr. Sharon O'Toole and Professor John O'Leary

An Abstract of the Thesis Presented
In Fulfillment of the Requirements for the
Degree of Doctor of Philosophy
(in Histopathology and Morbid Anatomy)
March 2021

This thesis encompasses an investigation into the function of plasminogen activator inhibitor 1 (PAI-1) - a serine protease inhibitor integral to coagulation and fibrinolysis that has been identified as both a key factor in and a potential regulator of the metastatic process – in high-grade serous ovarian cancer (HGSOC), and also investigates the potential role of platelets in the tumour microenvironment and in haematogenous metastasis. Herein, evidence is provided in support of the hypothesis that platelet-cancer cell interactions aid survival of CTCs in the blood, and that PAI-1 is a key driver of the metastatic process in epithelial ovarian cancer (EOC) with potential as an independent prognostic indicator.

For the purpose of this study, SK-OV-3 cells were used as a model of HGSOC. A panel of assays in which PAI-1 was transiently silenced via siRNA was employed to examine the downstream effects of silencing PAI-1. These assays included real-time polymerase chain reaction (RT-qPCR), migration,

invasion, wound-healing, cell-cycle analysis by flow cytometry, differential gene expression via ribonucleic acid (RNA) sequencing, and protein evaluation in both the cell line and patient cohorts by enzyme-linked immunosorbent assay (ELISA). Also interrogated were the behaviours and gene signatures of ovarian cancer cells that had been treated with consented healthy donor platelets isolated from whole blood, both in the context of otherwise untreated SK-OV-3 cells and in cells that had been treated with PAI-1 siRNA.

Results of all assays demonstrated that PAI-1 is a significant factor in the migration, invasion, wound-healing, and proliferation of ovarian cancer cells *in vitro*, and also demonstrated that the presence of platelets increases all of these processes. This suggested that platelet-cancer cell interactions increase PAI-1 in ovarian cancer cells, and also suggested that PAI-1 plays a central role in ovarian cancer metastasis. SERPIN E1, which encodes PAI-1 protein, was found to be significantly downregulated when PAI-1 was silenced via siRNA and significantly upregulated when platelets were co-incubated with otherwise untreated cells. Silencing PAI-1 resulted in the significant downregulation of many biological processes, including regulation of wound healing, regulation of cell-matrix adhesion, regulation of cell migration, and positive regulation of angiogenesis. Adding platelets to SK-OV-3 cells resulted in the significant upregulation of several molecular pathways, including cell migration, angiogenesis, regulation of response to wounding, and extracellular matrix organization.

In light of these results, plasma PAI-1 was evaluated in patient cohorts in

order to assess any association between plasma PAI-1 and metastatic disease and also to gain insight into the potential value of PAI-1 as a prognostic indicator. These cohorts included treatment-naïve patients, those who had undergone neoadjuvant chemotherapy, patients with recurrent disease, and a fourth cohort of patients with benign histology. A pilot study in a fifth, smaller cohort of breast cancer patients sought to correlate patient plasma PAI-1 with circulating tumour cells (CTCs). Plasma PAI-1 was found to be significantly higher in patients with advanced disease compared to that of patients with early-stage disease, implying a potential role for PAI-1 as a marker of advanced disease. It was also found to be significantly reduced in patients who had undergone neoadjuvant chemotherapy compared to treatment-naïve patients, suggesting a role for PAI-1 as a marker of treatment response. Plasma PAI-1 did not correlate with patient platelet counts. A positive Pearson correlation between plasma PAI-1 and neutrophils was observed. A Kaplan-Meier overall survival (OS) analysis of PAI-1 in late-stage patients in the treatment naïve cohort trended towards significance, suggesting a poorer prognosis for patients with higher plasma PAI-1. Preliminary results of a CTC study in a 5th, smaller cohort demonstrated a significant positive correlation between plasma PAI-1 and CTC counts in patients with breast cancer. This study is currently being expanded to include patients with HGSOC. These results provide evidence for a regulatory role for PAI-1 in the processes central to ovarian cancer metastasis, and further suggest that PAI-1 may have potential value as a prognostic indicator and in the management of HGSOC.

ACKNOWLEDGEMENTS

I wish to extend my sincerest thanks to Dr. Sharon O'Toole and Professor John O'Leary for their support, guidance, and dedication throughout my research. I also wish to thank the faculty and staff of the Department of Histopathology and Morbid Anatomy, and the faculty and staff of the Department of Obstetrics and Gynaecology at Trinity College Dublin, including Drs. Cathy Spillane, Yanmei Huang, Mark Ward, Cara Martin, Bashir Mohamed, and Lucy Norris, without whose support this work would not have been possible. Thank you to Anna Bogdanska for her assistance with the fluorescence microscopy. Many thanks to Dr. Karsten Hokamp at the Smurfit Institute of Genetics, Drs. Pierce Kavanaugh and James Spiers, and Mr. Kenneth Scott of the Pharmacology Laboratory, Professor Derek Doherty, and to Steve Wingett at the Babraham Institute (UK). Special thanks to Noreen Gleason, Feras Abu Saadeh, and Waseem Kamran of the Division of Gynaecological Oncology at St. James' Hospital in Dublin for their help with obtaining crucial patient samples, and also to the many brave women who have graciously and selflessly donated samples so that this research may be conducted.

DEDICATION

To my mother, Nancy Gail Adams Kelly, for always being there for me, to Ben for his unwavering support, and to Kevin for believing in me.

TABLE OF CONTENTS

LIST OF FIGURES

LIST OF TABLES

LIST OF ABBREVIATIONS

°C	Degrees Celsius
Ab	Antibody
ACD	Acid Citrate Dextrose
ADP	Adenosine Diphosphate
AJCC	American Joint Committee on Cancer
ALDH1	Aldehyde Dehydrogenase 1
AMNCH	Adelaide Meath and National Children's Hospital
ANOVA	Analysis of Variance
AT	Antithrombin
ATCC	American Type Culture Collection
BCA	Bicinchoninic Acid
BER	Base Excision Repair
BMI	Body Mass Index
BRCA	Breast Cancer Gene
CA-125	Cancer Antigen 125
CAM	Cell Adhesion Molecule
CCC	Clear Cell Carcinoma
CCOC	Clear Cell Ovarian Cancer
CD	Cluster of Differentiation
cDNA	Complementary DNA
CEA	Carcinoembryonic Antigen
CEP8	Chromosome 8 Centromeric Probe
CI	Confidence Interval
Ck	Cytokeratin
CPL	Central Pathology Laboratory
CSC	Cancer Stem Cell
CT	Computerised Tomography

CTC	Circulating Tumour Cell
CTL	Control
CXCL	C-X-C Chemokine Ligand
DAPI	4′,6-Diamidino-2-Phenylindole
DFS	Disease-free Survival
DMSO	Dimethyl Sulfoxide
DNA	Deoxyribonucleic acid
DPBS	Dulbecco's Phosphate-buffered Saline
DSB	Double-stranded Break
DVT	Deep Vein Thrombosis
EC	Extracellular
ECM	Extracellular Matrix
EDTA	Ethylenediaminetetraacetic Acid
EGFR	Endothelial Growth Factor Receptor
EHS	Engelbreth-Holm-Swarm
ELISA	Enzyme-linked Immunosorbent Assay
EMT	Epithelial-to-Mesenchymal Transition
EOC	Epithelial Ovarian Carcinoma
EpCAM	Epithelial Cell Adhesion Molecule
ER	Eostrogen Receptor
ERCC1	Excision Repair Cross-complementation Group 1
ESPR1	Epithelial Cell-type-specific Splicing Regulator 1
ETOH	Ethanol
FACS	Fluorescence-activated Cell Sorting
FBC	Full Blood Count
FBS	Foetal Bovine Serum
FDA	Food and Drug Administration
FIGO	International Federation of Gynaecology and Obstetrics
FISH	Fluorescence In Situ Hybridisation

FITC	Fluorescein Isothiocyanate
FM	Fresh Medium
FSC	Forward Scatter
FSH	Follicle Stimulating Hormone
FSS	Fertility-sparing Surgery
FTSEC	Fallopian Tube Secretory Epithelial Cells
GAPDH	Glyceraldehyde 3-phosphate Dehydrogenase
GnRH	Gonadotropin-releasing Hormone
h	Hours
HDR	Homology-directed Repair
HER2	Human Epidermal Growth Factor Receptor 2
HGF	Human Growth Factor
HGSOC	High-grade Serous Ovarian Carcinoma
HIF	Hypoxia-inducible Factor
HOX	Homeobox
HPMC	Human Peritoneal Mesothelial Cells
HRP	Horseradish Peroxidase
HRR	Homologous Recombination Repair
HRT	Hormone Replacement Therapy
ICC	Immunocytochemistry
IDS	Interval Debulking Surgery
IL	Interleukin
IOTA	International Ovarian Tumour Analysis
L	Liter
LCS	Lipofectamine Complex Solution
LGSOC	Low-grade Serous Ovarian Carcinoma
LH	Luteinising Hormone
LND	Lymph Node Dissection
LNM	Lymph Node Metastasis

LR	Logistic Regression
LRP1	Low-density Lipoprotein Receptor-related Protein 1
m	Minutes
M	Molar
mAb	Monoclonal Antibody
MEM	Modified Eagle's Medium
MET	Mesenchymal-to-Epithelial Transition
MHC	Major Histocompatibility Complex
miRNA/miR	Micro Ribonucleic Acid
mL	Millilitre
mM	Millimolar
MMP	Matrix Metalloproteinase
MMR	Mismatch Repair
MMS	Multimodal Screening
MMT	Mesothelial-to-Mesenchymal Transition
MOC	Mucinous Ovarian Carcinoma
MPER	Mammalian Protein Extraction Reagent
MRI	Magnetic Resonance Imaging
mRNA	Messenger RNA
MUC16	Mucin 16
NER	Nucleotide Excision Repair
ng	Nanogram
NHB	Non-Hispanic Black
NHEJ	Non-homologous End-joining
NHW	Non-Hispanic White
NIH	National Institute of Health
NK	Natural Killer
NLR	Neutrophil-to-Lymphocyte Ratio
nM	Nanomolar

OC	Ovarian Carcinoma
OC125	Ovarian Carcinoma
OR	Odds Ratio
OS	Overall Survival
OSE	Ovarian Surface Epithelium
PAI-1	Plasminogen Activator Inhibitor 1
PAp	Pan-apple
PARP	Poly-ADP-Ribose Polymerase
PBS	Phosphate-buffered Saline
PBST	Phosphate-buffered Saline with Tween 20
PCR	Polymerase Chain Reaction
PDGFR	Platelet-derived growth Factor Receptor
PDS	Primary Debulking Surgery
PET	Positron-emission Tomography
PFS	Progression-free Survival
PGE2	Prostaglandin E2
PI	Propidium Iodide
PLCO	Prostate, Lung, Colorectal, and Ovarian Cancer Screening
PLEK	Pleckstrin
PLR	Platelet-to-Lymphocyte Ratio
PLT	Platelet
PMT	Photomultiplier Tube
PPV	Positive Predictive Value
PROC	Platinum-resistant Ovarian Cancer
PRP	Platelet-rich Plasma
RT-qPCR	Quantitative Real-time Polymerase Chain Reaction
RCF	Relative Centrifugal Force
RCL	Reactive Center Loop
REL	Platelet Releasate

RNA	Ribonucleic Acid
RPM	Revolutions per Minute
RR	Risk Ratio
RS	Radical Surgery
RT	Room Temperature
s	Seconds
SEE-FIM	Sectioning and Extensively Examining the Fimbriated End
SERM	Selective Eostrogen Receptor Modulator
SERPIN	Serine Protease Inhibitor
siNEG	Inert siRNA
siRNA	Small Interfering Ribonucleic Acid
SJH	Saint James' Hospital
SSB	Single-stranded Break
SSC	Side Scatter
STIC	Serous Tubal Intraepithelial Carcinoma
t	Time
TF	Transcription Factor
TGF-β	Tumour Growth Factor Beta
TMB	3,3',5,5'-Tetramethylbenzidine
TNF-α	Tumour Necrosis Factor Alpha
TNM	Tumour - Node - Metastasis
tPA	Tissue Plasminogen Activator
TVUS	Transvaginal Ultrasound
UNT	Untreated
uPA	Urokinase Plasminogen Activator
uPAR	Urokinase Plasminogen Activator Receptor
UTR	Untranslated Region
VCAM	Vascular Cellular Adhesion Molecule
VEGF	Vascular Endothelial Growth Factor

VTE	Venous Thrombotic Event
vWF	von Willebrand Factor
WAR	Whole Abdominal Radiation
WR	Working Reagent
wt	Wild Type
ZO	Zonula Occludens
Δ	delta
λ	lambda
µL	Microliter

CHAPTER 1

INTRODUCTION

1.1. Epidemiology of Ovarian Cancer

Ovarian cancer is the 7th leading cause of cancer in women worldwide, and the 4th most frequent cause of cancer in women in North America and in northern and western Europe (Lukanova and Kaaks, 2005). It is the second-most common and the most lethal of all the gynaecological malignancies. There are approximately 250,000 new cases diagnosed worldwide annually (Fig. 1.1), and 152,000 deaths from this disease each year (Reid *et al*, 2017). It is estimated that this will increase by 55% to 371,000 cases by 2035, with mortality increasing by 67% to 254,000. In Ireland alone, there are close to 400 ovarian cancer diagnoses and approximately 272 deaths from this disease per annum (Irish Cancer Society, 1999-2021; National Cancer Registry Ireland).

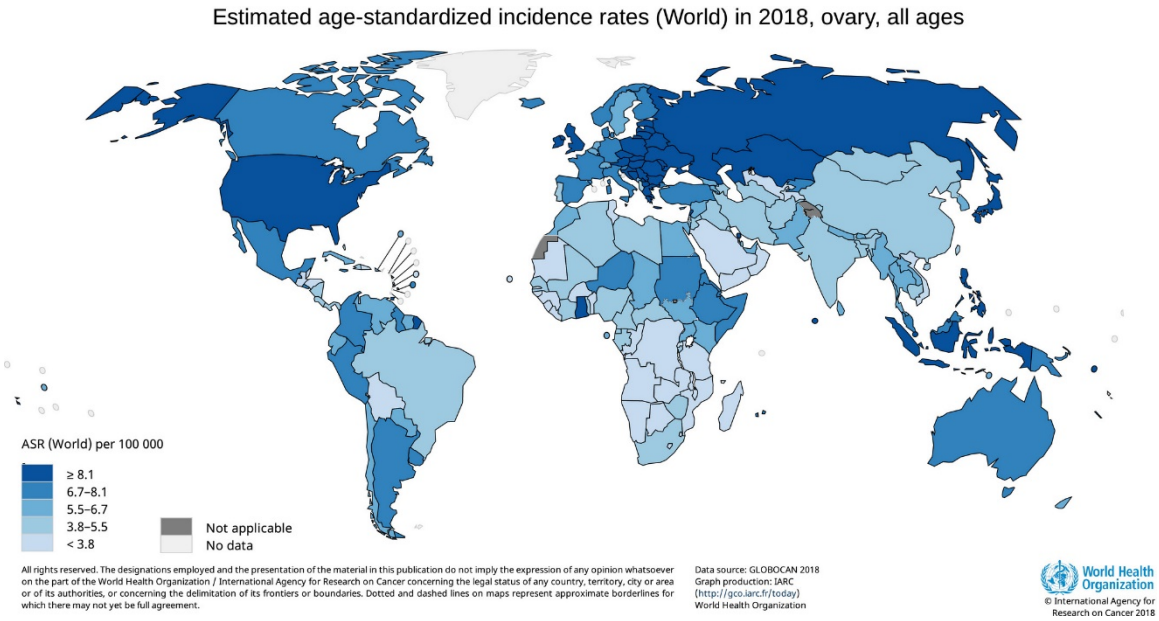

Fig. 1.1 Global distribution of ovarian cancer

It is well-documented that the risk of developing ovarian cancer is twice as high in industrialized nations than in less developed countries. Those

countries, such as China (34,575), India (26,834), and the United States (20,874), bear a greater annual disease burden due to higher populations (Reid *et al,* 2018). However, data vary from study to study, and there are many discrepancies among these. While the risk may be greater in the aforementioned nations, actual rates appear to be the highest in the United States and in Europe (Chornokur *et al*, 2013). These data may be skewed based on availability alone, and are also likely influenced by higher life-expectancies and earlier detection (Chornokur *et al*, 2013) in the United States and Europe. Diagnoses and treatments tend to be earlier and better in these countries, and these factors may also have an effect on reported incidence and survival numbers.

The highest rates of ovarian cancer in the United States occur in non-Hispanic white (NHW) women, with the lowest rates there occurring in women of African-American descent, even after adjusting for known risk factors (Ness *et al*, 2000). This may be due, in part, to the fact that African-American women were more likely to have had 5 or more pregnancies and were more likely to have had a hysterectomy, and that white women were more likely to have a long family history of ovarian cancer (Ness *et al*, 2000). This may also be due to the fact that for Black women and other women of color in the United States and worldwide, the data simply are not there (Ness *et al*, 2000).

One of the major points made in the World Ovarian Cancer Coalition Study is that the majority of the available epidemiology pertains to Caucasian or white North American and Western European women (Reid *et al*, 2018). A

prime example of how this presents obstacles to meaningful research is the fact that in the United States NHW women are more likely to be diagnosed with breast cancer, but non-Hispanic Black (NHB) women are more likely to die from it (Whitman *et al*, 2007). These statistics are also true for ovarian cancer, with African-American women being at greater risk of receiving delayed treatment, or no treatment at all, than Caucasian women. They were also less likely to receive surgery in addition to chemotherapy, whereas Caucasian women were more likely to receive both (Chornokur, *et al*, 2013). This is a direct result of a lack of access to health insurance, doctors, and treatment facilities, and it demonstrates the racial disparities in healthcare that still exist today even in the most developed of countries (Williams *et al*, 2001).

1.2 Ovarian Cancer Risk and Prevention

Genetic and lifestyle risk factors have been comprehensively analysed in order to ascertain whether or not they influence ovarian cancer incidences and outcomes. A woman's lifetime risk of developing ovarian cancer is roughly 2% in industrialized nations (Antoniou *et al*, 2003). Average cumulative risks by age 70 increase to 39% and 11% for women carrying BRCA1 and BRCA2 mutations, respectively. Women carrying these mutations and who have a family history of breast and/or ovarian cancer are at the highest risk. Risks appears to be less substantial in families without those histories, regardless of the presence of a BRCA1 or BRCA2 mutation (Antoniou *et al*, 2003).

In addition to BRCA1/2 mutations and family histories, several studies have looked at age of menarche/menopause, duration of ovulatory menstrual

cycles, and endogenous hormones. Lifestyle risk factors included pregnancy (including number of pregnancies and age of the mother), breastfeeding, birth control, hormone replacement therapy (HRT), tubal ligation, hysterectomy, obesity, physical activity level, smoking, and alcohol use (Lukanova and Kaaks, 2005).

1.2.1 Menarche, Menopause, and Pregnancy

While age is definitely a risk factor for OC, ages of neither menarche nor menopause appear to be risk-related in any studies (Lukanova and Kaaks, 2005). Pregnancy has been demonstrated to reduce OC risk, with a decrease in risk for each additional pregnancy. Pregnancy occurring at a later age also seems to confer a protective effect. Infertility appears to increase the risk of OC in both nulligravid and nulliparous women, but not in parous women. Breastfeeding and its duration may provide a protective effect, but this has not been definitively shown (Lukanova and Kaaks, 2005).

1.2.2 Ovulation and Hormones

In women of child-bearing age (usually 13-45) with normal menstrual cycles, ovulation occurs roughly on the 14th day of a cycle (this may vary due to longer or shorter follicular phases), with menses occurring 14 days post-ovulation (Fig. 1.2). Generally, gonadotropin-releasing hormone (GnRH) is secreted by the hypothalamus, and this in turn triggers a cascade of signaling events during which the anterior pituitary gland secretes follicle-stimulating hormone (FSH) and luteinizing hormone (LH), both of which communicate with theca cells and granulosa cells in the ovaries. Together, these keep a

balance of estradiol, progesterone, androgen, and testosterone, but once a month this is disrupted by an increase in FSH leading to the completion of meiosis I of a single ovum. The ovarian epithelium is thusly disrupted approximately 450 times during the course of a woman's life (Thiyagarajan DK, Basit H, Jeanmonod R. Physiology, Menstrual Cycle. [Updated 2019 Apr 24]. In: StatPearls [Internet]. Treasure Island (FL): StatPearls Publishing; 2019 Jan-. Available from: https://www.ncbi.nlm.nih.gov/books/NBK500020/).

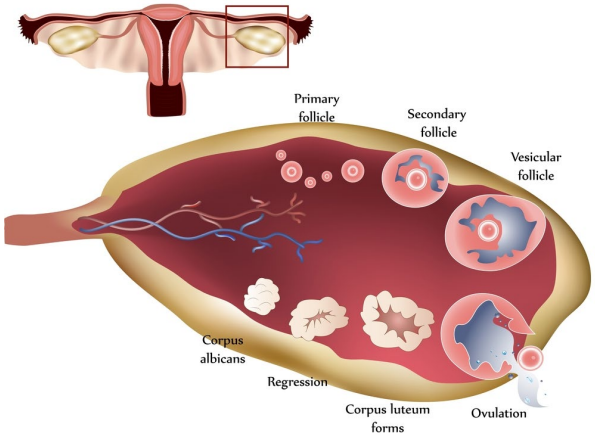

Fig 1.2 The ovulatory cycle (retrieved from https://sofatinfertility.com/news/ovulation-induction-in-india/)

The very first "hormonal hypothesis" was the "gonadotropin hypothesis" (Biskind and Biskind, 1944), which proposed that OC development was a result of excessive stimulation of the ovarian epithelium by luteinizing hormone (LH) and/or follicle-stimulating hormone (FSH). The data on this are inconclusive, and the very basis of this hypothesis has long been questioned, as the tumours induced in the rodents for the initial study were of non-epithelial origin.

The duration of ovulatory menstrual cycles, or "incessant ovulation" as a

cause of OC, is part of a hypothesis put forth by Fathalla in 1971 in his letter to *The Lancet*, "Incessant Ovulation – A Factor in Ovarian Neoplasia?". Birth control that suppresses ovulation has indeed long been shown to have a protective effect regarding OC, however the "incessant ovulation" hypothesis of ovarian carcinogenesis is no longer regarded as valid (Lukanova and Kaaks, 2004). HRT, on the other hand, *is* a risk factor for OC, particularly when estrogen is used alone rather than in conjunction with progesterone, although both formats are considered to increase a woman's risk of OC. Prolonged periods of use of both kinds of HRT have shown a 1.5-2-fold increased lifetime risk of developing OC. This is thought to impose the greatest risk for endometrioid and clear-cell subtypes (Lukanova and Kaaks, 2005). A country-wide Danish study has recently shown that progesterone-only HRT does not confer the protective effect against OC it was previously believed to (Iversen *et al*, 2018).

1.2.3 Weight and Body Mass Index

Studies are contradictory where body mass index (BMI) is concerned (Lukanova and Kaaks, 2004). Some studies show no correlation between BMI and OC risk, but do show that a significant risk correlation for OC exists regarding waist-to-hip ratio (Dal Maso *et al*, 2002; Anderson *et al*, 2004). A study of premenopausal women also found a correlation between hip-to-waist ratio and OC risk (Sonnichsen *et al*, 1990; Lukanova and Kaaks, 2004), however a fourth cohort found an association between BMI and OC risk, but no significant risk for the waist-to-hip ratio (Fairfield *et al*, 2002; Lukanova and Kaaks, 2004).

1.2.4 Diabetes

A case control study by Adler and colleagues in Washington and Utah investigated the possibility of an association between women with diabetes and ovarian cancer (Adler *et al*, 1996). This study used data from population-based cancer registries. Women were excluded from the study if surrogates were provided, and controls were excluded if they had undergone hysterectomy, bilateral oophorectomy, or if this status was unknown. Women with unknown diabetes history were also excluded. The study comprised 595 cases of ovarian cancer, and 1587 controls (Adler *et al,* 1996). While women with ovarian cancer were more likely to have never used birth control, never have been pregnant, and to have a higher BMI, no association was found between women with diabetes and those with ovarian cancer, regardless of histological subtype. While this was an interview-based study, diabetes was not found to be a risk factor for ovarian cancer (Adler *et al,* 1996).

1.2.5 Gynaecological Surgery

Gynaecological surgeries appear to reduce the risk of ovarian cancers. This is supported by a body of epidemiological research which shows that women who have undergone hysterectomy or tubal ligation have an overall lowered risk of ovarian cancer in the range of 30-40% (Reid *et al*, 2017). However, the highest risk reductions in these studies were seen in endometrioid and clear cell ovarian cancers, and not in the high-grade serous carcinomas that are responsible for so many deaths.

1.3 Symptoms of Ovarian Cancer

The symptoms of ovarian cancer are vague and poorly defined, but can include persistent abdominal bloating, fatigue, feeling of fullness in the abdominal area, and pelvic pain. Unexplained weight gain, bleeding after menopause, bowel issues, and an increase in frequency of urination can also be symptoms. However, these are also symptoms of many other conditions, and are therefore not definitive.

1.4 Ovarian Cancer Screening and Diagnosis

One of the many major drawbacks in women's healthcare at present is a lack of specific screening methodology for ovarian cancer. It is usually diagnosed by ultrasound or CT in the process of symptom investigation. As there is a strong correlation between stage at discovery and survival, it is crucial to uncover early detection methods. Five-year survival rates vary from approximately 80% for Stage I to 8% for Stage IV.

1.4.1 Current Diagnostic Methods

Diagnosis often includes a clinical exam, biopsy, blood tests, and both CT and MRI scans. Presently, there are two strategies used in early attempts at EOC diagnosis: a blood test which looks for cancer antigen 125 (CA-125), and transvaginal ultrasound (TVUS) to look for abnormalities in ovarian volume, cysts, blood vessel structure, and echogenicity (Rauh-Hain *et al*, 2011).

1.4.1.1 CA-125

CA-125 is a single transmembrane domain glycoprotein also known as mucin 16 (MUC16). It was discovered as the antigen for monoclonal antibody (mAb) OC125 (named so because it was the 125th mAb developed against

ovarian cancer by Bast in 1981), and has been shown to be useful in gauging EOC progression and response to treatment. However, it has not been shown to be useful as a diagnostic tool due to its association with other inflammatory conditions such as uterine fibroids, liver cirrhosis, pelvic inflammatory disease, endometriosis, and even normal menstruation (Bottoni and Scatena 2015).

1.4.1.2 Transvaginal Ultrasound

TVUS allows for detailed imaging of ovarian morphology, much more so than traditional transabdominal ultrasound (Rauh-Hain *et al*, 2011). Even so, acquired images are still dependent on interpretation by a skilled pathologist-radiologist. Screening protocols vary from country to country, and even from hospital to hospital, as do their morphologic criteria. There is no standard index at present, which often leads to different research results that are design-dependent and therefore contradictory within the context of meaningful comparison. The International Ovarian Tumour Analysis (IOTA) study compared 2 logistic regression (LR) models to pattern recognition by a Level III US operator in an effort to make better use of TVUS data. It was concluded that while these LR models yielded a highly sensitive first-stage test that could potentially be used in the outpatient setting, a different second-stage test would be necessary to rule out false positives (Nunes *et al*, 2018).

1.4.2 Ovarian Cancer Screening Trials

In spite of many ovarian cancer screening trials worldwide, none have demonstrated improved mortality. The University of Kentucky Ovarian Cancer Screening Project by van Nagell and colleagues, spanning 1987 – 2005, reported

TVUS results for 25,327 asymptomatic women over the age of 50, and asymptomatic women over the age of 25 with a family history of OC in an immediate or secondary family member (van Nagell *et al,* 2007; Rauh-Hain *et al,* 2011). Sensitivity was ranked at 85%, specificity at 98.7%, and PPV of an abnormal result was 14.01%. Many of these patients were from a high-risk group, so these results were determined to be skewed. The study concluded that TVUS was not a reliable OC detection method for women presenting with normal ovarian volumes (van Nagell *et al*, 2007; Rauh-Hain *et al*, 2011).

A similar study at Hirosaki University in Japan reported on a much larger sample size of 183,034, 51,500 of whom were presenting for screening for the first time (Sato *et al*, 2000; Rauh-Hain *et al*, 2011). Of these 51,500 participants on whom the study is actually based, there were roughly 25,000 each of pre- and post-menopausal status. 4452 women participated in secondary screening, with 324 (6.79%) of those women meeting the criteria for exploratory surgery. It was concluded that TVUS was a viable method of ovarian cancer screening, particularly as there was a significant difference in the number of cases that were determined to be Stage I, where they had been diagnosed at higher stages clinically.

Other studies, such as the Prostate, Lung Colorectal, and Ovarian Cancer Screening (PLCO) trial run by the National Institute of Health (NIH) in the United States screened 39,115 women aged 55-74 annually for ovarian cancer using CA-125 and TVUS, of which 28,506 had reported results. PPV for an abnormal CA-125 test was determined to be 3.7%, for TVUS was 1.0%, and

23.5% for abnormal results in both tests (Rauh-Hain *et al*, 2011).

The United Kingdom Collaborative Trial of Ovarian Cancer Screening - the largest ovarian cancer trial worldwide - broke its study design into three groups of roughly 67,546 participants each: control (no treatment), TVUS alone, and a multimodal screening group (MMS) which measured CA-125 on an annual basis and added TVUS if those levels were deemed to be elevated (Rauh-Hain *et al*, 2011; Menon *et al*, 2009; Jacobs *et al*, 2015). It also included results for malignant tubal neoplasms.

Preliminary results of this study reported sensitivity, specificity, and PPV at 89.4, 99.8, and 43.3 for the MMS cohort, and 84.9, 98.2, and 5.5 for the TVUS cohort, with a significant difference in specificity between the two cohorts (Rauh-Hain *et al*, 2011; Menon *et al*, 2009). Of the 2785 women with an abnormal ultrasound, 1894 underwent clinical assessment, with 854 requiring exploratory surgery. 24 of the women in the TVUS cohort were found to have ovarian malignancies. Longitudinal findings from this study were published in 2015 (Jacobs *et al,* 2015). Sensitivity, specificity, and PPV results were virtually unchanged and they did not show a significant reduction in overall mortality, but did show reduced mortality in the multimodal cohort when prevalent cases were excluded, therefore these data may be useful for newly-diagnosed cases.

While the results of this screening trial did not yield enough evidence for the NHS to implement a national ovarian screening program, research is still being conducted in this area in order to find screening methods that are consistently effective. The differences in all of these study designs and in their

reported results emphasize the need for standardized global testing criteria for ovarian cancer screening.

1.4.3 Pathological Classification and Pathogenesis

There are over thirty types of ovarian cancer, and all arise from three distinct cell types: epithelial, germ, and stromal. Epithelial ovarian carcinomas (EOC) account for 85-90% of all ovarian cancers, and 87% of these are diagnosed at stage III or stage IV (Lisio *et al*, 2019). There are currently five classifications of malignant EOC: clear-cell (CCOC), mucinous (MOC), low-grade serous (LGSOC), high-grade serous (HGSOC), and endometrioid. The focus of this thesis will be HGSOC, which is the deadliest of all ovarian cancer subtypes and has shown little to no improvement in overall survival over the course of several decades (Bowtell *et al,* 2015).

HGSOC currently comprises four molecular subtypes, which are C1/mesenchymal, C2/immune, C4/differentiated and C5/proliferative (Bowtell *et al,* 2015). While these encompass different types of cell involvement (immune, stromal, et c.) and different clinical outcomes, they are not currently employed in the clinical setting (Bowtell *et al,* 2015).

There are three schools of thought regarding the origins of HGSOC, and these are that genesis is in the ovarian surface epithelium (OSE), the fallopian tube, or in the peritoneal mesothelium. While origin in the peritoneal mesothelium is mentioned in several papers, it seems to only be mentioned as a potential source of OC due to its involvement at the time of many diagnoses, and none of the literature expands on this hypothetical origin.

Historically, it has been believed that genesis occurs directly in the OSE, arising from decades of ovulation and the continuum of rupture and repair cycles. OSE cells harbor both epithelial and mesenchymal markers, keratin and vimentin, respectively, as do cells lining the peritoneum. During foetal development, OSE cells are derived from the coelemic epithelium next to the gonadal ridge, whereas the epithelia of the fallopian tubes, uterus, and cervix derive from the paramesonephric ducts, and are Müllerian (Fig. 1.3) (Lengyel 2010).

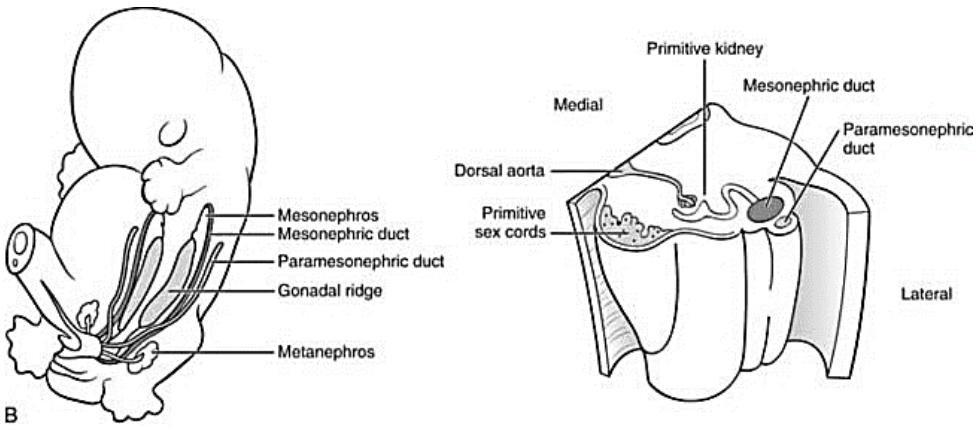

Fig.1.3 Diagram showing the gonadal ridge and paramesonephric duct (retrieved from https://oncohemakey.com/genetic-basis-of-gonadal-and-genital-development/)

Paradoxically, in advanced EOC there is generally involvement of the fallopian tube, cervix, and uterus, and so the involvement of non-Müllerian tissue in the larger picture was queried. A study of HOX genes in murine OSE did provide evidence for differentiation of previously undifferentiated OSE cells into a Müllerian-like morphology, but failed to provide any direct evidence for tumourigenesis in the ovarian epithelium itself (Lengyel 2010).

Compelling research has emerged, however, linking HGSOC to a genesis in the fallopian tube (Bowtell *et al*, 2015; Kroeger and Drapkin, 2016; Labidi-

Galy *et al*, 2017) via secretory epithelial cells (FTSECs). As previously discussed, among the risk factors for EOC are the BRCA1/2 mutations. These are mutations in the homologous DNA repair pathway (HDR), and mutations of this nature are seen in 50% of HGSOC cases (Bowtell *et al,* 2015; Kroeger and Drapkin, 2016). The discovery of these genes and their role in ovarian cancers led to many prophylactic salpingo-oophorectomies, which in turn led to the opportunity to more closely examine these tissues, as well as the subsequent development of the SEE-FIM (Sectioning and Extensively Examining the FIMbriated end) protocol (Kroeger and Drapkin, 2016).

Evaluation of the fallopian tubes of women carrying BRCA mutations showed early serous carcinomas in the distal ends, including serous tubal intraepithelial carcinomas (STICs), but no epithelial ovarian carcinomas were observed. Many of the fallopian tube samples contained non-proliferative regions of TP53-positive cells that contained DNA mutations that were identical to their corresponding STIC lesions (Figs. 1.4, 1.5). When these protocols were brought into the clinical setting, HGSOC patients were found to have the same TP53 mutation in lesions of the OSE, STIC, and in the non-proliferative p53-positive cells. This provided direct evidence for a fallopian tube origin of HGSOC.

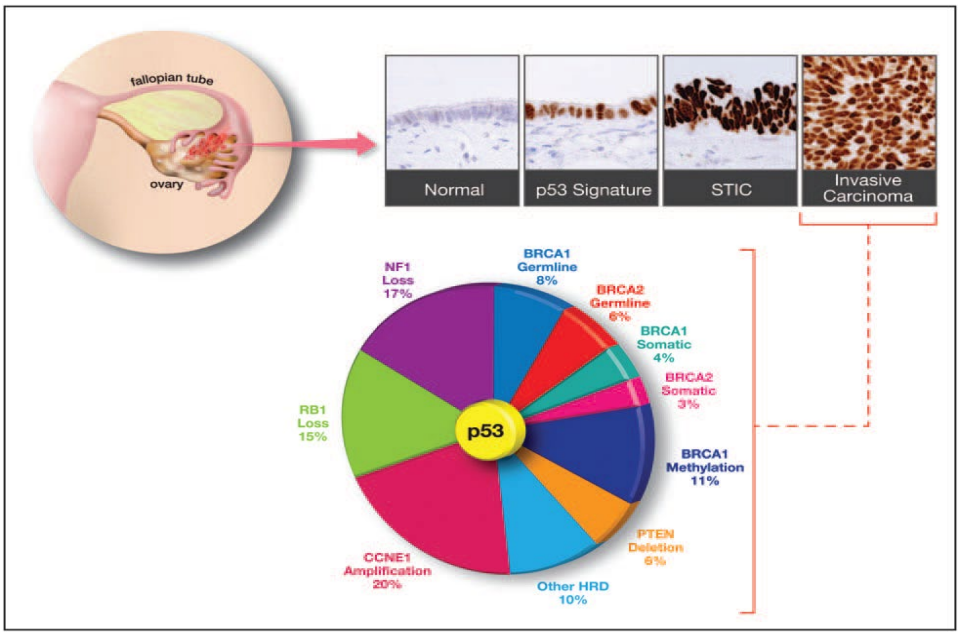

Fig. 1.4 Genomic and pathological composition of most HGSOCs (Kroeger and Drapkin 2016)

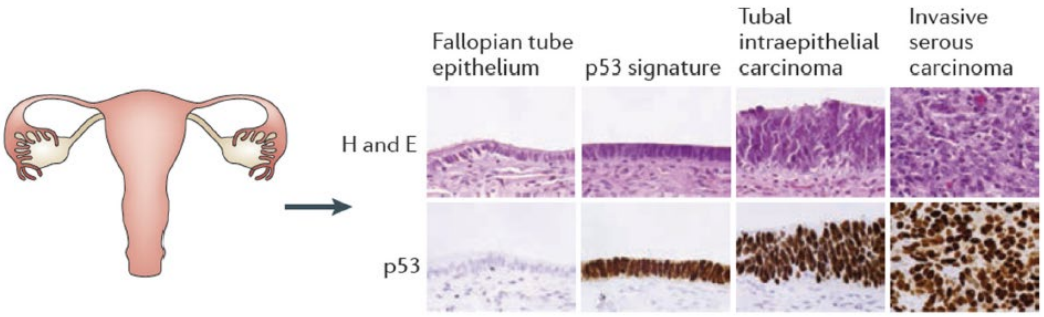

Fig. 1.5 p53 staining of the fallopian tube shows early clonal expansion in STIC lesions and eventual invasion (Botwell *et al,* 2015)

1.4.4 Staging

Ovarian cancers, once they have been diagnosed, are subject to a system of criteria by which they are staged and graded. There are currently two staging systems in use, and both use the three classification factors known as TNM (Tumour, Node, and Metastasis) (https://www.cancer.org/cancer/ovarian-cancer/detection-diagnosis-staging/staging.html). The International Federation of Obstetrics and Gynecology or FIGO (Fédération Internationale de Gynécologie et d'Obstétrique) grading system was introduced in 1954 by Swiss Professor Hubert de Watteville. The American Joint Committee on Cancer (AJCC) was formed in 1959, and uses practically identical criteria. Staging ranges from I through IV. It should be noted that FIGO updated its staging criteria for ovarian cancer in 2014 to include cancers of both the fallopian tube and peritoneum in an effort to streamline diagnoses and treatments for what their research deemed to be linked cancers (Javadi *et al*, 2016). FIGO's 2018 report states that it is the view of FIGO that cancers of these three areas should no longer be referred to as having an ovarian origin unless that is clearly the case (Berek *et al,* 2018; Bhatla and Denny, 2018). The paper also clarifies that as many as 80% of tumours thought to be of ovarian origin have been histologically and genetically shown to have originated in fallopian tube fimbria (Berek *et al*, 2018).

TNM gauges the size of the tumour (T), whether or not there is nodal involvement (N), and whether or not the cancer has metastasized (M) to other

sites or organs. There are four different kinds of staging: clinical staging (based on physical examination) pathological staging (also called surgical), post-therapy/post-neoadjuvant therapy staging, and restaging. Clinical staging is based on physical examination, imaging, and biopsies done prior to surgery, and pathological staging combines clinical findings with post-surgery laboratory data. Post-neoadjuvant therapy staging is used to stage the cancer that is left after treatment but prior to surgery or where no surgery is performed. Restaging is done in cases where there is a recurrence of the cancer after treatment in order to determine the best course of action for that particular patient. Staging can create a lot of confusion for the patient, particularly if the woman has had neoadjuvant chemotherapy to try to shrink the tumour prior to resection, as the pathological staging may then be very different from the initial clinical staging. The pathological staging generally gives better information regarding the patient's status, and is therefore typically used moving forward with treatment.

A tumour is said to be Stage I if it is confined to one or both ovaries, one or both fallopian tubes, and there is no nodal involvement and no metastasis. It would be described as T1-N0-M0. Stage IA is given to a tumour confined to one ovary or 1 fallopian tube with no cancer cells found in ascites or peritoneal washings. Stage IB status would be given if tumours were found in both ovaries or both fallopian tubes, with no cancer cells found in ascites or peritoneal washings. Stage IC, however can indicate potential advancement of the disease. It includes the criterion that there is tumour present in both ovaries

or both fallopian tubes, but also includes designations of 1, 2, or 3, with 1 being rupture of the ovarian capsule (tunica albuginea) during surgery, 2 being rupture of the capsule or of the tumour prior to surgery, and 3 being the presence of cancer cells in the ascites or peritoneal washings (Table 1.1).

It is unclear whether or not rupture of the ovarian capsule during or prior to surgery increases the risk of disease recurrence and death from EOC. It increases these risks in clear-cell carcinomas (CCC) of the ovary (Higashi *et al*, 2011). Literature regarding EOC is conflicting (Kim *et al*, 2012; Lynette Denny 2013), however the data regarding survival rates after surgical spill or pre-operative rupture of the ovarian capsule do not appear to be statistically significant (Higashi *et al*, 2011).

Stage II denotes that the cancer has spread to organs within the peritoneal cavity, such as the bladder, uterus, omentum, or sigmoid colon, or that there is primary peritoneal cancer. Stage III indicates that the cancer has spread to outside the pelvic area, with or without metastasis to retroperitoneal lymph nodes (Fig. 1.6), and Stage IV always involves distant metastasis (Table 1.1). It is these last two stages at which the vast majority of ovarian cancers are discovered.

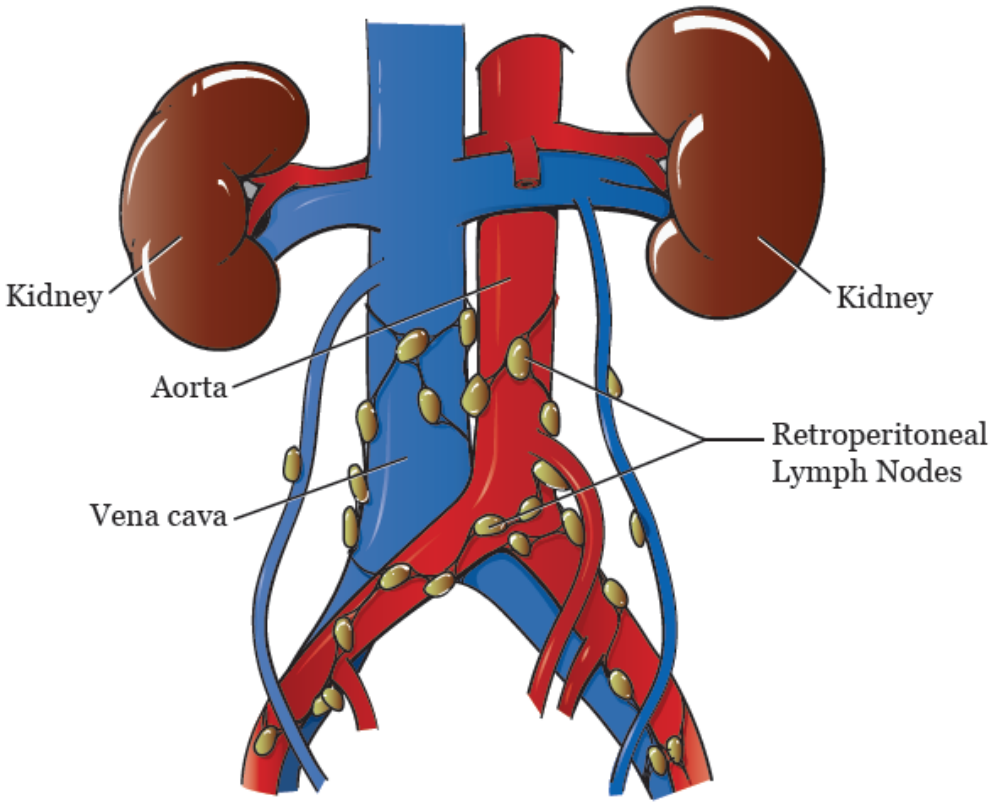

Fig. 1.6 Retroperitoneal lymph nodes (https://www.mskcc.org/cancer-care/patient-education/about-your-retroperitoneal-lymph-node-dissection)

Table 1.1 Current FIGO staging criteria for cancers of the ovary, fallopian tube, and peritoneum. (Berek *et al*, 2018)

FIGO Staging for Cancers of the Ovary, Fallopian Tube, and Peritoneum
Stage I: Tumor confined to ovaries or fallopian tube(s)
T1-N0-M0
IA: Tumor limited to 1 ovary (capsule intact) or fallopian tube; no tumor on ovarian or fallopian tube surface; no malignant cells in the ascites or peritoneal washings
T1a-N0-M0
IB: Tumor limited to both ovaries (capsules intact) or fallopian tubes; no tumor on ovarian or fallopian tube surface; no malignant cells in the ascites or peritoneal washings
T1b-N0-M0
IC: Tumor limited to 1 or both ovaries or fallopian tubes, with any of the following:
IC1: Surgical spill
T1c1-N0-M0
IC2: Capsule ruptured before surgery or tumor on ovarian or fallopian tube surface
T1c2-N0-M0
IC3: Malignant cells in the ascites or peritoneal washings
T1c3-N0-M0
Stage II: Tumor involves 1 or both ovaries or fallopian tubes with pelvic extension (below pelvic brim) or peritoneal cancer
T2-N0-M0
IIA: Extension and/or implants on uterus and/or fallopian tubes and/or ovaries
T2a-N0-M0
IIB: Extension to other pelvic intraperitoneal tissues
T2b-N0-M0
Stage III: Tumor involves 1 or both ovaries or fallopian tubes, or peritoneal cancer, with cytologically or histologically confirmed spread to the peritoneum outside the pelvis and/or metastasis to the retroperitoneal lymph nodes
T1/T2-N1-M0
IIIA1: Positive retroperitoneal lymph nodes only (cytologically or histologically proven):
IIIA1(i) Metastasis up to 10 mm in greatest dimension
IIIA1(ii) Metastasis more than 10 mm in greatest dimension
IIIA2: Microscopic extrapelvic (above the pelvic brim) peritoneal involvement with or without positive retroperitoneal lymph nodes
T3a2-N0/N1-M0
IIIB: Macroscopic peritoneal metastasis beyond the pelvis up to 2 cm in greatest dimension, with or without metastasis to the retroperitoneal lymph nodes
T3b-N0/N1-M0
IIIC: Macroscopic peritoneal metastasis beyond the pelvis more than 2 cm in greatest dimension, with or without metastasis to the retroperitoneal lymph nodes (includes extension of tumor to capsule of liver and spleen without parenchymal involvement of either organ)
T3c-N0/N1-M0
Stage IV: Distant metastasis excluding peritoneal metastases
Stage IVA: Pleural effusion with positive cytology
Stage IVB: Parenchymal metastases and metastases to extra-abdominal organs (including inguinal lymph nodes and lymph nodes outside of the abdominal cavity)
Any T, any N, M1

1.5 Treatment of Ovarian Cancer

Once a diagnosis of ovarian cancer has been made, treatment recommendations are discussed at a multidisciplinary team meeting, and depend on clinical stage, age, overall health of the patient, and whether or not fertility preservation is possible and/or desired. Treatment is generally a combination of surgery and chemotherapy. Other targeted therapies such as

mAbs or PARP-inhibitors may be used in conjunction with this, or used alone as either treatment or maintenance.

1.5.1 Surgery

Surgery is almost always performed, regardless of clinical stage, to verify scan findings, to remove visible cancer tissue, and to take samples that will provide more accurate staging information. Fertility-sparing surgery (FSS) is sometimes possible for pre-menopausal women with Stage IA cancers. This type of surgery removes only the one ovary and fallopian tube in which the cancer was found, and has been shown to have rates of overall survival (OS) and disease-free survival (DFS) comparable to radical surgery (RS) (Kajiyama *et al*, 2011).

Treatment for early-stage EOC typically involves primary debulking surgery (PDS). This encompasses bilateral salpingo-oophorectomy, as well as total hysterectomy (Kajiyama *et al*, 2011). Peritoneal washings and a biopsy of the omentum are also usually taken at this time. Lymph nodes may be resected during surgery, but the value of this procedure has come under questioning as it may lead to unnecessary removal of pelvic and paraaortic lymph nodes (Uccella *et al*, 2019). Only 20-25% of EOC is diagnosed as early-stage, and only 14-15% of these have metastasis to the lymph nodes. Research is currently underway in the Sentinel Lymph Nodes in Early-Stage Ovarian Cancer trial to determine the value of sentinel node biopsy versus complete pelvic and paraaortic lymphadenectomy in these cases (Uccella *et al*, 2019).

1.5.2 Chemotherapy

Post-surgical treatment is contingent upon pathological staging and substaging, per FIGO criteria in Table 1.1. It can also be dependent upon grading, which is based on how the cells look and behave: normal versus abnormal. Chemotherapy is standard, and can be administered as a neoadjuvant or adjuvant treatment. While it is typically delivered intravenously, it can also be administered intraperitoneally.

1.5.2.1 Neoadjuvant Chemotherapy

Current standard therapy for advanced EOC consists of three to six cycles of neoadjuvant chemotherapy administered prior to interval debulking surgery (IDS), with platinum-based drugs in combination with paclitaxel (https://www.nhs.uk/conditions/ovarian-cancer/treatment/). While still controversial, it has not been shown to be inferior to results achieved with PDS followed by adjuvant chemotherapy (Elies *et al,* 2018). It is most often administered in patients with late-stage diagnoses, and also in those for whom PDS poses an imminent risk. Carboplatin monotherapy may also be considered in some cases where a taxane is not suitable. Radiation is not typically used in the treatment of late-stage OC. Bevacizumab (a VEGF-inhibitor) may also be used in addition to standard treatment as first-line therapy for stage III and IV cancers, given every three weeks for as many as six cycle, and then given singly every three weeks for up to 16 further cycles (Marchetti *et al*, 2019). In patients with platinum-resistant recurrent disease, bevacizumab can be given in combination with paclitaxel, topotecan or doxorubicin

(https://www.hse.ie/eng/services/list/5/cancer/profinfo/chemoprotocols/gynaecology/).

1.5.2.2 Adjuvant Chemotherapy

Adjuvant chemotherapy for EOC is that which is administered post PDS, and generally consists of treatment with a combination of carboplatin and paclitaxel (Taxol®), given in three to six three-week cycles. Sometimes cisplatin is used in place of carboplatin, and docetaxel (a semisynthetic analogue of paclitaxel known commercially as Taxotere®) in place of paclitaxel. Radiation is not often used in OC, but may be used in early-stage cancers after PDS to eradicate any potential residual disease. Carboplatin monotherapy may also be used. Platinum-based cytotoxic drugs have proven to be effective in 80% of EOC solid tumours when combined with a taxane (Sato and Itamochi 2014), and this type of combination therapy confers a 5-year survival rate of approximately 45% (Marsh *et al*, 2007). Cancers that respond well to chemotherapeutic agents which contain the metal platinum, such as cisplatin and carboplatin, are described as being platinum-sensitive. Ovarian cancers treated with these particular chemotherapeutic agents that return after a period greater than six months are also considered to be platinum-sensitive, and recurrence may be treated with a PARP (Poly-ADP-ribose polymerases) inhibitor such as olaparib (https://www.hse.ie/eng/services/list/5/cancer/profinfo/chemoprotocols/gynaecology/).

1.5.2.3 Platinum-based Chemotherapeutic Agents

When Barnett Rosenberg and his colleagues discovered that some platinum compounds, including *cis*-Pt(IV)$(NH_3)_2Cl_4$, *cis*-Pt(II)$(NH_3)_2Cl_2$, Pt(II)$(NH_2CH_2CH_2NH_2)Cl_2$, and Pt(IV)$(NH_2CH_2CH_2NH_2)Cl_4$,were able to reversibly inhibit cell division in the Gram-negative rod bacteria *Escherichia coli* in 1969, he decided to test these compounds on cancers. He discovered that these compounds also inhibited sarcoma 180 and leukaemia L1210 in mice (Rosenberg *et al*, 1969). Cisplatin was the first platinum-based chemotherapy to earn FDA approval in 1978. Since then, platinum-based chemotherapy has become the standard treatment for roughly 50% of all cancers (Johnstone *et al*, 2014), including EOC.

The molecular mechanism of cisplatin (*cis*-diamminedichloroplatinum(II)) lies in its ability to cross-link with purines in DNA, thereby causing damage as well as interfering with DNA repair mechanisms, ultimately inducing apoptosis (Dasari and Tchounwou 2014). The antitumour activity of a platinum compound is dependent on several things, primarily a *cis* conformation which has cytotoxic properties, whereas the *trans* conformation does not (Schwab 2011). There must also be present two inert amine groups, and two chloride (or other) ligands which can form leaving groups with the DNA (Fig. 1.7) (Dasari and Tchounwou 2014).

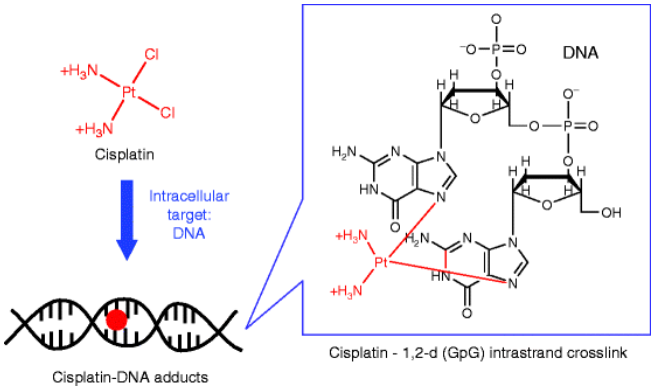

Fig. 1.7 Two chloride ligands form leaving groups with purines https://link.springer.com/referenceworkentry/10.1007%2F978-3-642-16483-5_1189

Carboplatin, or *cis*-diamine (1,1-cyclobutanecarboxylato) platinum (II) is an analogue of cisplatin, and is used to treat cancers of the lung, head, neck, testis, and ovary. It has a bidentate dicarboxylate as its ligand (Fig. 1.8), rather than the chloride ions of cisplatin that bind covalently to nitrogens in purines, and conveys similar activity to cisplatin, although it is not as fast-acting or as potent.

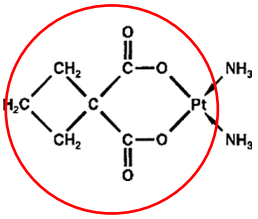

Fig. 1.8 Cisplatin has a bidentate dicarboxylate as its ligand, circled in red. (Hempel, 2004)

The resulting connections between the platinum and the DNA affect DNA rotation around the histone, and this determines how that particular segment of DNA is either presented for repair, or occluded (Sousa *et al,* 2014). Both cisplatin and carboplatin affect DNA repair mechanisms, and could be responsible for the loss of DNA mismatch repair (MMR). This may contribute to chemoresistance in ovarian cancer as apoptosis may be contingent upon both

the recognition of platinum adducts and the engagement of repair mechanisms (Sousa *et al*, 2014). Excision repair cross-complementation group 1 (ERCC1) protein in the nucleotide excision repair (NER) pathway is thought to be an important protein in the use of platinum-based chemotherapeutic agents (Sousa et al, 2014).

Some studies have shown that carboplatin has a lower excretion rate, and is retained by the body longer than cisplatin, but for the most part it leaves the body quickly, and up to 90% of administered carboplatin can end up in the patient's urine. While there are benefits to carboplatin, most notably decreased nephrotoxicity, lower blood cell and platelet production has been noted (Dasari and Tchounwou 2014).

1.5.2.4 Taxanes

Paclitaxel was isolated in 1971 from the Pacific Yew (Schwab *et al*, 2014). It functions in chemotherapy by binding specifically to microtubule polymers, subsequently blocking cells in the G_2/M phase from forming a normal mitotic spindle (Horwitz 1994). This ultimately results in apoptosis of the cell during the transition from anaphase to metaphase, at which time mitochondrial membrane potential is lost, and the membrane itself becomes permeabilized leading to the release of cytochrome c, caspase activation, and DNA fragmentation (Pasquier *et al*, 2004). It has been investigated as a stand-alone therapy for platinum-resistant ovarian cancer.

1.5.2.5 Topoisomerase Inhibitors

Topoisomerase inhibitors are used to treat ovarian cancer, small-cell

lung carcinoma, and cervical cancer. In ovarian cancer, they are typically employed after failure of first-line treatments. Topoisomerase I (type IB) creates single-stranded nicks in DNA that is tightly wound, relaxes the DNA and then reanneals the strand. Inhibiting this activity helps to prevent heterochromatin from being exposed during both transcription and replication, thereby suppressing both gene transcription essential to survival of the cell and also replication necessary for cell division and cancer progression. Topoisomerase I inhibitors include topotecan, irinotecan, and camptothecin (French *et al*, 2011).

Topoisomerase II inhibitors include etoposide, doxorubicin, and epirubicin. Topoisomerase II (type IIA) is important during S-phase. It creates double-stranded breaks in DNA and also prevents chromosomal breakage and loss (French *et al*, 2011). Inhibition of this important molecule prevents accurate DNA replication and induces a loss of chromosomal integrity thereby triggering apoptosis (Binaschi *et al*, 1995).

1.5.3 Radiation Therapy

Radiation therapy for cancer uses a precisely targeted beam of energy to kill cancer cells. The most common energy used is X-ray, but proton beams have also been used. Prior to the advent of chemotherapy, whole abdominal radiation (WAR) was widely used for the treatment of ovarian cancers. However, the low doses required to prevent damage to the kidneys, liver, and bowel often resulted in residual disease. Overall toxicity was often in itself fatal, and its use was largely displaced by cisplatin in the late 1970's (Fields *et al,* 2017). Recent advances in radiotherapy techniques are being investigated

for potential use in EOC, but at present it is not a standard treatment. It can be used in some recurrent cases where disease is confined to a single site, but proximity to the bowel is often prohibitive.

1.5.4 Hormone Therapy

Hormone or endocrine therapies are used to treat premenopausal women experiencing surgical menopause and also women with advanced disease who have experienced relapse following PDS and treatment with platinum-taxane chemotherapy, or for whom continued chemotherapy is not a viable option due to platinum-resistance or recurrent disease (George *et al*, 2017).

Tamoxifen is a selective estrogen receptor modulator (SERM) used to treat ER+ breast and ovarian cancers, with the caveat that it can induce endometrial and uterine cancers (Hu *et al,* 2015). It works by competing with estrogen for receptors on the surface of tumour cells. Letrozole is an aromatase inhibitor that lowers estrogen production. Both prevent tumour growth in ER+ cells by depriving them of estrogen.

A retrospective study of HGSOC patients treated with tamoxifen and letrozole included 97 women aged 20-92, with CA-125 levels, duration of response, and clinical benefit rate as secondary endpoints. It was concluded that both drugs were capable of stabilizing disease state for a prolonged period of time (George *et al*, 2017). However, it was noted that the use of letrozole increased duration of response when compared with tamoxifen. (George *et al*, 2018).

1.5.5 Targeted Therapies

As we learn more about the underlying mechanisms involved in cancer metastasis, we are able to design and direct therapeutics that cause less damage to surrounding tissues than conventional chemotherapeutic agents. These targeted therapies are also crucial for those patients with chemoresistant cancers and include a number of small-molecule inhibitors that are able to permeate the membranes of cancer cells, disrupting their normal progression.

1.5.5.1 Monoclonal Antibodies and Small-molecule Inhibitors

Monoclonal antibodies (mAbs) are a type of small-molecule inhibitor that have been employed in the fight against cancer, and can be used alone or in conjunction with other therapies. Anti-HER2 (Trastuzumab) has been used to treat breast, endometrial and uterine cancers with some success due to its ability to bind to cell surface receptors and block growth factors. However, it yielded disappointing results in the treatment of ovarian cancer, partially due to the fact that HER2 is not overexpressed in OC. 3 of 7 patients in one study did achieve complete remission after adding Trastuzumab to traditional chemotherapy, but these patients were heavily pre-treated and the cohort was very small (Guastalla *et al,* 2007).

Avastin® (Bevacizumab) works against vascular endothelial growth factor A (VEGF-A) signaling, functioning as an anti-angiogenic, and has been used in ovarian cancer in combination with platinum-based chemotherapy, followed by use as a single-agent maintenance therapeutic. In this scenario, it has been demonstrated to increase PFS from 12.0 months to 18.2 months.

Avastin® is approved for the treatment of platinum-sensitive recurrent EOC, and also of platinum-resistant recurrent EOC in women who have received two or fewer lines of platinum-based chemotherapy and who responded to first-line chemotherapy (non-refractory). Women with platinum-resistant disease showed an increase from 3.4 to 6.8 months in PFS, as well as a decrease in tumour size. Despite all of the advances in PFS, conclusions of the phase III clinical trials for use of bevacizumab in ovarian cancer were that OS was not significantly improved, but that BRCA and HRR testing remain vital in the context of post-chemotherapy maintenance, and that there is still a survival benefit for women with poor prognoses (Tewari *et al*, 2019).

Tyrosine kinase inhibitors Gefitinib and Erlotonib, which target endothelial growth factor receptor (EGFR), have not been shown to be useful in the treatment of ovarian cancer (Murphy and Stordal, 2011). Others such as Pazopanib target both vascular endothelial growth factor receptor (VEGFR) and platelet-derived growth factor receptor (PDGFR), and while the AGO-OVAR16 phase III study did show improved PFS for advanced ovarian cancer (AOC) patients, it did not show an improvement in OS (Vergote *et al*, 2019).

1.5.5.2 PARP Inhibitors

Poly-ADP-ribose polymerases (PARPs) are essential to base-excision repair (BER) pathways, and PARP inhibitors are a class of drug that disrupts this essential cellular repair mechanism. PARP inhibition results in a build-up of single-strand breaks (SSBs) in DNA, and these may lead to double-strand breaks (DSBs), which are much harder for the cell to repair. Coupled with

either a germline BRCA mutation or a deleterious mutation in the tumour, DNA repair mechanisms such as MMR and NER are severely hindered, while non-homologous end-joining (NHEJ) is encouraged leading to high rates of mutations and inevitable apoptosis (Mittica *et al,* 2018). In 2014, Olaparib was the first PARP inhibitor to gain approval for the treatment of ovarian cancer in patients with a BRCA1/2 mutation who had completed 3 lines of platinum-based chemotherapy. It has also been approved for maintenance in patients with recurrent platinum-sensitive ovarian cancer (Mittica *et al*, 2018). Recent clinical investigations are studying the effects of PARP inhibitors in conjunction with monoclonal antibodies like Bevacizumab, both with and without homologous repair deficiencies (HRD).

1.5.6 Challenges in Diagnosis and Treatment

There are currently no definitive blood tests for ovarian cancer, and it is often asymptomatic, thus it frequently remains undiagnosed until it has reached stage III or IV. As a result of this, the five-year survival rate is only in the range of 30-50%. 70% of women with advanced disease will have recurrence that results in relapse, with 20-25% of those with stage I and II diagnoses also experiencing recurrence (Ushijima 2010). The median time-frame of recurrence is 18-24 months. Recurrence is generally accepted to be both chronic and lethal, and treatments therefore focus on minimizing symptoms and improving quality of life. Platinum-sensitive patients may have longer progression-free survival (PFS) than those with platinum-resistant cancers, and reducing effects from toxicity is essential to quality of life for all

patients (Ushijima, 2010).

1.5.6.1 Platinum Resistance

Platinum resistance in ovarian cancer has traditionally been defined as cancer that recurs within 6 months of the completion of first-line platinum-based chemotherapy. It is now known to be a heterogeneous and complex group of diseases called Platinum Resistant Ovarian Cancer or PROC. Women in this category typically do not respond to further treatment with platinum-based chemotherapeutic agents, resulting in a PFS of only a few months and death within a year of relapse. Platinum sensitivity, as previously described, is defined as occurring in patients within a period of time occurring after 6 months from the completion of platinum-based chemotherapy. Women in this category typically do respond to further platinum-based chemotherapy and have a longer median survival of 2 years. It has become apparent over time, however, that platinum-sensitivity and resistance fall across a complex spectrum, and are not as black-and-white as a 6-month parameter (Davis *et al*, 2014).

There were three studies which took place between 1989 and 1991 that were used to define platinum-resistance, and these looked at symptoms, detectable disease, and radiological evidence of recurrence. Technological advances in computerised tomography (CT), magnetic resonance imaging (MRI), and positron-emission tomography (PET) scans, along with the discovery and implementation of the CA-125 biomarker to monitor disease progression and recurrence would likely paint a very different picture were

these studies to be repeated today. In light of this, it is crucial to constantly and consistently re-evaluate our definitions of platinum-resistance, and to adjust treatments both accordingly and in conjunction with molecular information gleaned from a field of constantly evolving laboratory insights (Davis *et al*, 2014).

1.6 Metastasis of Epithelial Ovarian Cancer

The primary route of metastasis in EOC is considered to be direct peritoneal spreading across the abdominal cavity (Van Berckelaer *et al*, 2016; Cannistra *et al*, 1993). Once cells dissociate from the primary tumour, they implant in to the peritoneal mesothelium that lines the abdominal cavity, or float freely in accumulating ascites. Implantation into the mesothelium is likely mediated by adhesion molecules, including integrin heterodimers that bind to fibronectin in the ECM (Cannistra *et al*, 1993). Transmembrane glycoproteins such as vascular cell adhesion protein 1 (VCAM-1, a member of the immunoglobulin superfamily) are also thought to play a role by binding to integrin α4ß1.

Osborn and colleagues first described the molecule VCAM-1 in 1989, and Elices and colleagues expounded on this by further elucidation of the cytokine-induced recruitment of leukocytes to extravascular tissue at sites of inflammation (Osborn *et al*,1989; Elices *et al*, 1990). Other mediators of adhesion include syndecan, CD44, and selectins, including the platelet-expressed P-selectin (CD62) (Cannistra *et al*, 1993).

An analysis by Deng and colleagues of 1481 EOC patients found that

distant metastases occur most often in the liver, followed by the lymph nodes, the lung, bone, and brain (Deng *et al*, 2018). As distant metastases only occur in roughly one third of cases, it has traditionally been thought that shedding of ovarian tumour cells into the circulation was a rare occurrence. However, recent studies show that haematogenous metastasis can arise as a result of circulating tumor cells (CTCs) (Pradeep *et al*, 2014).

It is theorised that CTCs arise from the site of the primary tumour. When the tumour grows to greater than 2cm, the tumour microenvironment becomes hypoxic. Hypoxia leads to cessation of HIF-1α subunit degradation by the ubiquitin-mediated proteasome, and begins a signaling cascade that facilitates angiogenesis, the hallmark of tumour progression. In this process, the HIF-1 heterodimer is able to form and translocate to the nucleus where it is a transcription factor (TF) for vascular endothelial growth factor (VEGF). Leaky vascular basement membranes create the "perfect storm" for epithelial-to-mesenchymal transition (EMT) and subsequent tumour cell intravasation.

1.7 Circulating Tumour Cells (CTCs)

Circulating Tumour Cells (CTCs) are viable tumour cells that have become loose from a primary tumour, intravasate at the primary tumour site, travel through the blood, and extravasate at a secondary site where, together with platelets, they form metastatic niches and subsequent tumours (Labelle *et al*, 2014) (Fig. 1.9).

CTCs are both rare and heterogeneous, making them difficult to detect, isolate, and culture (Barriere *et al,* 2014). Subpopulations include epithelial,

epithelial-mesenchymal, mesenchymal, and mesenchymal-stem, but it is important to acknowledge that these subtypes exist on a gradient that may change over time rather than as discrete subsets (Barriere *et al,* 2014). The normal epithelial-mesenchymal transition (EMT) observed during embryogenesis is very different from pathological EMT in that partial EMT is often sufficient to establish an invasive phenotype. Identification of CTCs has also brought to light a subset of self-renewing multipotent cancer cells known as circulating cancer stem cells, or CSCs (Barriere *et al,* 2014).

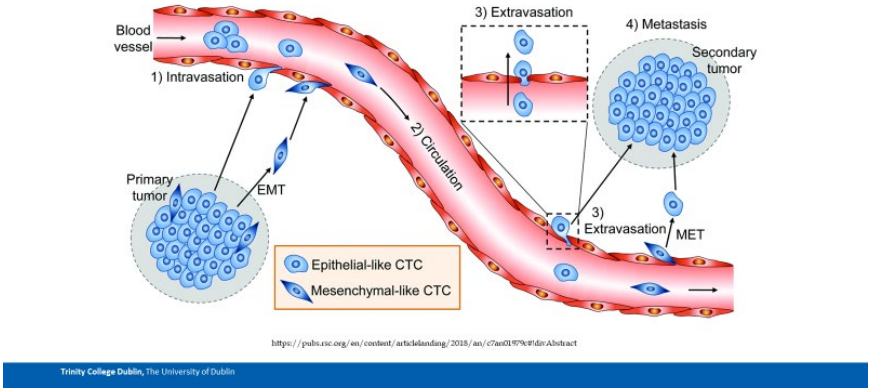

Fig. 1.9 EMT and intravasation of exfoliated primary tumour cells, and subsequent extravasation and MET at site of metastasis.

Use of CTCs has been demonstrated as a prognostic marker in breast cancer (Cristofallini *et al*, 2004) as well as other cancer types, including colorectal, gastric, lung, and prostate (Van Berckelaer *et al*, 2016). In EOC, smaller studies have yielded variable results regarding correlations between CTC enumeration, PFS, and OS, however larger studies have reported more encouraging results (Van Berckelaer *et al*, 2016). As there is no one specific marker expressed by all cancer cells, current detection is often achieved via size

and surface marker exclusion. Adding to this difficulty is a background of leukocytes that remains significant even after enrichment (Van Berckelaer *et al*, 2016).

Epithelial cellular adhesion molecule (EpCAM) is a glycoprotein expressed on the surface of cancer cells. This was the starting point for all CTC identification, beginning with the CellSearch system (Veridex, Warren, NJ, USA). Immunomagnetic enrichment by anti-EpCAM antibodies, followed by immunocytochemistry (ICC) or RT-qPCR has been the standard detection method for many years, however, the number of $EpCAM^+$ CTCs can be low in EOC. This may be due to the downregulation of EpCAM during EMT.

Cytokeratins (Cks) are often used in conjunction with EpCAM. These cancer cell-surface markers are lost just prior to intravasation, but can be used to enumerate CTCs with an epithelial phenotype, and residual expression may also help "track" cells. (Barriere *et al,* 2014). E-cadherin is another epithelial marker used in CTC identification, as its expression is decreased when cells adopt a mesenchymal state (Barriere *et al*, 2014).

Cells that have become mesenchymal can be identified with N-cadherin, which is increased when E-cadherin is decreased. Vimentin is also frequently used as an indicator of EMT, as well as Twist1, which has been used to identify CTCs in breast cancer together with Akt and Pi3K. Zeb1 can also be used, and was noted to be useful in identifying a hybrid epithelial-mesenchymal phenotype when coupled with miR-200 and pitted against miR-34/SNAIL in a "decision-making" assay (Barriere *et al*, 2014). It should be noted that purely

mesenchymal cells are rare, and that these markers serve to demonstrate EMT as an ongoing process rather than as an end result (Barriere *et al*, 2014).

Exclusion and enrichment methods for enhanced detection of CTCs are constantly evolving, with research into markers such as zonula occludens (ZO), epithelial splicing regulator 1 (ESPR1), alternative splicing proteins such as catenins, aldehyde dehydrogenase-1 (ALDH1), CD44, and stemness markers (Barriere *et al*, 2014). A study by Swisher and colleagues found CTC-specific p53 sequences in the peripheral blood of ovarian cancer patients (Swisher *et al*, 2005), and another study using negative selection by $CD45^{+}$ exclusion followed by fluorescence in situ hybridization (FISH) with a probe for chromosome 8 centromere (CEP8) showed a 76.2% sensitivity rate for detecting CTCs in patients with epithelial ovarian carcinoma (Van Berckelaer *et al*, 2016). Current research is also investigating single-cell RT-qPCR as well as single-cell RNA-Seq (Barriere *et al*, 2014).

CTC status has been shown to be positively associated with advanced tumor stage. It positively correlates with CA-125 levels, post-surgical residual cancer, and shorter survival rates (Van Berckelaer *et al*, 2016). CTCs are currently being investigated as a tool in ovarian cancer screening with the goal of producing a diagnostic "liquid biopsy." CTCs hold the key to tumour genomes and proteomes, and have the potential to guide earlier detection, prognosis, and treatments for ovarian cancer (Van Berckelaer *et al*, 2016).

1.8 Platelet-cancer Cell Interactions

The relationship between platelets and cancer cells is integral to

haematogenous metastasis in many cancer types, including EOC. High platelet count and thrombocytosis are frequently associated with advanced disease (Stone *et al*, 2012; Qi *et al*, 2015), whereas platelet deficiency is associated with lower risk of metastasis via an increase in the ability of NK cells to lyse CTCs (Lou *et al*, 2015).

Previous work in our laboratory and work by others has focused on interrogating the relationship between platelets and cancer cells (Egan *et al*, 2011; Lou *et al*, 2015). It was found that platelet adhesion occurs across multiple types of cancer (Fig.1.10), that platelets induce a mesenchymal phenotype in epithelial cancer cells, and that platelet adhesion and aggregation increases invasion, a pro-survival phenotype, and therefore the metastatic potential of ovarian cancer cells (Cooke *et al,* 2013; Egan *et al*, 2011).

Labelle and her colleagues demonstrated in a murine model that direct platelet-cancer cell interactions induce epithelial-mesenchymal transition (EMT) in cancer cells and promote metastasis (Labelle *et al,* 2011). In their work, it was shown that CTCs are "cloaked" by platelets, thereby triggering a mesenchymal phenotype which facilitates intravasation. Additionally, this "cloaking" physically protects CTCs from shear stress in the circulation (Egan *et al*, 2014), and also provides a means of immune evasion in which the platelets confer a self-protein MHC-I "decoy" that enables CTCs to evade detection by natural killer (NK) cells (Placke *et al*, 2012; Cluxton *et al*, 2019). Taken together, these point to the importance of platelets to CTC survival and to haematogenous cancer metastasis.

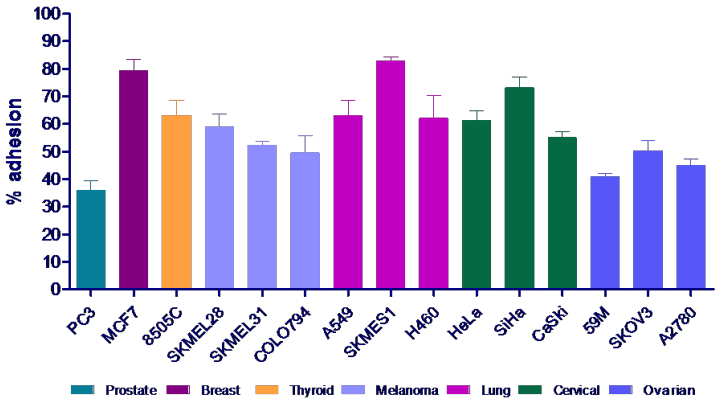

Fig. 1.10 Flow cytometry for detection of the platelet marker CD42b antigen indicates efficient platelet cloaking of tumour cell populations (Cluxton *et al*, 2019).

Independently, our group identified five genes as key drivers of platelet-CTC interactions (Spillane *et al*, submitted for publication). Of these five genes, PAI-1 was consistently altered in 90% of the cell lines investigated, which spanned 7 cancer types and 15 lines (Fig. 1.11).

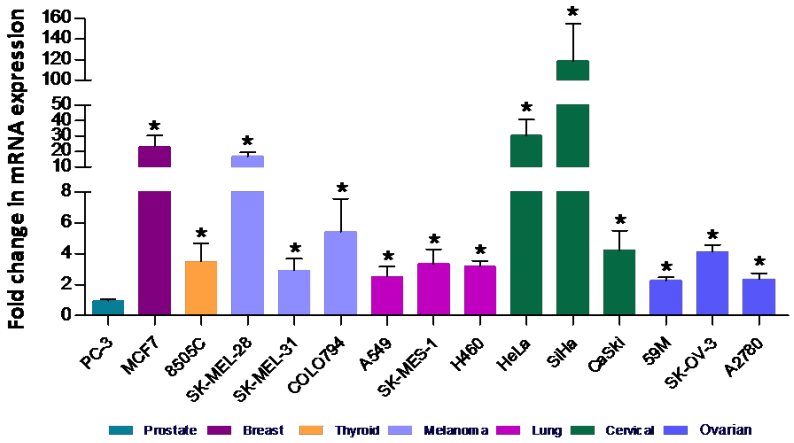

Fig.1.11 Expression-fold changes in PAI-1 mRNA across multiple cancer cell line types (Spillane *et al*, submitted for publication).

PAI-1 is an important molecule in cancer because it is directly involved in the ECM maintenance and remodelling that are part of tumourigenesis and maintenance of the tumour microenvironment (Kwaan *et al*, 2019). It is a ubiquitous endothelial element, and thanks to Armand Trousseau, we know that cancer patients are at an increased risk of developing blood clots, deep-

vein thrombosis (DVT), and thromboembolism (Kwaan *et al*, 2019). PAI-1 plays a large role in coagulation (Kwaan *et al,* 2019), and it is consistently altered across many types of cancer (Spillane *et al,* submitted for publication). Therefore, it is crucial to investigate this molecule and to evaluate its potential as a diagnostic marker, a therapeutic target, or both.

1.9 The Coagulation Pathways, Fibrinolysis, and PAI-1

The coagulation pathway works via a series of physical and chemical signals, which recruit coagulation factors to the site of an injury or wound to restore haemostasis. However, in instances of cancer, this can lead to dangerous clotting. Cancer has been referred to as "a wound that doesn't heal" (Dvorak, Harold F., 1986) due to many of the pathways involved in wound healing also being activated and/or repressed by the presence of a tumour. Fibrinolysis both affects and is affected by the tumour microenvironment, involving many factors including plasminogen, plasmin, uPA, tPA, uPAR, and PAI-1 (Kwaan *et al*, 2019).

1.9.1 The Coagulation Pathways

The Intrinsic or Long Pathway, and the Extrinsic or Short Pathway, both lead to the formation of a fibrin clot at the site of injury or tissue damage (Fig. 1.12). The Intrinsic Pathway is triggered by tissue injury, initiating Factor XII. The enzymatic form of Factor XII, Factor XIIa then converts Factor XI to Factor XIa, which in turn converts Factor IX to Factor IXa. Factor IXa then goes on to catalyse Factor X to Factor Xa. It is from this point that the Intrinsic and Extrinsic Pathways converge, and this is called the Common Pathway

(Chaudhry *et al*, 2020).

The Extrinsic Pathway arrives at the Common Pathway via a much shorter route involving the release of tissue factor (Factor III) from endothelial cells which along with an influx of calcium ions (Ca^{2+}) converts Factor VII to Factor VIIa. This, in turn, catalyses Factor X to Factor Xa (Chaudhry *et al*, 2020).

Regardless of the pathway taken to arrive at the Common Pathway, activated Factor Xa now acts as a catalyst for Factor V to cleave prothrombin (Factor II) into thrombin (Factor IIa). The thrombin then goes on to convert fibrinogen to fibrin. Fibrin combines with Factor VIII, carried by von Willbrand Factor (VWF), to form a fibrin mesh, and this mesh combines with platelets and VFW to form a plug (Chaudhry *et al*, 2020).

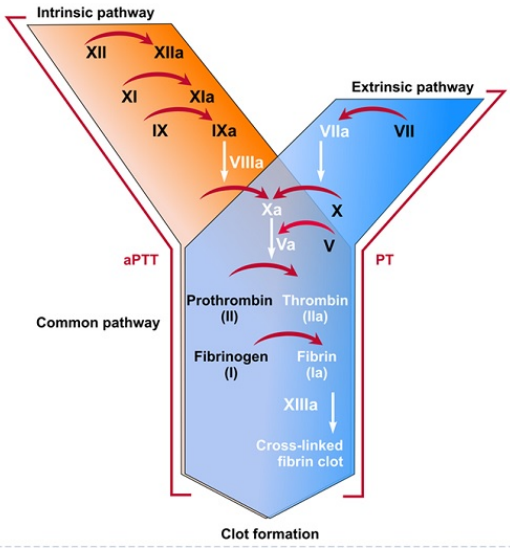

Fig 1.12 The intrinsic and extrinsic coagulation pathways. (retrieved from https://diapharma.com/coagulation/)

Thrombin goes on to act as part of the Intrinsic Pathway by activating other factors and cofactors necessary for haemostasis, but more importantly it acts as a negative feedback control to prevent over-coagulation by stimulating

the production of antithrombin (AT). Another way thrombin acts as a negative feedback control in the coagulation cascade is by activating plasminogen, the zymogen of plasmin (Chaudhry *et al*, 2020).

1.9.2 Fibrinolysis: Plasminogen and Plasmin Activation

Plasmin is integral to the breakdown of fibrin clots (fibrinolysis), and is involved in ovulation, embryonic development, tissue and extracellular matrix (ECM) remodelling, inflammation, and tumour invasion. Its zymogen, plasminogen, is encoded on the long arm of chromosome 6 in humans (Fig. 1.13), and is synthesised in the liver.

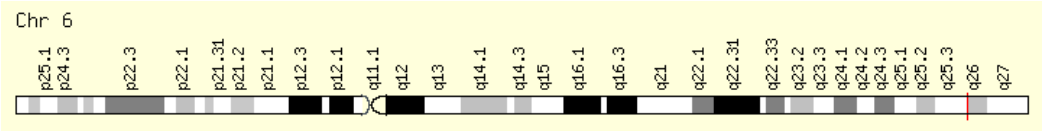

Fig 1.13 The red line marks the location of the plasminogen gene on human chromosome 6 (retrieved from https://www.genecards.org/cgi-bin/carddisp.pl?gene=PLG)

Plasminogen contains 7 domains, including 5 Kringle domains (KR1-5), a pan-Apple (PAp) domain located at the N-terminus, and a serine protease (SP) domain. It maintains an activation-resistant conformation in the circulation by virtue of interactions among Lys-50, Arg-68, and Arg-70 in the PAp domain, lysine-binding sites in the KR4 and KR5 domains, and serum chloride ions. Upon binding to clots, the activation site becomes open, and is able to be cleaved by tPA into the plasmin that will ultimately help degrade fibrin clots (Law *et al*, 2012).

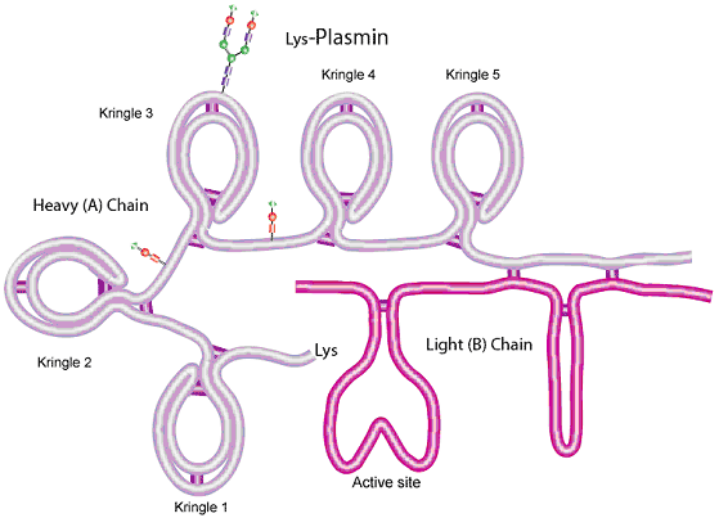

Fig. 1.14 Activated Plasmin molecule demonstrating 5 Kringle domains on the heavy chain, and the active site on the light chain.. (https://www.sigmaaldrich.com/life-science/metabolomics/enzyme-explorer/analytical-enzymes/plasmin.html)

Cleavage occurs between Arg561 and Val562, whereupon the amino terminus becomes the α heavy chain that houses the Kringle domains, and the carboxy terminus forms the ß light chain where the active site is located. The chains are joined by two disulphide bridges (Figs. 1.14,1.15) (retrieved from: https://www.sigmaaldrich.com/life-science/metabolomics/enzyme-explorer/analytical-enzymes/plasmin.html on 19 May, 2020).

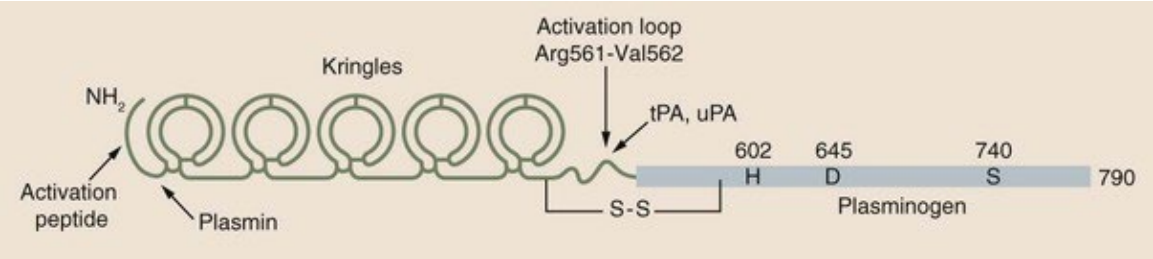

Fig. 1.15 Plasminogen cleavage site (Adapted from Dobrovolsky AB, Titaeva EV. The fibrinolysis system: regulation of activity and physiologic functions of its main components. Biochemistry [Mosc] 2002;67:99–108 and Castellino FJ, Ploplis VA. Structure and function of the plasminogen/plasmin system. Thromb Haemost 2005;93:647–54.)

Plasmin can be activated from plasminogen by tissue-type plasminogen

activator (tPA), which is a serine protease found on endothelial cells, in which case fibrin is the cofactor, or by urokinase plasminogen activator (uPA), which is a serine protease originally isolated from urine and found in the blood and ECM of humans and other animals, in which case uPAR is the cofactor. Once activated, plasmin participates in thrombolysis, fibrinolysis, and ECM breakdown and remodelling (Tang and Han, 2013).

1.9.3 PAI-1

Fibrinolysis is desirable in some cases, such as clot degradation, ovulation, or implantation of an embryo into the uterine lining, however, it is not desirable in all cases, and the body has mechanisms to prohibit these actions. In the case of plasminogen activation, these antifibrinolytic mechanisms are collectively known as serine protease inhibitors, or SERPINs. They are also known as plasminogen activator inhibitors, of which there are 3 types. The focus here will be on Plasminogen Activator Inhibitor Type 1 (PAI-1), also called SERPIN E1, whose importance is demonstrated in instances of heterozygous and homozygous PAI-1 deficiency where the absence of adequate PAI-1 has a clear effect similar to haemophilia (delayed bleeding after trauma, menorrhagia, and epistaxis), but without the spontaneous bleeding events normally associated with other coagulation disorders (Mehta *et al*, 2008).

PAI-1 is a single-chain glycoprotein with a molecular mass of approximately 45kDa that is located on the long arm of chromosome 7, q 22.1 in humans, SERPIN E1 spans 9 exons, and codes for a protein composed of 402 amino acids (aa) (Fig. 1.16). It is expressed by many different cell types, most

notably endothelial cells and platelets, and exists in 3 conformations: active, latent/inactive, and cleaved/substrate (Fig.1.17). It is the main suppressor of both tPA and uPA, and can be neutralized by thrombin, but only when in its procoagulant form in which it is complexed with vitronectin in the ECM (Erlich *et al*, 1991).

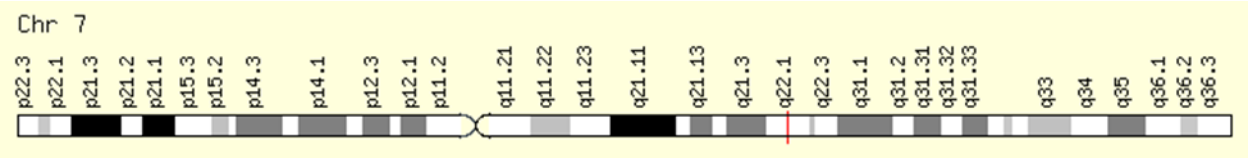

Fig. 1.16 The location of human SERPIN E1 on chromosome 7,q22.1 (http://www.genecards.or/cgi-bin/card.disp.pl? gene=SERPINE1)

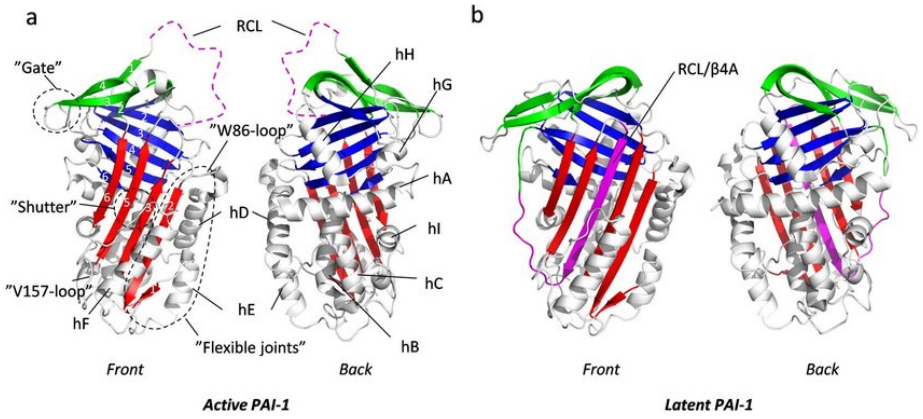

Fig. 1.17 Active and Latent PAI-1 conformations. (Petersen, Michael, Jeppe B. Madsen, Thomas J D Jørgensen, Morten B. Trelle "Conformational preludes to the latency transition in PAI-1 as determined by atomistic computer simulations and hydrogen/deuterium-exchange mass spectrometry. " Scientific Reports. December 2017.)

In its active conformation, PAI-1 like all SERPINs contains 3 β-pleated sheets, and 8 or 9 α-helices. It is a complex molecule with three well-characterized protein-binding domains (Fig. 1.17): one in the reactive center loop (RCL) where it binds to plasminogen activator (PA), one in the flexible joint region that binds to vitronectin, and one within helix D and helix F that binds to low-density lipoprotein receptor-related protein (LRP1) (DeClerck *et al*,

1992; V. Placencio and Y. DeClerck, 2015). When the reactive center loop (RCL) is exposed and cleaved, the associated protease – in this case, tPA or uPA – becomes covalently attached to the N-terminus of PAI-1. This causes a large portion of the protease molecule to be translocated to the SERPIN, whereby the part of the RCL that is attached to the protease is inserted into β-pleated sheet A of PAI-1. Thus, the plasminogen activator is trapped in the PAI-1 molecule (Petersen *et al*, 2017).

In the latent form of PAI-1, a similar action occurs with RCL insertion into β-pleated sheet A, but without the involvement of the protease (Fig. 1.17). This can be reactivated when denatured by certain proteins (Placencio *et al*, 2015). The substrate form was discovered by DeClerck and his colleagues (DeClerck *et al*, 1992), and is cleaved at the P_1-P_1' bond (Arg^{346}-Met^{347}).

PAI-1 is upregulated in conjunction with cellular plasticity in adults, most often during wound-healing (Wilkins-Port *et al*, 2010). It is an important molecule in terms of cellular migration, and in concert with LPR1, vitronectin, and the uPA/uPAR complex, assists in the modulation of the many requisite detachments and subsequent reattachments (Czekay *et al*, 2011) involved in this process. PAI-1 regulates cell adhesion by binding to the somatomedin (SMB) domain of vitronectin (Deng *et al*, 2001), and also by inhibiting binding mediated by uPAR (Fig. 1.19).

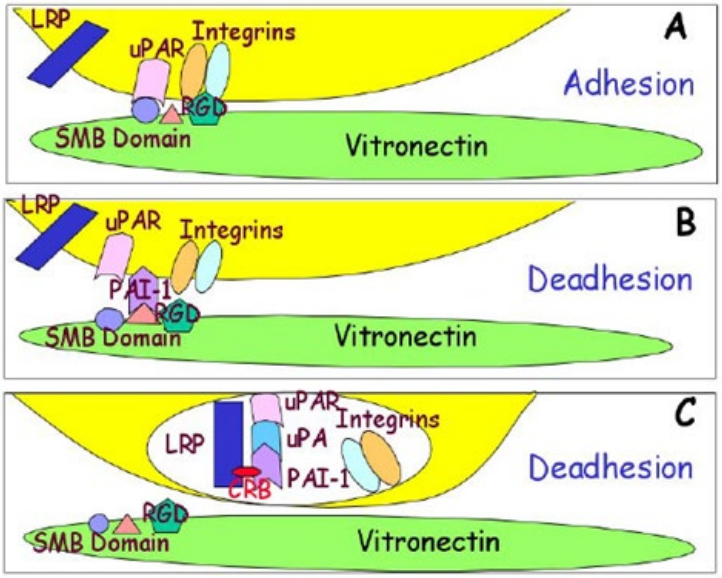

Fig. 1.18 PAI-1 binding to the uPA/uPAR complex and the SMB domain of vitronectin during cell adhesion, and the release during deadhesion (Lee *et al*, 2005).

1.10 PAI-1 in the Platelet

Platelets contain high levels of PAI-1, but due to a half-life of roughly one hour, only 5-10% of this is in active conformation, the majority being the inactive, or latent, form (Brogren *et al*, 2004). Conversely, other studies have reported high levels of active platelet PAI-1, and this led to the discovery of a calcium-dependent stabilization mechanism within the α-granules of the platelet (Lang *et al*, 1995). Platelets contain large amounts of transcriptionally active PAI-1 mRNA (as well as that of other genes), imparted to them by their megakaryocyte precursors, and thus undergo continuous *de novo* synthesis of active PAI-1 (Brogren *et al*, 2004). PAI-1 is released from platelet α-granules upon activation.

1.10.1 Platelet Genesis, Structure, and Activation

Platelets are anucleate cells formed by often multinucleate megakaryocyte precursors in the bone marrow (Fig. 1.20). They enter the

bloodstream through a "budding off" process, and one megakaryocyte can produce up to 3000 platelets. Despite a distinct lack of nuclei, platelets are metabolically active, and contain mitochondria, endoplasmic reticulum, and Golgi Apparatus (Yun *et al*, 2016). Importantly, during the budding process, the megakaryocyte imparts mRNA transcripts that the platelets can translate as they also contain ribosomes. Platelets are biconvex, discoid, and are roughly 20% the size of erythrocytes. Despite their importance, they make up only a tiny percent of the total blood volume.

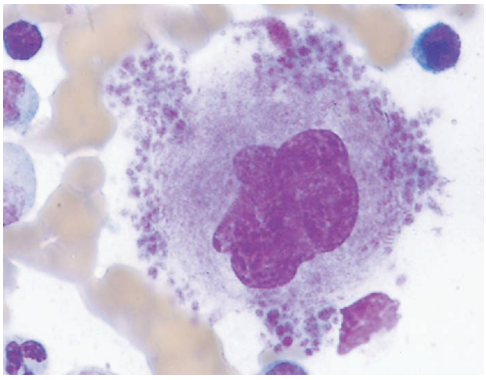

Fig. 1.19 A megakaryocyte producing platelets (retrieved from https://medical-dictionary.thefreedictionary.com/_/viewer.aspx?path=davisTab&name=m080p0.jpg&url=https%3A%2F%2Fmedical-dictionary.thefreedictionary.com%2Fmegakaryocyte)

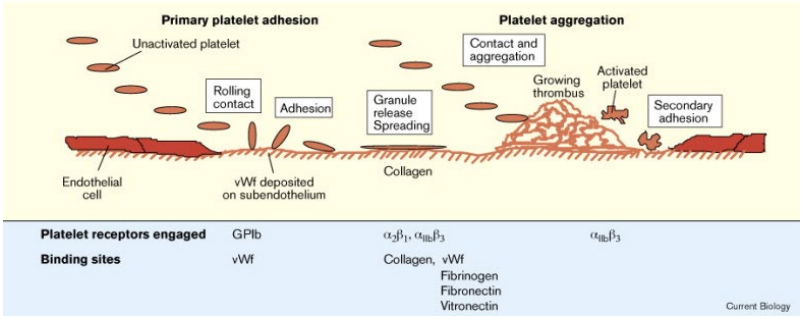

Fig. 1.20 Platelet activation and haemostatic plug formation (retrieved from https://www.sciencedirect.com/science/article/pii/S0960982299800633

Platelets aggregate at sites of vascular injury, and during coagulation become activated through pathways that include von Willebrand Factor (vWF) and membrane glycoproteins GP Ib-IX-V,GPIa/IIa, and GP VI (Fig. 1.21). Upon activation, platelets degranulate and release their contents, including ADP from dense granules, which binds G-coupled protein receptors $P2Y_1$ and $P2Y_{12}$. This in turn increases and sustains platelet activation (Yun *et al*, 2016).

1.11 PAI-1 and Cancer

Overexpression of PAI-1 in both tumour cells and the tumour stroma has been implicated in many cancers, including breast, bladder, colon, cervix, kidney, prostate, skin, and ovary (McMahon *et al*, 2001; Pappot *et al*, 1995). Vast clinical data support the hypothesis that stromal PAI-1 is essential to protecting tumours from uPA-mediated degradation (Pappot *et al*, 1995). It has been observed that while PAI-1 is produced by stromal cells in some cancers, such as adenocarcinomas of the colon and breast, and in glioblastomas, PAI-1 is produced only by the cancer cells and not by stromal cells in other cancers, such as skin squamous cell carcinomas (Pappot *et al*, 1995). Elevated plasma PAI-1 levels have been noted in patients with cancers of the pancreas, ovary, and urinary tract (Pappot *et al*, 1995).

PAI-1 can be produced by many cell types, including EC, fibroblasts, adipocytes, smooth muscle cells, and macrophages when stimulated by factors such as TGF-β, IL-6, and TNF-α (Placencio and DeClerck, 2015), and it is an integral part of angiogenesis in tumour progression (Isogai *et al*, 2001). The question that remains unanswered is the source of plasma PAI-1. It is

understandable that PAI-1 levels in plasma would be elevated due to acute injury or after a surgical procedure, but in cancer patients who have experienced neither, the source of their elevated plasma PAI-1 remains unclear. High levels of both PAI-1 and uPA are associated with poor prognosis in many cancers. However, high PAI-1 has been shown to prevent angiogenesis and tumourigenesis *in vitro*, while low PAI-1 has demonstrated opposite effects. Strangely, in PAI-1-deficient hosts, a distinct lack of angiogenesis and tumour progression has been noted.

1.11.1 tPA

tPA is expressed by endothelial cells, binds to fibrin, converts plasminogen to plasmin, and activates fibrinolysis. It is a crucial component of the circulatory system, serving to break up blood clots. Elevated PAI-1 in the circulation may lead to the formation of blood clots, putting cancer patients at an increased risk of both thrombotic events as well as intravasation of tumour cells. It is noteworthy that all active PAI-1 in the circulation is complexed to vitronectin, which stabilizes it and doubles its half-life. This complex also serves to neutralize thrombin (Stefansson *et al,* 1996), which then can no longer act as a negative feedback mechanism in coagulation, and can also no longer activate plasminogen, and this may further lead to thrombotic events.

1.11.2 Adhesion, Migration, and Invasion: The uPA/uPAR Complex

uPA, expressed by migrating cells, has a low affinity for fibrin, and instead binds its receptor uPAR to activate plasmin. Plasmin is then able to degrade glycoproteins and proteoglycans in the ECM, and promote cell

migration and invasion (Fig. 1.21A). Conversely, PAI-1 – which inhibits plasmin activation –contributes to cell adhesion (Fig. 1.21B).

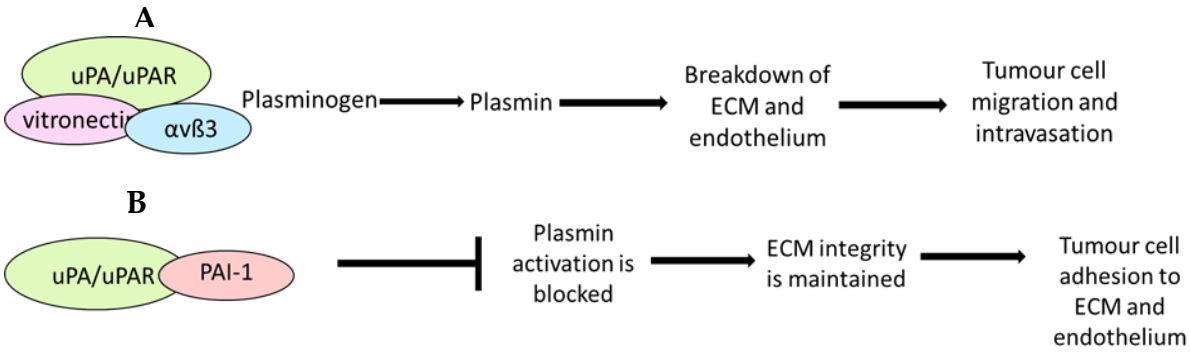

Fig. 1.21 A. Plasmin is activated by uPA/uPAR, **B.** Plasmin activation is blocked by PAI-1.

PAI-1 function is mediated by molecules such as heparin, vitronectin, fibronectin, collagen, integrins, and low-density lipoprotein receptor (LRP1). PAI-1 binds vitronectin, and inhibits ECM degradation while simultaneously inhibiting cellular migration and invasion. uPA is an anti-adhesion molecule, and similarly stimulates cell migration by catalyzing the cleavage of plasminogen to plasmin, which contributes to ECM degradation and the release of cells from their substratum (Lee *et al*, 2005). As PAI-1 inhibits uPA, it should follow that PAI-1 would inhibit cell migration in the same way that it promotes adhesion. However, it has been shown to have both anti- and pro-migratory capabilities that are dependent on both its location and concentration in the cell (Lee *et al*, 2005). When PAI-1 is bound by uPA/uPAR, it loses affinity for vitronectin, but its affinity for LRP increases, and this translocates the PAI-1/uPA/uPAR complex into endosomes which target PAI-1/uPA for degradation, and release uPAR and integrins back to a different area on the cell surface than which they began. In this way, a "leading edge" and a "trailing

edge" mechanism of chemical motion is created.

1.11.2 Tumour Growth and Regulation by p53

PAI-1's contribution to tumour growth is controversial, with contradicting studies showing both inhibitory effects and proliferative effects (Kubala and DeClerck, 2019). It has been demonstrated that PAI-1 modulates cancer cell growth through the inhibition of fibrinolysis. This directly promotes tumour cell adherence to the ECM, and also to the endothelium which contributes to intravasation, angiogenesis, and haematogenous metastasis (Kwaan and Lindholm, 2019).

p53 is required for the normal regulation of cell growth, and is mutated in most tumours. Functional p53 genes that are introduced into tumour cells have been shown to induce cell cycle arrest at G_1/S. As migration and invasion of tumour cells are dependent upon proteolytic degradation of the ECM, it was suspected that p53 could be involved in the regulation of this process. Christina Kunz and her team found that wt p53 inhibited the promoter and enhancer activity of uPA and tPA, and increased PAI-1 expression in several cancer cell lines, while p53 mutants inhibited PAI-1 promoter activity (Kunz *et al*, 1995). Shetty and colleagues demonstrated that transfection of p53 $^{-/-}$ H1299 human lung carcinoma cells with functional p53 increased the expression of PAI-1, and that p53 specifically binds to the 3' UTR of PAI-1 mRNA (Shetty *et al,* 2008).

Work by our group has identified PAI-1 as one of the top 5 genes that are differentially expressed when cancer cells are coincubated with platelets *in vitro*. Taken together with PAI-1's roles in cell adhesion, migration, ECM

degradation, and anti-apoptotic effects, this demonstrates both the significance and eminence of this protein in the cancer sphere.

1.12 PAI-1 and Epithelial Ovarian Cancer

In epithelial ovarian cancer, high levels of PAI-1 in tumour tissue extracts, serum, and plasma have been associated with poor survival rates (Aune *et al*, 2012; Chambers *et al*, 1998; Ho *et al*, 1999; Kuhn *et al*, 1999). PAI-1 has also been implicated in the peritoneal dissemination of metastatic ovarian cancer cells (Peng et al, 2019), and elevated plasma levels have been significantly associated with the presence of malignancy and late-stage disease (Ho *et al*, 1999).

1.12.1 Establishment and Metastasis

PAI-1's role in metastasis is well-documented, but it's contribution to tumourigenesis in ovarian cancer remains unclear. (Schmalfeldt *et al*, 1995). Astedt and Holmberg first defined proteolytic contribution to ovarian cancer metastasis in 1976 when they discovered elevated uPA in ovarian cancer tissue. Elevated PAI-1 levels were noted soon thereafter in both ovarian tissue and ascites (Scmalfeldt *et al*, 1995).

PAI-1 is suspected to contribute to establishment of metastatic OC in the peritoneum. Human peritoneal mesothelial cells (HPMCs) usually present a barrier to cancer cells, however hepatocyte growth factor (HGF) secreted by OC cells induce mesothelial mesenchymal transition (MMT) in HPMCs, making them susceptible to transformation into cancer-associated mesothelial cells or CAMs that secrete oncogenic factors (Peng *et al*, 2019). Peng and colleagues

demonstrated that PAI-1 secreted by metastatic OC cells instigates MMT and creates a positive feedback loop which increases dissemination of OC cells into the peritoneal mesothelium. PAI-1 was shown to upregulate the pro-metastatic chemokines IL-8 and CXCL5 via the NFκB pathway in cell lines, as well as *ex vivo* and *in vivo* (Peng *et al*, 2019).

A study by Schmalfeldt and colleagues examined PAI-1 in primary tumours, retroperitoneal lymph nodes, and the omenta of 39 patients with FIGO IIIc and IV stage OC. 7 patients with stage I early carcinoma were included for comparison. It was concluded that there was a statistically significant difference between PAI-1 in the primary tumour and that in the omentum, but not in lymph nodes versus the primary tumours (Schmalfeldt *et al*, 1995). A similar study by Dorn and colleagues yielded similar results, with an 86% increase in PAI-1 in the omenta as compared to primary tumours. This was statistically significant, but was not found to be a significant factor in PFS (Dorn *et al*, 2011).

1.12.2 PAI-1 as a Prognostic Indicator and Potential Treatment Target

Elevated PAI-1 levels in both tumour tissue and plasma have been associated with higher disease stage and poor prognosis. However, its clinical use for decision-making in treatment has yet to be elucidated as data are still both controversial and limited. Studies by Nakatsuka, Kuhn, Ho, Aune, Chambers and others all conclude that PAI-1 has power as a prognostic indicator for PFS and OS in patients with stages II-IV disease. Additionally, Nakatsuka found that use of the anti-PAI-1 inhibitor IMD-4482 successfully

blocked PAI-1 function in OC cell lines. Dose-dependent inhibition of cell adhesion to vitronectin in the PAI-1-positive cell lines SK-OV-3ipl - a highly-invasive cell line isolated from the ascites nu/nu mice that had been injected intraperitoneally with SK-OV-3 cells (Bourguignon *et al*, 1997) - and HEYA8 was noted, as well as inhibition of invasion. Inhibition of these things in PAI-1-negative cell line OVCAR3 was not observed, and when OVCAR3 cells were transfected with a SERPIN E1-inducing plasmid, inhibition of PAI-1 by IMD-4482 was observed (Nakatsuka *et al*, 2017).

Treatment of SK-OV-3ipl cells with IMD-4482 disrupted the association between PAI-1/uPAR and integrin αvß3, an integrin necessary in angiogenesis. IMD-4482 inhibited the dissemination of ovarian cancer cells in the peritoneum of a xenograft model. IMD-4882 was also observed to suppress proliferation via downregulation of CDK2 and Cyclin D3, and upregulation of p27kip1, and induce apoptosis, suggesting that PAI-1 serves as a mitogen in ovarian tumour cells (Nakatsuka *et al*, 2017). Other PAI-1 inhibitors such as TM5275 and TM5441 have been tested and shown to have anti-tumour and anti-angiogenic efficacy in colorectal and breast cancers (Placencio *et al*, 2015), and TM5275 has demonstrated anti-proliferative and pro-apoptotic effects in ovarian cancer cells (Mashiko *et al*, 2015).

Given the findings of research into PAI-1 in OC, it is clear that PAI-1 has potential as a prognostic indicator. Small-molecule inhibitors of PAI-1 have also shown promise, and have the potential to positively and significantly impact treatment, PFS, and OS for women with EOC.

1.13 Hypothesis

Platelet-cancer cell interactions aid survival of CTCs in the blood, and PAI-1 is a key driver of the metastatic process in EOC with potential as an independent prognostic indicator.

1.14 Specific Aims

1. To investigate platelet-cancer cell interactions in the context of PAI-1, and their contribution to an invasive and pro-metastatic phenotype in EOC.

2. To analyse differential gene expression using RNA sequencing of ovarian cancer cells where PAI-1 has been transiently silenced, and of ovarian cancer cells that have been treated with platelets. It is our hope that this will help to clarify the position of PAI-1 in the metastatic cascade.

3. To assess the potential use of PAI-1 as an independent prognostic factor in the clinical setting via a study of plasma PAI-1 levels and platelet counts in 5 HGSOC patient cohorts.

CHAPTER 2

MATERIALS AND METHODS

This chapter outlines the general materials and methods used in this thesis. More specific details regarding patient cohorts are outlined in Chapter 5.

2.1 SK-OV-3 Cell Culture

SK-OV-3 cells, adherent metastatic ovarian cells originally obtained from ATCC (American Type Culture Collection, Manassas, Virginia USA), were grown in McCoy's 5A medium (Sigma, USA) supplemented with 10%fetal bovine serum (FBS; Sigma, USA), 2 mM L-glutamine (Gibco, USA), and 100U penicillin + 0.1 mg streptomycin/mL (Sigma, USA). To establish cultures, cells were thawed at RT in a sterile laminar flow hood by adding 1 mL supplemented medium dropwise into the cryovial. The cells were then added to 10 mL medium in a 15 mL conical tube, and centrifuged for 10 min at 1000 rpm for the purpose of removing the dimethyl sulfoxide (DMSO; Sigma, USA) that is present in the freezing medium. The supernatant was decanted, cells were resuspended in supplemented medium, and added directly to pre-warmed medium in a vented T-25 culture flask (Sarstedt, Germany). A vented flask was employed as this cell line requires 5% CO_2. The flask was incubated at 37°C, 5% CO_2, and 87% humidity.

Cells were monitored for growth, and passaged as necessary by aspirating the medium, washing the monolayer with DPBS (Sigma, USA), and adding 4 mL trypsin-EDTA (Sigma, USA). Trypsinised cells were recovered in supplemented medium and either transferred to a new, larger T-75 flask with fresh medium, or frozen to replace stock.

Freezing of cells was accomplished by first counting. Cell counting was

performed using Trypan blue dye to dilute a sample of cells 2:1. 20 µl of this dilution were added to each side of a haemocytometer, which has a fill capacity of 10^{-4} mL (Fig. 2.1). Cells were counted in each of the outer four quadrants on both sides and then averaged, multiplied by the dilution factor of 2, and then multiplied by 10^4 to give cells per mL. This was then multiplied by the number of mLs present to give a total number of cells. These were then per ATCC protocol adjusted to a concentration of $5x10^6$ /mL in the complete growth medium described above that had been further supplemented with an additional 10% FBS plus 7% DMSO. Cells were aliquoted into cryovials at 1 mL each containing 5.0 x 10^6 cells/mL, frozen at -80°C overnight, and then transferred to liquid nitrogen storage the next day.

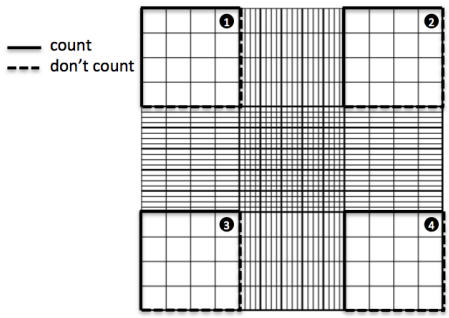

Fig 2.1 Example of an etched haemocytometer grid. Cells are counted in the four labeled quadrants, not counting cells that may fall on the dashed lines.

2.2 Platelet Isolation from Whole Blood

6mL of ACD (Appendix B) were placed in a 60 mL syringe, and a 19-gauge butterfly needle (Becton-Dickinson Vacutainer, USA) was used to draw 34 mL blood from an appropriately consented donor. The syringe was then inverted gently a few times to mix, and was placed on a rocker at 30 rpm for 15 min to avoid coagulation. The blood was divided into 8 x 5 mL aliquots in 15

mL Falcon tubes by rolling the blood slowly down the inside of each tube at approximately 45°. The tubes were centrifuged at 170 x g for 10 min at RT. The "up" brake was set at 2 and the "down" brake was set at 0 to prevent platelet activation. The upper layer of platelet-rich plasma (PRP) was carefully pipetted off and collected in a single 50 mL Falcon tube. The PRP was then acidified to an approximate pH of 6.5 by adding 10% ACD v/v and gently stirring with the pipet tip. Prostaglandin 2 (PGE2; Sigma, stock 5 mg/mL) was added in the same manner for a final concentration of 1 µM (1:1000). The PRP was centrifuged at 720 x g for 10 min at RT to pellet the platelets. The supernatant was carefully removed using a pipet, and the pellet was resuspended in JNL Buffer (Appendix B) in 1 mL increments, and transferred to a clean 50 mL falcon tube.

20 µL of platelet suspension were added to each of three 180 µL aliquots of JNL buffer, creating a 1:10 dilution, for the purpose of obtaining a count of the platelets using a Sysmex cell counter. These three counts were averaged and used to calculate a 1000:1 platelet: cell ratio for the assays included in this thesis**.** A 1:1000 ratio of 0.18 M $CaCl_2$ solution was added to the platelets just before adding them to the cells to give a final concentration of 0.18 mM.

2.2.1 Platelet Analysis by Flow Cytometry

To ensure that the platelets had not been activated during the isolation process, and to ensure that the end product contained only platelets, platelet activation was ruled out via flow cytometry using the marker CD62P (P-selectin) and were deemed to be platelets by marker CD42b. CD45 was used to

rule out contamination by other cell types. This was achieved by staining 10^6 platelets in 0.5 mL JNL buffer (Appendix B) containing APC Mouse Anti-Human CD42b (BD Pharmingen, Ex-Max 650 nm/Em-Max 660 nm), BB515 Mouse Anti-Human CD62P (BD Horizon, Ex-max 490 nm/Em-max 515 nm), and PE Mouse Anti-Human CD45 (BD Pharmingen, Ex-Max 496 nm/Em-Max 578 nm). Platelets were subsequently analyzed using the BD FACS-Melody flow cytometer. 10,000 events were recorded for each sample, using a 488 nm laser and a 586/42 longpass filter for excitation of the BB515 and PE conjugates, and a 640 nm laser and 660/10 longpass filter for the APC conjugate. Wavelengths are demonstrated in Fig. 2.2. Imaging was performed using FCSalyzer 0.9.18-alpha (open source, SourceForge, San Diego, CA USA).

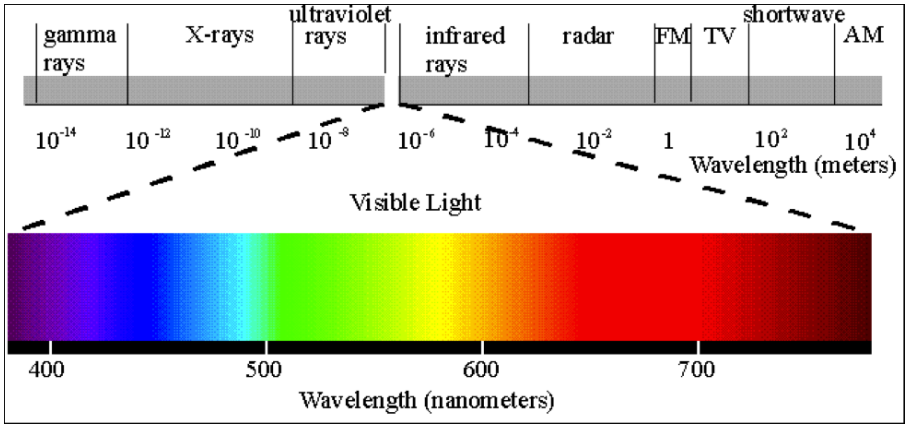

Fig. 2.2 Visible light spectrum. (https://commons.wikimedia.org/wiki/File:EM_spectrum.svg)

2.2.2 Principles of Flow Cytometry

A flow cytometer measures multiple characteristics of cells as they pass through a beam of light in a single-file stream. The sample must be completely fluid, as clumps of cells will clog the flow chamber. The sample is injected into a stream of sheath fluid. The pressures of both the sheath fluid and the sample

work in conjunction, and the sample pressure is always greater than that of the sheath fluid. These can be adjusted in order to control the width of the sample core. The flow of the sheath fluid accelerates the particles in the sample and also keeps them in the center of the sample core through a process called hydrodynamic focusing (BD Biosciences, 2000).

The cells in the sample are treated with specific fluorochromes that will produce specific wavelengths of light as they are excited by a laser. In instances where several fluorochromes are to be used at once, they are chosen if they are able to be excited at a similar wavelength, yet are different enough in their emission fluorescence to be distinguishable from each other. Background fluorescence that occurs naturally in the cells is used to set the parameters of these measurements, and the light emitted by the fluorochromes must be much stronger than this background in order to be picked up and registered by the light detectors. Signal compensation must also be used as the signal emitted from one fluorochrome may overlap the detector range for another. Running a sample stained with one antibody-fluorochrome while observing the output in all channels that will be used enables the operator to tune out any emission spectra overlap (BD Biosciences, 2000).

When the light from the laser hits the cells in the sample, some of this light is diffracted at small angles just off the axis of incidence of the laser, and this light is called forward scatter or FSC (Fig.2.3). FSC signals are collected by a photodiode. Light reflected and refracted is collected at approximately 90° to the laser and is called side scatter or SSC (Fig. 2.3). FSC is proportional to cell

size and surface area, whereas SSC is proportional to granularity and internal complexity of cells. It is the SSC that is subsequently split by the beam splitter(s) and then diverted to photomultiplier tubes (PMT's) (BD Biosciences, 2000).

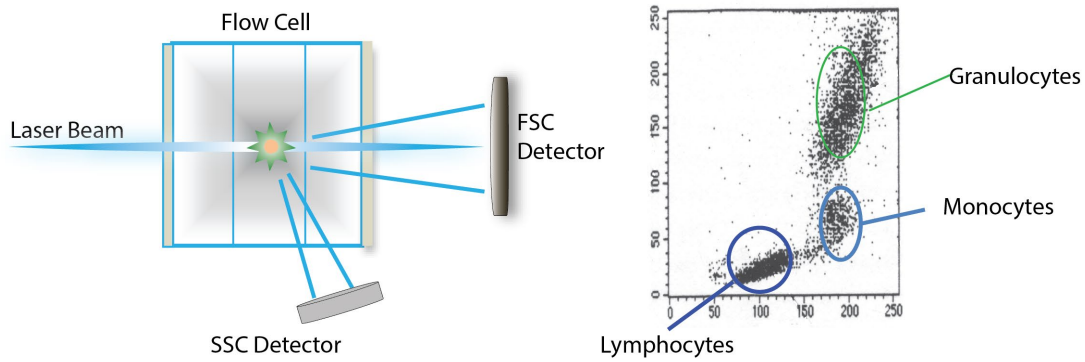

Fig. 2.3 Forward scatter (FSC) and side scatter (SSC) detectors are used to differentiate cell populations in a dot plot image. (https://flowcytometry.utoronto.ca/wp-content/uploads/2015/12/flow_diagram1-01.png

Beam splitters - or dichroic mirrors - and lenses direct different fluorescence wavelengths to appropriate detectors that will measure their respective intensities. Dichroic mirrors (Fig. 2.4) split light beams into two and reflect these beams at angles that are contingent upon their wavelengths: for example, a mirror may reflect a light wavelength of 420 nm at a 45° angle towards a specific light wavelength detector. The specificity of a detector for a specific fluorescence wavelength is created by placing a filter in front of each PMT that will only allow a certain range of wavelengths to pass through it. These are called bandpass filters. For example, the FITC filter is labeled 530/30. This means that it will only allow light at a wavelength of 530 nm ± 15 nm to pass through to the detector.

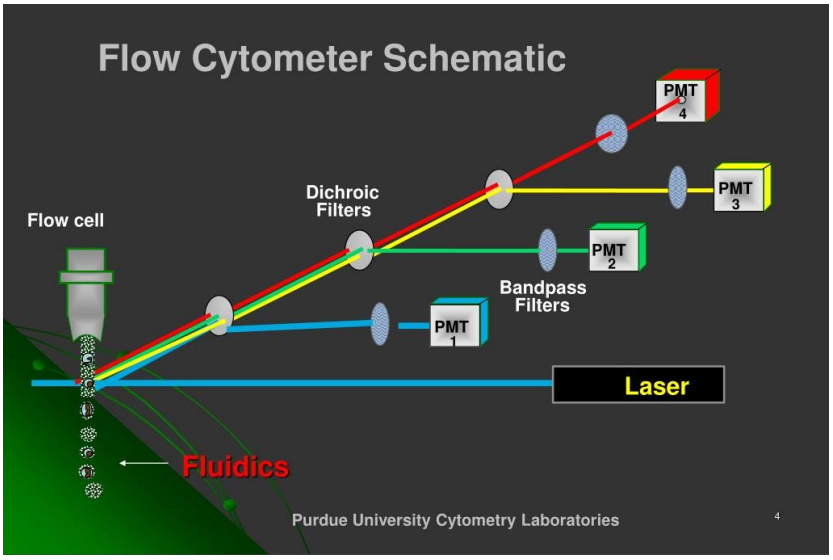

Fig.2.4 Dichroic mirrors reflect specific wavelengths towards their respective bandpass filters. Light signals proceed to photomultipliers and amplifiers where they are converted to digital signals for 2D analysis.

All of the signals generated by the events of the laser striking particles in the sample generate voltage pulses. When photons (light signals) hit the photodiode and PMT's, they are converted into a corresponding number of electrons that generate an electrical current. This travels to an amplifier creating a voltage pulse. The pulse is highest when the particle is in the center of the laser beam, and creates a rise to peak upon approach and a fall to baseline upon departure. The voltage pulse, which is between 0 and 1,000 mV, is assigned a digital value or channel number by an Analogue-to Digital Converter. This allows for our data to be plotted on a graph, such as a 2-D graph or a histogram (BD Biosciences, 2000).

Data analysis is performed by narrowing the search of output data to include only the subset of data you wish to work with in the gating process.

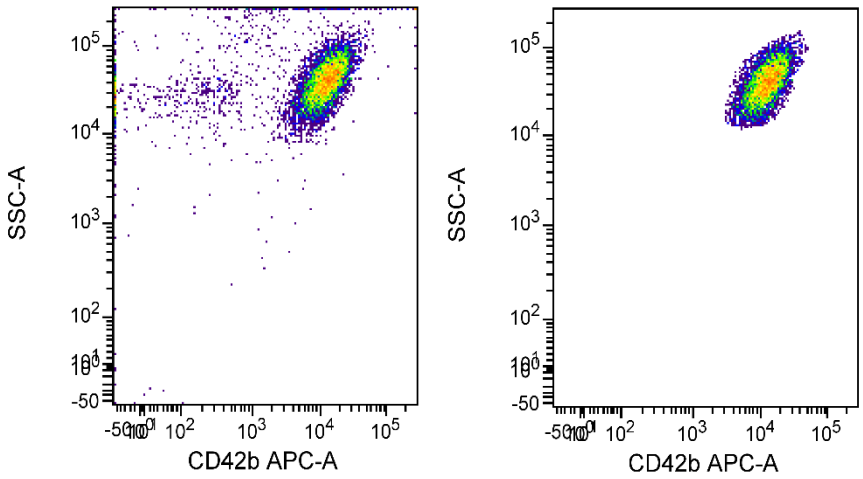

Fig.2.5 Gating strategy used to select platelets from samples.

For work here, a gate was created selecting only platelets, and that gate was then applied to the other fluorophore parameters to demonstrate that only unactivated platelets were present in the sample (Fig. 2.5).

2.3 Knockdown of Plasminogen Activator Inhibitor 1 (PAI-1) by siRNA

PAI-1 (SERine Protease INhibitor E1 or SERPIN E1) was transiently silenced in SK-OV-3 cells using small interfering ribonucleic acid (siRNA) in a forward transfection method. 10^5 cells were seeded in 9 wells of each of two 12-well tissue culture plates (Sarstedt, Germany). Wells were labelled "UNT" for untreated cells, "-CTL" for cells to be treated with an inert siNEG (negative control siRNA), and "siRNA" for cells to be treated with PAI-1 siRNA (Fig. 2.6). One plate was labelled "PLT" as these wells would receive an additional treatment of platelets in a 1000:1 platelet: cell ratio. Once seeded, the plates were incubated overnight at 37°C, 5% CO_2 in a humidified incubator.

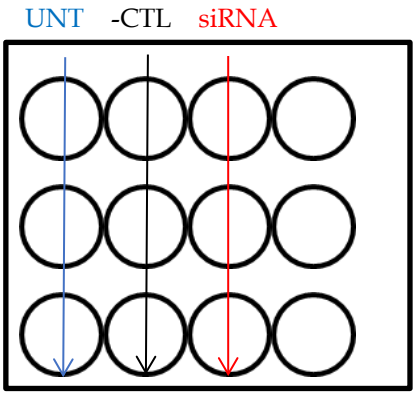

Fig. 2.6 Depiction of plate map for PAI-1 knockdown assay

For the transfection, and in strict accordance with the manufacturer's protocol, 7 µL of 10 mM PAI-1 siRNA (Ambion Silencer Select, Ambion USA) were added to Opti-MEM (Gibco, USA) to a total volume of 650 µL, and 1.75 µL of a 40 mM siNEG (Ambion Silencer Select ss#2, Ambion USA) were added to Opti-MEM to a total volume of 650 µL. Lipofectamine Complex Solution (LCS) was made per manufacturer's instructions by the addition of 39 µL of RNAi-MAX Lipofectamine (Thermo-Fisher USA) to 1261 µL Opti-MEM. 650 µL of LCS were added to the 650 µL of siRNA/Opti-MEM, and 650 µL LCS were added to the 650 µL of siNEG/Opti-MEM. These tubes were allowed to incubate at room temperature for 5 minutes, per the manufacturer's instructions.

Medium was aspirated from all wells of both plates, and the cell monolayers were washed with DPBS. 800 µL of antibiotic-free McCoy's 5A medium containing 10% FBS were added to all wells. UNT wells received 200 µL of Opti-MEM, -CTL wells received 200 µL of LCS/siNEG/Opti-MEM, and siRNA wells received 200 µL LCS/PAI-1 siRNA/Opti-MEM. Final concentrations of siNEG and siRNA (PAI-1) were 10 nM/well. Both plates

were returned to the incubator for 24 h, at which time freshly-prepared, washed platelets (as described in 2.1.2) were added to all wells of one plate (labeled "PLT") at a ratio of 1000:1.

After an additional 24 h, medium was aspirated from all wells, and cells were rinsed with DPBS. The cells were dissociated with 200 µL trypsin-EDTA per well, recovered with 800 µL antibiotic-free McCoy's medium containing 10% FBS, removed to 1.5 mL microcentrifuge tubes, and centrifuged at 1000 rpm for 10 minutes. The cell pellets were washed in 1 mL PBS for 10 min at 1000 rpm, allowed to air dry, and then frozen at -80°C. RNA was subsequently extracted using Qiagen's RNeasy Mini Spin Kit. This assay was performed a minimum of three times with three different cell passages, and three independent platelet donors.

2.4 RNA Extraction from SK-OV-3 Cells

Total RNA was extracted from the previously frozen cell pellets using Qiagen's RNeasy Mini Spin Kit according to the manufacturer's instructions. Frozen cell pellets were thawed on ice and resuspended in 350 µL Buffer RLT. These were centrifuged at 13,000 rpm for 3 min, and the supernatants transferred to fresh 1.5 mL microcentrifuge tubes. 350 µL 70% ethanol was added to each tube. The tubes were mixed by inverting 10 times and the contents were then added to RNeasy spin columns. These were centrifuged for 30 s at 13,000 rpm, and the liquid was decanted. 700 µL Buffer RW1 was added to each column. Tubes were centrifuged at 13,000 rpm for 30 s and the liquid decanted. 500 µL Buffer RPE was added to each column. Tubes were

centrifuged at 13,000 rpm for 30 s and the liquid decanted. An additional 500 µL of Buffer RPE were added to each column, and tubes were centrifuged at 13,000 rpm for 2 min. The spin columns were moved to new tubes and centrifuged at 13,000 rpm for 1 min to ensure there was no ethanol left on the membranes. Spin columns were then placed in fresh 1.5 mL microcentrifuge tubes, and 30 µL nuclease free H_2O were added to each membrane and allowed to rest at RT for 3min. The tubes were centrifuged at 13,000 rpm for 1 min, the spin columns discarded, and the RNA placed immediately on ice. RNA concentrations were quantitated via Qubit fluorometer (Thermo Fisher USA).

2.4.1 Quantitation of RNA by Qubit Fluorometer

To quantitate the RNA from the PAI-1 knockdown assays, the Qubit 3.0 Fluorometer (Thermo USA) was used with Invitrogen's Qubit RNA HS Assay Kit. Fluorometers employ a fluorescent intercalating dye, such as ethidium bromide, propidium iodide, or GelRed that binds between base pairs (Fig. 2.7), as opposed to a minor groove-binding dye like Hoechst or DAPI. They tend to be more accurate than UV spectrophotometers, which tend to overestimate nucleic acid concentrations.

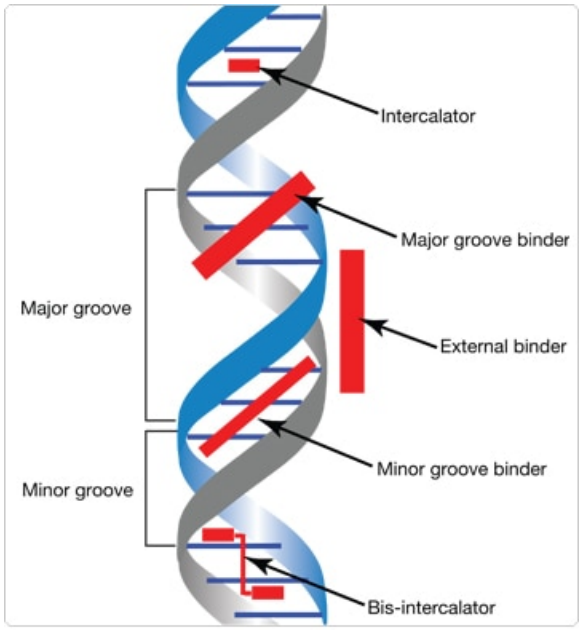

Fig. 2.7 Depiction of intercalating dye binding site. (https://www.thermofisher.com/ie/en/home/references/molecular-probes-the-handbook/nucleic-acid-detection-and-genomics-technology/nucleic-acid-stains.html)

The kit included a high standard, a low standard, RNA buffer, and RNA reagent/binding dye. RNA samples were thawed on ice. Preparations were made for 18 samples, plus a high and low calibrator by which to set the standard curve, plus 1 (21 samples total). 21 µL of RNA reagent were added to 4200 µL of RNA Buffer. Two thin-wall, clear 0.5 mL PCR tubes were prepared with 190 µL of the reagent/buffer solution, and labeled "1" and "2". 10 µL of low standard were added to tube "1", and 10 µL of high standard were added to tube "2". The tubes were then briefly vortexed per the manufacturer's instructions, and read by the Qubit to create a calibration curve. 18 additional PCR tubes were prepared with 199 µL of reagent/buffer solution, and labeled according to corresponding RNA samples. 1 µL of sample RNA was added to each tube, and the tubes were briefly vortexed per the manufacturer's instructions. The tubes were allowed to incubate at RT for 2 min, and were then

read three times each, with an average calculated for each sample. An average yield of at least 60 ng/µL per sample was desirable, with most samples yielding 88-100 ng/µL. These concentrations were marked on their corresponding parent RNA sample tubes, and used for future assays.

2.5 cDNA Synthesis

cDNA was synthesized via reverse-transcriptase PCR using Applied Biosystems' High-Capacity Reverse Transcription cDNA kit. 100 ng of total RNA in 10 µL molecular biology grade H_2O were used per reaction using Applied Biosystems' High-Capacity Reverse Transcription cDNA kit (Table B2, Appendix B). 10 µL H_2O containing 100 ng total RNA (previously quantitated by fluorometer) were added to 10 µL master mix for a total volume of 20 µL per reaction. PCR was performed using cycle times and temperatures listed in Table 2.1.

Table 2.1 cDNA synthesis thermocycler times and temperatures

Temperature (°C)	Time
25	10 min
37	120 min
85	5 sec
4	∞

2.6 Real-time Quantitative PCR (RT-qPCR)

RT-qPCR was performed using the Taqman Gene Expression Assay (Applied Biosystems, USA) for PAI-1, with glyceraldehyde 3-phosphate dehydrogenase (GAPDH) as the 'housekeeping" gene. GAPDH is an enzyme which catalyzes the 6th step of glycolysis, and is virtually omnipresent, making

it an appropriate choice. mRNA expression was evaluated using the $2^{-\Delta\Delta Ct}$ method. RT-qPCR is a method by which the total amount of RNA of a particular gene transcribed into mRNA can be quantitated through the implementation of a fluorescently-labeled primer/probe which binds to the gene of interest. In this experiment, a FAM reporter dye has been used, which emits a fluorescence signal at 535 nm. cDNA is first synthesized from total RNA in a standard reverse transcriptase PCR reaction. The cDNA is then mixed with a PCR reaction mix and a 5'-end reporter dye primer/probe that binds a specific DNA sequence and "reports" the amount of amplicon at the end of each cycle in the process for 40 cycles. This is accomplished by the cleavage of the quencher from the 3'-end of the primer (Fig. 2.8). Measured fluorescence is proportional to the amount of amplicon, with the cycles plotted on the x-axis (independent variable) and the fluorescent signal plotted on the y-axis (dependent variable). There is an exponential phase, during which the amount of amplicon approximately doubles each cycle, and a non-exponential phase, where the fluorescent signal plateaus.

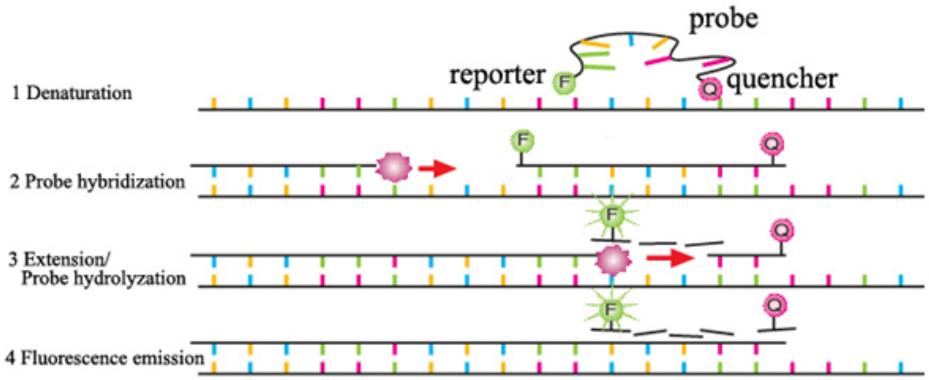

Fig 2.8 Binding of the reporter probe during hybridization, and subsequent quenching and release of the fluorescent signal during RT-qPCR.
http://www.sinobiological.com/real-time-pcr-service-gene-expression-analysis-by-qpcr-cro-service.html

A fixed threshold is set above the baseline in the exponential phase of fluorescence emission, and the point at which the signal crosses this threshold is called the C_t or C_q, depending on who you ask. ΔC_t is calculated using the C_t of a "housekeeping" gene, GAPDH in this case, and relative quantitation using the comparative C_t method allows one to analyze relative levels of the gene of interest across the submitted samples.

For this assay, a master mix was created for PAI-1 (20x PAI-1 Primer/Probe: Hs01126606_m1; Applied Biosystems, Lot #P170504-007 B03) and GAPDH (20x GAPDH Primer/Probe: Hu GAPDH FAM MGB; Applied Biosystems, Lot# 4352934-1301038) using the protocol listed in Table B3 in Appendix B. Both primers were inventoried, and the sequence information was not available. 18 µL of master mix were added to the wells of a 384-well optical plate, along with no-template controls for each primer/probe. 2 µL of cDNA were added to each appropriate well. Samples were run in triplicate, and mRNA transcripts quantitated by the $2^{-\Delta\Delta Ct}$ method (Livak and Schmittgen, 2001). In this method, the Cycle Threshold of the "housekeeping" gene is subtracted from that of the gene of interest to obtain a ΔC_t. Once these calculations have been performed, the ΔC_t of the control is subtracted from each ΔC_t of the test samples. In this case, the ΔC_t of the siNEG-treated cells was subtracted from the ΔC_t of the untreated samples, siRNA-treated samples, as well as the ΔC_ts of all samples that had been treated with platelets. These differences were then used as the exponents in a base 2 log transformation creating values equal to $2^{-\Delta\Delta Ct}$. These values were then compared to that of the

siNEG-treated sample, using that sample as the denominator in a ratio to obtain gene-fold expression values. These values were statistically analysed with GraphPad Prism 8.0, utilizing a one-way ANOVA with a Tukey post hoc multiple comparison test. This assay was performed a minimum of three times utilizing at least three independent sample sets.

2.7 PAI-1 Protein Analysis by ELISA

PAI-1 protein in SK-OV-3 cells from three independent sample sets was analysed using the Hyphen-BioMed Zymutest ELISA kit for human PAI-1 according to the manufacturer's instructions. This kit measures free PAI-1 as well as PAI-1 in complex with tPA, although the sensitivity for the latter is approximately 12 times lower than for the former (DeClerk *et al*, 1988). This was a sandwich ELISA, which utilizes an anti-PAI-1 monoclonal antibody (mAb) pre-coated plate, and a secondary capture antibody that has been conjugated to horseradish peroxidase (HRP). The kit includes high and low controls, and a standard curve was created using the PAI-1 protein standard provided in the kit.

SK-OV-3 cells were seeded into two 12-well cell culture plates, and were untreated, treated with 10nM siNEG, or treated with 10 nM PAI-1 siRNA as previously described (section 1.3.4). These were incubated at 37°C for 24 h, at which time all wells in one plate received platelets at a 1000:1 ratio (as described in section 2.2). Following an additional 24h incubation period, cells were pelleted, and protein lysates were obtained using 1 mL mammalian protein extraction reagent (MPER; Thermo Fisher, USA) per pellet. Total

protein was assessed by bicinchoninic acid assay (BCA assay; Pierce Thermo, USA), and equal amounts of total protein were added to the ELISA plate. The plate was incubated at RT on a shaker for 1 h, and wells were washed 3x with PBST (DPBS containing 0.1% Tween-20). The secondary antibody conjugate was added, and the plate incubated at RT on a shaker for 1 h. The wells were washed 3x with PBST, and 200 µL of 3,3',5,5'-tetramethylbenzidine (TMB) colorimetric reagent was added to all wells. This was incubated in the dark for 5 min, and the reaction was stopped using 100 µL 1 M HCl. The plate was read at 450 nm, and results were analyzed using both Microsoft Excel and GraphPad Prism 8.0. The same statistical analysis parameters were performed for protein concentrations as for mRNA gene-fold expression.

2.7.1 Bicinchoninic Acid Assay

The BCA Assay (also called the Smith Assay, after its inventor Paul K. Smith) is a colorimetric assay which employs copper reduction and chelation of copper with protein. When Cu^{+2} is reduced to Cu^{+1} in an alkaline environment, the reduced copper ion can then be bound by the acid at a ratio of two acid molecules per Cu^{+1} (Fig. 2.9). This second reaction creates a purple color that is readable at 562 nm to interpolate total protein concentrations from a standard curve (Walker, J.M. 1996). This assay was performed in accordance with the manufacturer's instructions against a BSA standard curve in which MPER was the diluent. Working Reagent (WR) was made using a 50:1 ratio of Reagent A: Reagent B, 25 µL of each sample and standard were loaded in triplicate into a 96-well plate. 200 µL of WR were then added to the wells, and the plate was

placed on a shaker for a few seconds to mix. The plate was incubated at 37°C for 30 min, cooled briefly, and read at 562 nm.

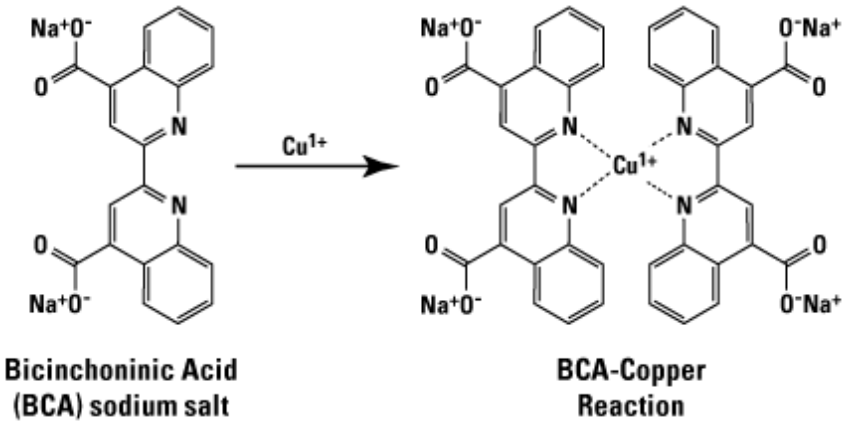

Fig. 2.9 Two BCA molecules chelate one copper ion. This creates the purple color that is used to measure protein concentrations. (Retrieved from https://www.thermofisher.com/ie/en/home/life-science/protein-biology/protein-biology-learning-center/protein-biology-resource-library/pierce-protein-methods/chemistry-protein-assays.html)

2.8 Wound-healing Assay

Cells were seeded at a density of 10^5 in 9 wells of a 12-well tissue culture plate and incubated overnight at 37°C and 5% CO_2 in a humidified incubator. Cells were rinsed with DPBS, and medium was replaced with serum-free and antibiotic-free McCoy's 5A. Platelets were isolated from whole blood (section 2.2), added to 6 of the wells at a 1000:1 ratio, and co-incubated for 24 h. At 24 h, the medium was aspirated from all wells, and cells were washed with DPBS. A scratch was made in each well with a 200 µL pipet tip. Untreated cells (labeled UNT) along with the three wells that had received platelets received fresh medium (labeled FM), and the other three wells treated with platelets (labeled REL) received platelet releasate obtained by centrifugation of the aspirated medium from those wells. Cells were incubated overnight, and photographed

at 0 h, 6 h, 20 h, and 24 h. Images were evaluated for wound closure with ImageJ software (NIH, public domain).

2.8.1 Evaluation of Wound Closure using ImageJ

The wound recovery rate shown in Results Table 3.1 is in mm^2, and assesses area. Percent wound recovery was calculated at each time point and graphed versus time. For example, at t = 6 h there were three area values for each n of each treatment type. The three n values for each treatment type were averaged, and those values were plotted versus 6 h. This was repeated for each treatment type at each time point to obtain a visual representation of percent wound recovery over time.

In order to properly assess wound edge migration, the area values were converted from mm^2 to mm by taking the quotients of the mm^2 values when they are divided by the constant y-axis values in mm. This gives a linear displacement value for each n of each treatment type at each time point. These values were used to calculate Δx, which was then used to determine wound edge migration velocity in the equation $\bar{v} = \Delta x/\Delta t$, where "$\Delta$" means "change in", "x" represents position or the distance traveled on the y-axis, and "t" represents time on the x-axis. $\Delta x/\Delta t$ is the calculation for slope "m" in the linear equation y = mx +b, and represents velocity (Fig. 2.10).

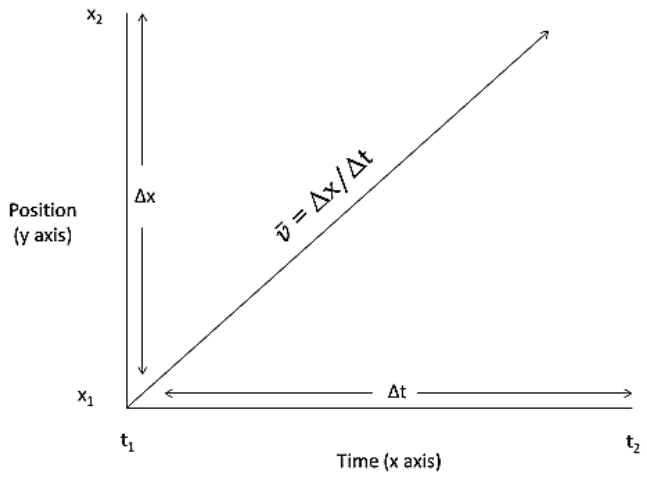

Fig. 2.10 Velocity is equal to the change in position over the change in time $\Delta x/\Delta t$, and is also the slope in a linear equation.

Three independent sample values were averaged for each treatment type at each time point and plotted on a graph of average velocity over time, which in turn represents acceleration. These results were then multiplied by 1000 to give velocity values in μm/h and acceleration values in μm/h/h, or μm/h^2. SI units of acceleration are m/s^2, but have been left in units of μm/h^2.

2.9 The Effect of Platelets and their Releasate on the Cell Cycle

SK-OV-3 cells were seeded in 12-well flat-bottomed polystyrene tissue culture plates (Sarstedt, Germany) at a density of 4.5 x 10^5 cells per well and labelled as depicted in Fig. 2.11.

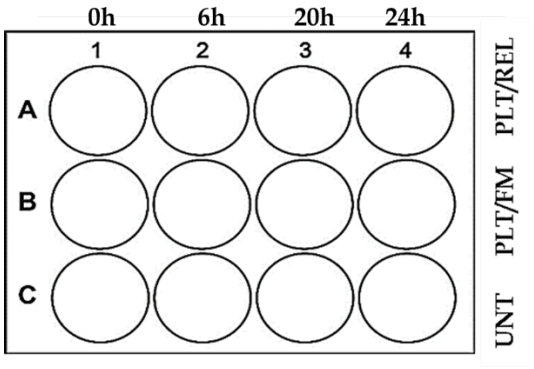

Fig. 2.11 Plate diagram for Cell Cycle Analysis assay

Platelets were isolated from whole donor blood (section 2.2). Wells labelled "PLT/FM" and "PLT/REL" received 1000 platelets per cell and wells labelled "UNT" received no platelets. The plates were returned to the incubator for 24 h. At 24 h, medium was aspirated from the wells, with medium from wells labelled "PLT/REL" centrifuged at 13,000 rpm and set aside in 3 x 1.5 mL Eppendorf tubes. Cells were washed in DPBS, and a scratch introduced in each well with a 200 µL pipet tip. The DPBS was aspirated, and wells labelled "UNT" received 1 mL fresh medium (FM), wells labelled "PLT/FM" received 1mL FM, and wells labelled "PLT/REL" received 1mL of the supernatant from the medium that had been previously set aside. Cells of each treatment type were stopped at each time mark (0 h, 6 h, 20 h, or 24h), and fixed in 70% ETOH. This assay was performed 3 times with three different cell passages and three different platelet donations.

2.9.1 Fixing and Staining of SK-OV-3 Cells for Flow Cytometry

Cells were fixed according to the methods set forth by Piotr Pozarowski and Zbigniew Darzynkiewicz in their 2004 publication "Analysis of Cell Cycle by Flow Cytometry". At each time point, the cells were removed to 15 mL

falcon tubes, and washed in DPBS at 300 x g for 10 min. The cells were resuspended in 0.5 mL DPBS. These were pipetted gently to create a suspension with minimal aggregation. The cells were then fixed by transferring this suspension dropwise into tubes containing 4.5 mL of ice-cold 70% ETOH while gently vortexing the tube. Cells were kept in the ETOH at 4°C for a minimum of 2 h. When cells from all time points had been fixed, the cells were centrifuged for 5 min at 300 x g, and the ETOH decanted. Cells were resuspended in 5 mL DPBS and centrifuged for 5 min at 300 x g. The DPBS was decanted, and the cells were resuspended in 1 mL propidium iodide (PI) staining solution (Appendix B). PI is an orange-red fluorescing DNA intercalating dye with a maximum excitation of 493 nm, and a maximum emission of 636 nm (Fig.2.2). Work here was performed using the 488 nm (blue/green) excitation laser and readout with a 560LP mirror and 586/42 (orange/red) longpass filter setting as these represent the most accurate available combination for PI excitation/emission. Cell cycle analysis was performed using Becton-Dickinson's FACS-Melody. FlowJo version 10.6.1 (BD, USA) software was used to gate and identify cell populations, and to create histograms.

2.10 Combination PAI-1 Knockdown and Wound-healing Assay

A wound-healing assay which incorporated a PAI-1 knockdown was performed. This was achieved by combining the protocols in sections 2.3 and 2.8. Cells were seeded at a density of 10^5 cells per well and incubated overnight. A forward transfection was performed to transiently silence PAI-1. Wound

healing was measured using ImageJ software (NHS, public domain).

2.11 Invasion Assay of SK-OV-3 Cells treated with PAI-1 siRNA ± Platelets

SK-OV-3 cells were grown in McCoy's 5A supplemented with 10% FBS, 2 mM L-Glutamine, and 100 U penicillin + 0.1 mg streptomycin/mL. Cells were washed, trypsinised, and counted. 4.0×10^4 cells were seeded in serum-free and antibiotic-free McCoy's 5A in the wells of a 12 well plate and allowed to grow for 24h. Per the manufacturer's protocol, cells were serum-starved for 24 h prior to seeding in the invasion assay chambers.

For the PAI-1 knockdown: medium was aspirated from all wells, and cells washed in DPBS. 800 µl fresh medium were added to all wells, and a forward transfection was performed with untreated cells ("UNT") receiving 200 µL Opti-MEM, siRNA ("siRNA) wells receiving 200 µL of 50 nM PAI-1 siRNA/Lipofectamine complex (10 nM final concentration in wells), and siNEG wells ("-CTL") receiving 200 µL of 50 nM siNEG /Lipofectamine complex (10nM final concentration in wells). Both forward and reverse transfections were attempted, and it was determined that the forward transfection method was optimal for this particular experiment.

For assays receiving platelets: platelets were isolated from whole blood (section 2.2) and added at a ratio of 1000:1 at 2 4h post knockdown. The invasion assay chambers were seeded after another 24 h.

25 µL of previously aliquoted ECM gel (stock concentration = 9.72 mg/mL) were thawed on ice and added to 975 µL of ice-cold Tris-NaCl coating buffer (Appendix B), per the manufacturer's protocol, for a final concentration

of 250 µg/mL. 100 µL of this solution were pipetted into each of 9 0.8 µM PET cell culture inserts, and incubated at 37°C for 2 h.

After 2h, the remaining liquid was carefully pipetted off, and 700 µL of McCoy's 5A containing 5% FBS as chemoattractant were added to the lower chambers. 2.5 x 10^4 cells were added in serum-free medium to individual wells labelled according to their treatment type, with a full set of matching controls (no ECM gel). These were returned to the incubator and allowed to incubate overnight.

Cells were removed from the apical side of the inserts using unsupplemented McCoy's 5A and cotton swabs. Cells remaining on the basolateral sides of the inserts were fixed in ice-cold 100% methanol (Acros Organics, USA) for 2 h. Crystal violet stain was made by dissolving 0.125 g crystal violet in 50 mL of 20% methanol. Cells were counted manually by microscopy photography according to the manufacturer's protocol. This was accomplished by photographing 5 random fields per insert, manually counting cells per field, and then taking an average. Counting was also performed using ImageJ (NIH, USA) rather than a visual count, and no difference was noted between the two methods.

2.12 PAI-1 IF Staining of SK-OV-3 Cells

An 8-chamber slide (Merck) was coated with poly-L-lysine, and SK-OV-3 cells were seeded and grown on the slide. Cells were transfected with PAI-1 siRNA, inert negative control siNEG, or untreated. Identically treated chambers were also treated with platelets isolated from whole donor blood

following the protocol in section 2.2. Cells were subsequently stained with an anti-PAI-1 monoclonal antibody (mAb).

2.12.1 Coating of Chamber Slide with Poly-L-Lysine

50 µL of poly-L-lysine (Sigma; stock 0.01% w/v) were added to each chamber of an 8-chamber slide in a laminar flow hood and incubated for 5 min at RT. The liquid was aspirated out of each chamber, and the chambers were rinsed 3X with cell culture grade H_2O, and allowed to dry for 2 h.

2.12.2 Cell Growth, Transfection, and Fixation

SK-OV-3 cells were seeded at a density of $2x10^4$ per chamber in 0.5 mL McCoy's 5A medium supplemented with 10% FBS, 100 U penicillin + 0.1 mg streptomycin/mL, and 2 mM L-Glutamine. The slide cover was replaced, and the slide was incubated overnight at 37°C with 5% CO_2 to allow the cells to adhere. After 24 h, the medium was aspirated, and all chambers were gently rinsed with DPBS. The medium was replaced with 0.4 mL antibiotic-free medium. LCS/PAI-1 siRNA and LCS/siNEG solutions were prepared according to the protocol outlined in section 2.3. Following the legend in Table 2.5, cells in chambers 2 and 6 received 100 µL siNEG in LCS for a final concentration of 10 nM, while those in chambers 3 and 7 received 100 µL PAI-1 siRNA in LCS for a final concentration of 10 nM. Chambers 1, 4, 5, and 8 received 100 µL Opti-MEM only. The slide was returned to the incubator for 24 h, at which point wells 5 -8 received platelets isolated from whole donor blood (as described in section 2.2) at a ratio of 1000 platelets per cell. The slide was incubated for an additional 24 h, and the media from all wells was then

aspirated, the wells washed in DPBS and the cells fixed in 100% ice-cold methanol on ice for 1 h.

Table 2.2 Chamber slide legend

Chamber	Treatment	Platelets	Primary	Secondary
1	Untreated		✓	✓
2	siNEG		✓	✓
3	siRNA		✓	✓
4	Untreated			✓
5	Untreated	✓	✓	✓
6	siNEG	✓	✓	✓
7	siRNA	✓	✓	✓
8	Untreated	✓		✓

2.12.3 Staining with Monoclonal Antibody 33H1F7

After fixation, the cells were blocked with a 3% fraction V bovine serum albumin (BSA; Sigma, USA) in PBST (PBS+ 0.1% Tween 20) for 30 min on rocker at RT (Table B4, Appendix B). The blocking solution was aspirated, and 400 µL of anti-PAI-1 mAb-33H1F7 (Thermo MA1- 40224) at a 1:50 dilution in PBST with 3% BSA were added to each chamber (Table B4, Appendix B), with the exception of chambers 4 and 8, and the slide was incubated overnight at 4°C. The next day, the primary antibody solution was aspirated, and the chambers were washed 3x for 5 min each in DPBS. 400 µL of AlexaFluor 488 goat anti-mouse secondary antibody (Invitrogen IgG H+L AlexaFluor 488 A11001) at a 1:1000 dilution in PBST with 3% BSA (Table B4, Appendix B) were added to each chamber, and the slide was incubated in the dark for 1 h at RT. The secondary antibody solution also contained 1 µg/mL Höechst 33342 (Thermo Pierce). The secondary antibody was aspirated, and the chambers were washed 3x for 5 min each with DPBS in the dark. The slide was dried,

and a coverslip applied. Imaging was performed via fluorescence microscopy using the Nikon Eclipse TE300.

2.13 RNA Sequencing

RNA sequencing, or RNA-Seq, is a high-throughput sequencing technology that allows for in-depth transcriptome analysis of both coding and non-coding regions. It enables the identification of all species of genome transcript, including 5′ and 3′ ends, and post-translational modifications under different conditions (Wang *et al*, 2009), including gene expression changes during mouse embryogenesis (Cloonan *et al*, 2008) and yeast meiosis (Nagalakshmi *et al*, 2008). 5′ and 3′ ends can be mapped much more accurately - often to within 10-50 bp, with 3′ ends being much more precisely mapped - than with previous techniques utilising poly-A tail location (Wang *et al*, 2009). RNA-Seq is one of the most important tools available to modern science, surpassing some of the available hybridization techniques that may be limited by cross-reactivity, and is less expensive than higher-end hybridization tiling-arrays or the Sanger EST method (Wang *et al*, 2009).

Once the RNA has been analysed for integrity, it is typically processed using a ribosomal RNA (rRNA) depletion enrichment method or a poly-A tail depletion method. rRNA depletion is used for total RNA analysis, whereas the poly-A method selects only mRNA that has been transcribed and tagged for translation. cDNA is then synthesized using the polymerase chain reaction (PCR). Smaller RNAs, such as miRNAs and siRNAs, are able to be sequenced directly after ligation of cDNA in the library creation step, but larger RNAs like

mRNAs must be fragmented by RNA hydrolysis/thermal fragmentation (Shanker *et al*, 2015) prior to cDNA synthesis. Additional cDNA fragmentation is also sometimes required to create 200-500 bp fragments (Shanker *et al*, 2015), and can be done with DNase I or sonication (Wang *et al,* 2009). To control for potential PCR artefacts, biological replicates are necessary in order to ascertain whether or not they are true short RNA transcripts (Wang *et al*, 2009). After the fragmentation and cDNA creation steps, the DNA fragments are selectively enriched, meaning that only those fragments with annealed adapters at their ends are subject to PCR amplification. Those without adapters are largely considered to be artefactual. PCR cycles are kept to a minimum to avoid overrepresentation in the libraries. The PCR products are then cleaned, and the libraries are validated and quantified.

2.13.1 RNA Integrity Analysis by Bioanalyzer (Agilent)

RNA quantitation by Qubit was performed as previously described in section 2.4.1. RNA integrity was analysed using the RNA 6000 Nano kit (Agilent) and the Bioanalyzer 2100 (Agilent) according to the manufacturer's protocol. The 16- pin bayonet electrode cartridge was decontaminated with RNaseZAP (Ambion) prior to the sample runs. A new syringe was installed in the chip priming station, and the base plate adjusted. The chip selector was adjusted to the correct position for accommodation of RNA chips. The ladder was denatured at 70°C for 2 min, and all reagents were equilibrated to RT for 30 min. 1 µL of Nano dye concentrate was added to 65 µL of filtered gel matrix. This was vortexed and then centrifuged at 13,000 rpm for 10min at RT. A chip

was placed on the priming station, and 9 µL of the gel/dye mixture were pipetted into the well marked "G". The syringe plunger was positioned at 1mL, the chip priming station closed, and the plunger depressed until held by the plunger clip. After 30 s, the plunger was released and watched until it had moved back to the 0.3 mL mark. After 5 s, the plunger was drawn back to the 1 mL mark, and the chip priming station was opened.

9 µL of gel/dye mixture were then pipetted into the two wells directly above the well marked "G", and 5 µL of ladder were pipetted into the marked ladder well, and into each sample well. Samples were denatured at 70°C for 2 min, and 1 µL of each sample was pipetted into each sample well. The chip was then horizontally vortexed for 60 s at 2400 rpm. The chip was then placed into the Bioanalyzer and processed.

2.13.2 Preparation of RNA and Construction of cDNA Libraries

All RNA preparation and library construction was performed by Trinity College Dublin's TrinSeq facility using TruSeq mRNA Sample Prep (Illumina, San Diego, CA USA) in strict accordance with the manufacturer's instructions. Once the RNA had been analysed for integrity, it was enriched using a poly-A depletion method. The process employed by the Trinity TrinSeq facility purified 500 ng of each sample of the poly-A containing mRNA molecules using magnetic beads with attached poly-T oligos during two rounds of purification. During the second purification, preparation for cDNA synthesis was also performed by heat fragmentation of the RNA and the addition of random hexamers for priming.

First Strand cDNA synthesis was performed using Illumina's First Strand Act D Mix and SuperScript II Reverse Transcriptase (Invitrogen). Blunt-end Second Strand cDNA was then created in a process that replaces dDTP with dUTP, and purifies the cDNA with AMPure XP beads (Beckman Coulter™ Agencourt). The 3′ ends were then adenylated to prevent ligation to each other during adapter ligation. The adapter contains a corresponding "T" to ensure correct ligation of the adapters to the cDNA fragments. DNA fragments were then enriched by PCR using a primer cocktail designed to anneal to the adapters. PCR product clean-up was performed again using AMPure XP Beads. DNA libraries were validated and quantified using the Agilent High Sensitivity DNA Assay, which is run on the Agilent Bioanalyzer 2100, and is analogous to the aforementioned RNA integrity assay (2.13.1). Libraries were then pooled and normalized.

2.14 Analysis of Plasma PAI-1 by ELISA

All samples were tested by ELISA using the R&D Human Serpin E1/PAI-1 DuoSet and its companion ancillary kit. This kit measures the active and latent forms of PAI-1, as well as PAI-1 complexed with vitronectin. It does not detect PAI-1 in complexes with uPA or tPA. Optimisation of sample testing conditions was performed using a standard curve with five samples used neat, and also diluted 1:5, 1:10, and 1:20. All dilutions proved to be too low for at least one sample, and it was determined that testing the samples undiluted would be the most accurate method to employ.

All reagents were prepared with strict adherence to the protocol

provided with the ELISA kit. 720 µg of primary/capture antibody was supplied in lyophilized form. This was reconstituted to a stock solution of 400 µg/mL by the addition of 1.8 mL DPBS. This was aliquoted to minimize freeze/thaw cycles, and stored at -20°C until needed. One stock aliquot was thawed at RT and was further diluted to its working concentration of 4 µg/mL for each individual plate, of which there were 6, by the addition of 100 µL of stock solution to 9.9 mL DPBS. 100 µL of working concentration capture Ab were added to each well, and the plate was covered and incubated overnight at RT.

The next day, wash buffer (stock solution 25X) was prepared by adding 20mL of stock solution to 480 mL sterile cell culture grade H2O. Reagent diluent (stock solution 10X) was prepared by adding 10 mL to 90 mL sterile cell culture grade H2O, and was freshly prepared each day. The primary Ab was aspirated from all wells, and all wells were washed 3X in wash buffer. For the blocking step, 300 µL of reagent diluent were added to each well, and the plate was covered and incubated at RT for 1 h.

The reagent diluent was aspirated from the well, and all wells were washed 3X with wash buffer. A stock solution of PAI-1 standard was prepared by first reconstituting the supplied 135 ng of lyophilized standard with 0.5 mL of Reagent Diluent for a stock concentration of 270 ng/mL. Using the stock solution and the reagent diluent, a 7-point standard curve was prepared using 2-fold serial dilutions (Fig. 2.12).

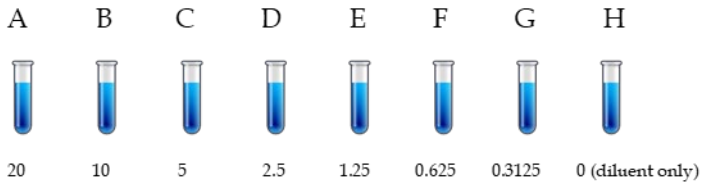

Fig. 2.12 Standard curve preparation

Patient plasma samples were thawed in a 37°C water bath, and 100 µL of the standards and the patient samples were loaded into the plate. A pooled normal plasma sample and a reagent diluent "blank" were included as controls. The plate was covered and incubated at RT for 2 h. At 2 h, the samples were aspirated, and the plate was washed 3X in wash buffer. A 50 µg/mL stock solution of secondary/detector antibody had previously been prepared by reconstituting the provided 72 µg of lyophilized antibody in 1.44 mL of reagent diluent. This was aliquoted and frozen at -20°C to minimize freeze/thaw cycles. One aliquot was thawed at RT, and 10 mL of 50 ng/mL antibody were prepared by adding 10 µL of stock solution to 9.99 mL reagent diluent. 100 µL were then added to each well, and the plate was covered and incubated at RT for 2 h.

At 2 h, the secondary Ab was aspirated, and the wells washed 3X in wash buffer. A 200X stock solution of streptavidin-HRP was provided with the kit, and a 1X solution was prepared by adding 50 µL to 9.950 mL reagent diluent. 100 µL were added to each well, and the plate was covered and incubated in the dark for 20 min. When 20 min had elapsed, the streptavidin-HRP was aspirated, and the wells were washed 3X in wash buffer. 5 mL of

TMB A solution was mixed with 5 mL TMB B solution in a 10 mL Falcon tube, and 100 µL of the resulting solution were added to each well. The plate was incubated in the dark for 7 min, at which point 50 µL of 2 M sulphuric acid were added to each well to stop the reaction. The plate was then read at 450 nm with a correction λ of 540 nm.

Standard curves for each individual plate were created using a sigmoidal 4PL curve in GraphPad Prism, and the data were interpolated to give PAI-1 values for each individual sample in ng/mL.

2.15 Statistical Analysis

Statistical analyses for all assays were carried out using either GraphPad Prism 8.4.3 or SPSSv26 (IBM). Log10 transformations were implemented for data that were not normally distributed (such as those in Chapter 5). Data are presented as either mean ± SD or mean ± SEM. A minimum of three independent biological replicates were performed for each experiment, the exception being fluorescence microscopy which was not possible due to issues created by scheduling and Covid19. Details of statistical tests used are included in each method above, and further details are provided in each chapter, where appropriate.

CHAPTER 3

ASSESSMENT OF PAI-1 FUNCTION AND THE EFFECT OF PLATELETS IN AN OVARIAN CANCER CELL LINE MODEL

3.1 Introduction

Ovarian cancer (OC) is the 7th leading cause of cancer in women worldwide (Lukanova and Kaaks, 2005). Epithelial ovarian carcinomas (EOC) account for 85-90% of all ovarian cancers, and the majority have late-stage diagnoses (Lisio *et al*, 2019). Of the five classifications of malignant EOC: clear-cell (CCOC), mucinous (MOC), low-grade serous (LGSOC), high-grade serous (HGSOC), and endometrioid, our work here will focus on HGSOC.

Metastasis in EOC has historically been considered to be the result of direct peritoneal spreading (Van Berckelaer *et al*, 2016; Cannistra *et al,* 1993). However, evidence of haematogenous metastasis has been demonstrated in research regarding circulating tumor cells (CTCs) (Pradeep *et al*, 2014).

Platelet-cancer cell interactions are integral to haematogenous metastasis across many cancers, including EOC. As previously mentioned, high platelet counts are often associated with advanced disease stage (Stone *et al*, 2012; Qi *et al*, 2015), and platelets contain high levels of PAI-1. Previous work in our and other laboratories has elucidated the relationship between cancer cells and platelet aggregation in the form of a platelet "cloak" (Egan *et al*, 2011; Lou *et al*, 2015; Cluxton *et al*, 2019), with PAI-1 being identified as a consistently altered molecule in the platelet-cancer cell transcriptome. The platelet cloak has been shown to induce a mesenchymal phenotype in epithelial cancer cells, and increases the metastatic potential of ovarian cancer cells (Egan *et al*, 2011). As PAI-1 is directly involved in extracellular matrix (ECM) maintenance, remodeling, and tumourigenesis, we have chosen to investigate PAI-1 in the

context of wound-healing (migration), invasion, and mitosis in EOC. Here, we present evidence that PAI-1 is a key driver of the metastatic process in EOC, and contribute to a growing body of evidence that provides the foundation for research into PAI-1 as a diagnostic and/or prognostic marker in the clinical setting.

3.1.1 Hypothesis

Platelet-cancer cell interactions aid survival of CTCs in the blood, and PAI-1 is a key driver of the metastatic process in EOC with potential as an independent prognostic indicator.

3.1.2 Specific Aims

1. To investigate platelet-cancer cell interactions in the context of PAI-1, and their contribution to an invasive and pro-metastatic phenotype in EOC.

3.2 Materials and Methods

SK-OV-3 cells were utilised as a model of epithelial ovarian cancer (EOC) (Fig. 3.1). Cells were cultured in supplemented McCoy's 5A (Sigma) as described in chapter 2, section 2.1, and platelets for all assays were isolated from consented donor whole blood according to the methods outlined in section 2.2. Silencing of PAI-1 was accomplished via siRNA transfection as outlined in section 2.3, and RNA extraction and quantitation were performed following the methods in section 2.4. All assays were performed a minimum of three times, using three different cell passages, unless otherwise noted.

cDNA synthesis was performed by reverse-transcriptase PCR using Applied Biosystems' High-Capacity Reverse Transcription cDNA kit according to the manufacturer's instructions, and is detailed in section 2.5. Subsequent Real-time PCR (RT-qPCR) analysis was performed using the PAI-1 Taqman Gene Expression Assay (Applied Biosystems), and this is outlined in section 2.6. A corresponding PAI-1 protein analysis was performed by ELISA (Hyphen BioMed) and is described in section 2.7.

Wound-healing assays with and without platelets were performed according to the methods in section 2.8, and a combination wound-healing/PAI-1 knockdown assay is detailed in section 2.10. Cell cycle analysis was performed on untreated cells (UNT), cells treated with platelets and then fresh medium (PLT/FM), and cells treated with platelets and then platelet releasate obtained by centrifugation of supernatants (PLT/REL). These cells were subject to the same conditions as the wound-healing assay described in

section 2.8, and were stopped and fixed at identical time points. When all time points and treatments had been collected, fixed cells were stained with propidium iodide and analysed using Becton-Dickinson's FACS-Melody flow cytometer. This assay is detailed in section 2.9.

Invasion assays were performed on cells treated with inert negative control siRNA and PAI-1 siRNA. Cells were synchronized via serum deprivation for 24h prior to seeding in 0.8μm pore PET membranes that had been coated with Engelbreth-Holm-Swarm (EHS) mouse sarcoma ECM gel. This was performed both with and without the addition of platelets. Details of these assays are outlined in section 2.10.

Immunofluorescence staining for PAI-1 was performed *in situ* on cells grown in a chamber slide that were left untreated, treated with an inert negative control siRNA, or treated with PAI-1 siRNA. An identical set of these treatment types was treated with platelets for 24h. All cells were fixed in 70% ETOH, incubated with anti-PAI-1 mAb-33H1F7 (Thermo), and then stained with AlexaFluor 488 goat anti-mouse secondary antibody (Invitrogen). Details of this assay are outlined in section 2.12.

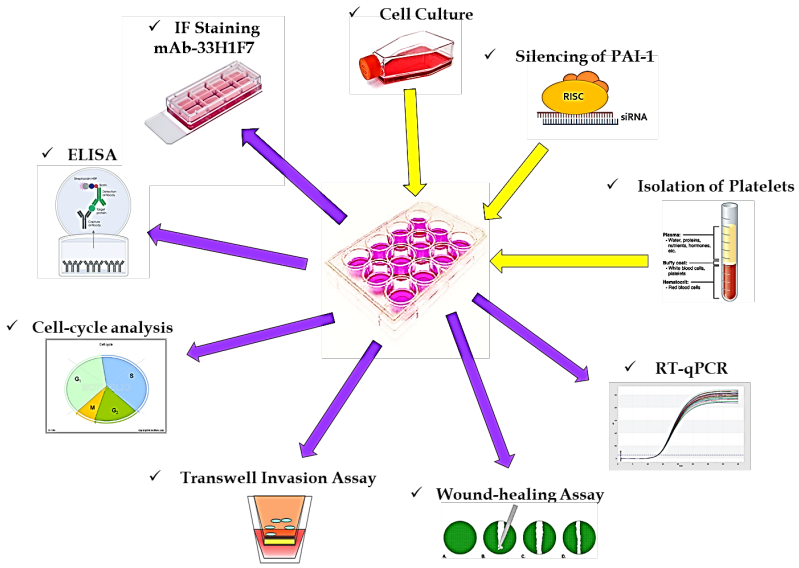

Fig. 3.1 Schematic of materials and methods used in this chapter

3.3 Results

3.3.1 Platelets were not activated during Isolation

Debris were removed by gating for CD42b (Fig. 3.2), and all cells were determined to be platelets, with little to no CD45 emission (Fig. 3.3), likely due to overlying spectra. All cells were $CD42b^+$ and $CD62p^-$, indicating that there was no activation of the platelets during the isolation process (Figs. 3.2 through 3.5). Unstained cells emitted no fluorescence signals in any of the channels used (Figs. 3.3A, 3.4A, and 3.5A).

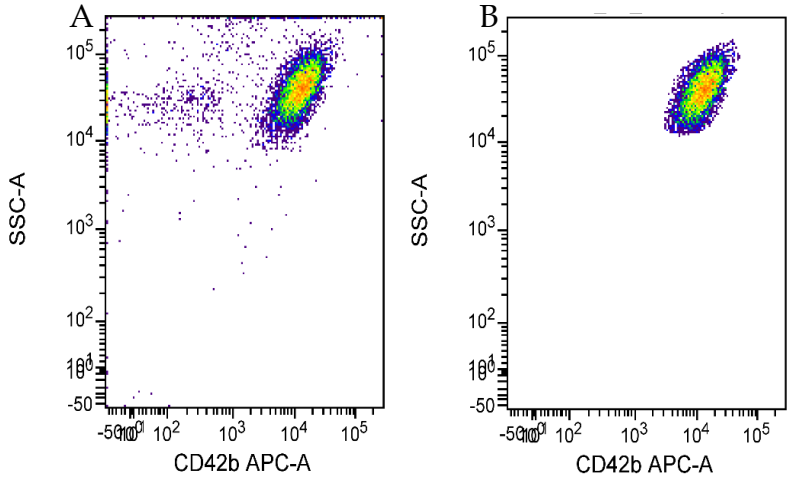

Fig. 3.2 Gating to exclude potential debris: **A** Stained, ungated platelets and **B** Stained platelets gated for CD42b

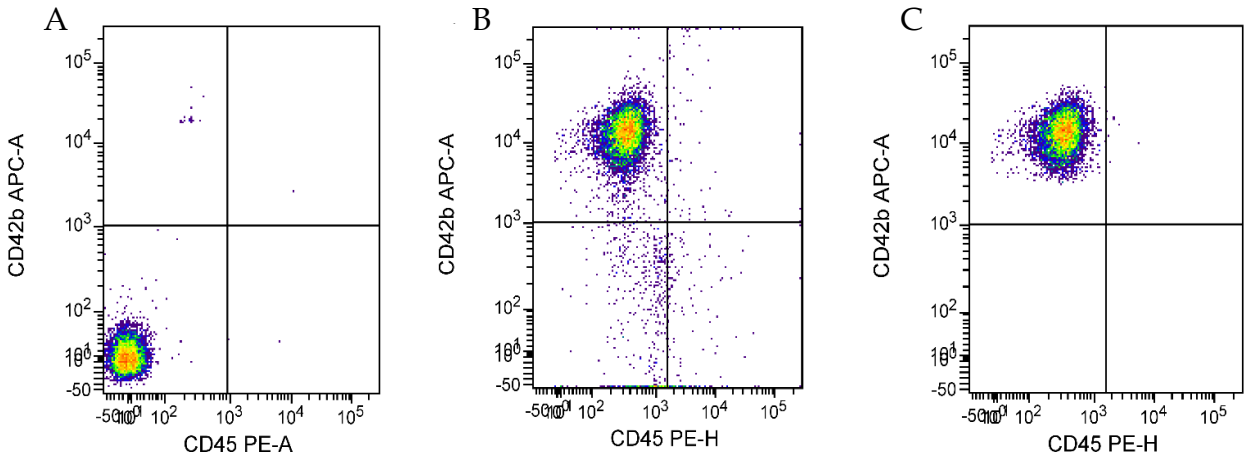

Fig. 3.3 Platelets are negative for CD45: **A** Unstained platelets are $CD42b^-/CD45^-$, **B** Stained platelets are $CD42b^+/CD45^-$, **C** Stained platelets gated for CD42b+ are $CD42b^+/CD45^-$.

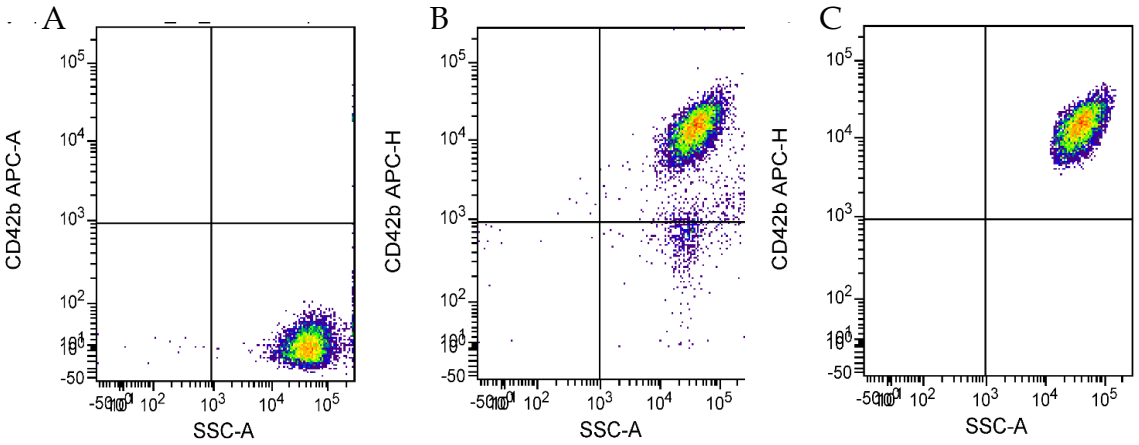

Fig. 3.4 Platelets are positively stained for CD42b: **A** Unstained platelets show no staining, **B** Stained platelets, **C** Stained platelets gated for CD42b+

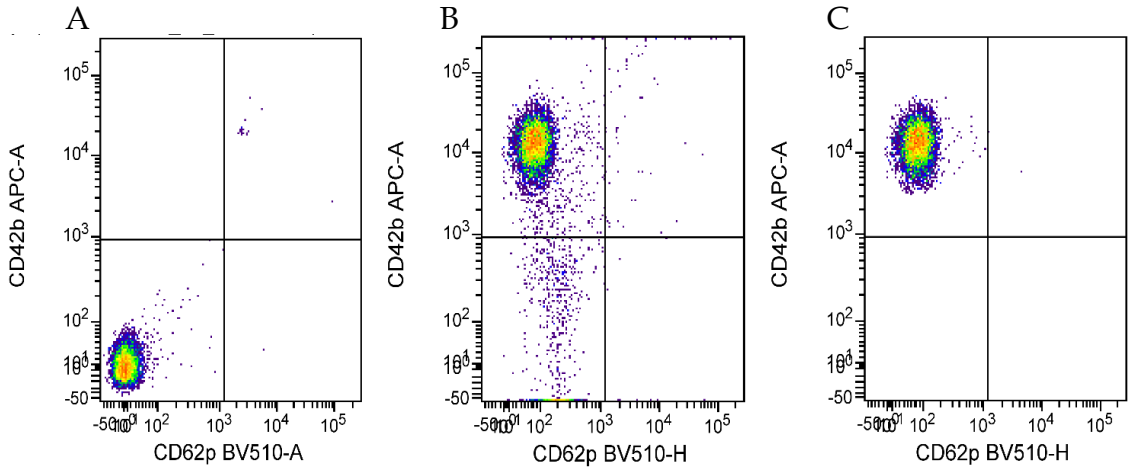

Fig. 3.5 Platelets are negative for CD62p: **A** Unstained platelets are $CD42b^-/CD62p^-$, **B** Stained platelets are $CD42b^+/CD62p^-$, **C** Stained platelets gated for CD42b+ are $CD42b^+/CD62p^-$.

3.3.2 Platelets increased PAI-1 in SK-OV-3 Cells

To validate previous research in which platelets demonstrated an ability to induce an increase in PAI-1 in cancer cells, (Cooke *et al,* 2015), SK-OV-3 cells were co-incubated with platelets. mRNA was measured using the TaqMan Gene Expression Assay (Applied BioScience). The addition of platelets to SK-OV-3 cells resulted in a significant increase in PAI-1 mRNA (Fig. 3.6 A; n = 3, p

= 0.0097), with an average fold gene expression increase of 3.31. PAI-1 protein concentrations (Fig.3.6 B; n = 3, p = 0.006) were quantitated by ELISA, and validated the RT-qPCR results (Fig. 3.6 A). Adding platelets to SK-OV-3 cells yielded a significant 9.3-fold increase in PAI-1 protein (Fig. 3.6 B).

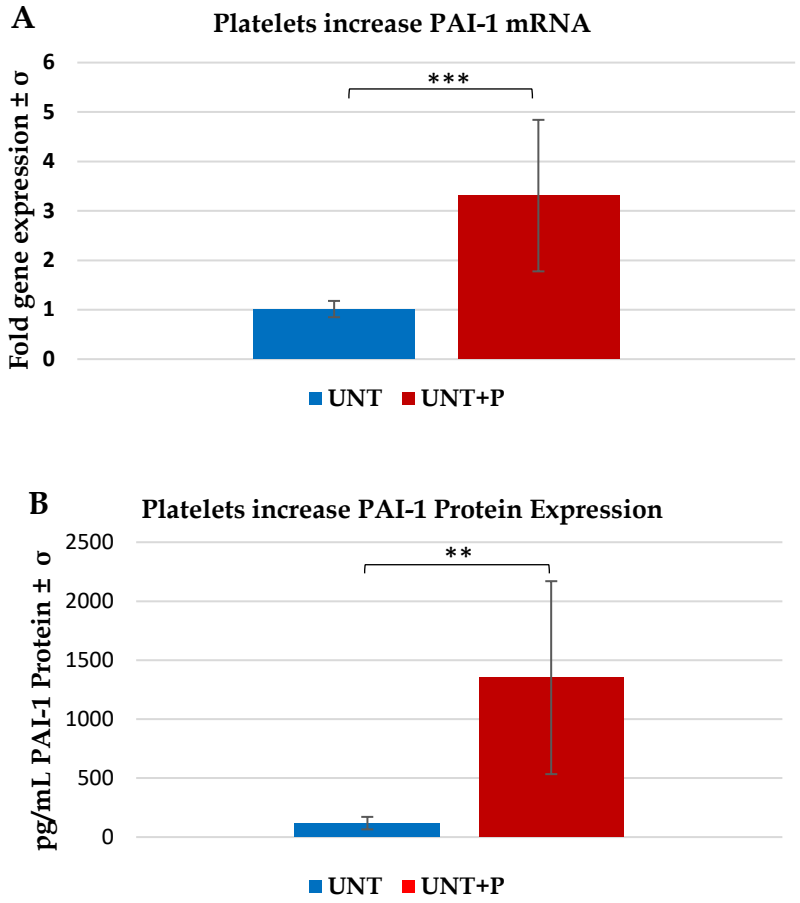

Fig. 3.6 Platelets increase: **A** PAI-1 mRNA, n= 3, graphed as fold gene expression and **B** PAI-1 protein, graphed as pg/mL, n=3, **p ≤ 0.01, ***p ≤ 0.001

3.3.3 Silencing of PAI-1 in SK-OV-3 Cells

SK-OV-3 cells were treated for 48 hours with PAI-1 siRNA. Real-time PCR revealed an average 78.4% loss of PAI-1 mRNA transcripts in SK-OV-3 cells treated *in vitro* with siRNA versus those cells treated with an inert siNEG (Fig. 3.7 A; p < 0.0001). This was further validated by a 73.25% loss of PAI-1

protein (Fig. 3.7 B; n = 3, p = 0.0069) in siRNA-treated cells versus those treated with an inert siNEG. There was no significant difference in either mRNA transcripts or in protein concentrations between the siNEG-treated cells and the untreated cells.

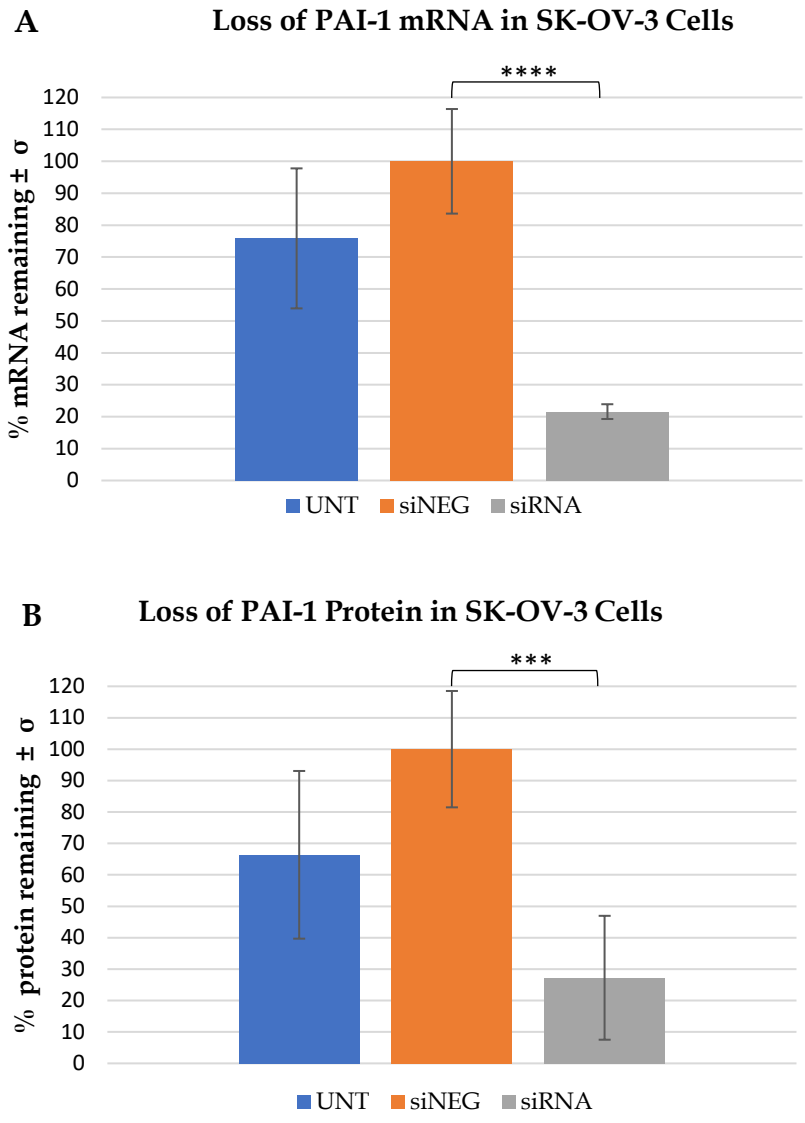

Fig. 3.7 Transfection with siRNA significantly reduces: **A** PAI-1 mRNA transcripts, n= 3, and **B** PAI-1 protein expression, n=3, ***p<0.001, ****p<0.0001

3.3.4 Evaluation of the Effect of Platelets on Cancer Cells when PAI-1 was Silenced

The addition of platelets to SK-OV-3 cells treated with negative control siRNA resulted in a fold increase of 3.1 ± 0.55 in mRNA transcription (Fig. 3.8 A; n = 3, p = 0.0143). A 5.5-fold increase in PAI-1 protein expression validated the RT-qPCR results (Fig. 3.8 B, n=3, p = 0.0327). The amount of PAI-1 protein lost was not as pronounced as the reduction in mRNA transcripts, and this may have been due to the first assay not working as well as the subsequent two assays. However, the fold-change in protein expression followed the same trend towards significance as that of the mRNA, and this occurred across all treatment types. Variations in donor platelet PAI-1 levels were expected. Both PAI-1 mRNA transcripts and protein were increased by the addition of platelets when PAI-1 was transiently silenced, however, the platelets alone were not able to recover PAI-1 to its pre-knockdown status.

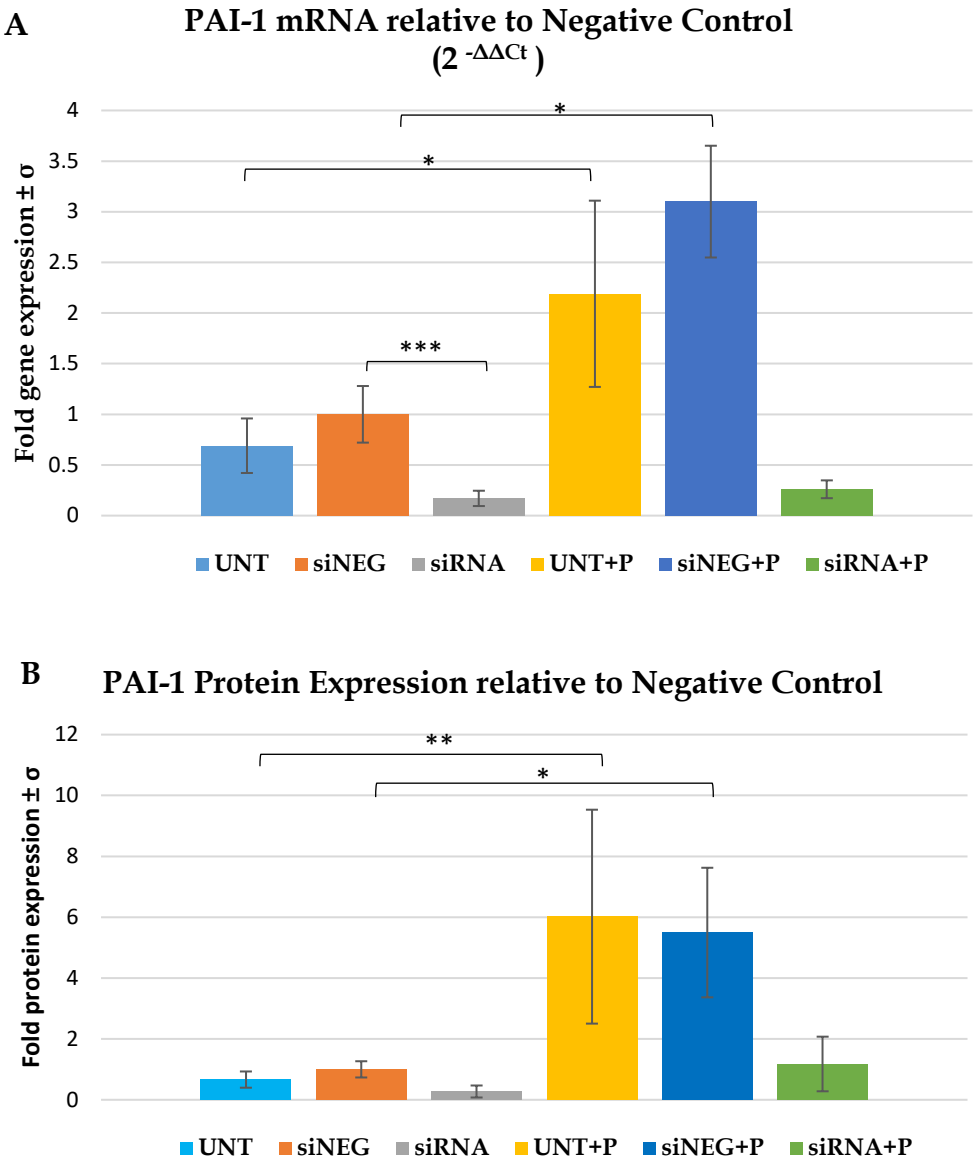

Fig. 3.8 A. Real-time PCR results (n=3) show a reduction in PAI-1 mRNA transcripts as compared to the negative control, and an increase in PAI-1 where platelets are added, n=3. **B.** ELISA results validate the RT-qPCR, n=3. * $p<0.05$, ** $p<0.01$, *** $p<0.001$

3.3.5 Platelets increased intracellular PAI-1 in SK-OV-3 Cells, and silencing PAI-1 decreased intracellular PAI-1

Untreated SK-OV-3 cells (Fig.3.9 A) showed intracellular PAI-1 (indicated by red arrow), as did cells treated with an inert negative control siNEG (Fig.3.9 B, indicated by red arrow). Their respective platelet-treated counterparts showed a marked increase in intracellular PAI-1 (Fig. 3.9 E and F,

indicated by red arrows). SK-OV-3 cells treated with PAI-1 siRNA (Fig. 3.9 C) showed a lack of intracellular PAI-1, and those cells where PAI-1 was silenced also did not show intracellular PAI-1 even when platelets were added (Fig. 3.9 G), although the platelets were clearly visible (indicated by red arrow). Control wells of untreated cells (Fig. 3.9 D) and untreated cells plus platelets (Fig.3.9 H) receiving only the secondary conjugate did not show any PAI-1 staining, as expected.

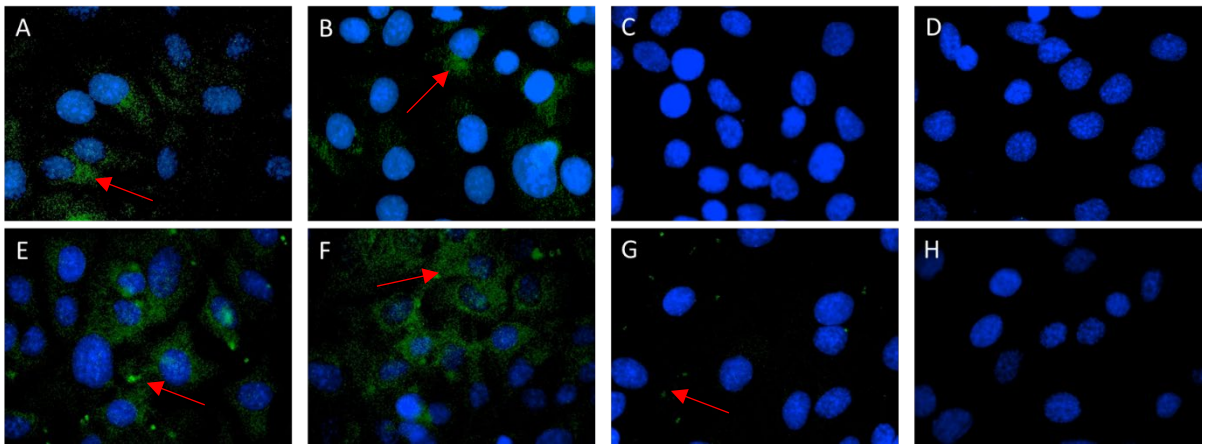

Fig. 3.9 PAI-1 protein in SK-OV-3 cells visualized by fluorescence microscopy at 40x. All wells were incubated with a 1:500 dilution of mAb-33H1F7 (monoclonal murine IgG1 against PAI-1) stained with 10µg/mL Höechst (seen in blue) and a 1:1000 dilution Alexa Fluor 488 –conjugated goat anti-mouse IgG (seen in green), with the exception of wells D and H, which received fluorophore-conjugated secondary IgG only. **A.** Untreated cells, **B**. Cells treated with siNEG (inert siRNA), **C.** Cells treated with PAI-1 siRNA, **D.** Untreated cells, **E.** Untreated cells incubated with platelets for 24h, **F.** Cells treated with siNEG (inert siRNA) and incubated with platelets for 24h, **G.** Cells treated with PAI-1 siRNA and incubated with platelets for 24h, **H.** Untreated cells incubated with platelets for 24h.

3.3.6 Platelets and their Releasate expedited wound-healing in SK-OV-3 Cells in vitro

The effect of platelets and their releasate on the motility of SK-OV-3 cells was assessed by a wound-healing assay. Exposure to platelets and their releasate increased the rate of wound closure in these cells significantly from 0-6h, with a p-value of 0.0096, with an overall one-way ANOVA p-value of

0.0118. Figs. 3.10A and 3.11 demonstrate that at 24h, there was a marked difference among total average percent wound closures: 59.2% in untreated cells, 79.9% in cells treated with platelets/fresh medium, and 83.6% in cells treated with platelets/releasate.

Table 3.1 shows average rates of wound closure in mm^2/hour, and tables 3.2 and 3.3 demonstrate respective velocities and accelerations of wound edge migration. One-way ANOVA of velocities was significant, with an overall p-value of 0.0054 and significance between untreated cells and cells treated with platelets and then releasate at the 6h mark having a p-value of 0.0388. Fig. 3.10 B represents respective accelerations of wound-edge migration, and Fig. 3.11 clearly depicts accelerated wound closure in cells treated with platelets or platelets and releasate versus untreated cells.

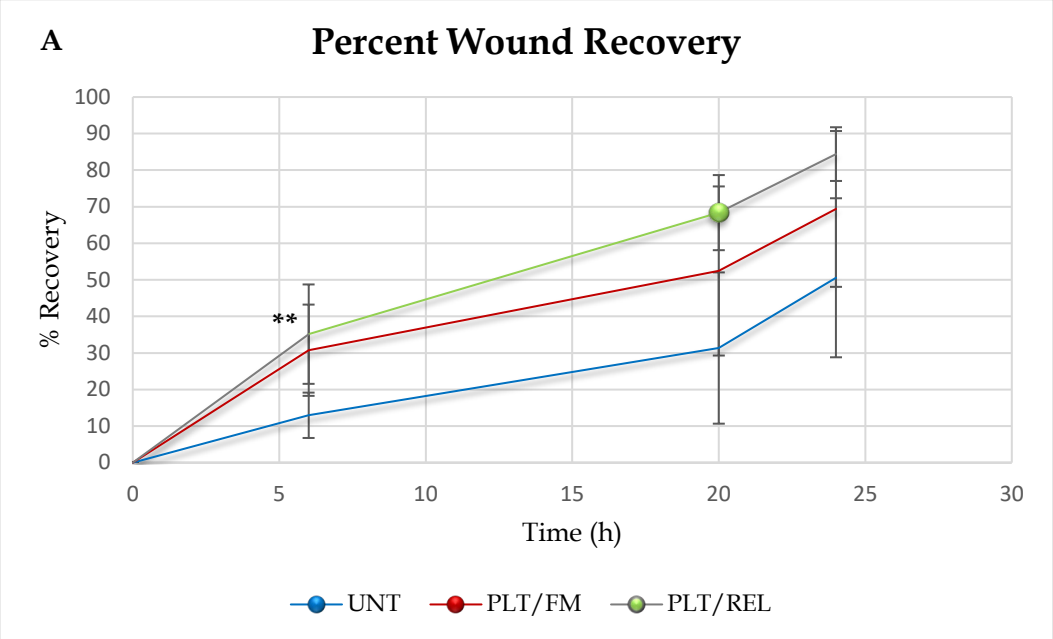

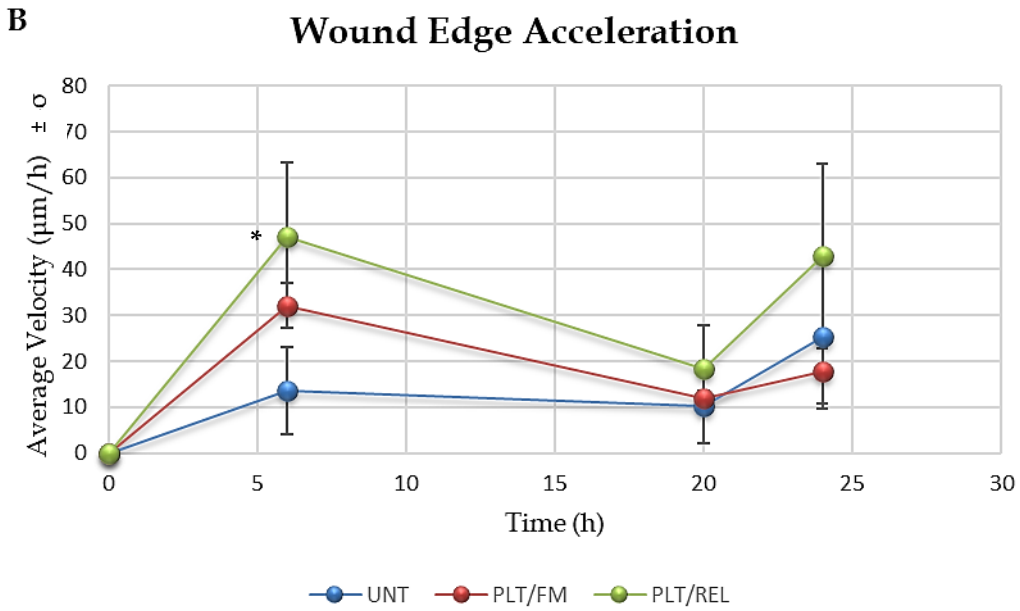

Fig. 3.10 A. Percent wound recovery achieved by untreated cells (blue line), cells treated with platelets and then fresh medium (red line), and cells treated with platelets and then platelet releasate (green line) at 0h, 6h, 20h, and 24h, shown in mm^2/h, n = 3 **B.** Graph of acceleration of wound edge migration seen in untreated cells (blue line), cells treated with platelets and then fresh medium (red line), and cells treated with platelets and then platelet releasate (green line). All are shown in μm/h. Sharp increases can be seen in both red and green lines from t=0h to t=6h, and again in the green line from 20-24h, n = 3. *p ≤ 0.05, **p ≤ 0.001

Table 3.1 Average rate of wound closure in mm^2/hour, broken down by treatment type (n=3). Untreated cells achieve a faster recovery rate during the period from 20-24 hours. Cells treated with platelets/fresh medium or platelets/releasate achieve faster recovery during the first 6 hours following wound introduction. Wound recovery was significant at t=6h between UNT and PLT/REL (p=0.0096). Data points for calculations taken from Fig.3.4.

Wound Recovery Rate (mm^2/h)			
Elapsed Time(h)	**UNT**	**PLT/FM**	**PLT/REL**
0-6	0.94758	4.58466	6.90616**
6-20	0.66561	1.23565	2.14428
20-24	4.80021	3.68068	2.75759

Table 3.2 Average velocity: $\bar{v} = \Delta x/\Delta t$ = rate of edge migration in micrometers per hour (n=3). Untreated cells move faster during the 20-24 hour period, while cells treated with platelets/fresh medium or platelets/releasate move faster during the 0-6 hour period. Velocity was significant between UNT and PLT/REL (p=0.0388). Data points used in calculations were taken from Fig.3.4.

Average Velocities of Wound Edge Migration (µm/h)			
Elapsed Time (h)	**UNT**	**PLT/FM**	**PLT/REL**
0-6	13.5888	32.0836	47.1435975*
6-20	10.1263	11.7729	18.26118987
20-24	25.3892	17.6229	42.97097295

Table 3.3 Average acceleration of wound edge migration in µm/h^2: $\bar{a} = \Delta v/\Delta t$., n=3. Untreated cells experience greater acceleration during the period from 20-24 hours, while cells treated with platelets/fresh medium or platelets/releasate experience greater acceleration during the period from 0-6 hours. Cells from all treatment types experience deceleration during the time period from 6-20 hours. Data points used in calculations were taken from Fig.3.5.

Average Accelerations of Wound Edge Migration (µm/h^2)			
Elapsed Time (h)	**UNT**	**PLT/FM**	**PLT/REL**
0-6	0.88115	3.374414139	6.472150029
6-20	-0.1845	-0.931529986	-2.008744026
20-24	1.74498	2.272492254	4.641850481

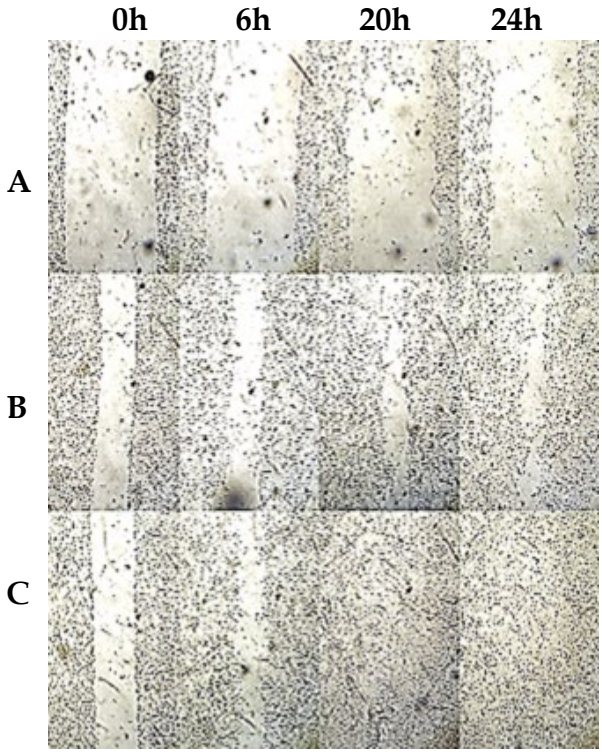

Fig. 3.11 Platelets and releasate expedite wound-healing in SK-OV-3 cells *in vitro.* **A** Untreated cells, **B** Cells treated with platelets and fresh medium, **C** Cells treated with platelets and releasate.

3.3.7 Silencing PAI-1 Inhibited Wound-healing in SK-OV-3 Cells, even in the Presence of Platelets

Photographs taken at 0h pre-wound induction and at 24h post wound induction, and analyzed using ImageJ, demonstrated that the ability of SK-OV-3 cells treated with platelets and fresh medium or treated with platelets and releasate-conditioned medium to close an induced wound was significantly inhibited *in vitro* when PAI-1 was knocked down (Figs. 3.12 and 3.13). Cells treated with a negative control prior to wound induction and receiving fresh medium post wound induction achieved an average wound closure of 17.4%. Cells treated with a negative control and platelets pre-wound induction and receiving fresh medium post wound induction achieved an average wound closure of 50%, while cells treated with a negative control and platelets pre-wound induction and receiving releasate-conditioned medium post wound induction achieved an average wound closure of 83.6%. Cells treated with PAI-1 siRNA prior to wound induction and receiving fresh medium post wound induction achieved an average wound closure of 17.4%. Cells treated with PAI-1 siRNA and platelets prior to wound induction and receiving fresh medium post wound induction achieved an average wound closure of 23.6%. Cells treated with PAI-1 siRNA and platelets prior to wound induction and receiving releasate-conditioned medium post wound induction achieved an average percent wound recovery of 20.4%. Platelets and releasate significantly expedited wound-healing in SK-OV-3 cells when compared to cells receiving fresh medium only, and cells treated with both platelets and releasate achieved significant closure when compared to cells treated with platelets and then fresh

medium. Transiently silencing PAI-1 in these same cells significantly inhibited wound closure, even in the presence of platelets and releasate.

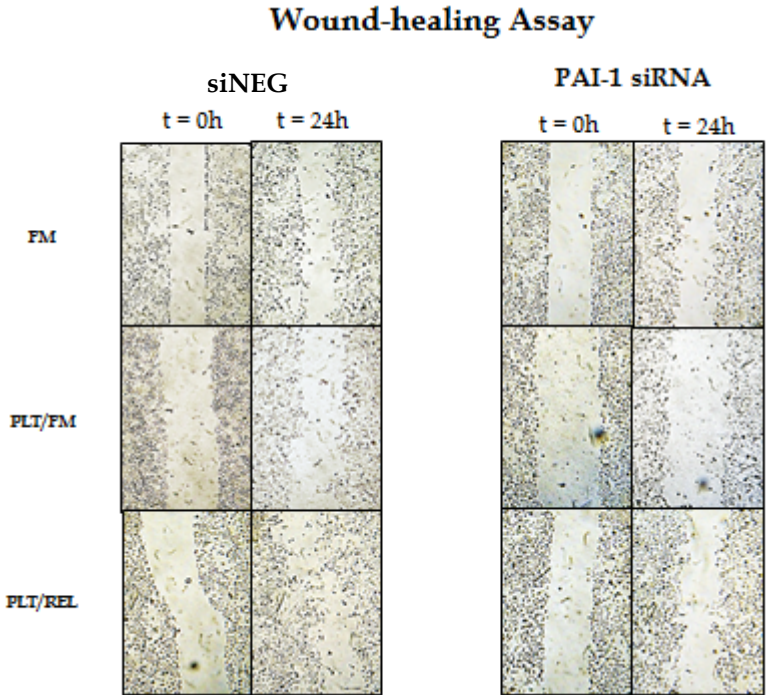

Fig. 3.12 Results of a combination knockdown/wound-healing assay demonstrate significantly inhibited wound-healing in SK-OV-3 cells treated with PAI-1 siRNA, even when pre-treated with platelets. The top row across (FM) shows cells treated with fresh medium only. The middle row across (PLT/FM) shows cells treated with platelets prior to wound induction and then with FM post wound induction. The bottom row across (PLT/REL) shows cells treated with platelets prior to wound induction and then with releasate post wound induction.

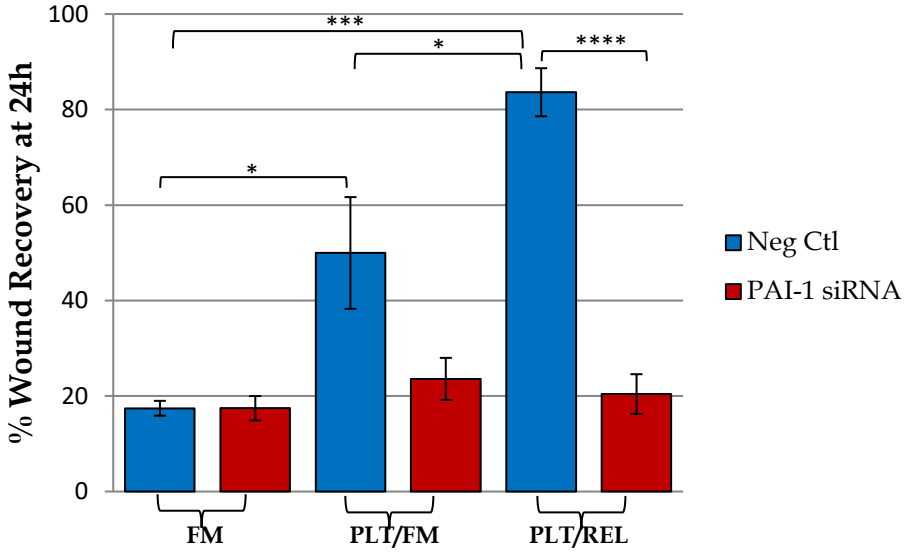

Fig. 3.13 Percent wound closure is decreased in SK-OV-3 cells treated with PAI-1 siRNA compared with cells treated with a negative control when cells are treated with platelets (PLT) prior to wound creation. The greatest difference is seen in cells treated with platelets before wound creation and with releasate (REL) after wound creation., n=3, *p<0.05, **p<0.01,***p<0.001, ****p<0.0001

3.3.8 Reducing PAI-1 inhibited the Invasiveness of SK-OV-3 Cells <u>in vitro</u>

Invasion of SK-OV-3 cells through a polyethylene terephthalate (PET) membrane coated with Engelbreth-Holm-Swarm (EHS) mouse sarcoma cell-secreted extracellular matrix (ECM) protein was significantly impeded when cells were treated with PAI-1 siRNA for 48 hours (Fig. 3.14) as compared to cells treated with an inert negative control (siNEG), with a reduction from 94.97% to 47.7% ($p = 0.008$). Fig. 3.15D clearly illustrates the reduced capacity of SK-OV-3 cells to invade through ECM when treated with PAI-1 siRNA. There was no significant difference in invasion between untreated cells and cells treated with siNEG (data not shown).

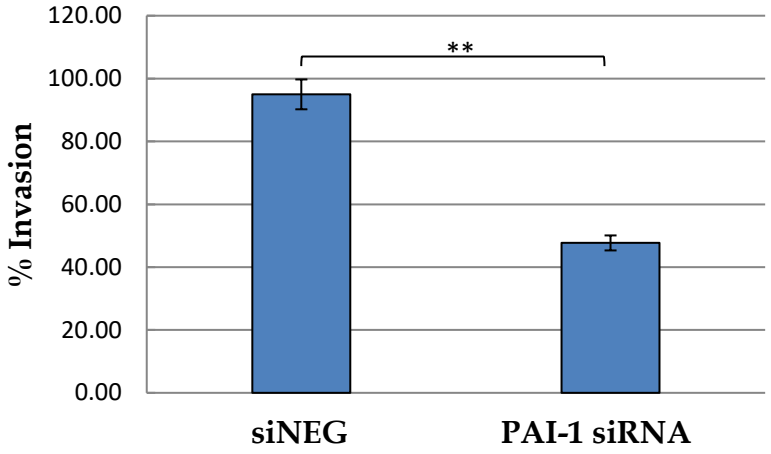

Fig. 3.14 Cells treated with PAI-1 siRNA were 47.7% less invasive than cells treated with a negative control (n=3). **p<0.01

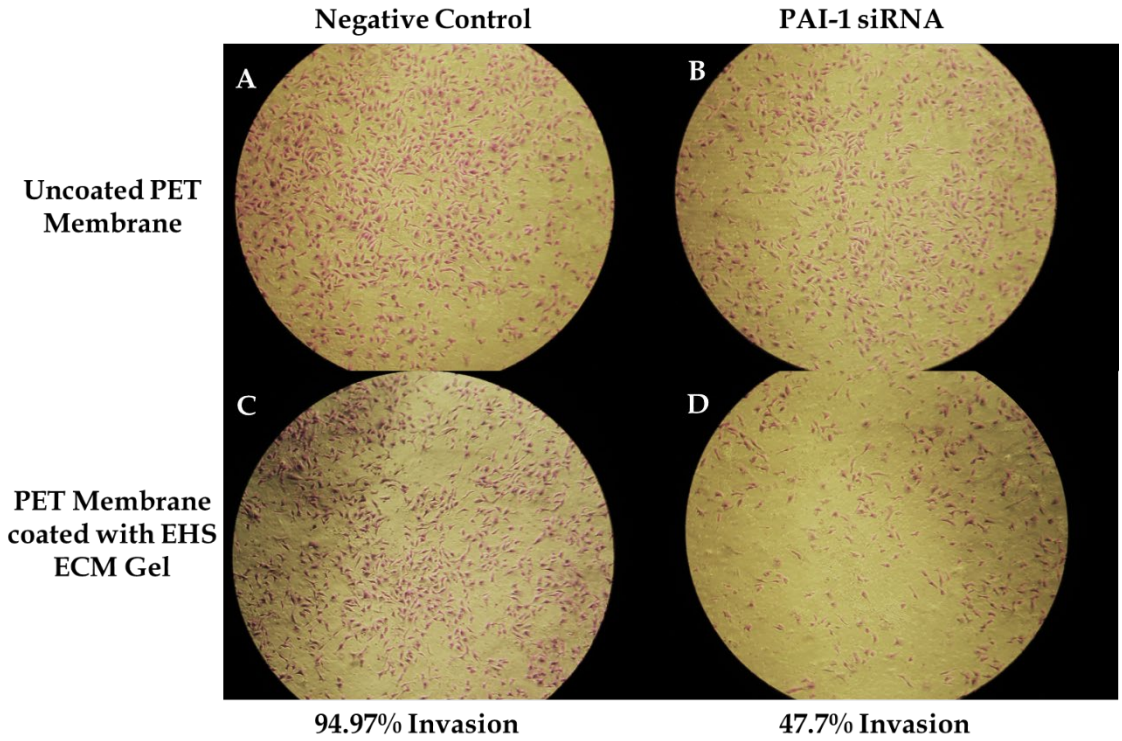

Fig. 3.15 Stained SK-OV-3 cells fixed to the basolateral side of a polyethylene terephthalate (PET) membranes at 40x: **A.** Cells treated with siNEG pass through an uncoated control PET membrane, **B.** Cells treated with PAI-1 siRNA pass through an uncoated control PET membrane, **C.** Cells treated with siNEG pass through a PET membrane coated with Engelbreth-Holm-Swarm (EHS) mouse sarcoma cell-secreted ECM protein, and **D.** Cells treated with PAI-1 siRNA pass through a PET membrane coated with EHS mouse sarcoma cell-secreted ECM protein.

3.3.9 Platelets increased Invasion in SK-OV-3 Cells

SK-OV-3 cells treated with PAI-1 siRNA were observed to be 42% less invasive than cells treated with an inert negative control (Figs. 3.16, 3.17), and these results were both significant and similar to those shown in section 3.3.8. The addition of platelets to both treatment types did increase the invasiveness of cells in both treatment groups, but these results were not significant.

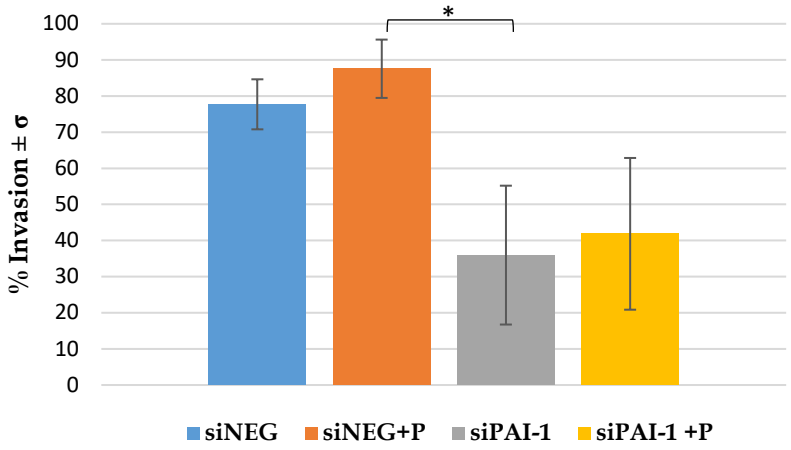

Fig. 3.16 SK-OV-3 cells treated with PAI-1 siRNA are 42% less invasive than those treated with an inert negative control siRNA (siNEG). Data are shown as mean value + SD, n=3, p = 0.0012. *p<0.05

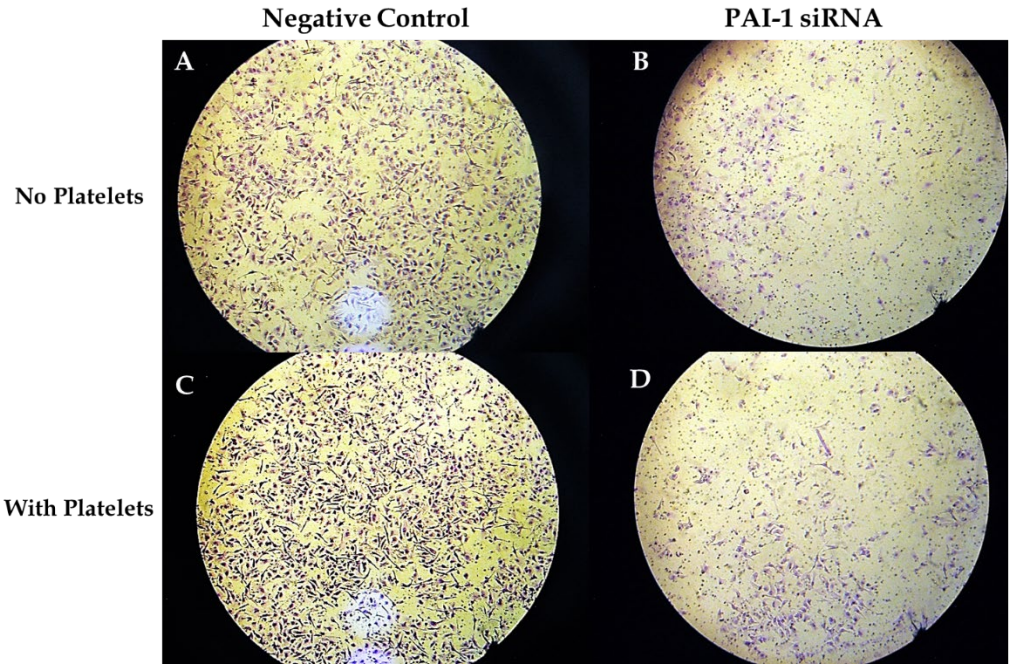

Fig. 3.17 A.SK-OV-3 cells treated with 10nM siNEG, B. SK-OV-3 cells treated with 10nM PAI-1 siRNA, C. SK-OV-3 cells treated with 10nM siNEG and platelets, D. SK-OV-3 cells treated with 10nM PAI-1 siRNA and platelets. All images at 40x.

3.3.10 Platelets and their Releasate increased Mitosis in SK-OV-3 Cells

The proportion of cells in each phase across treatment types was practically identical at t=0h (Fig 3.18 A, B, C), with the untreated cells (UNT) (Fig. 3.18A) having slightly more cells in G2 at this time, but not significantly more than either the platelet and fresh medium-treated group (PLT/FM) (Fig.3.18B) or the platelet and releasate-treated group (PLT/REL) (Fig. 3.18C). The majority of cells in all groups were in the G_0/G_1 resting phase, and this was expected. There were no significant differences in specific cell-cycle percentages among the treatment groups at the starting point, as demonstrated in the histograms in Fig. 3.18. Figs. 3.18-3.21 show histograms created in FlowJo (BD, USA) using data from one sample set. As with any cell cycle analysis, populations are not always perfectly defined, and overlap may occur between G_0/ G_1 and S phases, and also between S and G_2/M phases. For this reason, the percentages in these figures may not add up to exactly 100%. Other software packages are able to generate histograms, but do not define the populations, which can then be difficult to discern from a visual representation alone. FlowJo was thusly determined to be the best software available for this type of analysis.

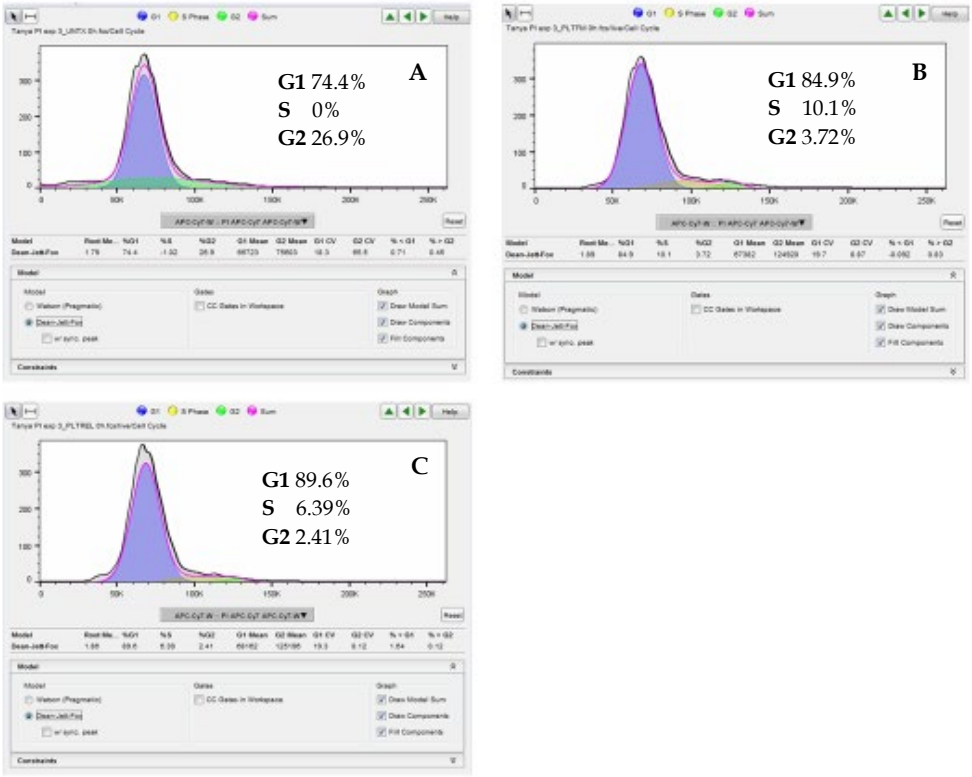

Fig. 3.18 t = 0h, histograms of sample set 1 **A.** UNT **B.** PLT/FM **C.** PLT/REL. G1 is seen in blue, S in yellow, and G2 in green.

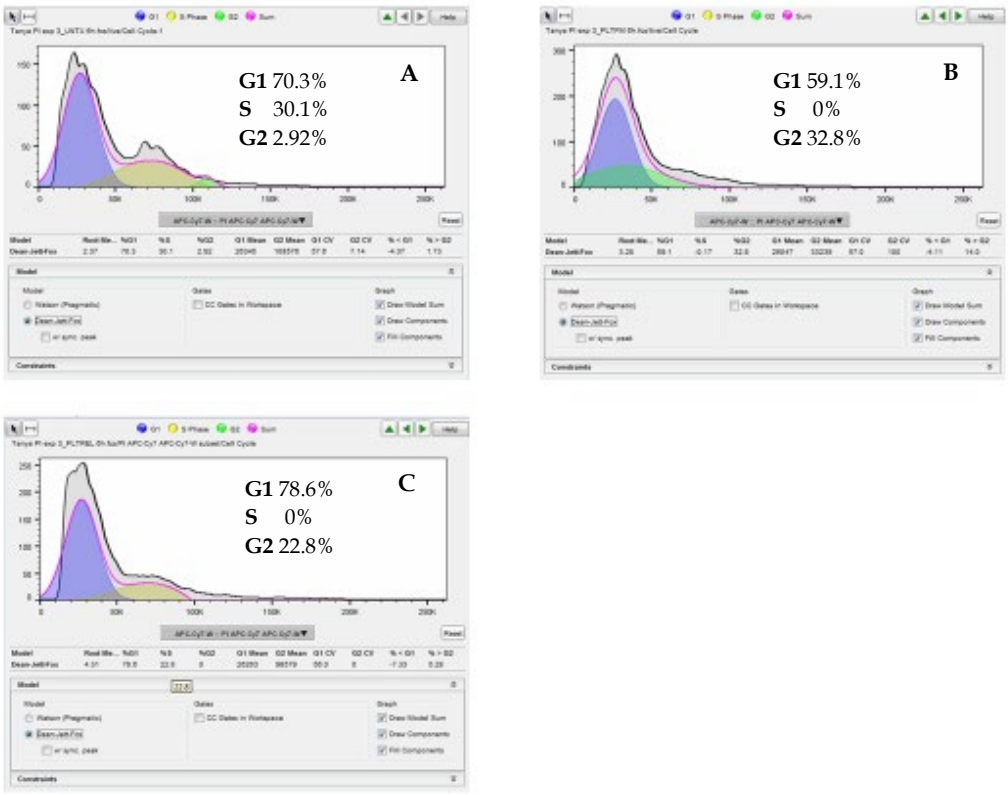

Fig. 3.19 t = 6h, histograms of sample set 1 **A.** UNT **B.** PLT/FM **C.** PLT/REL. G1 is seen in blue, S in yellow, and G2 in green.

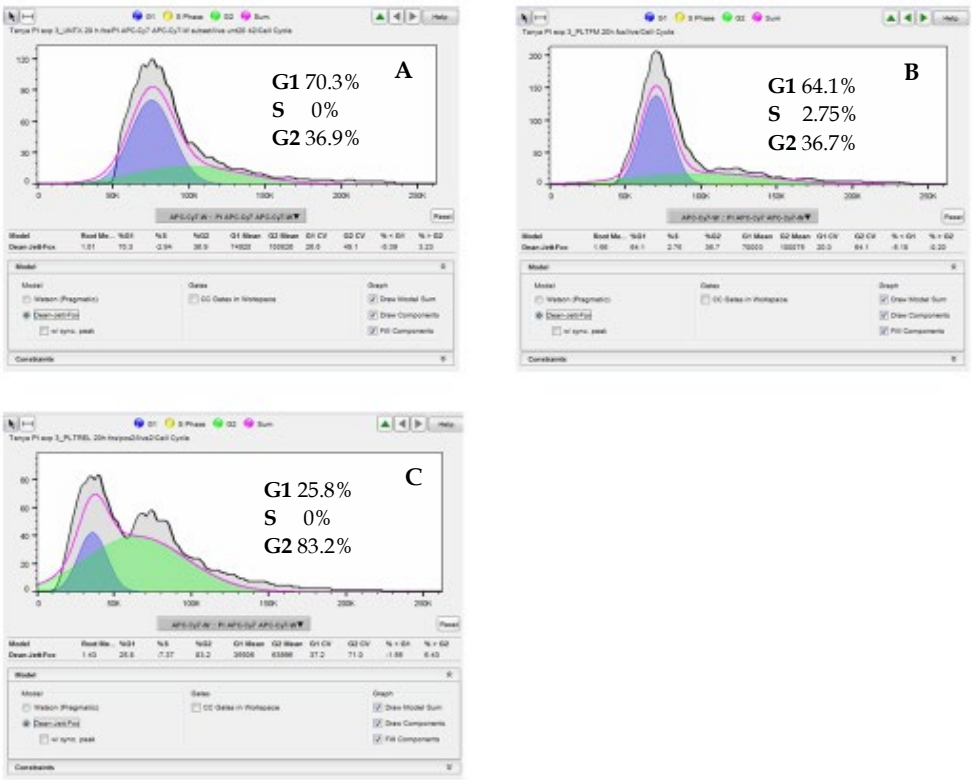

Fig. 3.20 t = 20h, histograms of sample set 1 **A.** UNT **B.** PLT/FM **C.** PLT/REL. G1 is seen in blue, S in yellow, and G2 in green.

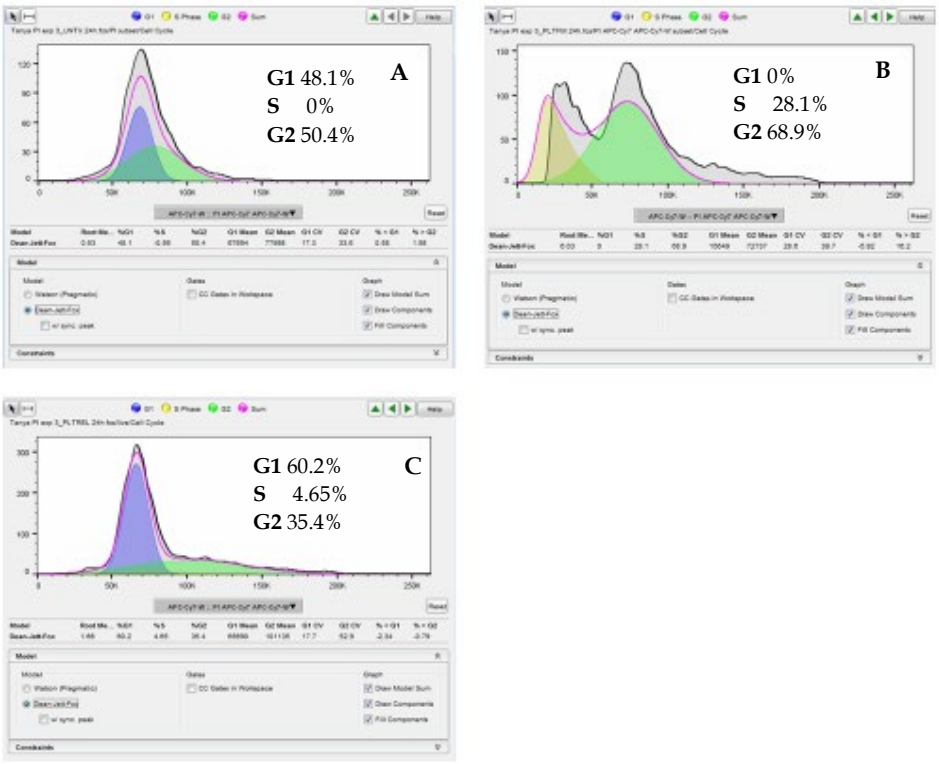

Fig. 3.21 t = 24h, histograms of sample set 1 **A.** UNT **B.** PLT/FM **C.** PLT/REL. G1 is seen in blue, S in yellow, and G2 in green.

At t=6h, there were equal percentages of cells in the G_0/G_1 population across treatment types (Fig. 3.19 A, B, C), and the majority of each cell population in all three groups remained in this phase. There were virtually no cells in S phase in either UNT (Fig. 3.19 A) or PLT/FM cells (Fig. 3.19 B), and approximately 14% of cells in the PLT/REL group were in S phase (Fig. 3.19 C). Roughly 10% of cells comprised the G_2 population in both the UNT and PLT/REL groups, however this was increased to approximately 25% in the PLT/FM group. There was no significance between any two treatment groups for any cell-phase population at t=6.

At t=20, we saw UNT and PLT/FM cells still maintaining a fairly consistent and equal percentage of cells in G_0/G_1 (Fig. 3.20 A, B). Cells in S

phase across all groups were similar at less than 10%. The percentage of cells in G_0/G_1 decreased in the PLT/REL group as cells in the G_2 population experienced a sharp increase (Fig. 3.20 C). Despite this stark departure from the UNT and PLT/FM treatment groups at t=20h, results remained insignificant but were trending towards significance.

At the 24h mark, there was an increase in the percentage of cells in S and G_2 phases in the UNT (Fig. 3.21 A) and PLT/FM (Fig. 3.21 B) groups, as indicated by the positive slope between t=20h and t=24h, with a decrease in the percentage of cells in G_1, as indicated by the negative slope between t=20h and t=24h. In the PLT/REL group (Fig. 3.21C), the opposite was true, with a decrease in the percentage of cells in S and G_2 and an increase in the percentage of cells in G_1.

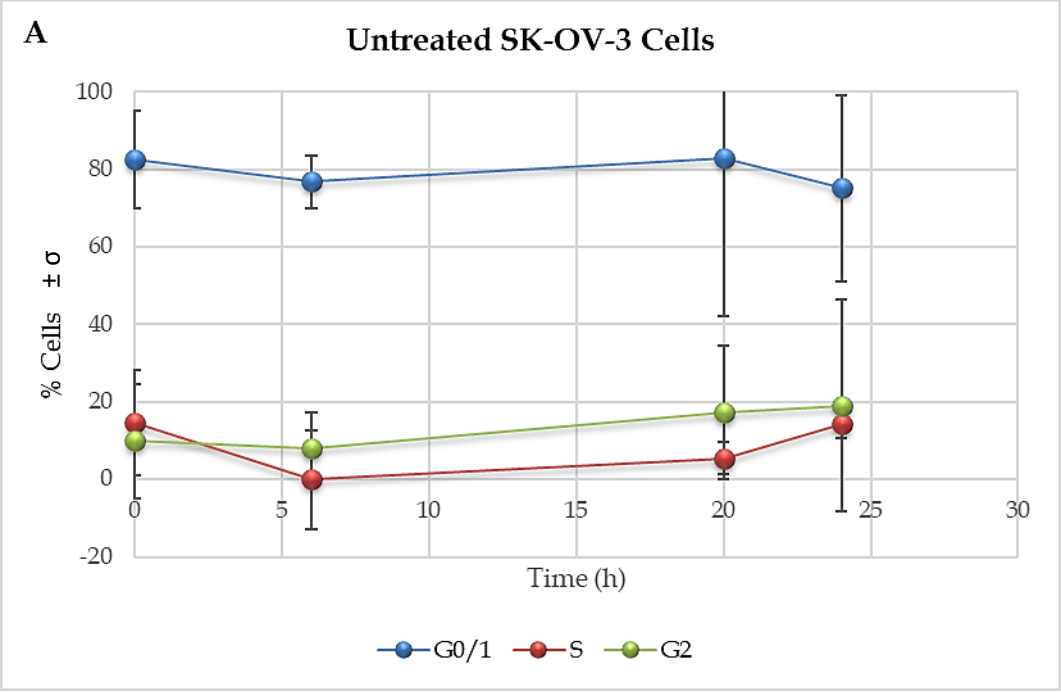

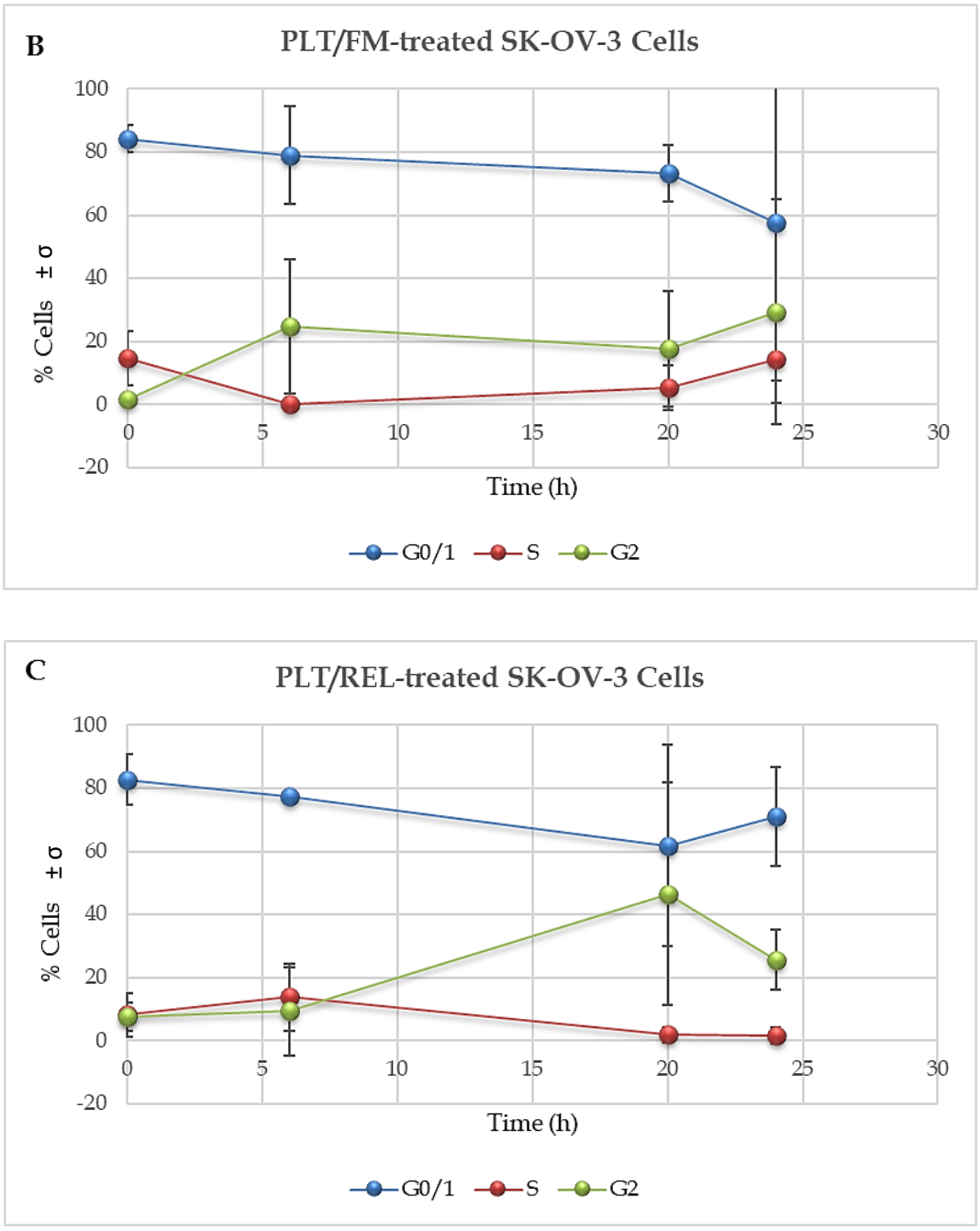

Fig. 3.22 A. Percentage of untreated cells in G_1 (blue), S (red), and G_2 (green) phases. **B.** Percentage of cells treated with platelets and then fresh medium in G_1 (blue), S (red), and G_2 (green) phases. **C.** Percentage of cells treated with platelets and platelet releasate in G_1 (blue), S (red), and G_2 (green) phases. n = 3 for all 3 graphs.

3.4 Discussion

The objective of the research presented in this chapter was to investigate the function of platelets and PAI-1 within the context of epithelial ovarian cancer (EOC), with specific regard to a platelet-driven increase of PAI-1 in EOC cells and in CTCs, as this model may have implications for CTCs *in vivo*. It was our goal to demonstrate that platelet PAI-1 directly impacts wound-healing, migration, invasion, proliferation, and metastasis in EOC. Our objective was further demonstrated by the significant loss of these cancer-cell characteristics when PAI-1 is transiently silenced with a targeted siRNA.

3.4.1 Platelets increase PAI-1 in SK-OV-3 Cells at mRNA and Protein Levels

Platelets have been shown to be a major driver of PAI-1 in cloaked cells (Cooke *et al*, 2015), and this is supported by the results shown in section 3.3.2. SK-OV-3 cells themselves contain high levels of PAI-1 (Brogren *et al*, 2011), and together with platelets this may provide an anti-apoptotic environment compatible with proliferation, migration, invasion, and subsequent metastasis. As PAI-1 has been shown to influence apoptosis via inhibition of caspase-3 (Schneider *et al*, 2008), an increase in PAI-1 in the microtumour environment as well as in the circulation may contribute to tumour cell survival at the tumour origin, in the circulation, and at distant sites of metastasis.

3.4.2 Silencing of PAI-1 in SK-OV-3 Cells

PAI-1 is significantly reduced at both the mRNA and protein level when SK-OV-3 cells are treated with siRNA, as demonstrated by results in section 3.3.3. The loss of motility, adhesion, migration, and invasion that accompany the loss of PAI-1, as demonstrated throughout the results in section 3.3,

supports existing research in which PAI-1 is shown to be integral to the maintenance of the ECM, to cell-cell adhesion, and to tumour progression (Isogai *et al*, 2001; Kwaan *et al*, 2019; Lee *et al*, 2005; Pappot *et al*, 1995).

Previous work by our group has shown that PAI-1 is a key driver of EMT, and that its functionality may be interlinked with many other genes, including TGF-ß, PLEK2, CLCX2 (Spillane *et al*, submitted for publication). There is also evidence that PAI-1 may be part of a link between ß-catenin and the tetraspanin CD63 that is involved in EMT, cell adhesion and migration, and the maintenance of the ECM (Seubert *et al*, 2014). A CD63 knockdown reduced ß-catenin as well as its downstream targets MMP-2 and PAI-1 in ovarian cancer cells *in vitro* and *in vivo*, and was shown to help maintain an epithelial phenotype in these cells, whereas an increase of CD63 was shown to contribute to tumour aggressiveness (Seubert *et al*, 2014). It stands to reason that if decreasing CD63 decreases PAI-1, then conversely an increase in PAI-1 may lead to an increase in CD63 and thereby contribute to tumour progression and metastasis.

The results in section 3.3.3 show that PAI-1 can be silenced, and results throughout section 3.3 demonstrate that silencing this gene produces a change in phenotype that is counterintuitive to ovarian cancer progression.

In addition to examining the phenotypic effects of silencing PAI-1 on SK-OV-3 cells, RNA-Seq was performed on 3 sample sets where cells are treated with PAI-1 siRNA, platelets, neither, or both to investigate any changes that may occur in the transcriptome. This will be discussed in Chapter 4, and will

enable us to gain a clearer picture of the effects of PAI-1 on differential gene expression, and may help to elucidate its position in relevant signaling cascades.

3.4.3 Evaluation of the Effect of Platelets on Cancer Cells when PAI-1 is Silenced

Platelets were utilised in many assays in this thesis to investigate their effects on ovarian cancer cells. This included assays where PAI-1 was transiently silenced via transfection with siRNA. Although PAI-1 mRNA and protein were both increased when platelets were added to cells where PAI-1 had been silenced, as shown in section 3.3.4, the recovery provided by the platelets was not sufficient to bring those levels back to normal (Fig. 3.8). This suggests that platelet PAI-1 alone is not able to recover a loss of intracellular PAI-1, and that there is an interdependent relationship between the two that is necessary to drive the metastatic phenotype. Knocking down PAI-1 produces a massive effect on the functionality of PAI-1 in the cell – and the cells themselves - even in the presence of platelets, which are a source of PAI-1.

As demonstrated by results throughout section 3.3, PAI-1 is crucial to cell motility, wound-healing, migration, and invasion. Knocking down PAI-1 significantly inhibits the ability of ovarian cancer cells to perform these functions, which are integral to maintaining the tumour and its microenvironment. Platelets, while a rich source of PAI-1, are not solely capable of providing enough PAI-1 to recover these cell functions in cells where PAI-1 has been lost. Therefore, it is clear that it is the relationship between the

platelets and the cancer cells that is primarily responsible for the maintenance of PAI-1 in the tumour microenvironment, and that this may occur by *de novo* synthesis of PAI-1 in the platelets (Brogren *et al*, 2004), by a positive feedback mechanism involving platelet PAI-1 as a transcription factor (TF) for intracellular PAI-1 in the cancer cell, or by a combination of both.

3.4.4 Platelets increase intracellular PAI-1 in SK-OV-3 cells in vitro, and transiently silencing PAI-1 decreases intracellular PAI-1

Immunofluorescence staining with anti-PAI-1 monoclonal antibody mAb-33H1F7 clearly demonstrates an increase in intracellular PAI-1 when EOC cells are treated with platelets, as seen in section 3.3.5 (Fig.3.9 E, F). It also demonstrates an observable loss of intracellular PAI-1 when those same cells are transfected with PAI-1 siRNA (Fig. 3.9 C, G). This supports the hypothesis of a TF and/or positive feedback mechanism for PAI-1 created in the cancer cell by the presence of the platelets, and potentially by platelet PAI-1 (Fig. 3.23). This is particularly important in the context of circulating tumour cells.

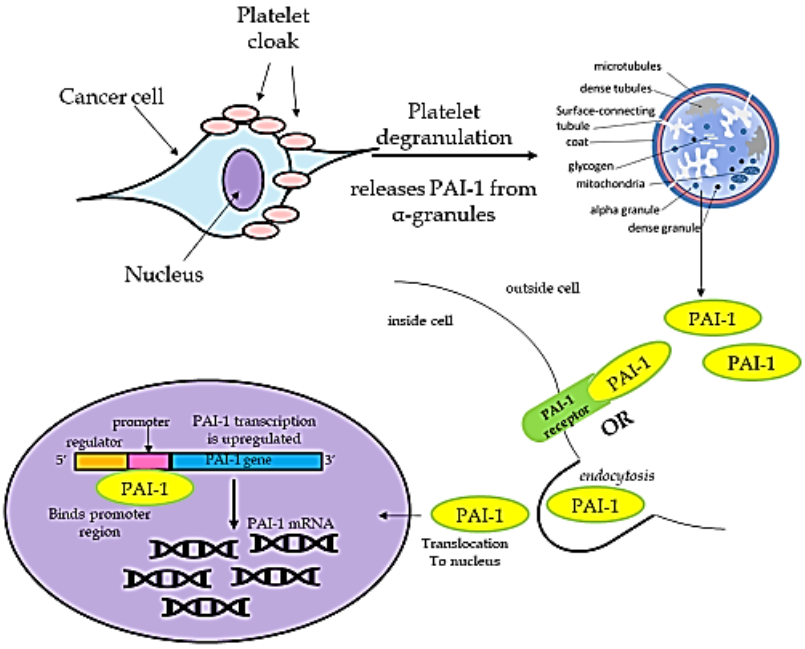

Fig. 3.23 Possible upregulation of PAI-1 induced by platelet PAI-1 as a direct result of platelet cloaking of CTCs. (Platelet diagram picture only is by Dr Graham Beards - Own work, CC BY-SA 3.0, https://commons.wikimedia.org/w/index.php?curid=21906052)

However, this leads to a primary question: if platelet PAI-1 is a TF for PAI-1 in the cancer cell, then what is the mechanism that enables platelets to drive the increase in PAI-1 in the cancer cell? There are several possibilities. Platelets degranulate and release PAI-1, and some of that PAI-1 is going to complex with vitronectin, but not all of it. Some of it may be taken up by the CTCs. One possible mechanism is that the platelet membranes merge with cell membranes and release some contents into the cell by membrane fusion. This could release PAI-1 protein, or PAI-1 mRNA into CTCs. A second possibility is horizontal transfer of mRNA with no membrane fusion, but this would require a transmembrane channel in the phospholipid bilayer through which the mRNA could enter the CTC, a lipid extracellular microvesicle that could encapsulate the mRNAs, or a carrier molecule such as an ion. As PAI-1 is a glycoprotein, it

seems much more likely that it would have an easier time binding to and crossing the plasma membrane in this form rather than as a negatively-charged transcript.

Other possible mechanisms exist, for example when the uPA/uPAR/PAI-1 complex is endocytosed during cell migration, the uPA and PAI-1 are typically tagged for proteasomal degradation, but perhaps there is an intracellular malfunction where the PAI-1 is not being tagged. Perhaps this is a chemically-stimulated process analogous to how the hypoxic tumour environment inhibits the degradation of HIF-1α. It is also possible that PAI-1 protein or mRNA are being directly endocytosed along with TGF-ß, PDGF, and other coagulation factors from the platelets, or there could be an undiscovered PAI-1 receptor or transmembrane protein that functions as a receptor. These unanswered questions along with these results indicate that further research is warranted into platelet PAI-1 and its contribution to the metastatic phenotype in EOC.

3.4.5 Platelets and their Releasate expedite Wound-healing in SK-OV-3 Cells in vitro

Calculating rates of wound closure, average velocities and accelerations for each time period and cell treatment type yielded three consistent sets of data (Tables 3.1, 3.2, 3.3), as shown in section 3.3.6. This made it possible to map out migration/wound-healing rates in EOC cells, and demonstrated that platelet activation and continuous exposure to platelet releasate directly affect cell migration and wound-healing in these cells.

It might appear at first, according to Fig. 3.10 A, that in cells treated with platelets prior to wound introduction, there is very little difference in the amount of wound recovery and wound edge migration achieved between cells receiving fresh medium and those receiving platelet releasate after wound introduction. However, charting the accelerations of wound edge migration (Fig. 3.10 B) tells a different tale. Sharp increases in velocity from 0-6h are seen both in cells treated with platelets and then fresh medium and cells treated with platelets and then releasate, yet there is a marked difference in the acceleration of the latter, being twice that of the former (Fig. 3.10 B). This suggests that it is not merely platelet degranulation that affects migration and wound recovery in these cells in the short term, but that continued exposure to the platelet releasate plays a fundamental role over a longer period of time, and supports previous research by Egan and colleagues which found that platelets and their releasate are able to mediate pro-survival signaling in ovarian tumour cells (Egan *et al,* 2011).

When cells are wounded, the wounded cells signal surrounding cells to invade and assist with repair (Bleaken *et al*, 2016). This is true of both injury and tumour progression (Harold F. Dvorak, 1986; Kalluri and Zeisberg, 2006). Platelets increase the ability of wounded cells to recover, as demonstrated by a sharp acceleration in growth from 0-6h (Fig. 3.10 B). This shows the ability of platelets to accelerate wound healing, and supports the hypothesis that platelet activation and degranulation accelerates the growth and subsequent migration of these tumour cells, much in the same way they would assist in wound-

healing *in vivo*. As platelet degranulation releases PAI-1, this strongly suggests that PAI-1 from the platelets is involved in wound-healing and migration processes, not only by direct exposure to the protein itself, but also possibly by horizontal transfer of functional PAI-1 mRNA transcripts to other cells (Kirschbaum *et al*, 2015; Spillane *et al*, submitted for publication). As described in above sections, this could in turn increase transcription and subsequent translation of PAI-1 by the SK-OV-3 cells themselves, and also supports the hypothesis of a positive feedback mechanism in which PAI-1 acts as a transcription factor for itself. The increase in PAI-1 when platelets are added to ovarian cancer cells demonstrated by RT-qPCR also provides support for this. The same number of platelets added to the tissue culture wells were tested alone by RT-qPCR, which did not yield enough PAI-1 mRNA to emit a signal (Spillane *et al*, submitted for publication), showing that the PAI-1 mRNA readings from the platelet-treated cells are not merely the result of the presence of the platelets, but are the result of an interaction between the platelets and the cancer cells. This strongly suggests that there is a component in the platelet that is serving as a TF for PAI-1 in the cloaked CTCs, and there is evidence to suggest that this is PAI-1 itself.

3.4.6 Silencing PAI-1 Inhibits Wound-healing in SK-OV-3 Cells even in the Presence of Platelets

Silencing PAI-1 in SK-OV-3 cells prior to induction of a "wound" resulted in a reduced capacity for wound recovery in these cells. These results are shown in section 3.3.7. As seen in the previous wound-healing assays

where PAI-1 was not inhibited (section 3.3.6), untreated cells recovered from an induced "wound" neither as quickly nor as completely as cells treated with platelets/fresh medium, or as those treated with platelets/releasate. However, cells treated with PAI-1 siRNA prior to wound induction were unable to achieve the same level of wound recovery, even when treated with platelets/fresh medium or platelets/releasate. These data further support that PAI-1 is fundamental to epithelial ovarian tumor progression and metastasis.

Stromal PAI-1 has been shown to protect tumours from uPA-mediated degradation via the inhibition of fibrinolysis (Pappot *et al*, 1995). This was surprising, given the pro-tumourigenic contribution of uPA to angiogenesis, invasion, and metastasis (Placencio and DeClerck, 2015). PAI-1 has been implicated in the inhibition of apoptosis (Placencio and DeClerck, 2015), and the dysregulation of tumour cell growth via p53 (Kunz *et al*, 1995; Shetty *et al,* 2008). There is evidence for TGF-ß, IL-6, and TNF-α stimulation of PAI-1 production in the tumour microenvironment (Placencio and DeClerck, 2015), and DNA elements termed CAGA boxes in the PAI-1 promoter region that interact with Smad3 and Smad4 and mediate TGF-ß's ability to regulate transcription of PAI-1 have been identified (Dennler *et al*, 1998). In this process, threonine-kinase receptor II phosphorylates threonine-kinase receptor I upon binding of TGF-ß. This in turn phosphorylates Smad3, which forms a heteromeric complex with Smad4, translocates to the nucleus, and binds the CAGA boxes of the PAI-1 promoter region to induce transcription of PAI-1 mRNA (Fig. 3.24). Mutations in these CAGA boxes were shown to completely

inhibit TGF-ß response, making a functional PAI-1 promoter region as essential to TGF-ß as TGF-ß is to PAI-1 (Dennler *et al*, 1998). This symbiotic regulatory relationship lends itself to support of our hypothesis that PAI-1 is a key regulatory protein in tumour progression and the metastatic process.

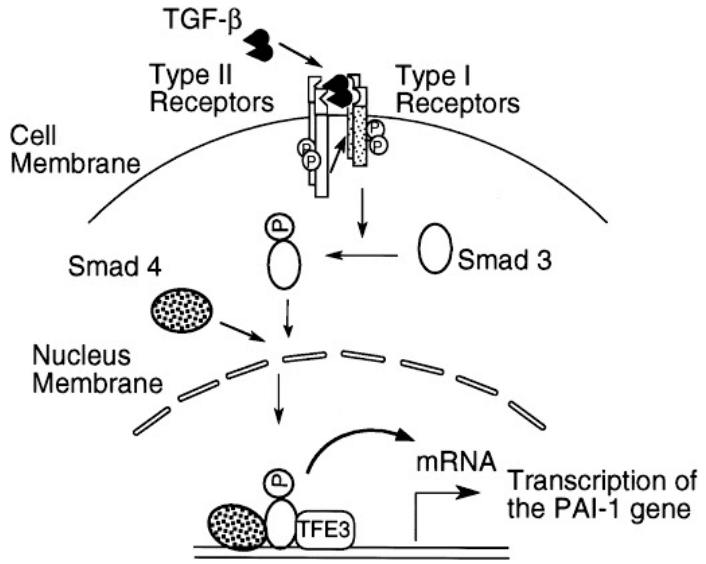

Fig. 3.24 TGF-ß induces PAI-1 transcription (Hua *et al,* 1998).

3.4.7 Transiently silencing PAI-1 inhibits Invasion of SK-OV-3 Cells in vitro

Results from transwell invasion assays in section 3.3.8 demonstrated that silencing PAI-1 in SK-OV-3 cells significantly reduces their capacity to move through ECM, and it is this reduced capacity for invasion that suggests a reduced capacity for metastasis. This also emphasises the importance of PAI-1 in the establishment of an invasive phenotype, as PAI-1 is directly involved in ECM maintenance and cell migration and invasion.

Epithelial-mesenchymal-transition (EMT) is the process by which epithelial cells lose polarity and adopt a mesenchymal phenotype with stem-like properties. This is essential in facilitating intravasation by exfoliated

primary tumour cells, however the reverse process of MET is thought to be necessary for the actual establishment of the secondary tumour in metastasis (Liao and Yang, 2017). Cancer shares many characteristics with embryonic development, and many studies to date have interrogated cancer cells in the context of gene expression, particularly the expression of stemness markers as several of these such as ZEB1, Snail, Slug, and Notch are involved in EMT. The epithelial marker E-cadherin and mesenchymal markers vimentin and N-cadherin are also used to study EMT. EMT is characterised by the loss of adherens and tight junctions, and increased cell motility, all of which are processes in which PAI-1 is involved (Liao and Yang, 2017). Research by Xu and colleagues found that triple-negative breast cancer (TNBC) cell express elevated levels of PAI-1 as a result of EMT. This suggests that PAI-1 is an essential molecule for highly invasive breast cancers, and could easily translate into the ovarian platform (Xu *et al*, 2018).

The question remains, however, as to whether or not elevated PAI-1 induces EMT, whether or not EMT induces PAI-1 expression, or if there exists a combination of two intertwined signaling cascades in which PAI-1 serves as a "switch". Which came first? The chicken or the egg? Platelets appear to be a "missing link". They are readily available at intravasation sites, as they are drawn to sites of vascular injury including sites of angiogenesis, and they supply an "extra boost" of PAI-1 directly into that site by degranulation and also by cloaking exfoliated tumour cells as they enter the bloodstream. TGF-ß is a known inducer of PAI-1 (Dennler *et al*, 1998), and research has been

conducted concerning the elements of this pathway, but data concerning PAI-1 as an independent transcription or activation factor remains elusive.

3.4.8 Platelets increase Invasion in SK-OV-3 Cells

As shown in section 3.3.9, platelets did increase invasion in cells that were treated with siNEG, but not significantly, and platelets only very slightly increase invasion in cells where PAI-1 has been transiently silenced. This is consistent with the previous assays performed here which demonstrate that adding platelets to cells where PAI-1 has been knocked down did not enable those cells to recover full functionality with regard to migration and wound-healing.

Previous invasion assays by others have shown a significant increase in invasion in these cells, however the cells, while seeded in serum-free medium, were not serum-deprived for 24 hours prior to seeding (Cooke *et al*, 2011) due to the already invasive nature of SK-OV-3 cells. This presents a special conundrum for this cell line, which has been repeatedly demonstrated to be a good model for metastatic high-grade serous ovarian cancer. 59M cells were determined by others in our lab to not be a good model of HGSOC, and OAW42 cells were found to contain little to no PAI-1, so they would not have been a useful model here. With SK-OV-3 cells, it is possible to have a significant increase in invasion with the addition of a 1000:1 platelet ratio, as seen in Cooke's research, if the cells are *not* serum-deprived for 24 hours prior to seeding in the transwell chambers. It is also possible to have a significant loss of invasion via transfection with PAI-1 siRNA if the cells *are* serum-deprived

for 24 hours prior to seeding in the transwell chambers, as demonstrated in section 3.3.8, Fig. 3.15. It is not, however, possible to have both, and the results from these two protocols are mutually exclusive. A series of optimisations completed prior to assay performance supports this.

The importance of serum-starvation is well-documented, and it is generally accepted as standard protocol for transwell assays, including the Corning protocol used here in this research. Serum-deprivation suppresses cell proliferation that may interfere with actual migration and/or invasion, and use of this technique is a crucial component of these kinds of assays (Grada *et al*, 2016), therefore the use of serum-deprivation is justified here.

3.4.9 Cell-cycle Analysis of SK-OV-3 Cells: Platelets and their Releasate increase Mitosis

When cells are replicating, they do not migrate as demonstrated by the deceleration of the wound edge during the 6h-20h time period in the aforementioned scratch assays (section 3.3.6) on which this cell-cycle analysis is based. Flow cytometry results in section 3.3.10 show that cells treated with platelets and then platelet releasate post wound-induction (PLT/REL) have G_2 populations that correlate inversely with the deceleration of wound edge migration from 6-20 hours. Untreated cells (UNT), as well as those receiving platelets and then fresh medium (PLT/FM) post wound-induction also follow this same trend, with the percentage of PLT/REL-treated cells that are in G_2 being much higher than in the other two treatment types. This supports the hypothesis that continued exposure to the platelet releasate drives a higher rate

of completed cell replication. More cells are in S phase in PLT/REL group at t=6 because they have been exposed to the platelet releasate, which contains mitogen that has been shown to expedite clearance through cell cycle checkpoints (Giacoia *et al*, 2014).

Giacoia and colleagues found evidence that high levels of PAI-1 are associated with aggressive cancers of the bladder and cervix. He and his team demonstrated that overexpression of PAI-1 increased cell proliferation by "pushing" cells into S phase, effectively bypassing DNA mutation and repair checkpoints. Conversely, they found that PAI-1 knockdowns inhibited cellular proliferation and led to an increase in the number of cells in the G_0/ G_1 phase, and a corresponding decrease in the number of cells in S phase (Giacoia *et al*, 2014). These data along with research presented here strongly suggest that PAI-1 is not only an integral molecular gear in the machinery of tumor progression and metastasis, but also provides evidence for PAI-1 as a mitogen, and suggests that wound healing may be due as much to increased proliferation as it is to migration.

3.5 Conclusion

Results presented in this chapter support findings that PAI-1 and platelets are essential to ovarian cancer metastasis, and specifically to the establishment and maintenance of a metastatic phenotype in ovarian cancer. Research by our group has identified PAI-1 as a key factor in EMT and ovarian cancer metastasis (Cooke *et al*, 2015). This supports previous research by Labelle and colleagues, which demonstrated that platelets are integral to the

formation of early metastatic niches (Labelle *et al*, 2014), research by Giacoia pointing to PAI-1 as a mitogen (Giacoia *et al*, 2014), and also research by Mashiko and colleagues, which suggests that PAI-1 is a potential therapeutic target (Mashiko *et al*, 2015). In addition to these bodies of work, PAI-1 has been well studied for its effects on cell adhesion, ECM maintenance and remodeling, signaling, and its capacity to influence apoptosis (Schneider *et al*, 2008). The significance of the results achieved here provide a strong foundation for the investigations in the following chapters, which will examine the potential effects of increases/decreases in PAI-1 on differential gene expression in EOC cells, and also seek to examine the potential of plasma PAI-1 as diagnostic/prognostic factor in women with HGSOC.

CHAPTER 4

INTERROGATING THE ROLE OF PAI-1 AND THE CONTRIBUTION OF PLATELETS TO METASTATIC DISEASE IN AN OVARIAN CANCER CELL LINE MODEL USING RNA-SEQUENCING

4.1 Introduction

PAI-1 was previously identified using Affymetrix arrays by our group as one of the top five genes that are dysregulated when cancer cells are co-incubated with platelets. Here, the effects of silencing PAI-1 in an ovarian cancer cell model, adding platelets to cells, or both simultaneously have been investigated through the lens of RNA sequencing analysis. A loss of PAI-1 mRNA via PAI-1 siRNA in Chapter 3 resulted in the loss of both migratory and invasive phenotypic properties of SK-OV-3 cells in vitro. These data support current research demonstrating that PAI-1 is integral to ECM maintenance and remodeling, and also to cancer cell migration and invasion (Lee *et al*, 2005; Kwaan *et al*, 2019).

Results of a study by Mashiko and colleagues suggested that inhibiting PAI-1 via siRNA directly encouraged G_2/M cell-cycle arrest and subsequent apoptosis in an ovarian cancer cell line model (Mashiko *et al*, 2015). Results of a separate study by Giacoia in ovarian cancer cells found that downregulation of PAI-1 by shRNA vector or inhibition by small-molecule tiplaxtinin (PAI-039) significantly decreased cellular proliferation via cycle halting at G_0/G_1 in accordance with depletion of cyclin D3/cdk4/6 and cyclin E/cdk2. Similarly, Giacoia's study also determined that overexpression of PAI-1 promoted unchecked entry into S-phase, resulting in a significant increase in cellular proliferation (Giacoia *et al*, 2014). We also found that adding platelets to SK-OV-3 cells resulted in an increase in proliferation, which suggested a role for PAI-1 as a mitogen, or as part of a mitogenic pathway. These studies clearly

demonstrate the importance of PAI-1 in ovarian cancer cell proliferation, and could have implications for the diagnosis and treatment of ovarian cancer as discussed by Mashiko and colleagues (Mashiko *et al*, 2015).

PAI-1 expression has also been found to be associated with poor prognosis in glioblastoma multiforme (GBM). Research by Fidan Seker and colleagues demonstrated that silencing PAI-1 interfered with tumour growth and invasion in the brain, and that PAI-1 was an important element in GBM regulation (Seker *et al*, 2019).

Additionally, PAI-1 was shown to play a key role in chemoresistance – specifically carboplatin – in EOC (Pan *et al*, 2017). Pan and colleagues found that cisplatin induced PAI-1 expression in cisplatin-resistant OC cells, thereby inducing EMT. A subsequent knockdown of PAI-1 inhibited EMT in these same cells (Pan *et al*, 2017).

It is well known that TGF-ß is involved in transcriptional regulation of the SERPIN E1 gene (Dennler *et al*, 1998). There are several miRNAs that also affect regulation via binding to the 3′ UTR of SERPIN E1, including members of the miR-30 family (McCann *et al*, 2019). Low expression of miR-30c in conjunction with high expression of PAI-1 was recently found to be a predictor of decreased survival in a cohort of breast cancer patients. This same study proposed that there may be an axis that exists among TGF-ß, PAI-1, and miR-30c in the endothelial cells of the tumour vasculature that creates a "perfect storm" for angiogenesis via fibrin production pathways (McCann *et al*, 2019). Additionally, platelets have been shown to be involved in tumour growth,

angiogenesis (Egan *et al*, 2011; Isogai *et al,* 2001), induction of EMT (Labelle *et al*, 2011), intravasation, protection of tumour cells in the circulation (Egan *et al*, 2014) , and the establishment of metastatic niches at secondary sites (Labelle *et al*, 2014).

To further investigate the role of PAI-1 in ovarian cancer, and in platelet-cancer cell interactions, RNA samples isolated from three independent sets of knockdown and invasion assays were sequenced by Trinity College Dublin's TrinSeq facility using the Illumina NovaSeq 6000. Differential gene expression employing RNA-Seq has rapidly become ubiquitous in the fields of genomics and proteomics. Previous work in our laboratory, as outlined in chapter one, identified PAI-1 as one of five key drivers of platelet-CTC interactions (Spillane *et al*, submitted), where gene expression assays were performed in the form of Affymetrix microarrays. Platelet-cancer cell interactions have also been shown to be integral to the metastatic process, with TGF-ß/SMAD and NF-κB pathways in cancer cells being directly affected by these interactions (Labelle *et al*, 2011). TGF-ß/SMAD is also involved in the transcriptional regulation of the SERPIN E1 gene, and the subsequent expression of PAI-1 protein. Here we employ RNA-Seq for further verification and characterisation of PAI-1 in order to gain better insight into PAI-1's potential role in the regulation of gene expression during ovarian cancer metastasis, and the potential contribution of platelet-cancer cell interactions to this process.

4.2 Hypothesis

PAI-1 is central to the platelet-cancer cell interactome, and contributes to ovarian cancer metastasis.

4.3 Specific Aims

1. To investigate the effects of transiently silencing PAI-1 on gene expression in an ovarian cancer cell line model.

2. To investigate the contribution of platelets on ovarian cancer metastasis.

4.4 Materials and Methods

The methods used to obtain our RNA (Fig. 4.1) began with culturing of SK-OV-3 cells as described in chapter 2, section 2.1. Cells were counted and plated, PAI-1 was silenced via siRNA transfection for 24h, and donor platelets were isolated and added to plated cells for an additional 24h. These cells were subsequently used for invasion assays and PAI-1 mRNA quantitation by RT-qPCR.

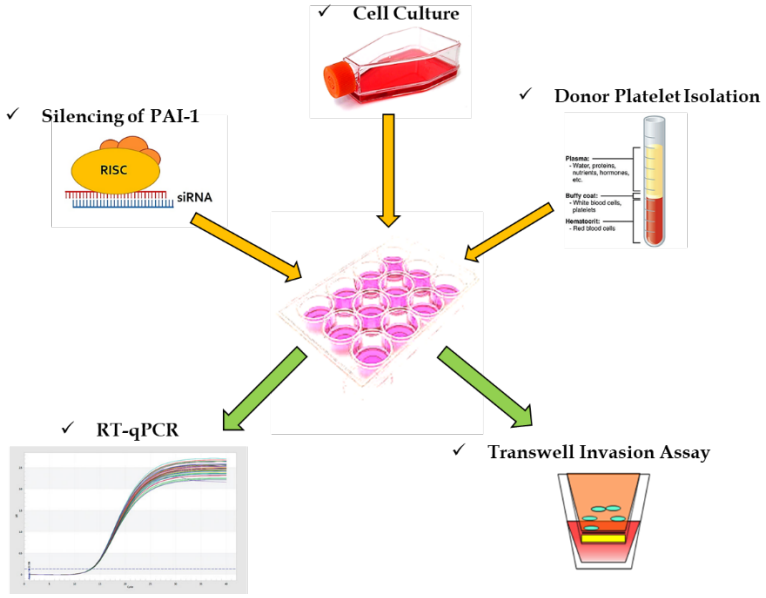

Fig. 4.1 Materials and methods diagram

4.4.1 Sample Set Generation

As described in the methods in chapter two, cell culture, PAI-1 transfection by siRNA (chapter 2, section 2.2), donor platelet isolation (chapter 2, section 2.3), invasion assay, and RT-qPCR assays were employed to obtain RNA samples for RNA-Seq analysis. Three independent sets of biological RNA

replicates were isolated. Six invasion assays were performed using six different cell passages, and also using six different platelet isolations performed specifically for each assay. RT-qPCR assays were performed on Applied Biosystems' AB7900, using Applied Biosystems' TaqMan Gene Expression Assay for SERPIN E1, with GAPDH as the "housekeeping" gene. RNA samples had been isolated using Qiagen's RNeasy Mini Kit according to the manufacturer's instructions (chapter 2, section 2.4), and quantitated using Invitrogen's Qubit™ 3.0 fluorometer with Invitrogen's Qubit™ RNA HS Assay Kit (chapter 2, section 2.4.1). All RNA samples were stored at -80°C until needed. **Two of these RT-qPCR assays were performed on RNA samples from cells grown in the same cell culture plates as each of two of our six independent invasion assays** (Fig 4.2). That is to say that ***two of the six invasion assays and two of the three RT-qPCR assays were directly linked,*** and the two sets of RNA from these linked assays accounts for two of the three sets of RNA sent to the sequencing facility. This is important because it demonstrates that the phenotype is directly linked to gene transcription. A third RT-qPCR assay was performed on RNA isolated from an independent PAI-1 knockdown assay that was not linked to an invasion assay (Fig 4.2).

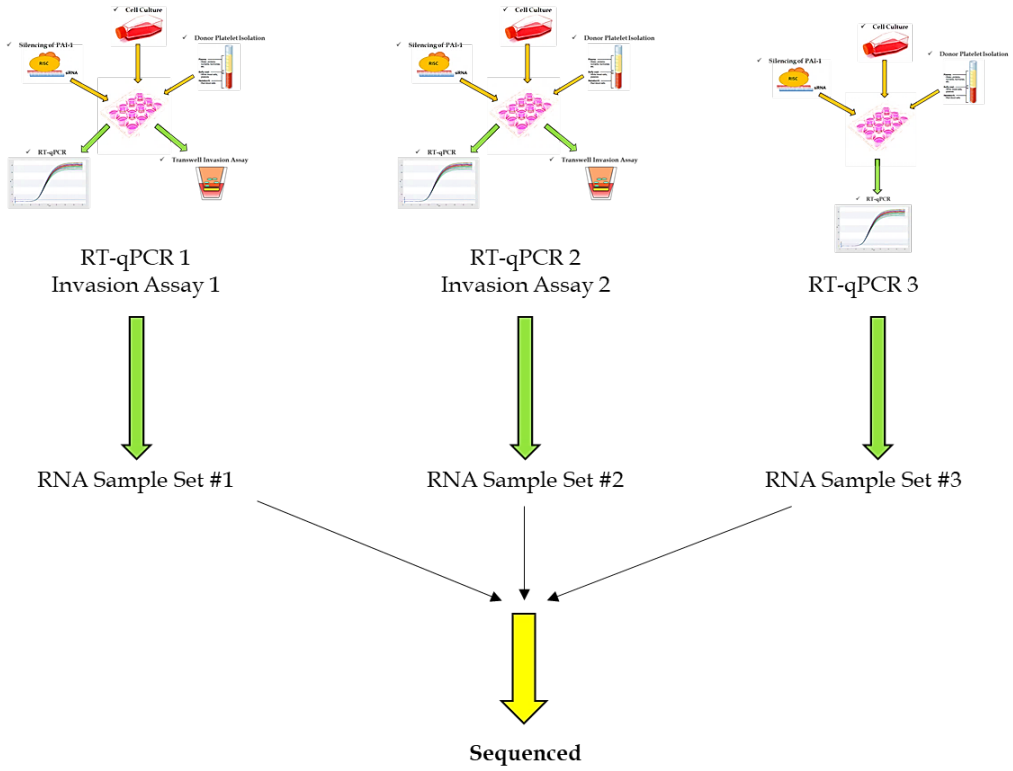

Fig. 4.2 Diagram depicting RNA sample set origin

Each set was composed of the following treatment types: untreated (UNT), treated with an inert negative control siRNA (siNEG), treated with PAI-1 siRNA (siRNA), untreated with the addition of platelets for 24h post-transfection (UNT +P), negative control with the addition of platelets for 24h post-transfection (siNEG+P), and PAI-1 siRNA treated with platelets for 24h post-transfection (siRNA +P). RT-qPCR results were log10 transformed and analysed using GraphPad Prism 8.0 to perform a one-way ANOVA with Tukey's post hoc multiple comparisons test. Invasion assay results were analysed without log10 transformation by the same methods. Previous invasion assays have demonstrated that there was no significant difference in invasion between UNT and siNEG treated cells. Samples will be referred to by their previously parenthetically referenced labels throughout this chapter.

4.4.2 Sequencing

RNA samples as described above were labeled according to the following table:

Table 4.1 Sample tube legend

Tube #	Sample	Tube #	Sample	Tube #	Sample
1	UNT 1	**7**	UNT 2	**13**	UNT 2
2	siNEG 1	**8**	siNEG 2	**14**	siNEG 3
3	siRNA 1	**9**	siRNA 2	**15**	siRNA 3
4	UNT+P 1	**10**	UNT+P 2	**16**	UNT+P 3
5	siNEG+P 1	**11**	siNEG+P 2	**17**	siNEG+P 3
6	siRNA+P 1	**12**	siRNA+P 2	**18**	siRNA+P 3

Sample sets were transported on ice to the TrinSeq facility housed at the Trinity Translational Medicine Institute (TTMI). Once received, the samples were checked for integrity by BioAnalyzer (Agilent, Santa Clara, CA USA) as outlined in chapter 2, and converted to cDNA. cDNA libraries were constructed as outlined in chapter 2. Those libraries were then enriched by poly-A+ selection and run in paired-end (PE) reads on Illumina's NovaSeq 6000 (Illumina, San Diego, CA USA) per TrinSeq's standard operating procedure (SOP).

4.4.3 Bioinformatics and Statistical Analysis

Sample reads were checked for integrity and quality by Dr. Karsten Hokamp at the Smurfit Institute of Genetics at Trinity College Dublin using

FastQC (Babraham Bioinformatics, UK), and also checked for quality and contamination against human, mouse, rat, and plasmid index genomes by myself using FastQ Screen (Steve Wingett, Babraham Bioinformatics, UK) and the Bowtie2 sequence alignment tool (Ben Langmead, Center for Computational Biology, Whiting School of Engineering, Johns Hopkins University, Baltimore, MD, USA). Sequences were then trimmed and were further corrected for potential batch effect using the negative binomial method of ComBat-Seq as described by Zhang (Zhang *et al*, 2020), and this was also performed by Dr. Hokamp.

The resulting read counts data text file obtained was then uploaded to iDEP92 (Bioinformatics, South Dakota State University, Brookings, South Dakota, USA) and analysed using siNEG-treated cells as the comparitor. iDEP92 is an analysis engine which uses DESeq2 (Love *et al*, 2014), and which employs the Benjamini-Hochberg (Benjamini, Yoaav and Yosef Hochberg, 1995) procedure for decreasing false discovery rate (FDR). To investigate any potential differences in results from read counts being normalised and subsequently analysed as an entire groups versus read counts from only one comparison – for example, our PAI-1 knockdown compared to our negative control – being normalised and analysed, three additional text files were created in which only the two treatments being compared were included. This also enabled us to look for any differences in gene expression that might be considered an off-target effect of the negative control. These were the following: siRNA versus siNEG, UNT+P versus UNT, siRNA+P versus siRNA. These are

discussed in more detail in their corresponding sections.

Analysis of transformed read counts of our PAI-1 knockdown (SK-OV-3 cells treated with PAI-1 siRNA) compared to our negative control (SK-OV-3 cells treated with an siNEG) in iDEP92 produced a DESeq2-generated list of differentially expressed genes, their Log2-transformed expression-fold change values, and their corresponding Benjamini-Hochberg adjusted p-values. This list was sorted by adjusted p-value, and only those genes demonstrating significant differential expression with adjusted p-values ≤ 0.05 were kept. The resulting list of significant genes was then sorted largest to smallest by Log2 expression-fold change. Those with positive Log2 expression-fold changes represented genes that were upregulated, while those with negative values represented genes that were downregulated. The Log2 expression-fold change values were then back-transformed by the equation $2^{|Log2|}$ resulting in actual expression-fold change values. Only those values ≥ 1.5 were considered for downstream analysis. Our iDEP92 analysis of significantly differentially expressed genes (DEGs) returned a list of genes whose comprehensive analysis was far beyond the scope of this thesis. Significant DEGs were separated into the following categories: genes that were downregulated when PAI-1 was silenced, genes that were upregulated when PAI-1 was silenced, genes that were upregulated when platelets were added to untreated cells, genes that were downregulated when platelets were added to untreated cells, genes that were upregulated when platelets were added to a PAI-1 knockdown model, and genes that were downregulated when platelets were added to a PAI-1

knockdown model. These 6 gene lists were then uploaded into ShinyGOv0.61 for further gene enrichment and pathway analysis (Bioinformatics, South Dakota State University, SD USA; Ge *et al*, 2020).

Binary alignment map (BAM) files obtained were uploaded to the Integrative Genomics Viewer (IGV – Broad Institiute, UC San Diego, CA USA), which gave a visual image of mapped reads. A BAM file is a compressed binary version of a sequence alignment map (SAM) file, which is the standard file format that is used to save alignment information regarding short reads mapped against reference sequences.

4.5 Results

4.5.1 Sample Selection

The three sets of independent biological replicates were assayed by RT-qPCR, and results showed a significant loss of PAI-1 mRNA when PAI-1 was silenced via siRNA (Fig, 4.3A, p = 0.0003), as well as a significant increase in PAI-1 mRNA when platelets were added to both untreated cells (Fig, 4.3A , p = 0.0124) and cells treated with a negative control siRNA (Fig, 4.3A ,p = 0.0143). The overall ANOVA p-value was less than 0.0001. Invasion assays demonstrated a significant loss of the invasive phenotype when PAI-1 was silenced with siRNA (Fig. 4.3B, p = 0.0033), with an overall ANOVA p-value of 0.0002.

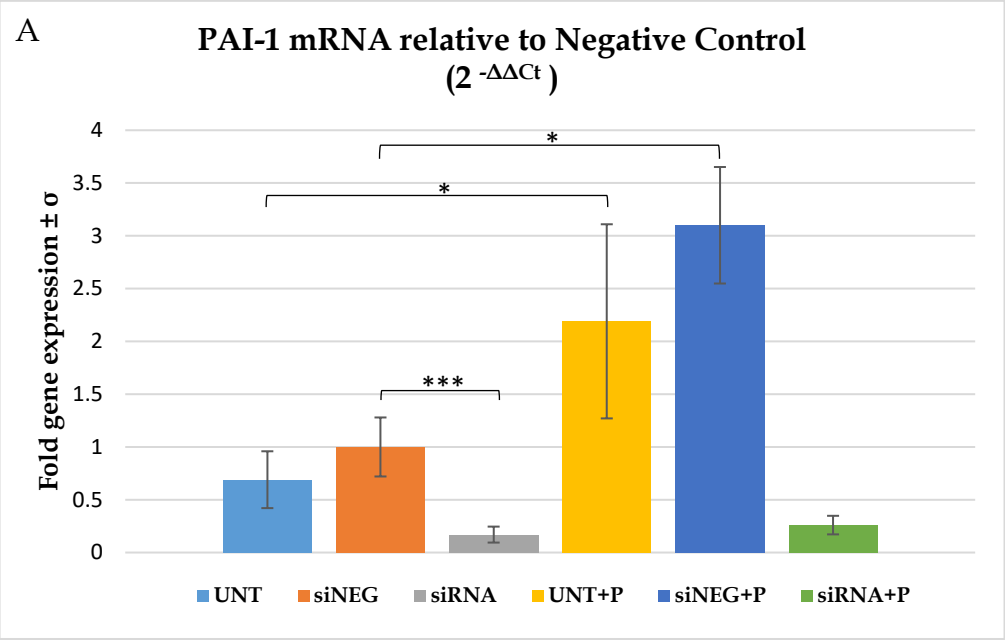

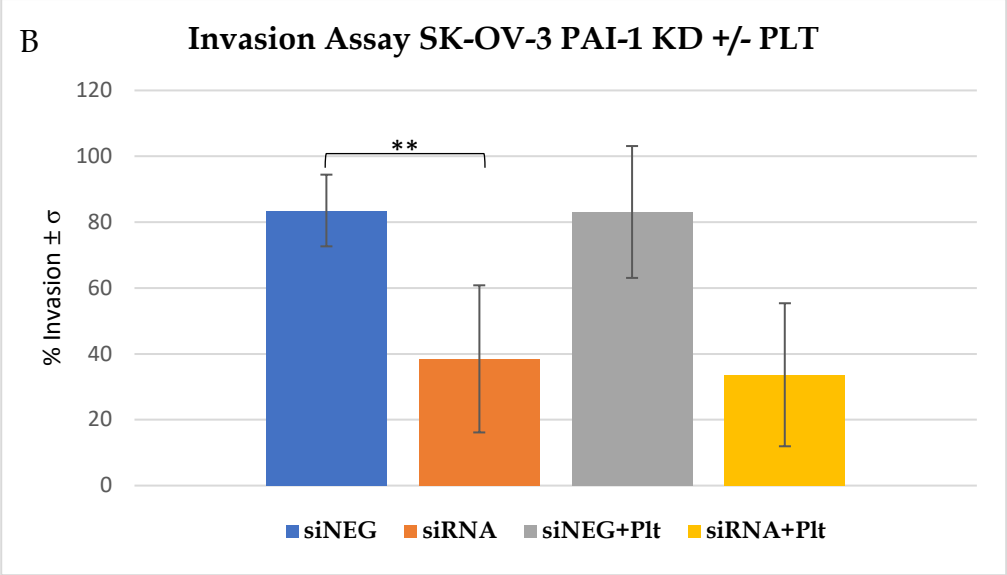

Fig. 4.3 A RT-qPCR of samples sent for RNA-Sequencing, n=3, overall p-value < 0.0001, **B** Percent invasion of pooled samples, including those sent for RNA-Sequencing, n=6, overall p-value = 0.0002 *p ≤ 0.05, **p ≤ 0.01, ***p ≤ 0.001

4.5.2 Sample Quality Control

All samples were deemed by TrinSeq to be of excellent RNA integrity (Fig. 4.4) and subsequent DNA libraries were also of excellent quality (Table 4.2). Resulting reads were mapped to GRCh38 using FastQ Screen (Babraham Bioinformatics, UK) and Bowtie2 (Johns Hopkins University, Baltimore, MD, USA), and were not found to contain any contamination by non-human genomes (Fig. 4.5). Total read counts before and after normalisation within DESeq2 are shown in Fig. 4.6.

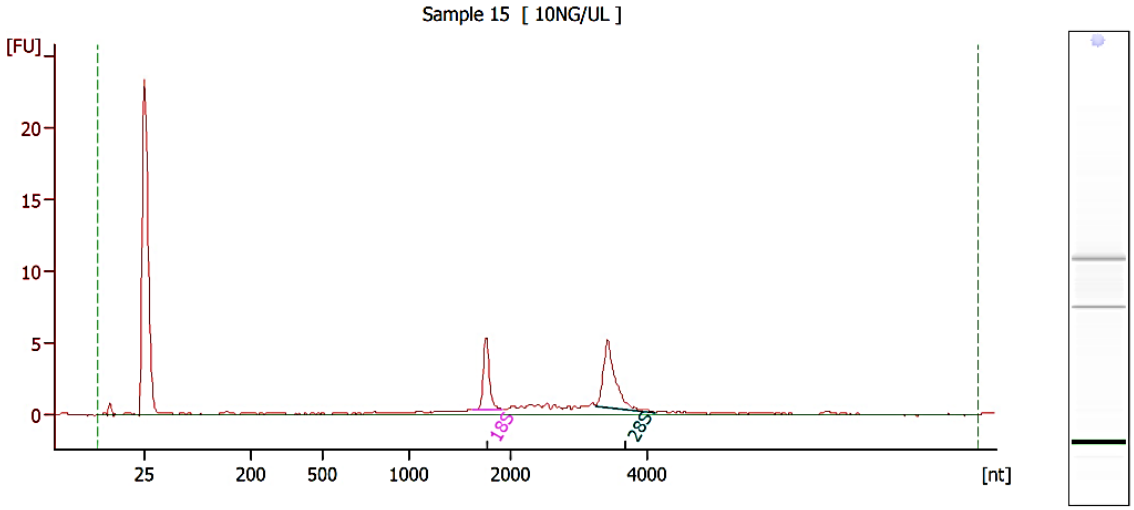

Fig. 4.4 Example of Bioanalyzer results demonstrating RNA integrity

Table 4.2 Sample DNA library QC

Sample No	Sample ID	ng/ul	size in bp	nM DNA
1	UNT1	41.5	450	142.1
2	siNEG1	36.3	450	124.3
3	siRNA1	33.4	450	114.4
4	UNT+P1	38.4	450	131.5
5	siNEG+P1	35.8	450	122.6
6	siRNA+P1	35.8	450	122.6
7	UNT2	38.5	450	131.8
8	siNEG2	37.3	450	127.7
9	siRNA2	36.7	450	125.7
10	UNT+P2	37.5	450	128.4
11	siNEG+P2	36.4	450	124.6
12	siRNA+P2	39.4	450	134.9
13	UNT3	35.9	450	122.9
14	siNEG3	38	450	130.1
15	siRNA3	39.5	450	135.3
16	UNT+P3	41.5	450	142.1
17	siNEG+P3	40.7	450	139.4
18	siRNA+P3	40.9	450	140.0

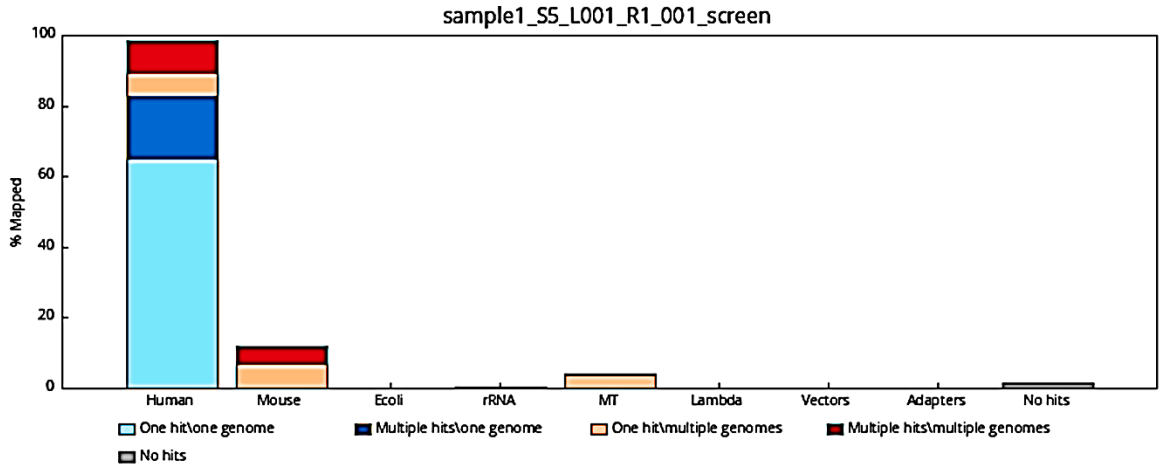

Fig. 4.5 Genome alignment to GRCh38 of Sample 1 using FastQ Screen and Bowtie2 shows no contamination by other genomes. (Babraham Bioinformatics, UK)

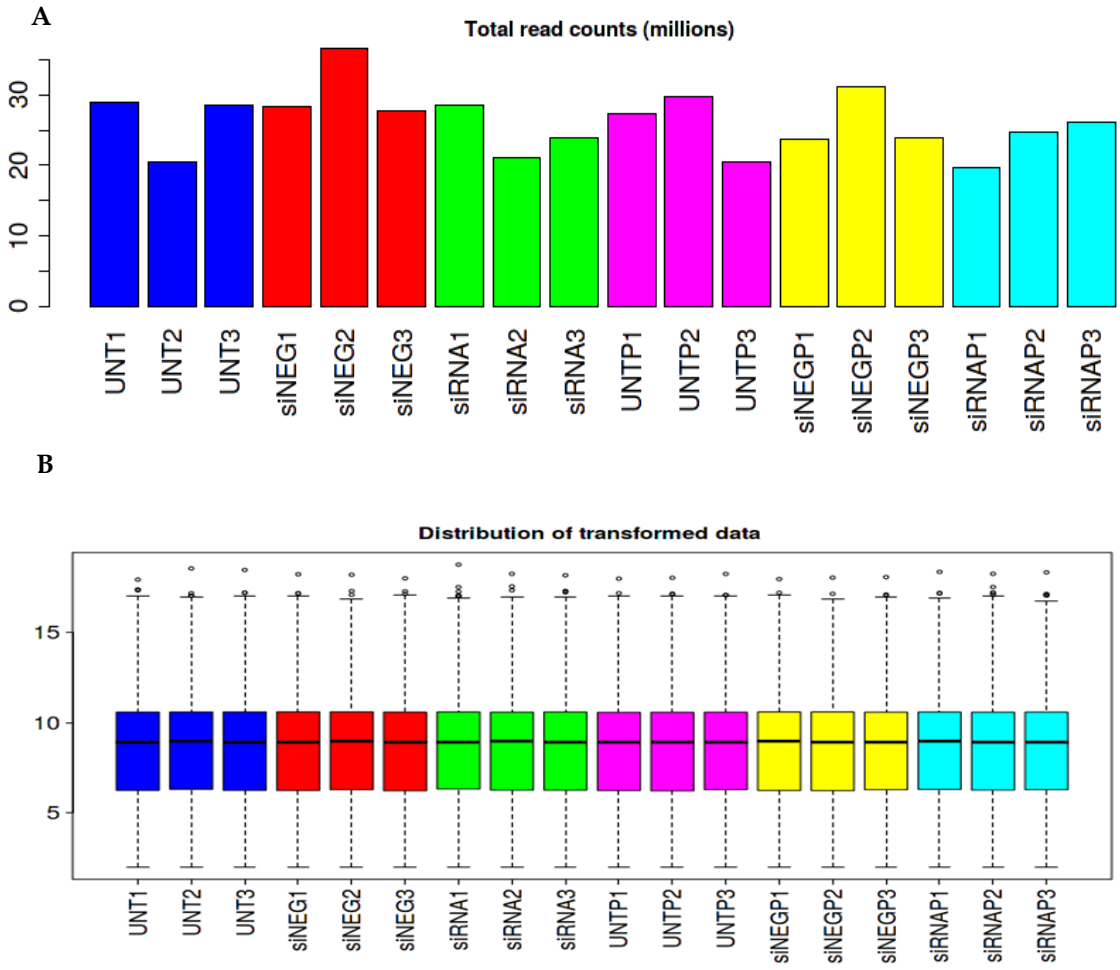

Fig. 4.6 A Total read counts before normalisation, **B** Distribution of transformed data (http://bioinformatics.sdstate.edu/idep92/)

4.5.3 Differential Gene Expression when PAI-1 has been silenced in an Ovarian Cancer Cell Model, with and without the Addition of Platelets

Analysis of transcript read counts across all treatment types was performed using iDEP92 (Fig. 4.7). Overall analysis demonstrated that transiently silencing PAI-1 in SK-OV-3 cells resulted in significant downregulation of 430 genes, and significant upregulation of 290 genes (Fig. 4.8, Table 4.3), and a Venn diagram (Fig. 4.9) shows total dysregulated genes for each treatment type, and also the number of overlapping genes in each treatment. Adding platelets to untreated cells resulted in 57 significantly upregulated and 59 significantly downregulated genes, whereas as adding platelets to our PAI-1 knockdown resulted in significant upregulation of 3 genes and significant downregulation of 3 genes (Fig. 4.9, Table 4.3).

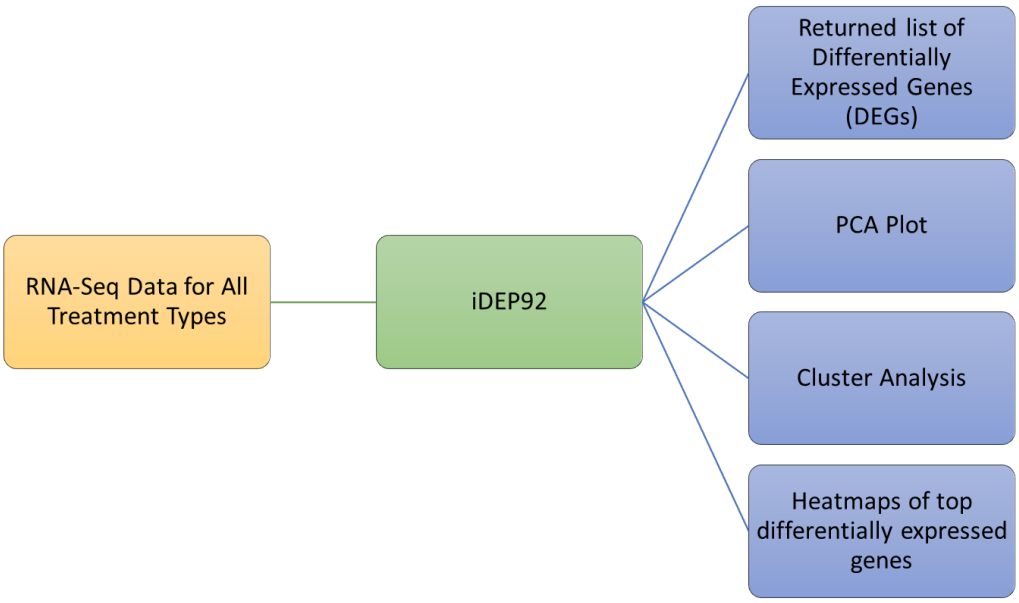

Fig. 4.7 Flowchart showing how data were analysed in iDEP92

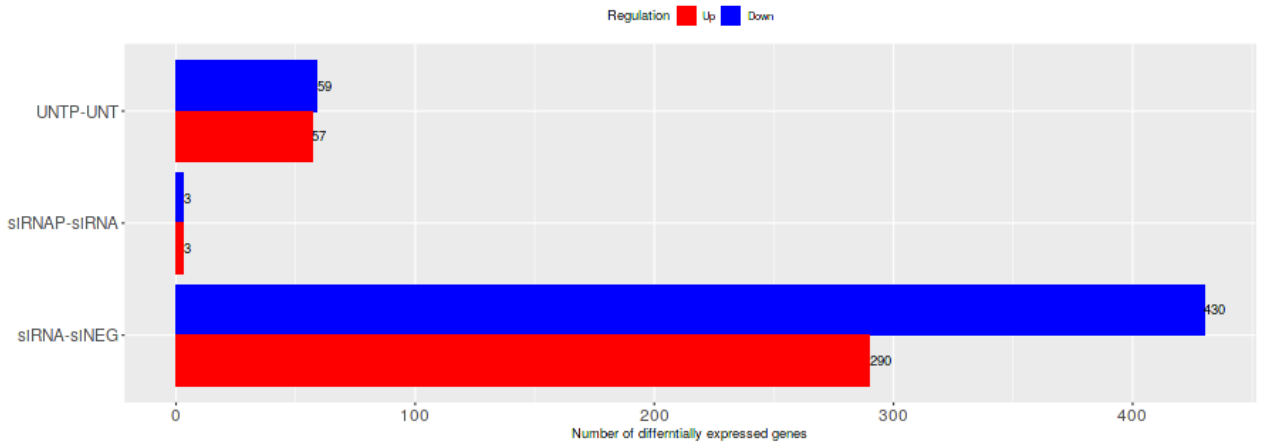

Fig. 4.8 Differentially expressed genes as analysed in DESeq2 (http://bioinformatics.sdstate.edu/idep92/)

Table 4.3 Gene expression comparisons

Comparisons	Up	Down
UNTP-UNT	57	59
siRNAP-siRNA	3	3
siRNA-siNEG	290	430

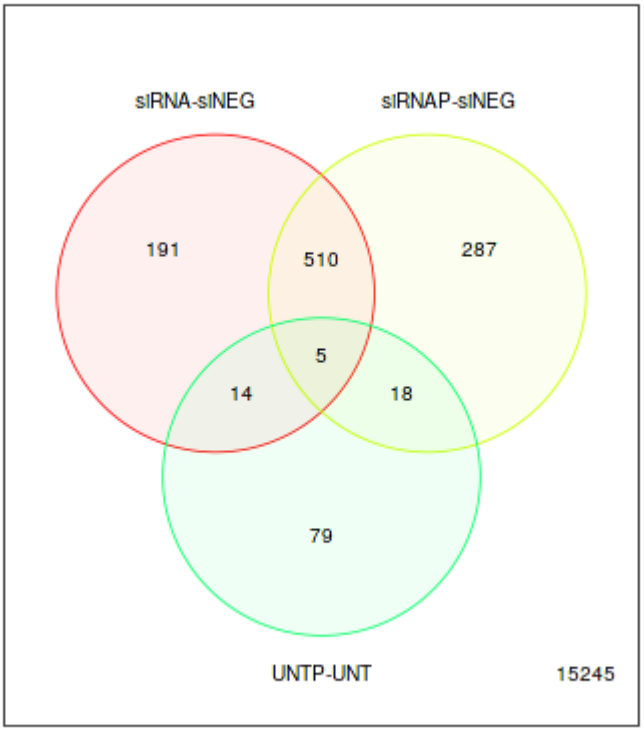

Fig. 4.9 Venn diagram of differentially expressed genes and overlap between treatment groups (http://bioinformatics.sdstate.edu/idep92/)

A principal component analysis (PCA) of all of our samples, which had been corrected for any potential "batch effect" that may have occurred using Combat-Seq (Zhang et al, 2020), demonstrated good grouping for each sample "n" within each treatment type (Fig. 4.10).

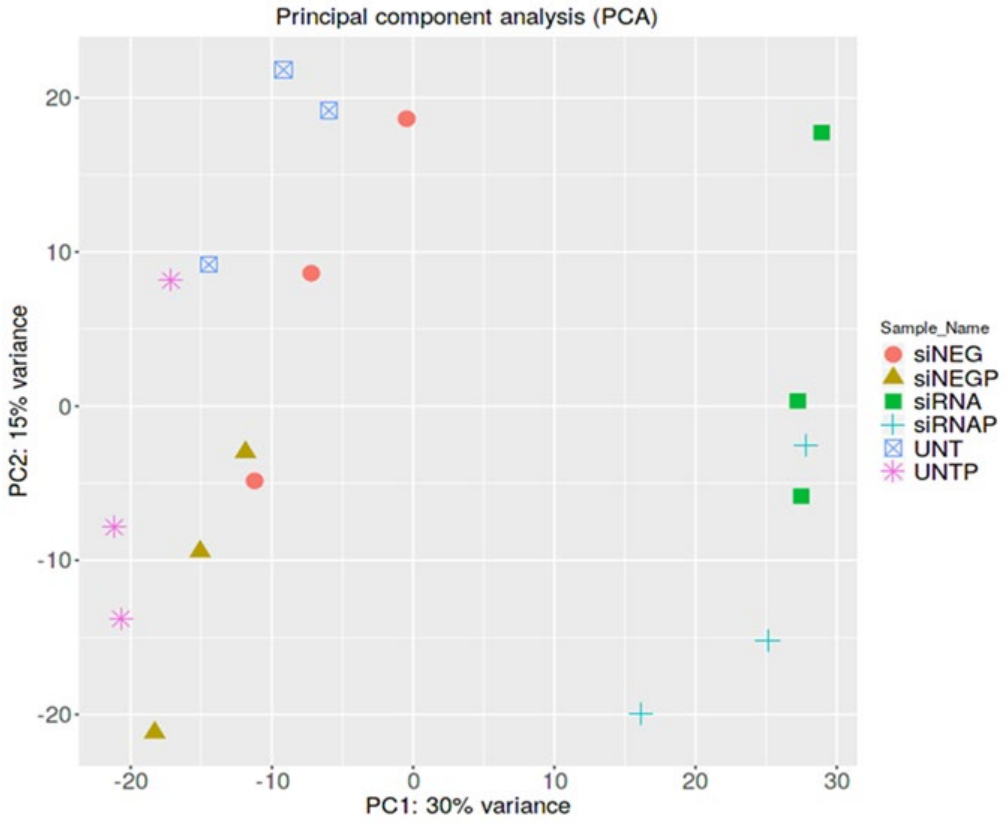

Fig. 4.10 Principal component analysis of all samples shows grouping of treatment types: samples treated with an inert negative control are shown as orange circles, samples treated with an inert negative control and then platelets are shown as gold triangles, samples treated with PAI-1 siRNA are shown as green squares, samples treated with PAI-1 siRNA and then platelets are shown as blue crosses, untreated samples are shown as blue squares containing an "x", and untreated cells that received platelets are shown as a pink star.(http://bioinformatics.sdstate.edu/idep92/)

A heatmap was created in iDEP92 of the top 1000 variable genes among treatment types (Fig. 4.11). Clustering was evident among downregulated (green) and upregulated (red) genes within the grouped treatment types particularly where PAI-1 had been silenced and where platelets had been added to untreated cells and to our negative control-treated cells. Both untreated and siNEG-treated cells displayed extremely similar gene expression with very little variation.

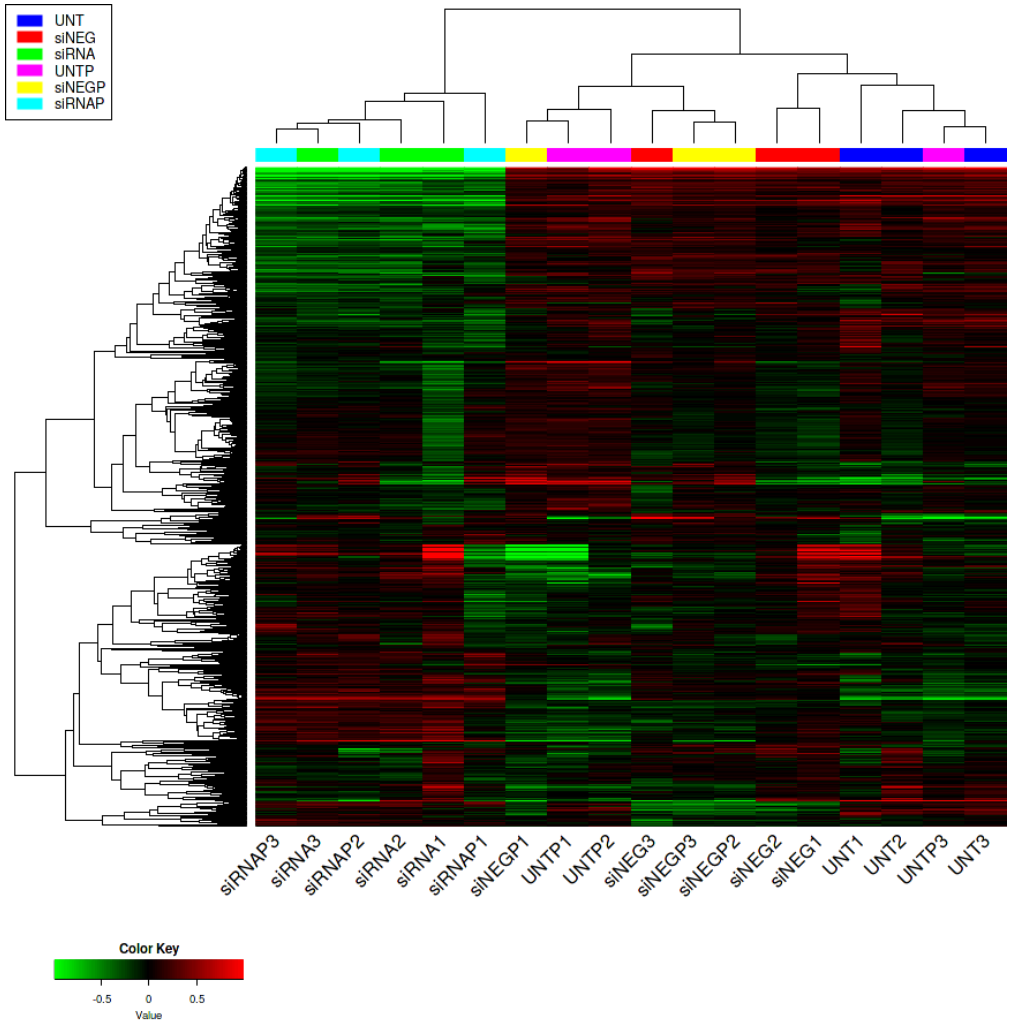

Fig. 4.11 A Top 1000 variable genes heatmap, (http://bioinformatics.sdstate.edu/idep92/)

A cluster analysis (Fig. 4.12) was performed on the top 1000 variable genes, divided into 6 clusters, A-F, which demonstrated downregulation (green) and upregulation (red) of genes corresponding to separation of treatment types in response to having PAI-1 silenced (siRNA), platelets added to an untreated or negative control (UNT+P or siNEG+P), untreated or negative control alone (UNT or siNEG), or platelets added after PAI-1 was silenced (siRNA+P). Details of these clusters are listed in the appendix (Appendix A Table A4-1).

Cluster A, which was composed of 224 genes involved in the biosynthetic processes of sterols, cholesterols, and lipids as well as their metabolic processes was less defined with regard to clear separation of upregulation (red) and downregulation (green) by treatment type, but did tend to show a platelet effect of downregulation in these groups of processes.

Cluster B was much more clearly defined in terms of genes that were upregulated in response to knocking down PAI-1, as was cluster C. The 144 dysregulated genes in cluster B were those involved with acute-phase response, leukocyte migration, and inflammatory response, while 119 dysregulated genes in cluster C were described as those involved in the processes of protein glycosylation, glycoprotein biosynthesis, and transsynaptic signaling by soluble gases.

125 variable genes comprised cluster D, and mainly showed an upregulatory response to the addition of platelets to our untreated and negative control samples, and were those involved in response to bacterial infection, cytokine stimulation, cytokine-mediated signaling, cellular response to oxygen-containing compounds, and immune response.

Cluster E was composed of 166 variable genes that were highly downregulated (green) in response to the loss of PAI-1, and were highly upregulated (red) in response to the addition of platelets. Genes in this cluster included those involved in tissue development, anatomical structure morphogenesis, cell proliferation, epithelial development, angiogenesis, and the positive regulation of cell migration.

Finally, cluster F encompassed a group of 222 genes that were highly downregulated in response to the loss of PAI-1 (green). This cluster was composed of genes of the pathways concerning the response to viruses, type 1 interferon signaling, immune response, and the negative regulation of viral genome replication. The sections that follow provide a closer look at how some of the major gene groups and pathways discovered by this analysis were affected in our ovarian cancer cell line model by the various treatments mentioned here.

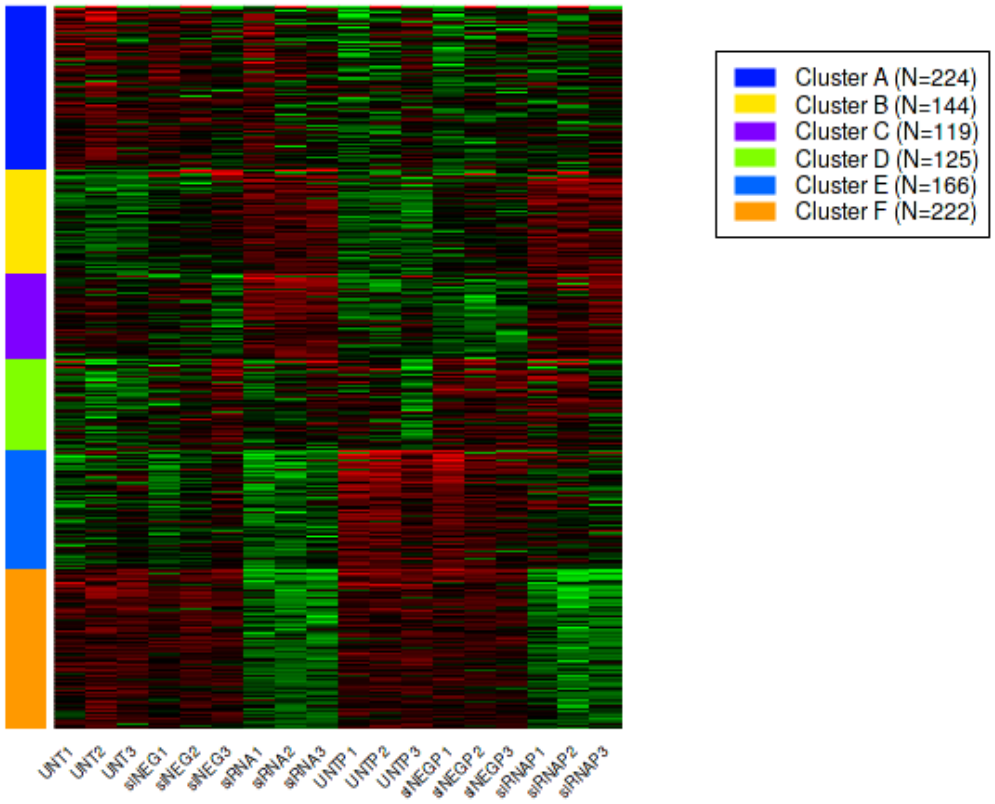

Fig. 4.12 K-means heatmap of top 1000 genes with 6 clusters (http://bioinformatics.sdstate.edu/idep92/)

As our gene of interest was SERPIN E1, we uploaded our binary alignment map (BAM) files to the Broad Institute's integrative genomics viewer (IGV), which created a visual map of the differences in SERPIN E1 gene

expression across our samples (Fig. 4.13). As expected, the most visible changes appeared in our PAI-1 knockdown (Fig. 4.13 dark pink and light pink sections, outlined in a red rectangle). Interestingly, there appeared to be quite a lot of altered gene expression not only in the exons, but also in the introns. There is virtually no gene expression in the intragenic regions of samples where PAI-1 has not been silenced, and consistent expression in the introns of samples where PAI-1 has been silenced, including those samples treated with PAI-1 siRNA that also received platelets. Slight differences in exon mapping were also visible in our siNEG-treated samples, which do correspond to the data shown in our PCA plot (Fig. 4.10).

Fig. 4.13 Integrative Genomics Viewer (IGV) image of samples aligned to the SERPIN E1 gene (Broad Institute, UC San Diego, CA USA)

Further analyses of transcript read counts were performed by separating read count data by treatment type, and analysing one comparison at a time. These analyses were: siRNA v siNEG, UNT+P v UNT, and siRNA+P v siRNA (Fig. 4.14). Performing these individual analyses facilitated a more comprehensive understanding of the functional properties of PAI-1 in ovarian cancer cells, and also of the effect that platelets exert on these cells, both with PAI-1 intact and within the context of a PAI-1 knockdown model. iDEP92 analyses yielded robust lists of differentially expressed genes (DEGs) obtained via DESeq2 which were then uploaded to ShinyGOv0.61 according to treatment type, and with regard to upregulation or downregulation. Individual lists of genes corresponding to specific pathways were also evaluated, and pathways obtained via iDEP92 and ShinyGO were cross-referenced. These results are reported in the sections that follow in this chapter, and refer back to the following Fig. 4.14 throughout.

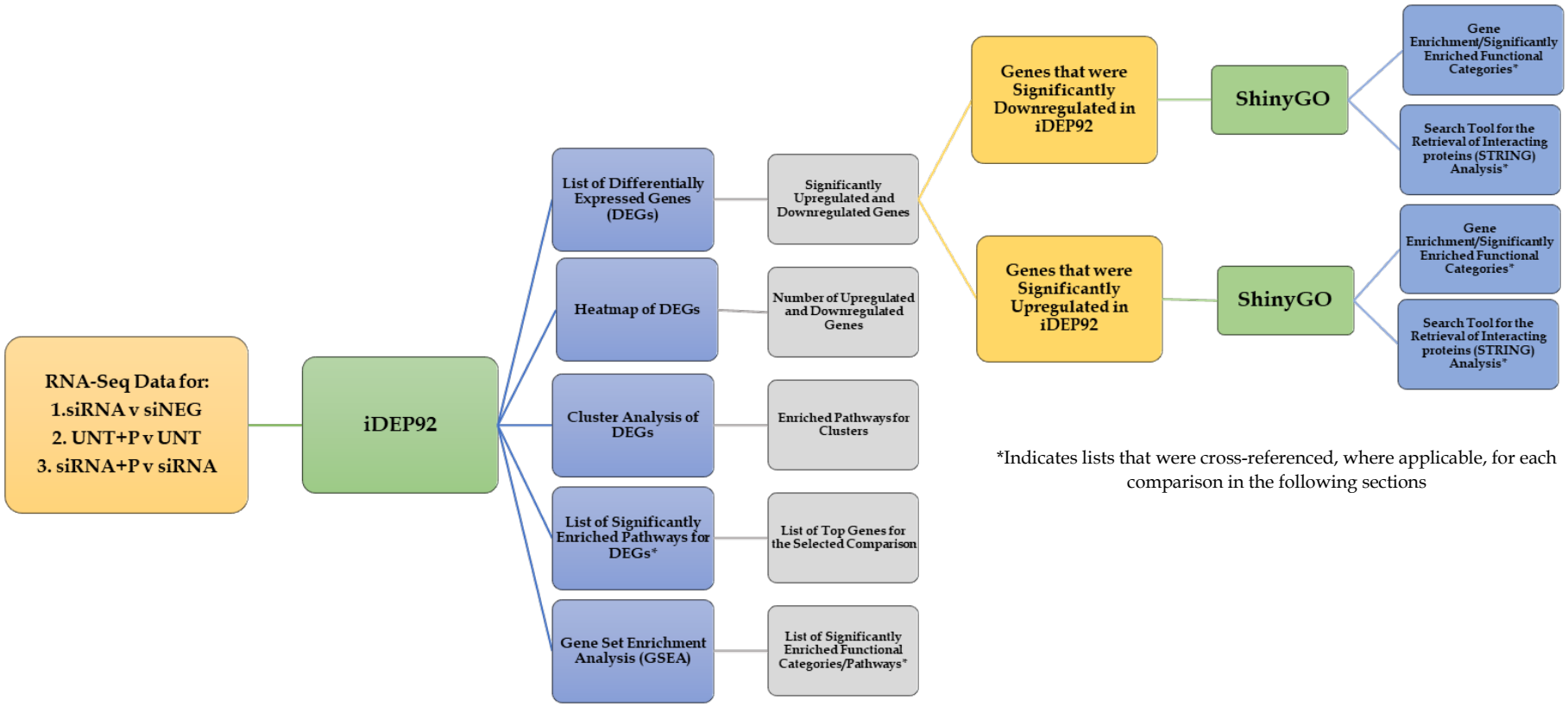

Fig. 4.14 Workflow diagram of separate analyses by treatment type

4.5.3.1 Differential Gene Expression when PAI-1 has been transiently silenced in an Ovarian Cancer Cell Model

Individual analysis in iDEP92 of transiently silencing the PAI-1 protein expressed by the SERPIN E1 gene via siRNA compared to the negative control showed the significant downregulation of 424 genes, and the significant upregulation of 257 genes (Figs. 4.15, 4.16, and 4.17). This analysis yielded a gene list that was essentially identical to the overall analysis performed on all treatment types simultaneously in section 4.5.3, but subsequent cluster and gene enrichment analyses were more specific than those of the overall analysis. Running separate analyses on specific treatment types did not change the differential expression results, but rather this breakdown allowed for a closer look at affected pathways between two treatment types that might not have been immediately apparent in a broader analysis.

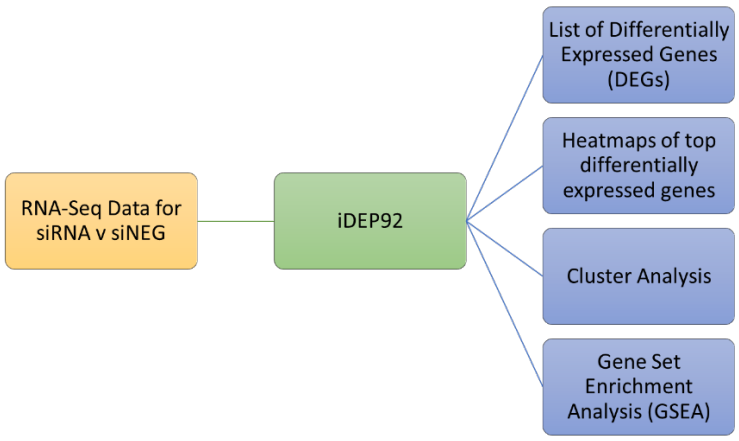

Fig. 4.15 Analysis of siRNA v siNEG in iDEP92

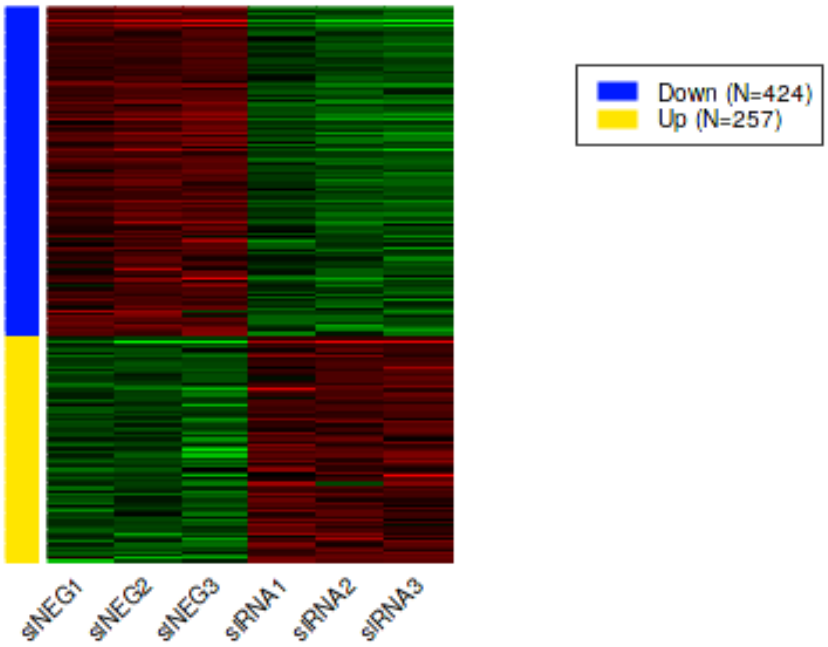

Fig. 4.16 Heatmap of differentially expressed genes (http://bioinformatics.sdstate.edu/idep92/)

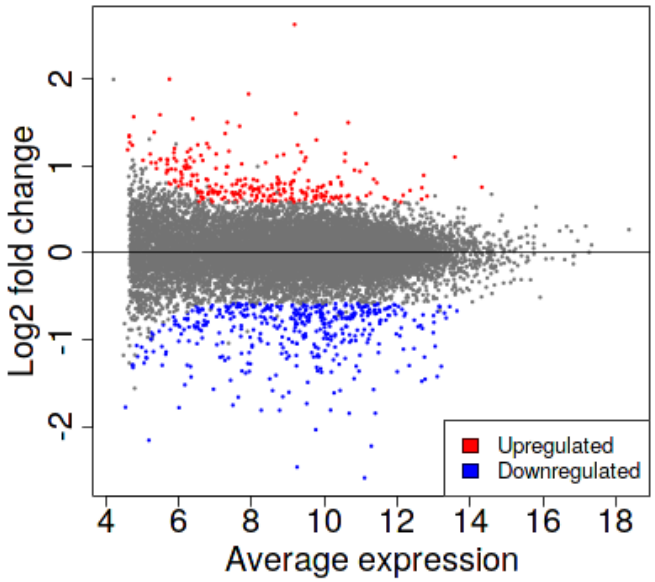

Fig. 4.17 MA plot of average gene expression (http://bioinformatics.sdstate.edu/idep92/)

An enrichment pathway analysis in iDEP92 (Fig. 4.18) showed significant downregulation of 13 molecular pathways including those associated with the regulation of cellular migration, phosphorylation,

anatomical structure morphogenesis, intracellular signal transduction, cellular protein modification, and the stress-activated protein kinase signaling cascade (Appendix A Table A4-2). 9 significantly upregulated molecular pathways included glycosylation, protein glycosylation, homophilic cell adhesion via plasma membrane adhesion molecules, cell-cell adhesion, and the biosynthetic processes of several molecules including glycoproteins and carbohydrate-derived products (Appendix A Table A4-2). Genes selected for comparison were listed (Appendix A Table A4-3), where a negative (-) Log_2 fold change indicated downregulation of a specific gene, and a positive Log_2 expression-fold change indicated upregulation of a particular gene.

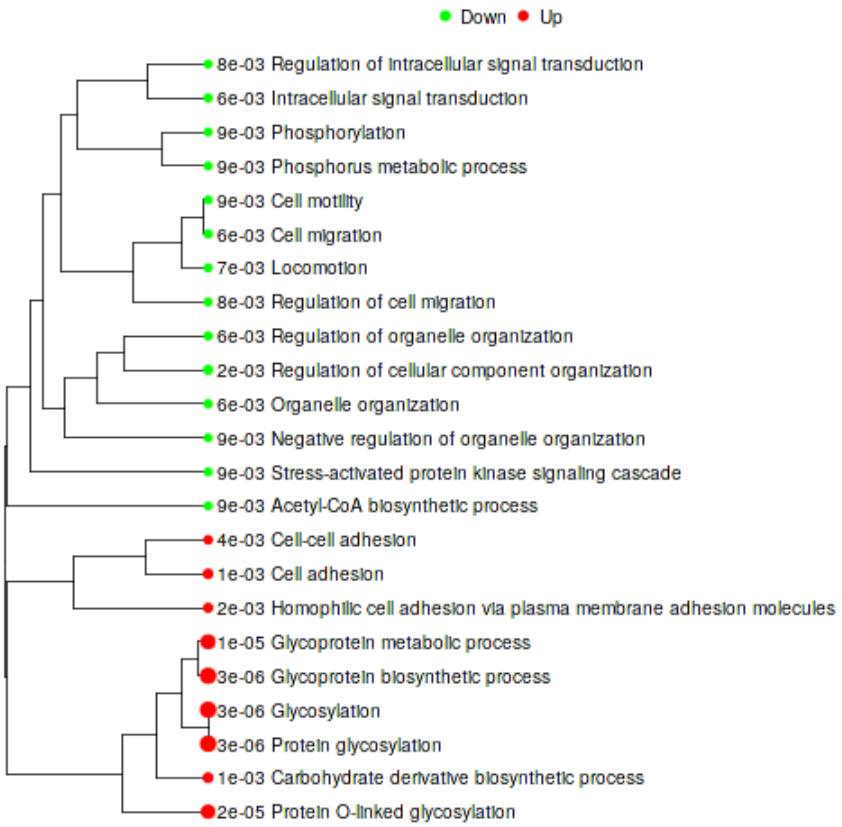

Fig. 4.18 Enrichment pathway for siRNA v siNEG, with green dots representing downregulation, red dots representing upregulation, and larger dots representing smaller p-values (http://bioinformatics.sdstate.edu/idep92/)

A cluster analysis (Fig. 4.19) demonstrated that the pathways involving cell motility, locomotion, and regulation of cell migration were significantly downregulated when PAI-1 was transiently silenced, while glycosylation and glycoprotein biosynthesis were upregulated (Appendix A Table A4-5). Gene set enrichment analysis (GSEA) yielded 12 significantly downregulated pathways and 18 significantly upregulated pathways (Appendix A Table A4-4). Downregulated pathways included homologous recombination, regulation of blood coagulation, histone ubiquitination, and negative regulation of wound healing. Upregulated pathways included glycosylation, protein glycosylation, glycoprotein metabolic processes, and homophilic cell adhesion via plasma membrane adhesion molecules. Examples of the downregulated pathway regulation of blood coagulation and the upregulated pathway protein glycosylation are shown in Fig. 20 and Fig. 21, respectively.

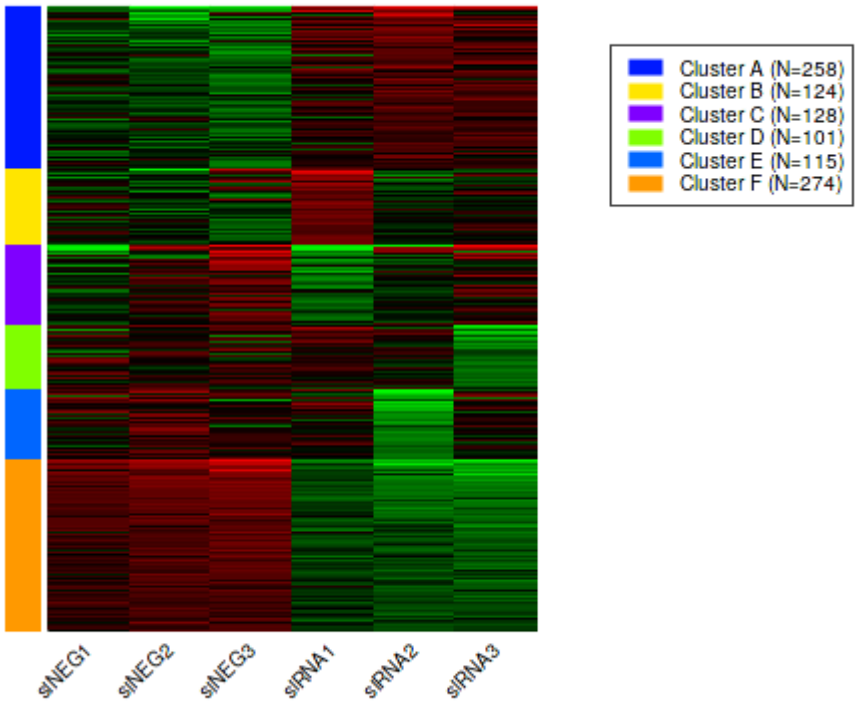

Fig. 4.19 Cluster analysis of siRNA v siNEG (http://bioinformatics.sdstate.edu/idep92/)

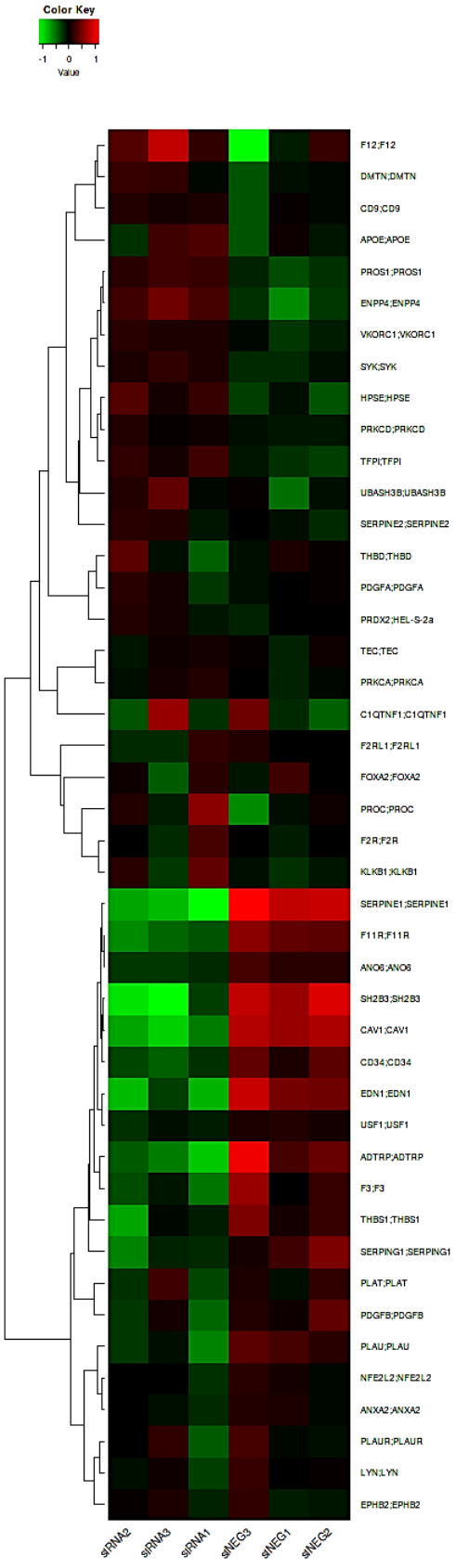

Fig. 4.20 Regulation of blood coagulation is significantly downregulated when PAI-1 is silenced in SK-OV-3 cells, p = 0.009 (http://bioinformatics.sdstate.edu/idep92/)

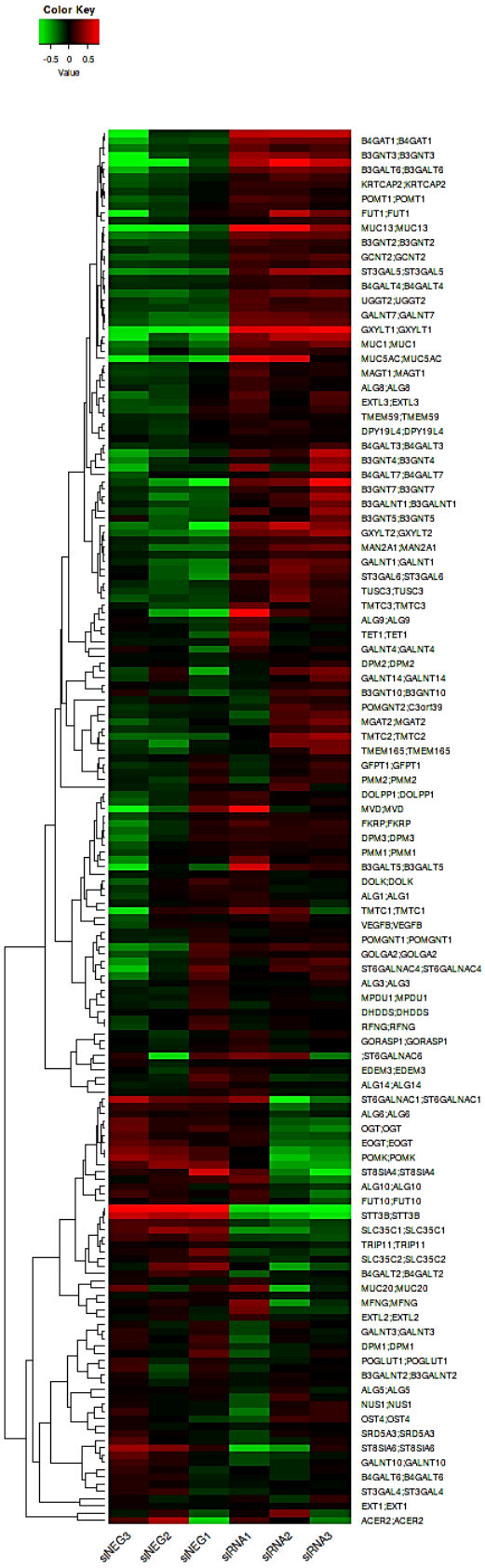

Fig. 4.21 Protein glycosylation is significantly upregulated when PAI-1 is silenced in SK-OV-3 cells, p = 0.0024 (http://bioinformatics.sdstate.edu/idep92/)

4.5.3.1.1 Significantly downregulated Pathways in an Ovarian Cancer PAI-1 Knockdown Model

A workflow analysis procedure was developed and was previously demonstrated in Fig. 4.14. Analysis of pathways that were significantly downregulated when PAI-1 was silenced via siRNA was performed by uploading the list of significantly downregulated genes obtained from our iDEP92 analysis to ShinyGO v0.61 (Fig. 4.22, Bioinformatics, South Dakota State University, SD, USA).

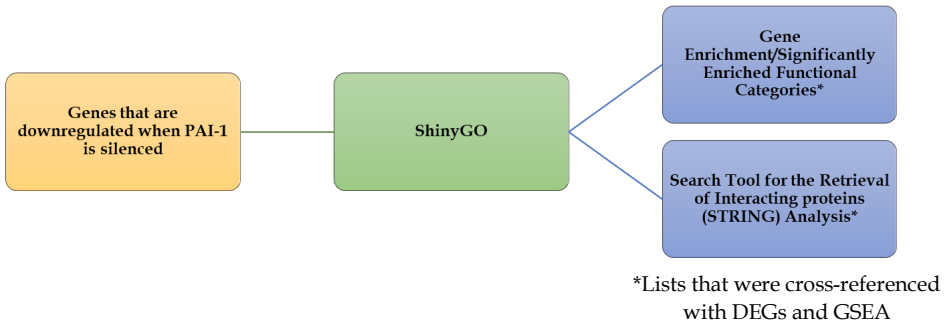

Fig. 4.22 Analysis of downregulated genes in a PAI-1 knockdown in ShinyGO

ShinyGO employs thousands of Ensembl 92-based gene sets and databases. This returned a list of 13 functional categories (Fig. 4.23, Appendix A Table A4-6) that were significantly affected when PAI-1 is silenced, including acetyl-CoA biosynthetic process, detection of virus, and regulation of cell migration. Search Tool for the Retrieval of Interacting proteins (STRING) analysis results were also obtained through the ShinyGO engine. Functional categories from this analysis included cell migration and cell motility, but also included categories such as regulation of response to stress, inflammatory response, and regulation of protein transport (Appendix A Table A4-7).

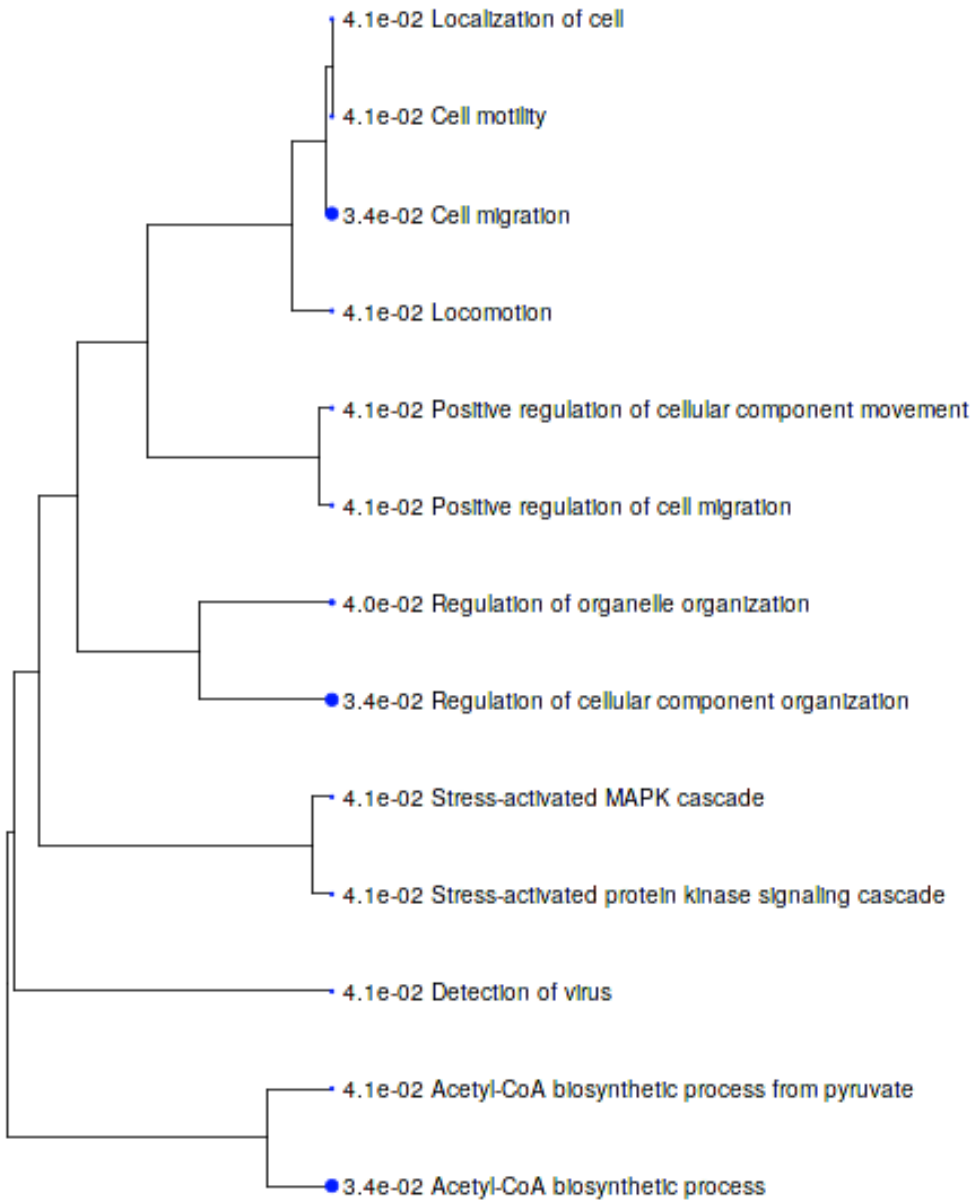

Fig. 4.23 A hierarchical clustering tree showing the connections among significant pathways that are downregulated when PAI-1 is silenced. Larger dots represent smaller p-values. (http://bioinformatics.sdstate.edu/go)

Cross-referencing of significantly downregulated pathway lists obtained via analyses in DEGs, GSEA, ShinyGO, and STRING (Figs. 4.14 and 4.22) revealed a subset of significant pathways present in 2, 3, or all 4 analyses (Appendix A Table A4-7), however all returned results were deemed to be relevant. Analyses of all the resulting categorical pathways, and certainly all of the genes within those pathways, was beyond the scope of this thesis. Here, we have focused on three significantly downregulated functional categories or pathways that were returned in both DEGs and ShinyGO. GSEA returned gene lists in a format that was not conducive to further analysis, and STRING did not return a list of genes at all, and so further investigation into the functional categories from these two analyses was simply not possible. However, it was possible to enter our gene lists from chosen pathways into STRING, and these are reported below. The functional pathways chosen were relevant to our chapter 3 results and to ovarian cancer metastasis, and included SERPIN E1. These pathways were cell migration (Fig. 4.24, Appendix A Table A4-8), cell motility (Fig. 4.25, Appendix A Table A4-9), and regulation of cellular component organisation (Fig. 4.26, Appendix A Table A4-10). Uploading the list of genes associated with cell migration directly to the STRING website created a gene map of this pathway (Fig. 4.27), which contained both known and predicted interactions. Color-coding of genes within this map demonstrated that our gene of interest, SERPIN E1, is central to many of the biological processes involved in ovarian cancer metastasis, including negative regulation of cell adhesion mediated by integrin (shown in blue), regulation of

wound healing (shown in orange), positive regulation of interleukin-8 (IL-8) production (shown in purple), regulation of cell-matrix adhesion (shown in yellow), regulation of cell migration (shown in green), and positive regulation of angiogenesis (shown in red). Many of the same genes listed in our iDEP92 analysis were also listed in our 3 chosen pathways, and so to avoid redundancy only one color-coded map was created for this section.

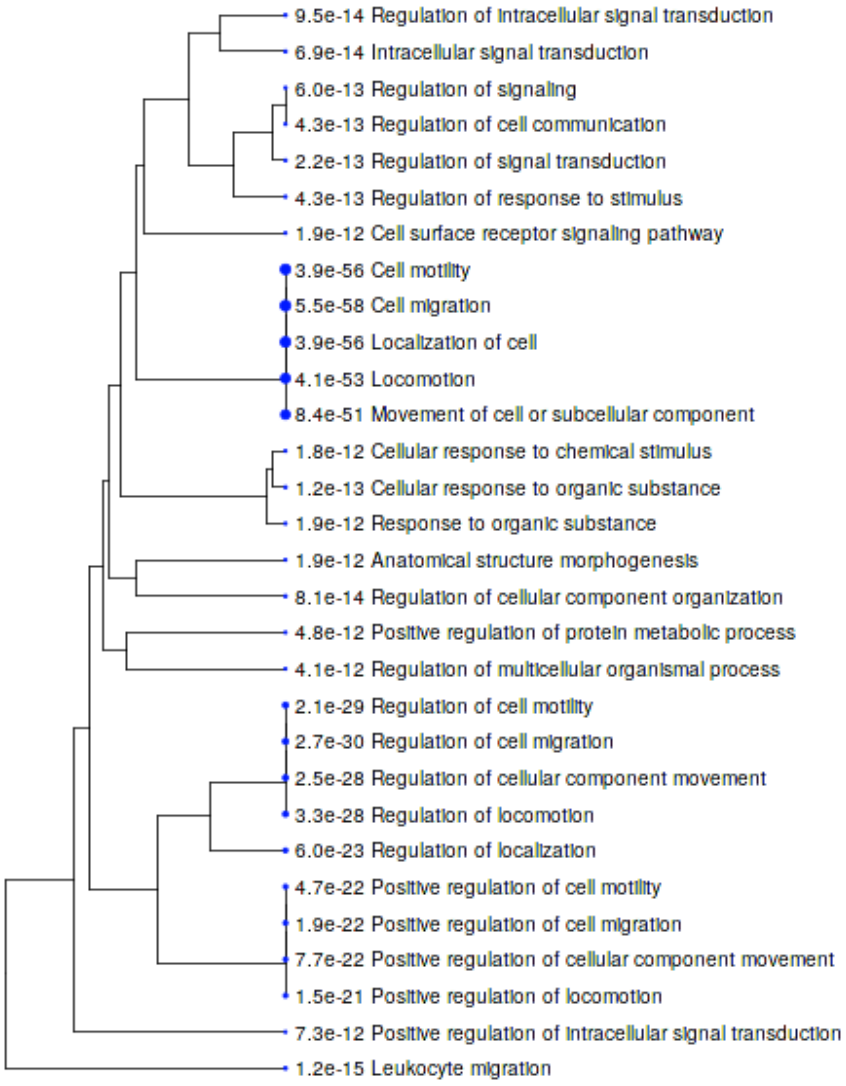

Fig. 4.24 A hierarchical clustering tree showing the connections among pathways involved in cell migration that are significantly downregulated when PAI-1 is silenced. Larger dots represent smaller p-values. (http://bioinformatics.sdstate.edu/go)

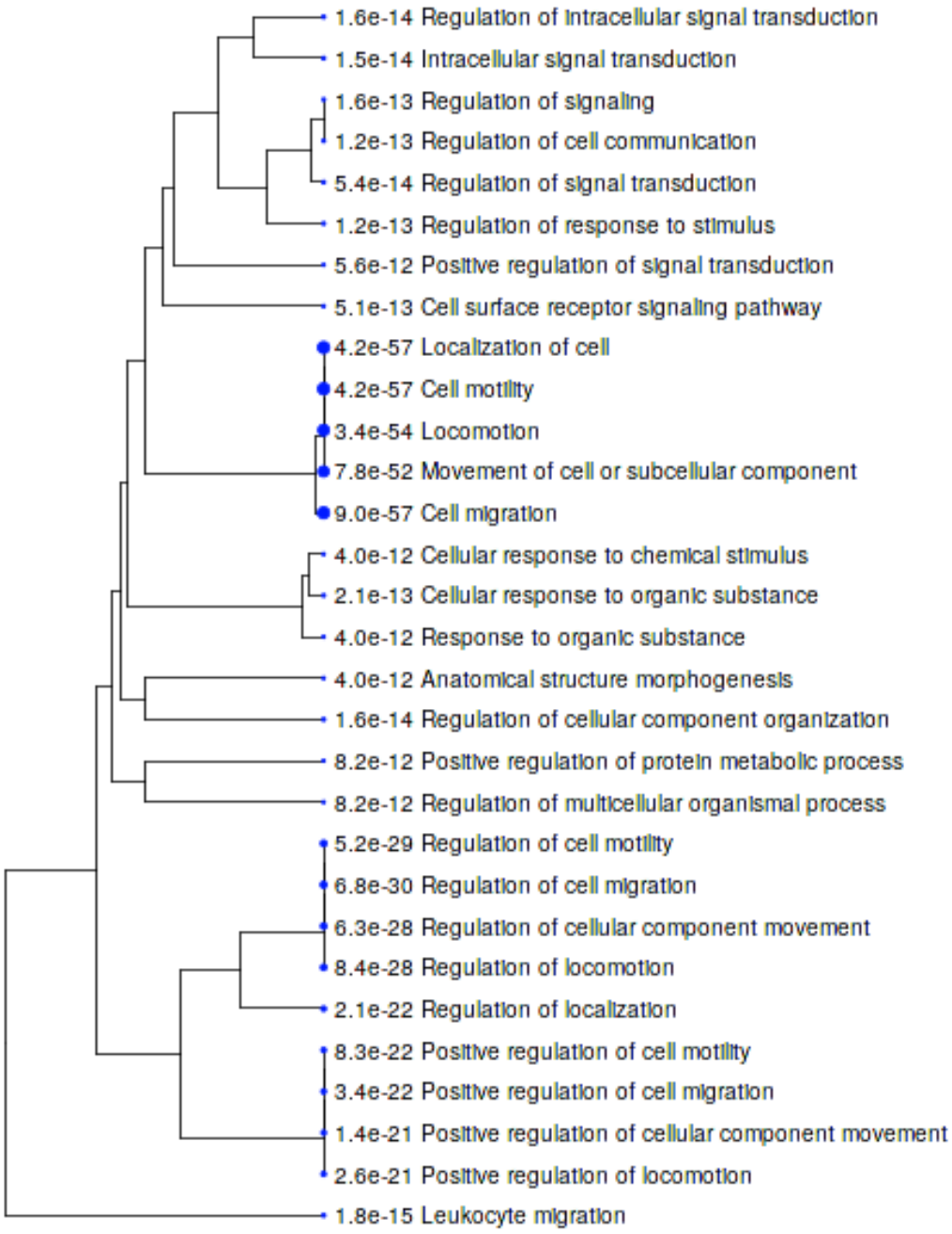

Fig. 4.25 A hierarchical clustering tree showing the connections among pathways involved in cell motility that are significantly downregulated when PAI-1 is silenced. Larger dots represent smaller p-values. (http://bioinformatics.sdstate.edu/go)

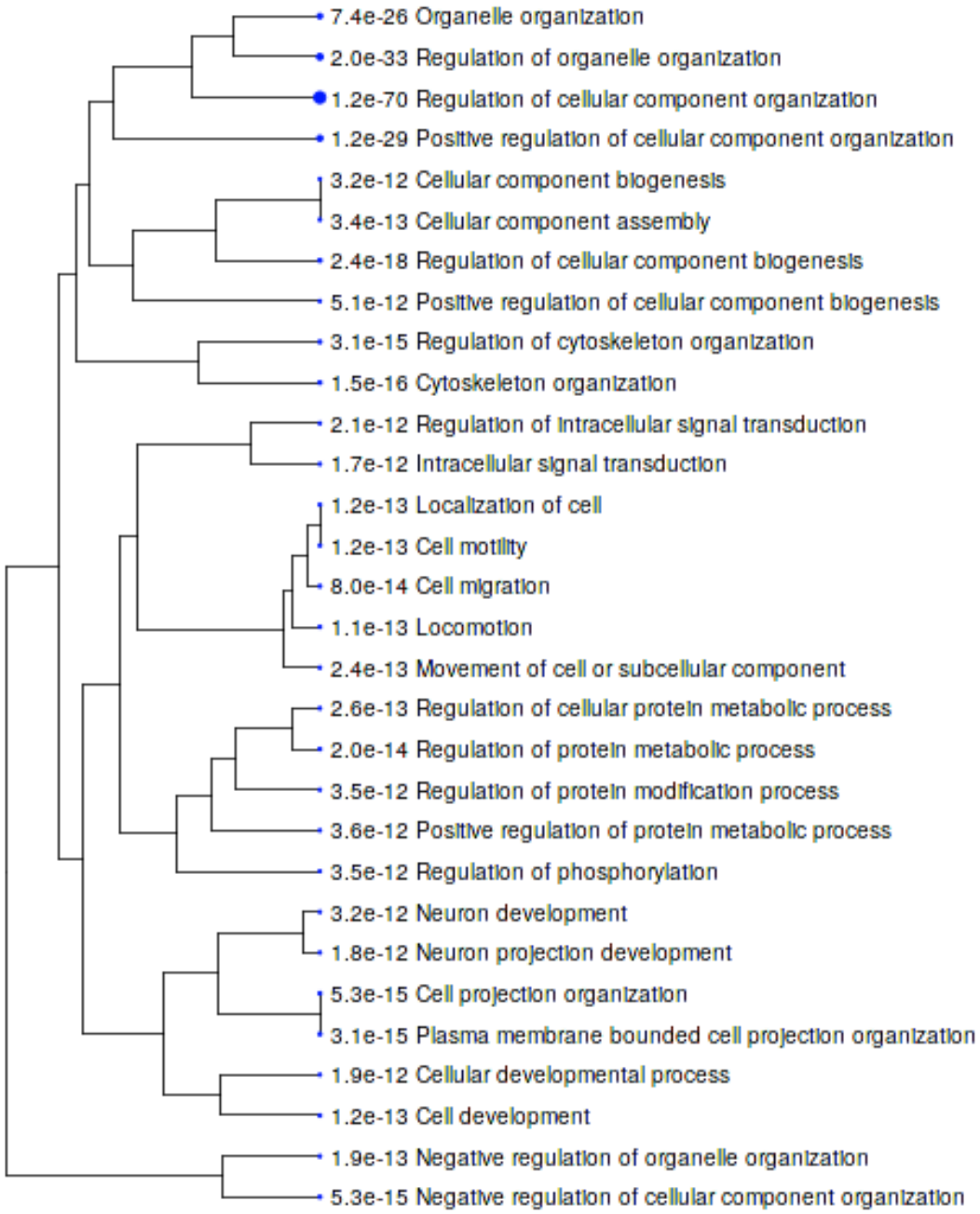

Fig. 4.26 A hierarchical clustering tree showing the connections among pathways involved in regulation of cellular component organisation that are significantly downregulated when PAI-1 is silenced. Larger dots represent smaller p-values. (http://bioinformatics.sdstate.edu/go)

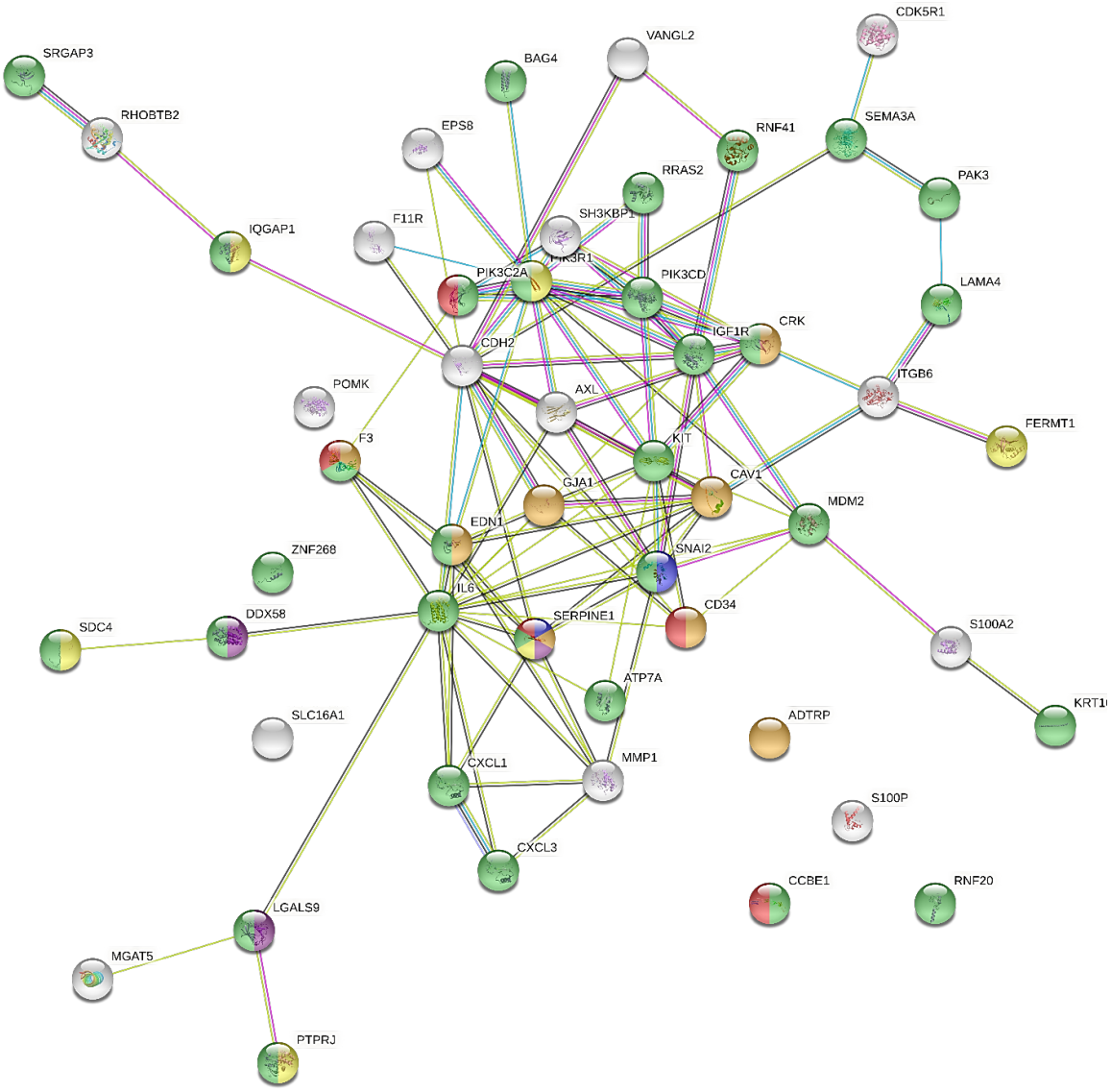

Fig. 4.27 Gene mapping in STRING demonstrated that SERPIN E1 was central to many biological processes. Color coding indicates the biological processes each gene is involved in; negative regulation of cell adhesion mediated by integrin (blue), regulation of wound healing (orange), positive regulation of interleukin-8 (IL-8) production (purple), regulation of cell-matrix adhesion (yellow), regulation of cell migration (green), and positive regulation of angiogenesis (red). Gene representations containing objects indicate genes for which 3-D structures have been obtained.

4.5.3.1.2 Significantly upregulated Pathways in an Ovarian Cancer PAI-1 Knockdown Model

As with our significantly downregulated genes, a list of genes that were significantly upregulated when PAI-1 was transiently silenced was uploaded to ShinyGO for analysis (Figs. 4.14 and 4.28). This analysis resulted in a list of 20 significantly enriched functional categories (Fig. 4.29, Appendix A Table A4-11), which included protein glycosylation, cell-cell adhesion, and regulation of metallopeptidase activity. Results of a STRING analysis were also returned and was identical to the aforementioned enriched functional categories.

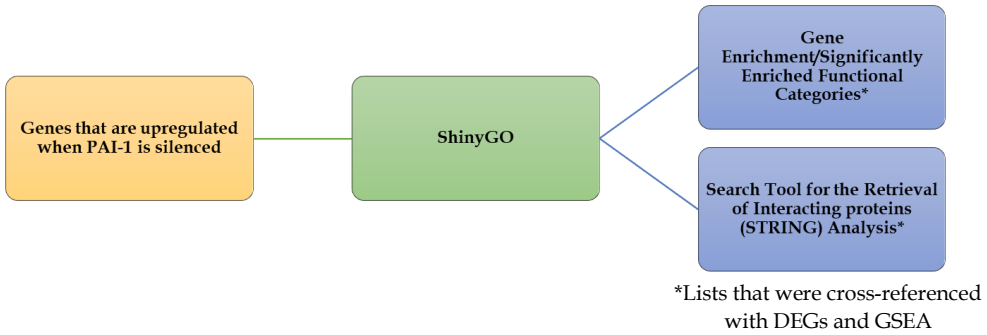

Fig. 4.28 Analysis of upregulated genes in a PAI-1 knockdown in ShinyGO

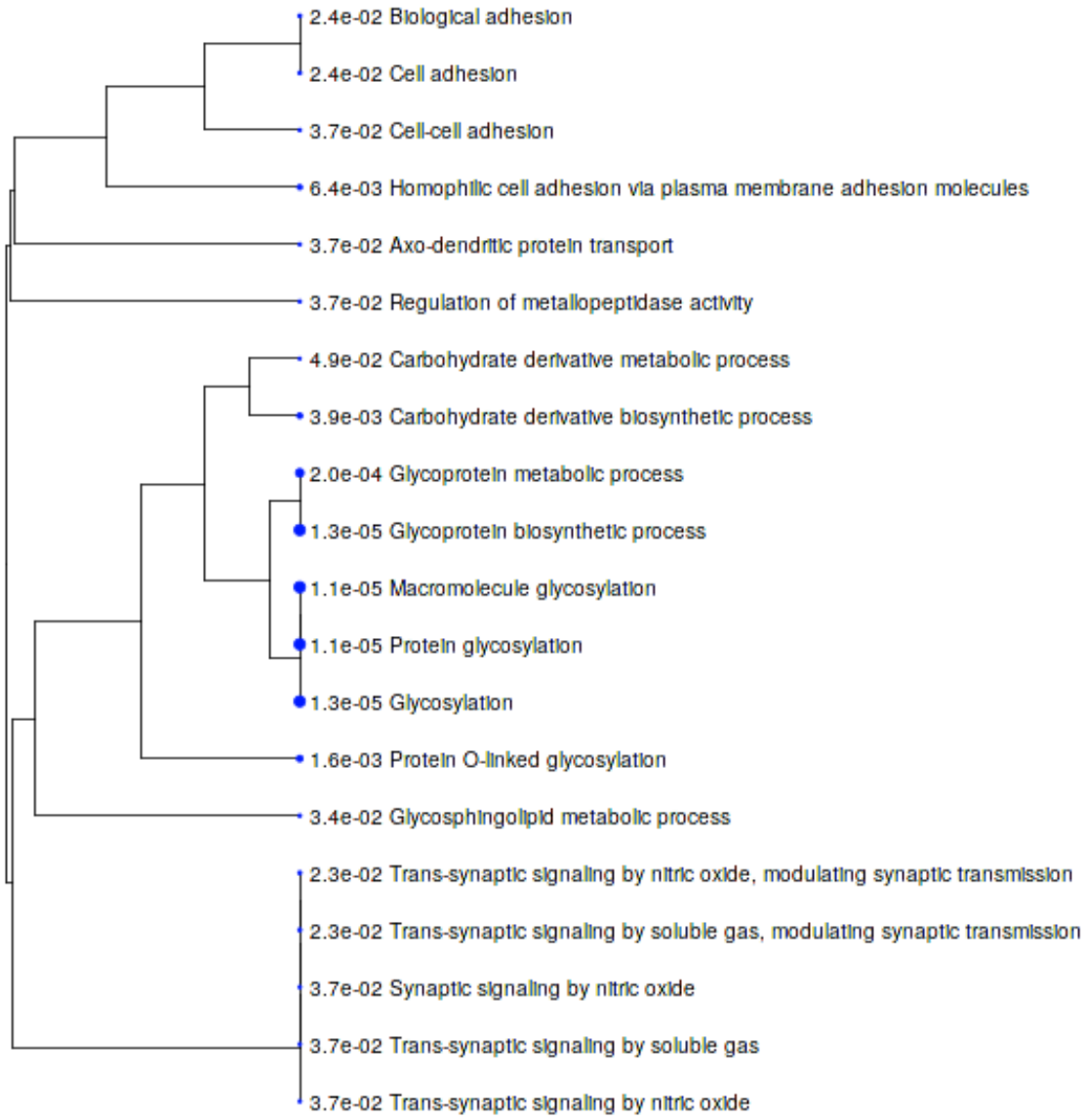

Fig. 4.29 A hierarchical clustering tree showing the connections among significant pathways that are upregulated when PAI-1 is silenced, with larger dots indicating smaller p-values. (http://bioinformatics.sdstate.edu/go)

As with our downregulated gene pathways, this resulted in an enormous amount of data, and it was not possible to comprehensively analyse all of these data within this thesis. Three pathways returned in the enrichment analysis in ShinyGO and also in iDEP92 that were relevant to the results of research performed in chapter 3, and to ovarian cancer metastasis were chosen for further analysis (Appendix A Table A4-12). These pathways were glycosylation (Fig. 4.30, Appendix A Table A4-13), homophilic cell adhesion via plasma membrane adhesion molecules (Fig. 4.31, Appendix A Table A4-14), and cell adhesion (Fig. 4.32, Appendix A Table A4-15).

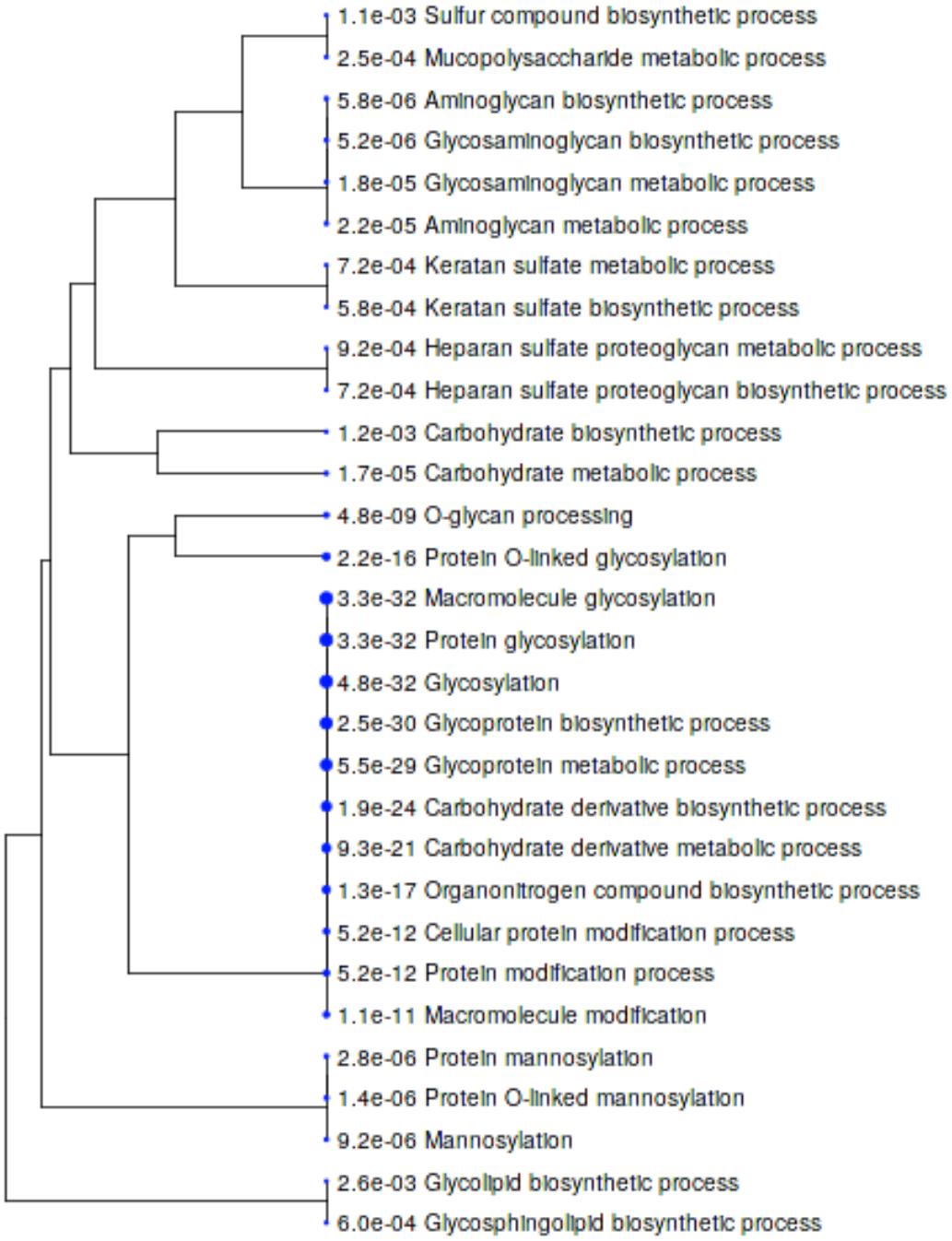

Fig. 4.30 A hierarchical clustering tree showing the connections among pathways involved in glycosylation that are significantly upregulated when PAI-1 is silenced, with larger dots representing smaller p-values. (http://bioinformatics.sdstate.edu/go)

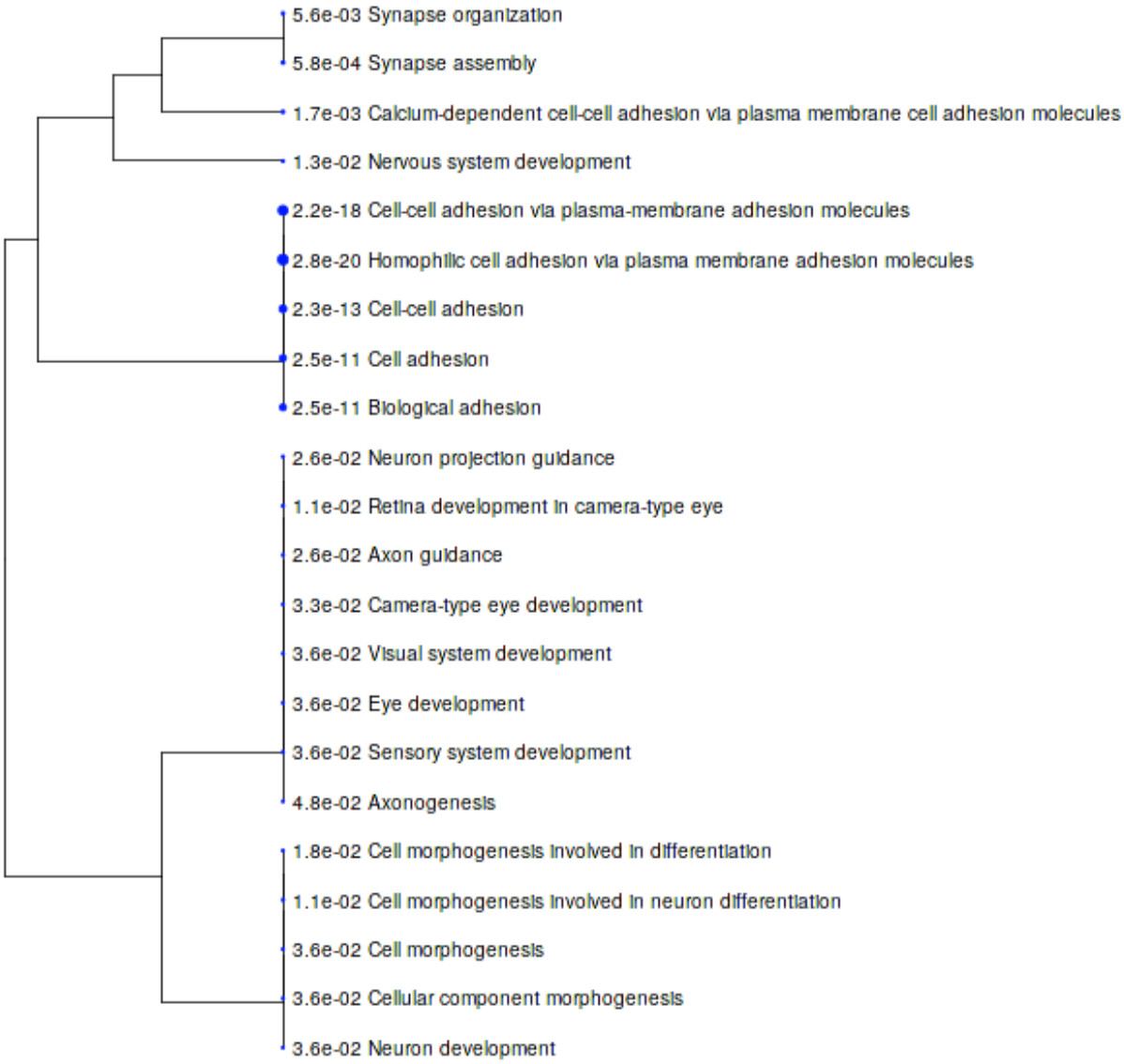

Fig. 4.31 A hierarchical clustering tree showing the connections among pathways involved in homophilic cell adhesion via plasma membrane adhesion that are significantly upregulated when PAI-1 is silenced, with larger dots representing smaller p-values. (http://bioinformatics.sdstate.edu/go)

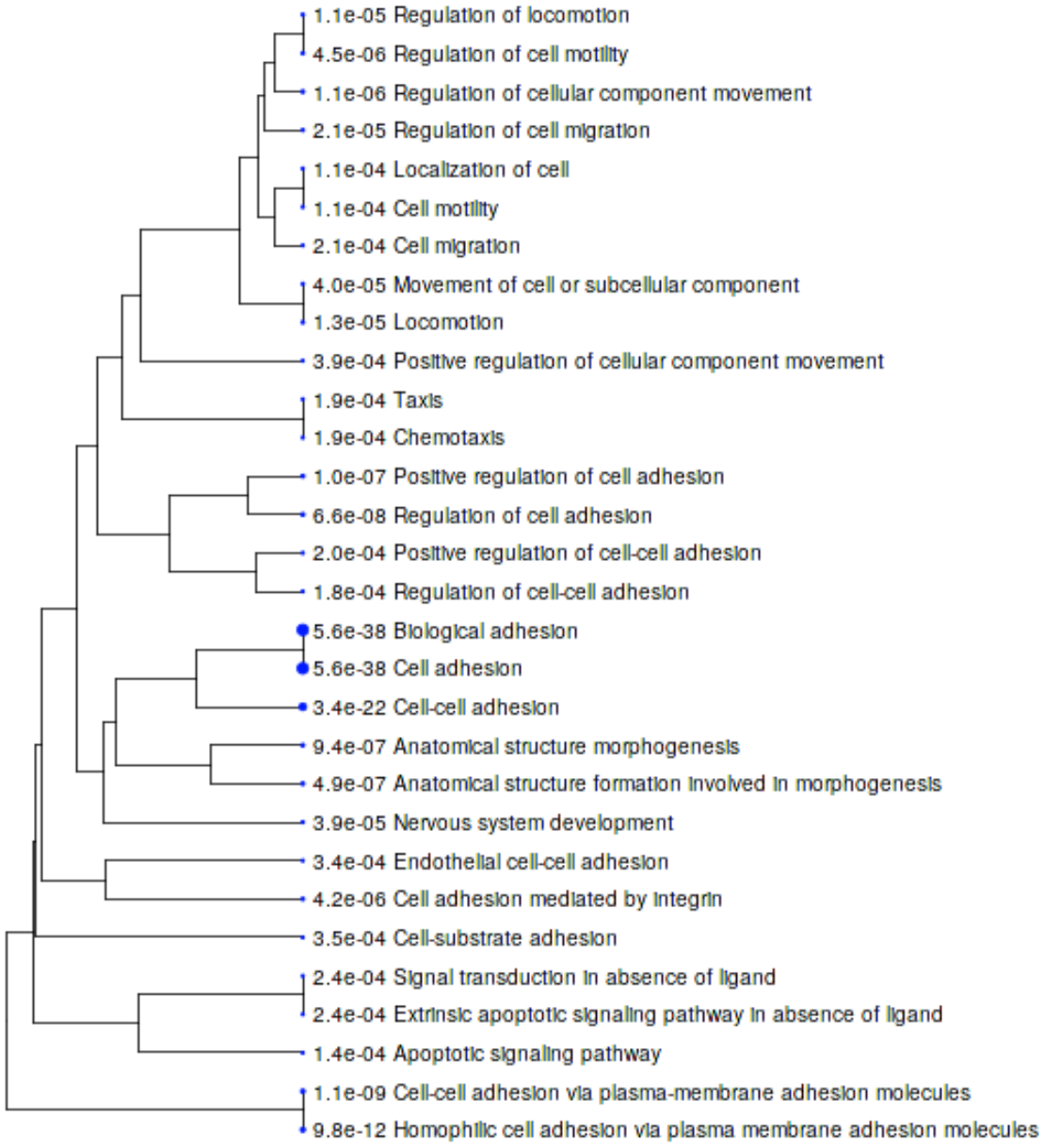

Fig. 4.32 A hierarchical clustering tree showing the connections among pathways involved in cell adhesion that are significantly upregulated when PAI-1 is silenced, with larger dots representing smaller p-values. (http://bioinformatics.sdstate.edu/go)

4.5.3.2 Differential Gene Expression in an Ovarian Cancer Cell Model when Platelets have been added to untreated Cells

Individual analysis in iDEP92 of the effects of platelets on an otherwise untreated ovarian cancer cell line (Figs. 4.14 and 4.33) yielded a total of 59 genes that were significantly upregulated, and 54 genes that were significantly downregulated (Figs. 4.34 and 4.35). The results of this analysis were essentially identical to those of the analysis performed on all treatment types simultaneously, but subsequent cluster and gene enrichment analyses were more focused. Our gene of interest, SERPIN E1, was significantly upregulated when platelets were added to ovarian cancer cells, with an expression-fold change of 2.04, and $p < 0.0001$.

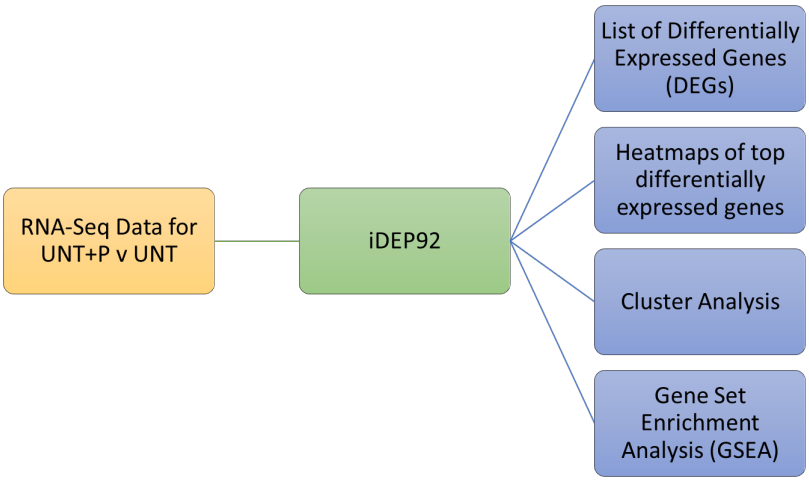

Fig. 4.33 Analysis of UNT+P v UNT in iDEP92

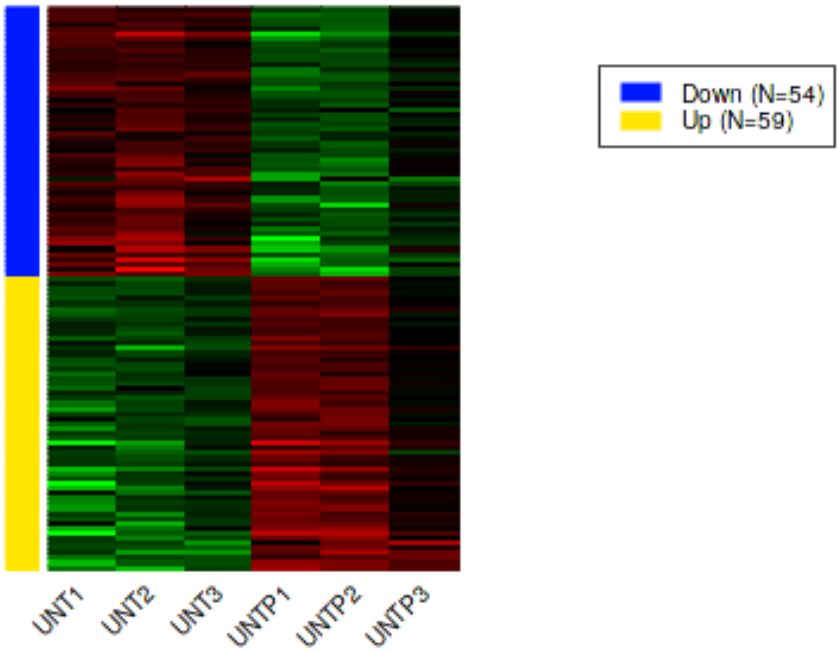

Fig. 4.34 Heatmap of gene expression: UNT+P v UNT (http://bioinformatics.sdstate.edu/idep92/)

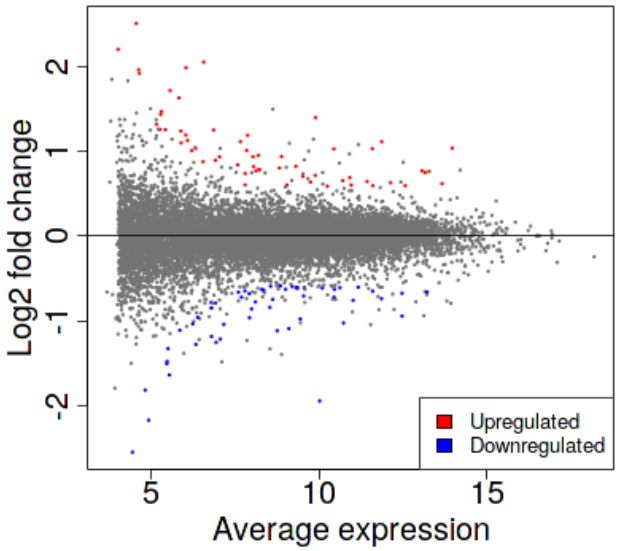

Fig. 4.35 MA plot: UNT+P v UNT (http://bioinformatics.sdstate.edu/idep92/)

Enrichment pathway analysis in iDEP92 (Fig. 4.36) showed significant upregulation of 10 molecular pathways, including cell migration, regulation of cell migration, and animal organ development (Appendix A Table A4-16). There were no significantly downregulated molecular pathways reported. Genes selected for comparison were listed (Appendix A Table A4-17), where a negative (-) Log_2 fold change indicated downregulation of a specific gene, and a positive Log_2 expression-fold change indicated upregulation of a particular gene.

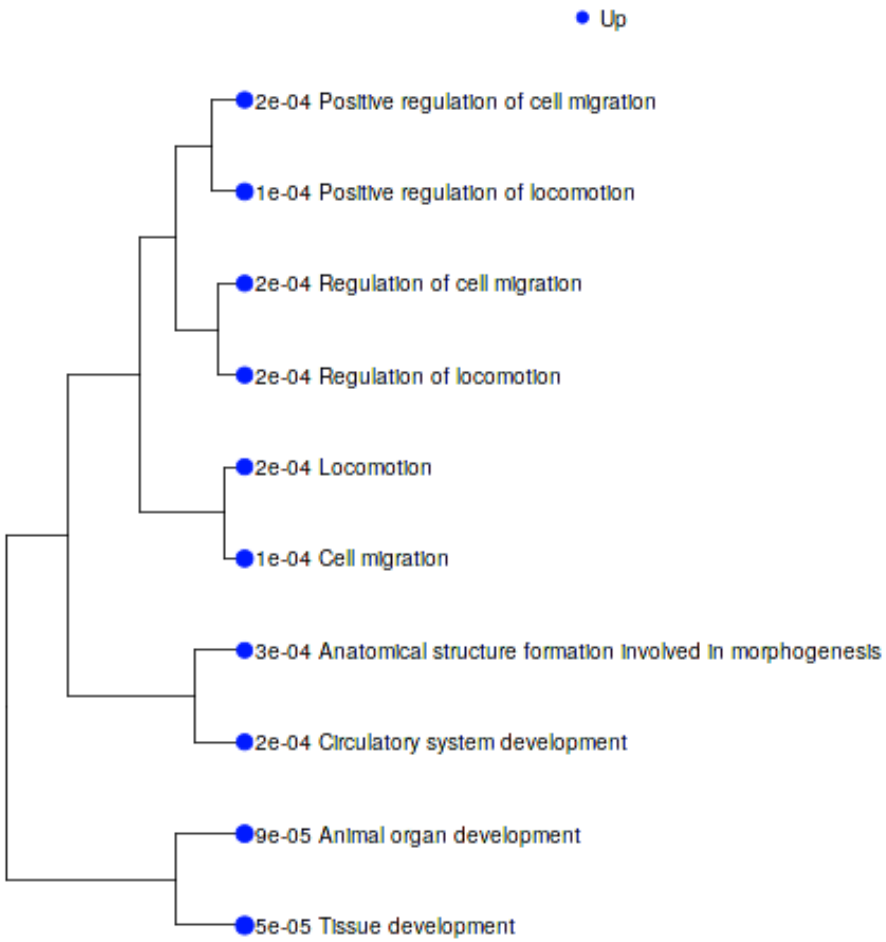

Fig. 4.36 DEGs enrichment pathways for SK-OV-3 cells treated with platelets versus untreated cells. Larger dots indicate smaller p-values. (http://bioinformatics.sdstate.edu/idep92/)

A cluster analysis (Fig. 4.37) demonstrated that pathways involving cell differentiation, extracellular matrix organisation, circulatory system process, response to virus, immune response, and leukocyte migration in our ovarian cancer cell model were all significantly altered in the presence of platelets (Appendix A Table A4-19). Gene set enrichment analysis (GSEA) yielded 17 significantly upregulated pathways that included cell cycle DNA replication, negative regulation of interferon-gamma production, and interstrand crosslink repair. It also returned a list of 13 significantly downregulated pathways that included cholesterol metabolic process, response to type I interferon, and type I interferon signaling pathway (Appendix A Table A4-18). Examples are shown for the upregulated pathways interstrand crosslink repair and the downregulated pathway response to type I interferon in Fig. 4.38 and Fig. 4.39, respectively.

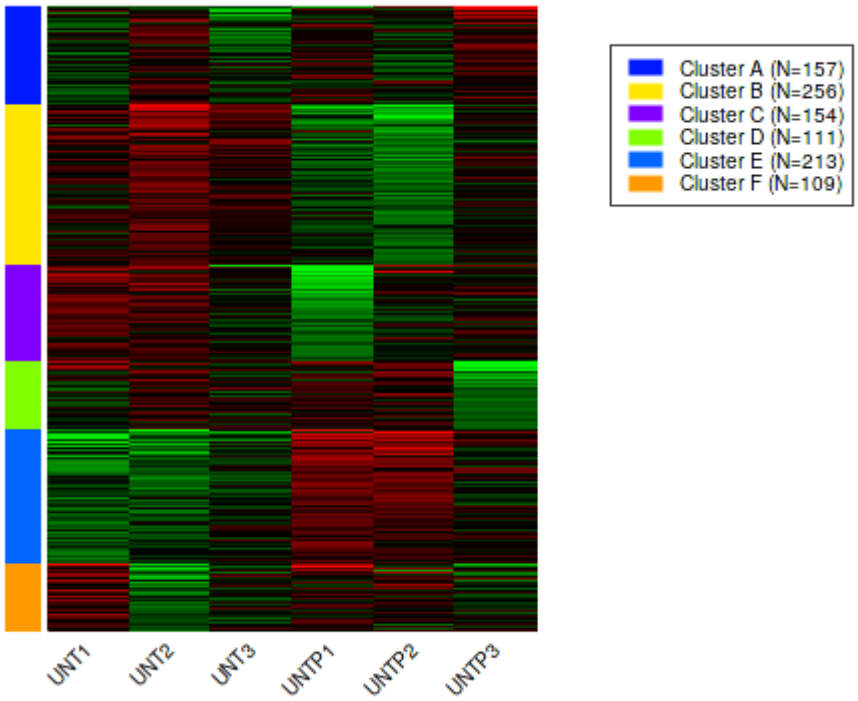

Fig. 4.37 Cluster analysis: UNT+P v UNT (http://bioinformatics.sdstate.edu/idep92/)

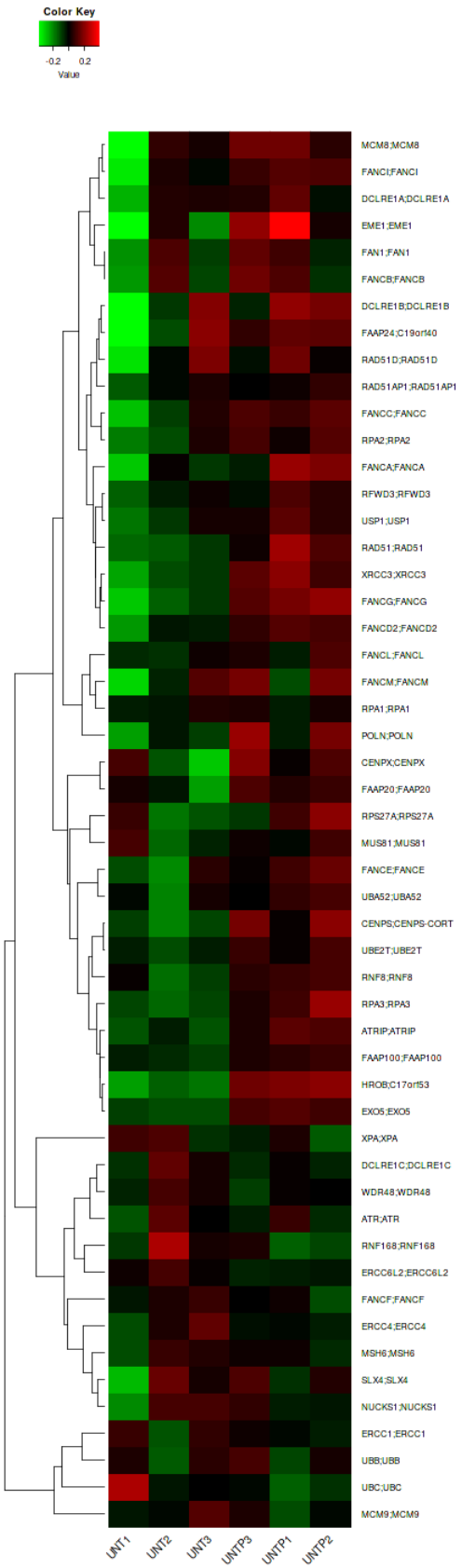

Fig. 4.38 Interstrand crosslink repair is significantly upregulated in the presence of platelets

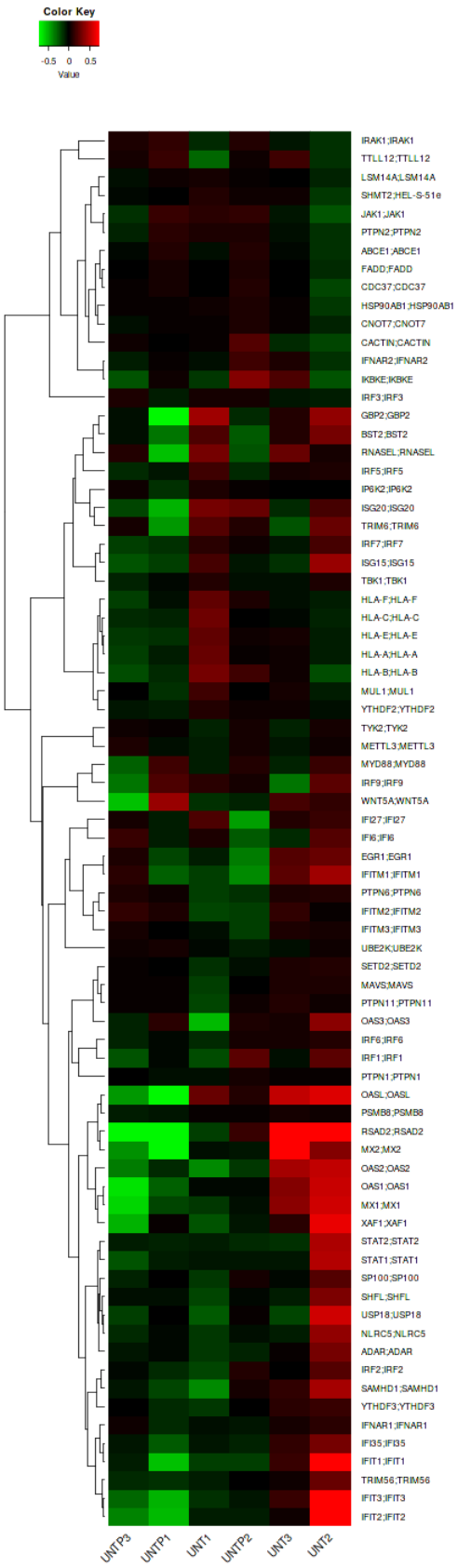

Fig. 4.39 Response to type I interferon is significantly downregulated in the presence of platelets

4.5.3.2.1 Pathways that were significantly upregulated when Platelets were added to Ovarian Cancer Cells

A workflow procedure was developed for the analysis of pathways that were significantly upregulated when platelets were added to SK-OV-3 cells (Fig. 4.14). Analysis of pathways that were significantly upregulated when our ovarian cancer cell line model was co-incubated with platelets was performed by uploading the list of significantly upregulated genes obtained from our iDEP92 analysis to ShinyGO (Fig 4.40).

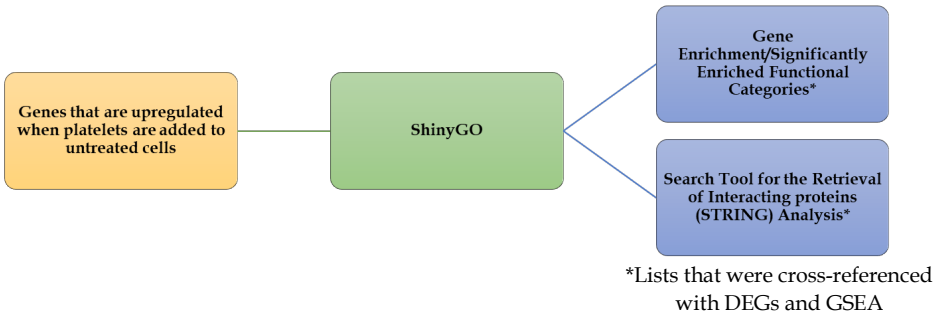

Fig. 4.40 ShinyGO analysis of genes that are upregulated when platelets are added to ovarian cancer cells

30 functional categories were significantly affected by the presence of platelets on ovarian cancer cells including cell migration, angiogenesis, regulation of response to wounding, and extracellular matrix organisation (Fig. 4.41).

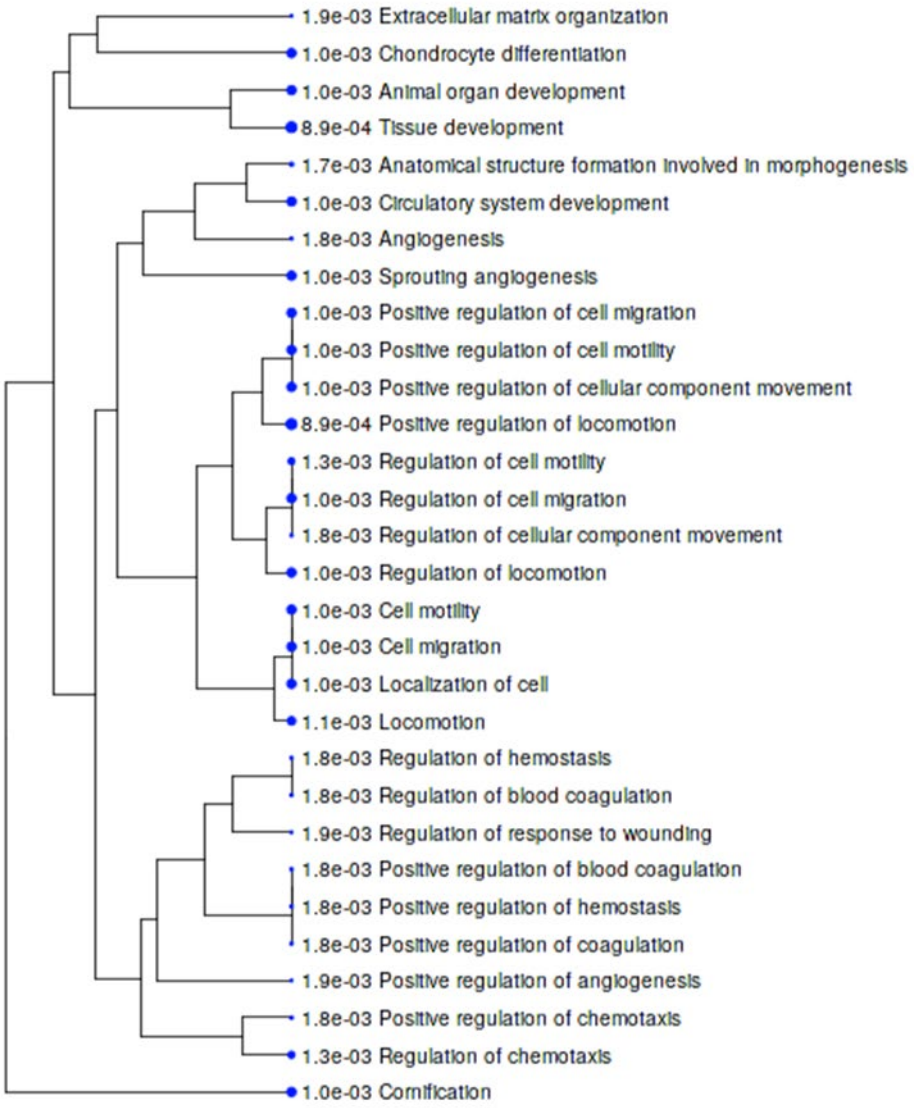

Fig. 4.41 Hierarchical clustering tree showing the correlation among enriched pathways that are significantly upregulated when platelets are added to ovarian cancer cells. Larger dots indicate smaller p-values. (http://bioinformatics.sdstate.edu/go/)

STRING analysis returned fewer affected functional categories, all of which were discovered in the initial ShinyGO analysis (Appendix A Table A4-20). However, uploading our list of significantly upregulated genes directly to the STRING website for gene-mapping yielded ontology which demonstrated that SERPIN E1 is central to biological processes associated with genes that are upregulated in ovarian cancer cells by the addition of platelets (Fig. 4.42).

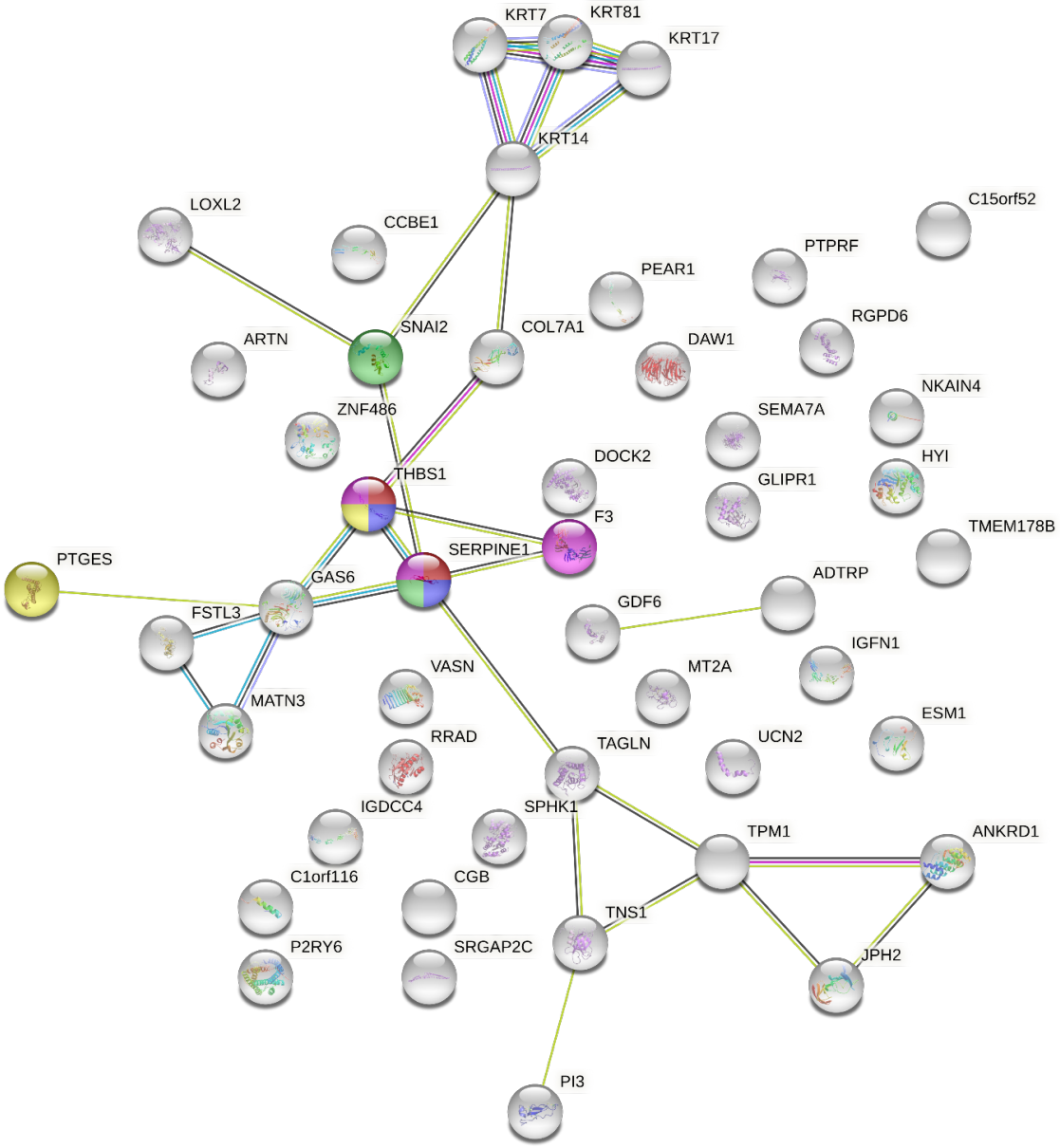

Fig. 4.42 Gene mapping demonstrates that SERPIN E1 is central to biological processes that are upregulated when platelets are added to ovarian cancer cells, including the negative regulation of plasminogen activation (red), the negative regulation of fibrinolysis (blue), the negative regulation of cell adhesion mediated by integrin (green), and the positive regulation of blood coagulation (purple). Circles containing images represent genes for which 3-D structures have been identified. (https://string-db.org/cgi/network?taskId=befshGD4GV1S&sessionId=brITvoqzWbvV)

Resulting enriched pathways in ShinyGO were cross-referenced with enriched pathways returned by DEGs in iDEP92, GSEA, and String (Appendix A Table A4-21). Some were present in all analyses, and some were only present in one. All were considered relevant. As the list of genes that were significantly upregulated in the presence of platelets was much shorter than for our PAI-1 knockdown analysis, some of these pathways did not contain enough genes for further analysis, and as in our siRNA analyses, GSEA did not return genes in a usable format, and STRING did not return a list of genes. Here, we have focused on three pathways from DEGs or ShinyGO that are significantly upregulated in the presence of platelets, that are relevant to cancer, and are potentially relevant to ovarian cancer cell metastasis. These pathways are anatomical structure formation involved in morphogenesis (Fig. 4.43, Appendix A Table A4-22), cell migration (Fig. 4.44, Appendix A Table A4-23), and angiogenesis (Fig 4.45, Appendix A Table A4-24).

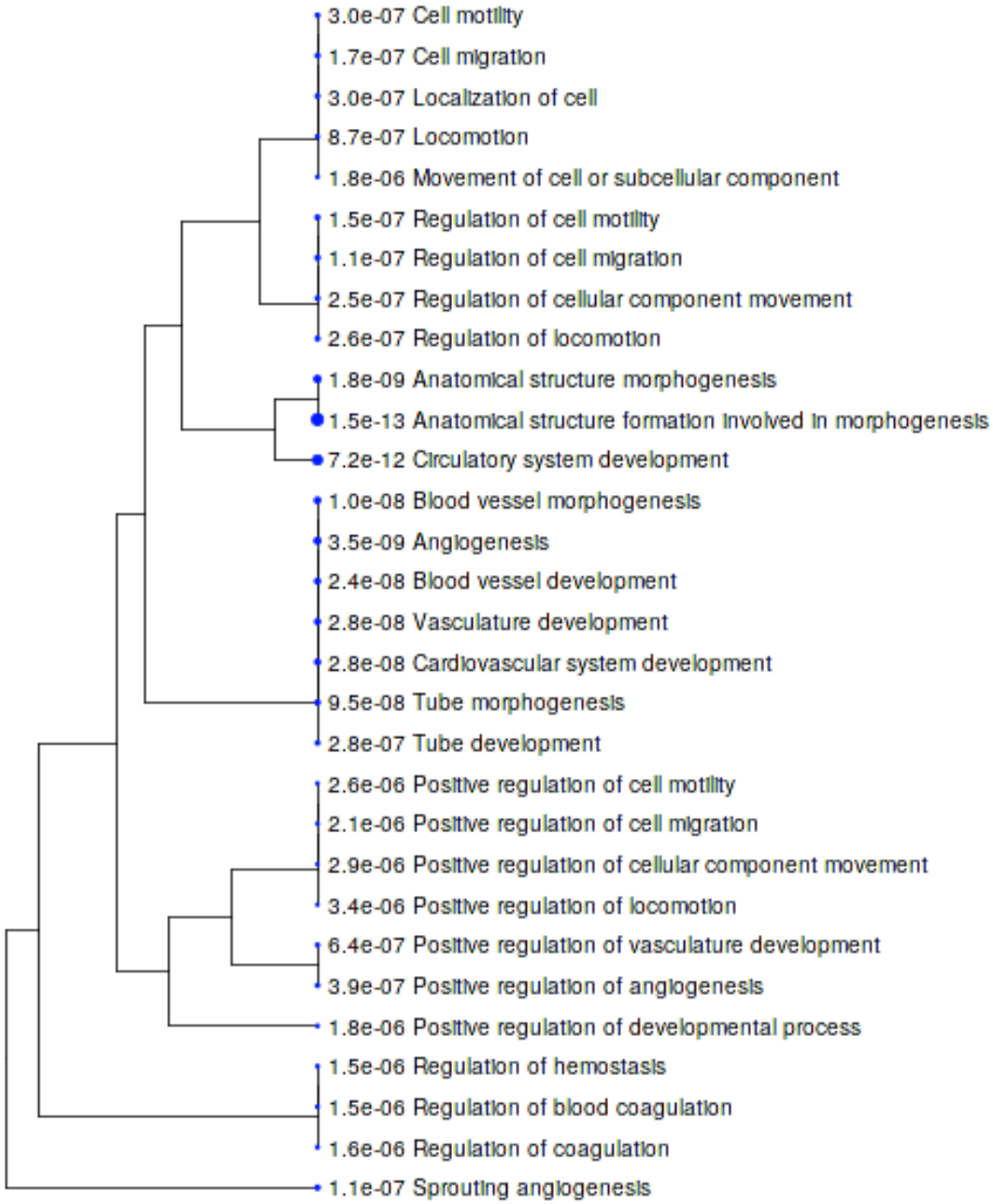

Fig. 4.43 A hierarchical clustering tree showing the connections among pathways involved in anatomical structure formation involved in morphogenesis that are significantly upregulated when platelets are added to SK-OV-3 cells. Larger dots indicate smaller p-values. (http://bioinformatics.sdstate.edu/go)

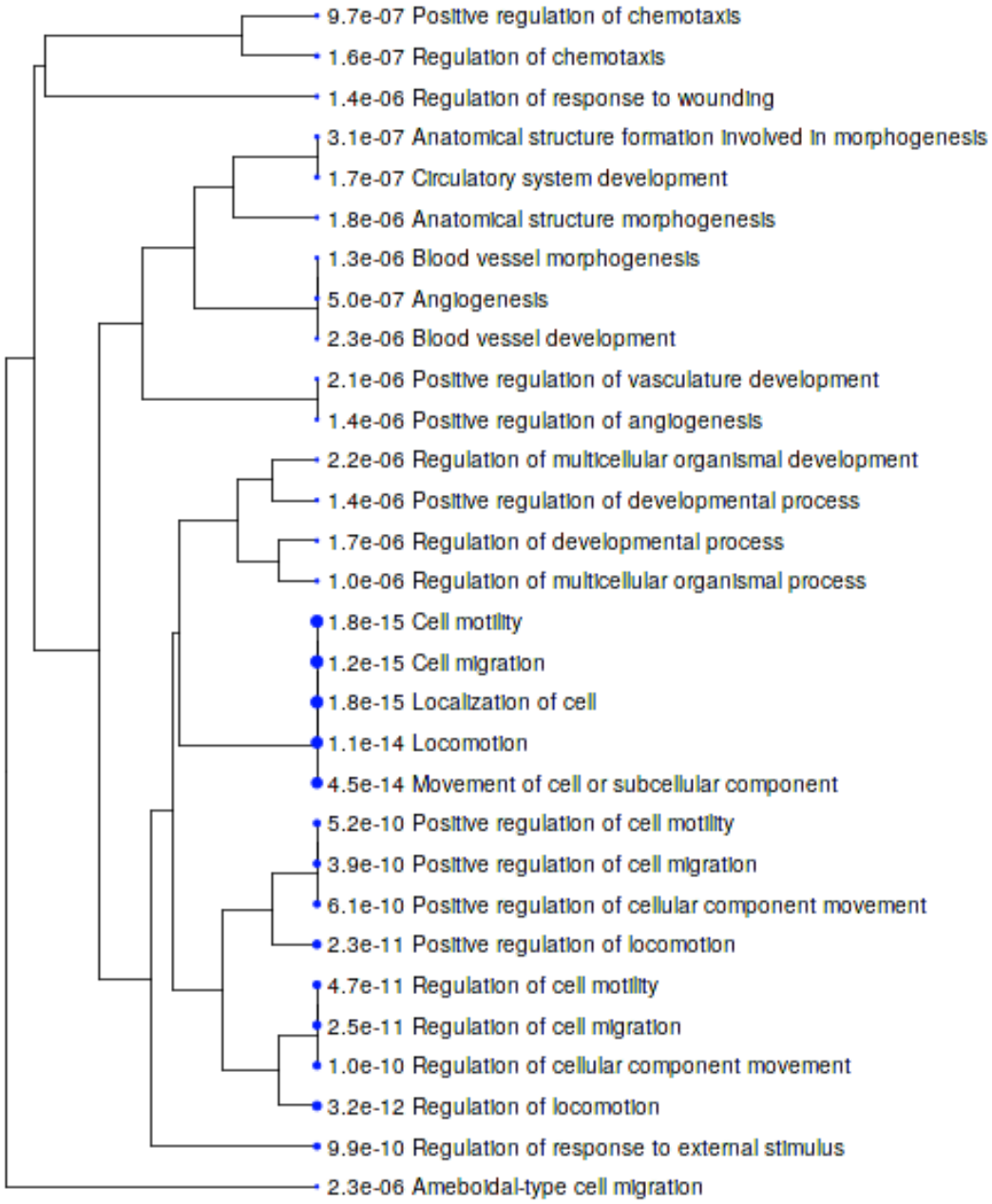

Fig. 4.44 A hierarchical clustering tree showing the connections among pathways involved in cell migration that are significantly upregulated when platelets are added to SK-OV-3 cells. Larger dots represent smaller p-values. (http://bioinformatics.sdstate.edu/go)

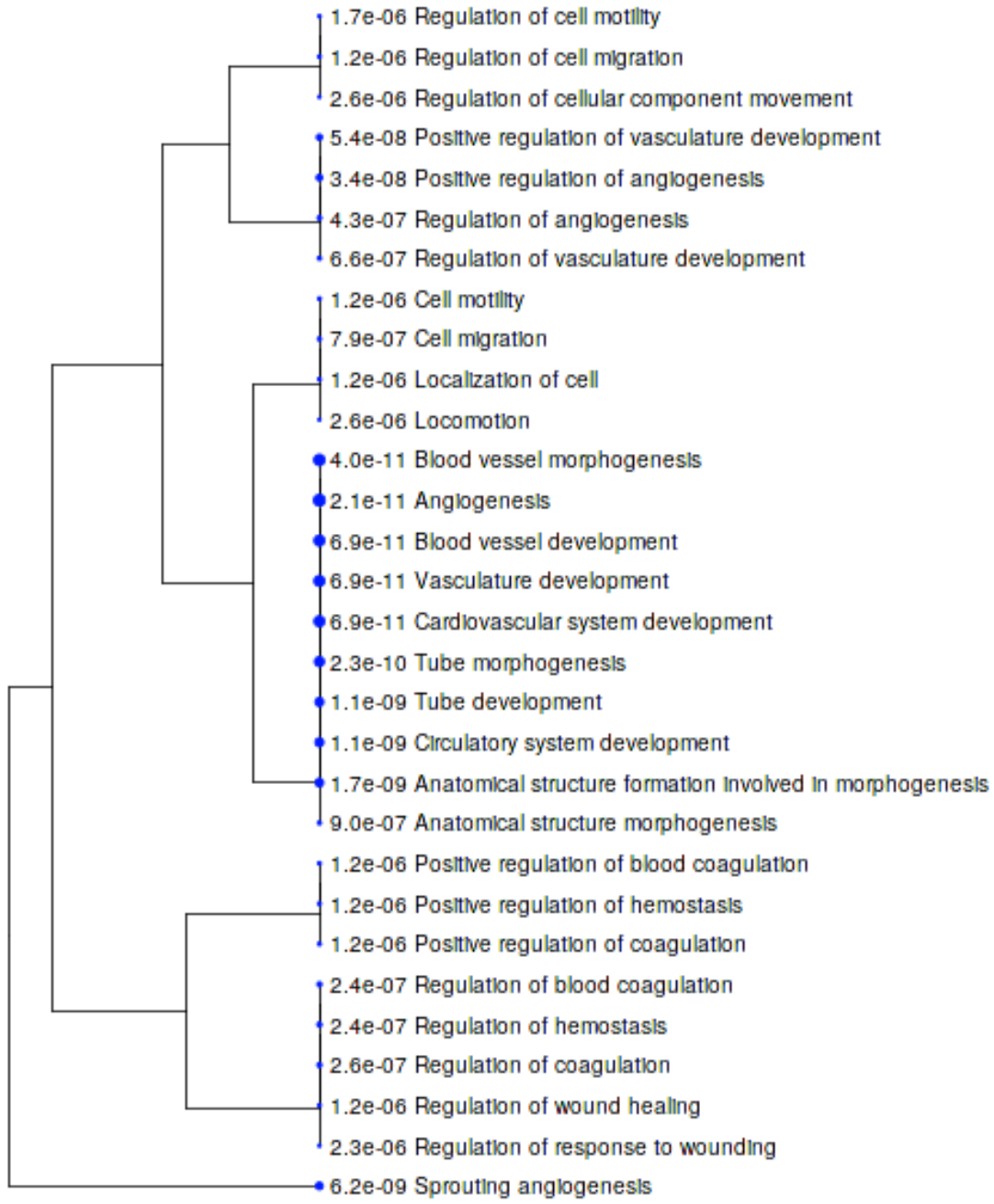

Fig. 4.45 A hierarchical clustering tree showing the connections among pathways involved in angiogenesis that are significantly upregulated when platelets are added to SK-OV-3 cells. Larger dots represent smaller p-values. (http://bioinformatics.sdstate.edu/go)

4.5.3.2.2 Pathways that were significantly downregulated when Platelets were added to Ovarian Cancer Cells

A workflow procedure was outlined for the analysis of pathways that were significantly downregulated when platelets were added to SK-OV-3 cells (Fig. 4.14). Analysis of the molecular pathways/functional groups in our ovarian cancer cell line model that were significantly downregulated by the addition of platelets was performed by uploading the list obtained in iDEP92 of significantly downregulated genes to ShinyGO (Fig. 4.46).

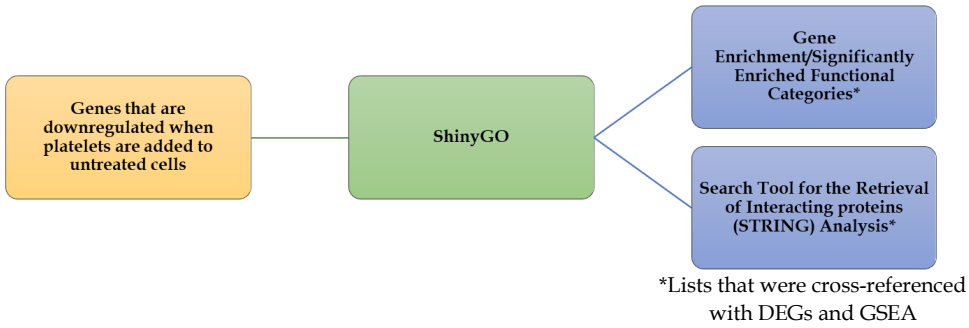

Fig. 4.46 ShinyGO analysis of genes that are downregulated when platelets are added to ovarian cancer cells

ShinyGO analysis did not find significant enrichment for any biological processes involving the downregulated gene list. STRING analysis within ShinyGO also found no significant enrichment. No cross-referencing was performed as there was only one enrichment analysis that yielded a result, and that was GSEA which did not return a gene list that was in a usable format. Further analysis using the STRING website was then attempted by submitting our list of significantly downregulated genes directly to their gene-mapping engine to visualise any interactions that might exist. This yielded gene ontology related to cellular components, specifically membrane and plasma membrane,

but as with the STRING analysis tool associated with ShinyGO, no significant enrichment for any biological processes was found.

4.5.3.3 Differential Gene Expression when Platelets have been added to an Ovarian Cell Line Model where PAI-1 has been transiently silenced

In order to study the effects of platelets on our ovarian cancer cell PAI-1 knockdown model, we engaged an iDEP92 analysis of genes that are differentially expressed when platelets were added to SK-OV-3 cells where PAI-1 has been knocked down via siRNA (Figs. 4.14 and 4.47).

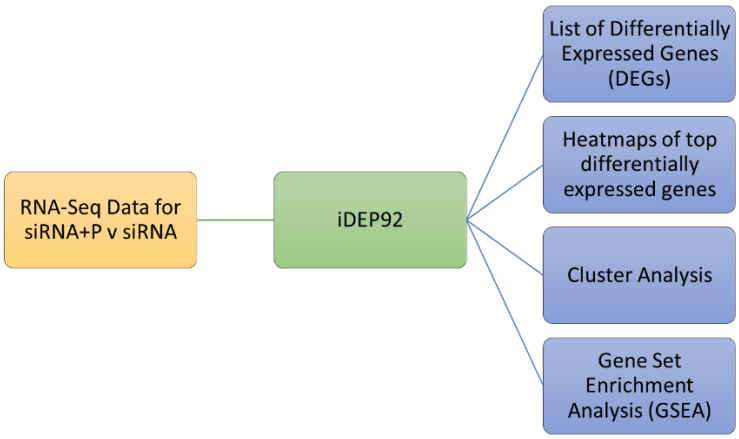

Fig. 4.47 Analysis of siRNA+P v siRNA in iDEP92

This returned a significant result of 11 upregulated genes and 6 downregulated genes (Table 4.4, Figs. 4.48 and 4.49). A list of genes included in the analysis was generated (Appendix A Table A4-25), however no significant gene enrichment was found.

Table 4.4 Genes that were significantly dysregulated as a result of adding platelets to ovarian cancer cells where PAI-1 had been silenced

UPREGULATED GENES: siRNA+P v siRNA				
Row-names	**Symbol**	**siRNAP-siRNA___log2FoldChange**	**Expression-fold Change**	**siRNAP-siRNA___padj**
ENSG00000108342	CSF3;CSF3	2.381327916	5.210160863	0.001863342
ENSG00000189052	CGB5;CGB3	1.831341908	3.558679255	0.004274264
ENSG00000213030	CGB8;CGB3	1.431449027	2.697174806	0.015219634
ENSG00000101198	NKAIN4;NKAIN4	1.31383331	2.486012086	0.002592665
ENSG00000171631	P2RY6;P2RY6	1.296260193	2.455914257	0.004274264
ENSG00000149591	TAGLN;DKFZp686P11128	0.831570765	1.779621909	1.23312E-05
ENSG00000198732	SMOC1;SMOC1	0.807959891	1.750733986	0.031297509
ENSG00000128422	KRT17;KRT17	0.806037453	1.74840263	0.004274264
ENSG00000120708	TGFBI;TGFBI	0.739530118	1.669631955	0.004274264
ENSG00000124225	PMEPA1;TMEPAI	0.691672855	1.615155262	0.001863342
ENSG00000105825	TFPI2;TFPI2	0.6080966	1.524246887	0.009089654
DOWNREGULATED GENES: siRNA+P v siRNA				
Row-names	**Symbol**	**siRNAP-siRNA___log2FoldChange**	**Expression-fold Change**	**siRNAP-siRNA___padj**
ENSG00000137648	TMPRSS4;TMPRSS4	-0.76836257	1.703335434	0.025458055
ENSG00000162591	MEGF6;MEGF6	-0.82766663	1.774812513	0.000340919
ENSG00000180638	SLC47A2;SLC47A2	-0.875271797	1.834353637	0.031297509
ENSG00000197635	DPP4;DPP4	-0.913447946	1.883541664	0.000282483
ENSG00000108602	ALDH3A1;ALDH3A1	-0.951358593	1.933692769	5.11681E-06
ENSG00000242574	HLA-DMB;HLA-DMB	-1.103340974	2.148516675	0.000340919

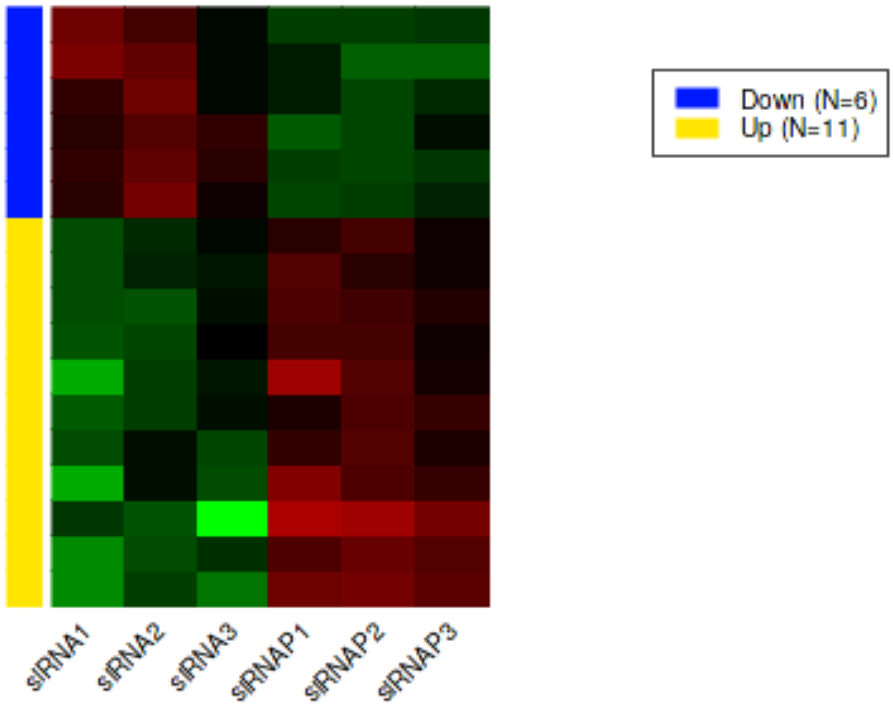

Fig. 4.48 Heatmap of gene expression: siRNA+P v siRNA (http://bioinformatics.sdstate.edu/idep92/)

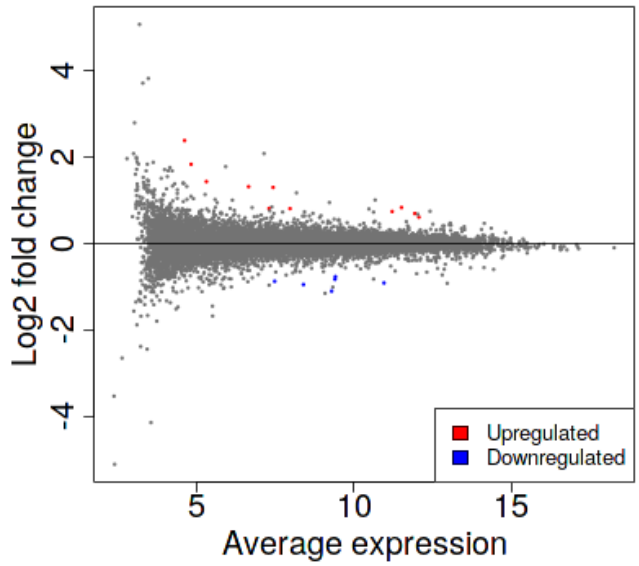

Fig. 4.49 MA plot average expression of siRNA+P and siRNA (http://bioinformatics.sdstate.edu/idep92/)

The significantly upregulated genes (Table 4.4) were colony-stimulating factor 3 (CSF3), chorionic gonadotropin subunits ß5 (CGß5) and ß8 (CGß8), sodium/potassium transporting ATPase interacting 4 (NKAIN4), pyrimidinergic receptor P2Y6 (P2RY6), transgelin (TAGLN), secreted modular calcium-binding protein 1 (SMOC1), keratin 17 (KRT17), transforming growth factor ß 1 (TGFßI), prostate transmembrane protein, androgen induced 1 (PMEPA1) and tissue factor pathway inhibitor 2 (TFPI2). Interestingly, although CSF3, SMOC1, TGFß1, PMEPA1, and TFPI2 were significantly upregulated when platelets were added to our PAI-1 knockdown, they were not significantly affected when platelets were added to untreated cells.

Significantly downregulated genes (Table 4.4) were identified as transmembrane protease serine 4 (TMPRSS4), multiple epidermal growth factor-like domains protein 6 (MEGF6), solute carrier family 47 member 2 (SLC47A2), dipeptidyl-peptidase 4 (DPP4), aldehyde dehydrogenase 3 family, member A1 (ALDH3A1), and HLA class II histocompatibility antigen DM beta chain (HLA-DMB). There were 6 genes that were significantly upregulated when platelets were added to our PAI-1 knockdown model that were also significantly upregulated when platelets were added to otherwise untreated ovarian cancer cells: CGß5, CGß8, NKAIN4, P2RY6, TAGLN, and KRT17.

Similarly, there were 3 genes that were significantly downregulated when platelets were added to our PAI-1 knockdown model that were also significantly downregulated when platelets were added to untreated cells, and these were SCL47A2, ALDH3A1, and DPP4. TGFß1 was not significantly

downregulated in our PAI-1 knockdown model in section 4.5.3.1.1, yet was significantly downregulated here when platelets were added to a PAI-1 knockdown model. KRT17 was significantly downregulated when platelets were added to cells treated with PAI-1 siRNA, and was the only gene in the siRNA+P v siRNA analysis that was also significantly downregulated when PAI-1 was knocked down without the addition of platelets.

TMPRSS4 was significantly upregulated in our PAI-1 knockdown, with an expression-fold change of 2.08, and p = 2.70139E-07, but was significantly downregulated here when platelets were added to a PAI-1 knockdown. Similarly, HLA-DMB was significantly upregulated in our PAI-1 knockdown, with an expression-fold change of 2.14, and p = 1.64878E-07, but was significantly downregulated here when platelets were added to the PAI-1 knockdown. Interestingly, the alpha chain HLA-DMA was found to be significantly downregulated when platelets were added to otherwise untreated ovarian cancer cells.

A cluster analysis of the top 100 dysregulated genes (Fig. 4.50, Appendix A Table A4-26) revealed enriched pathways that were downregulated by the presence of platelets (green) including response to type I interferon, negative regulation of viral genome replication, and immune effector process. Pathway clusters that were upregulated in the presence of platelets (red) included acute inflammatory response, response to bacterium, and positive regulation of prostaglandin biosynthetic process. While no significant enrichment was found for differentially expressed genes (DEGs), gene set enrichment analysis (GSEA)

did return a list of 7 significantly downregulated functional categories (Appendix A Table A4-27), including fatty acid metabolic process, carboxylic acid metabolic process, and several mechanisms related to lipid metabolism. An example of this – the carboxylic acid metabolic process - is shown in Fig. 4.51.

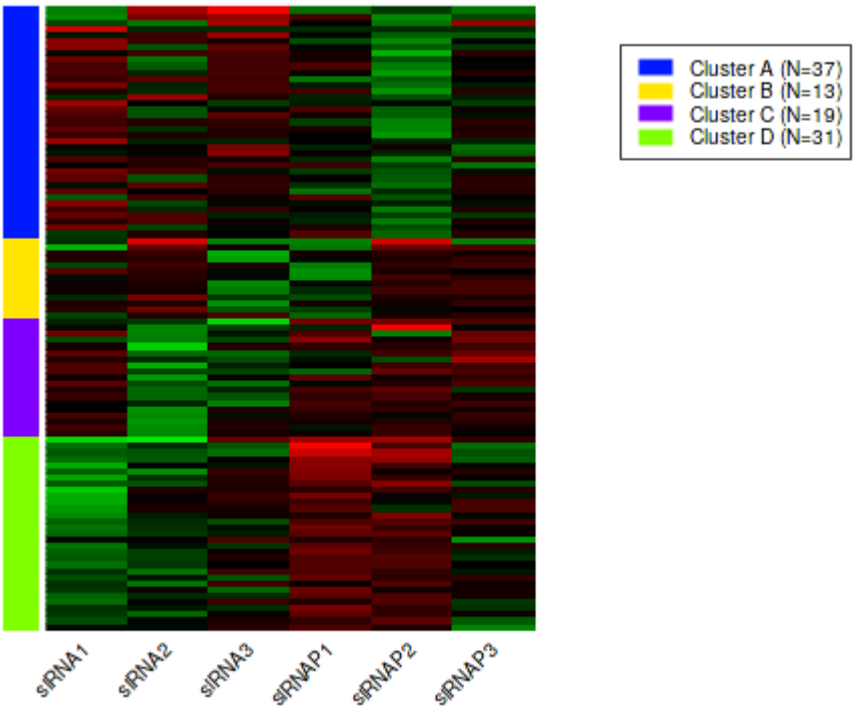

Fig. 4.50 Cluster analysis of the top 100 genes that are dysregulated when platelets are added to ovarian cancer cells where PAI-1 has been silenced

(http://bioinformatics.sdstate.edu/idep92/)

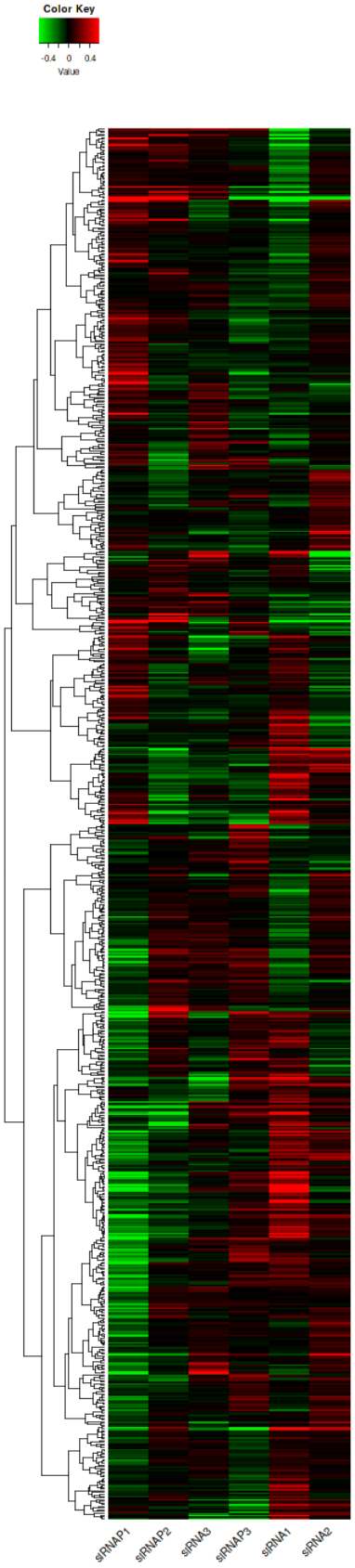

Fig. 4.51 Carboxylic acid metabolism is significantly downregulated when platelets are added to an ovarian cancer PAI-1 knockdown model (http://bioinformatics.sdstate.edu/idep92/)

4.5.3.3.1 Pathways that were significantly upregulated when Platelets were added to an Ovarian Cell Line Model where PAI-1 had been transiently silenced

A workflow chart was created for the investigation of pathways that are significantly upregulated when platelets are added to ovarian cancer cells where PAI-1 has been silenced (4.14). The list of genes that were significantly upregulated when platelets were added to our ovarian cancer cell PAI-1 knockdown model was submitted to ShinyGO (Fig. 4.52).

Fig. 4.52 ShinyGO analysis of genes that are upregulated when platelets are added to ovarian cancer cells where PAI-1 has been silenced

This yielded four significantly enriched upregulated pathways, all related to hormone signaling (Fig. 4.53, Appendix A Table A4-28). Further analysis in STRING did not find any gene enrichment.

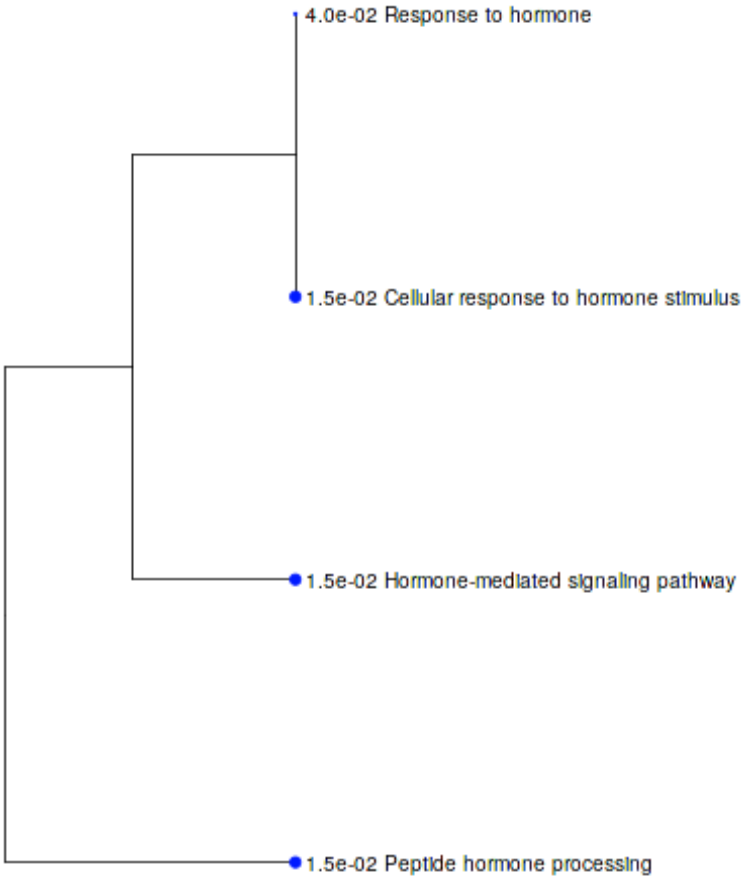

Fig. 4.53 Hierarchical clustering tree showing the correlation among enriched pathways that are significantly upregulated when platelets are added to ovarian cancer cells where PAI-1 has been silenced. Larger dots represent smaller p-values. (http://bioinformatics.sdstate.edu/go/)

4.5.3.3.2 Pathways that were significantly downregulated when Platelets were added to an Ovarian Cell Line Model where PAI-1 had been transiently silenced

As with our upregulated pathways, a workflow chart was created for the investigation of pathways that were significantly downregulated when platelets were added to ovarian cancer cells where PAI-1 has been silenced (4.15). The list of genes that were significantly downregulated when platelets were added to our ovarian cancer cell PAI-1 knockdown model was submitted to ShinyGO (Fig. 4.54).

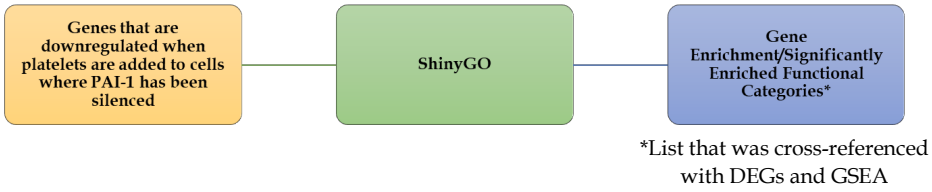

Fig. 4.54 ShinyGO analysis of genes that are downregulated when platelets are added to ovarian cancer cells where PAI-1 has been silenced

This yielded 25 significantly enriched downregulated regulated pathways, including response to hypoxia, regulation of T-cell activation, and positive activation of leukocyte activation (Fig. 4.55, Appendix A Table A4-29). It is of note that our gene list only included 6 genes, and that 22 of these functional categories included only DPP4 and HLA-DMB from our gene list. Two other categories – cell proliferation and regulation cell proliferation – also included ALDH3A1. A final category - response to drug - included only the two genes ALDH3A1 and SLC47A2. Analysis of gene distribution was not significant, and a STRING analysis did not return any significant gene enrichment. Our

downregulated functional categories did not contain the requisite number of genes required for further analysis.

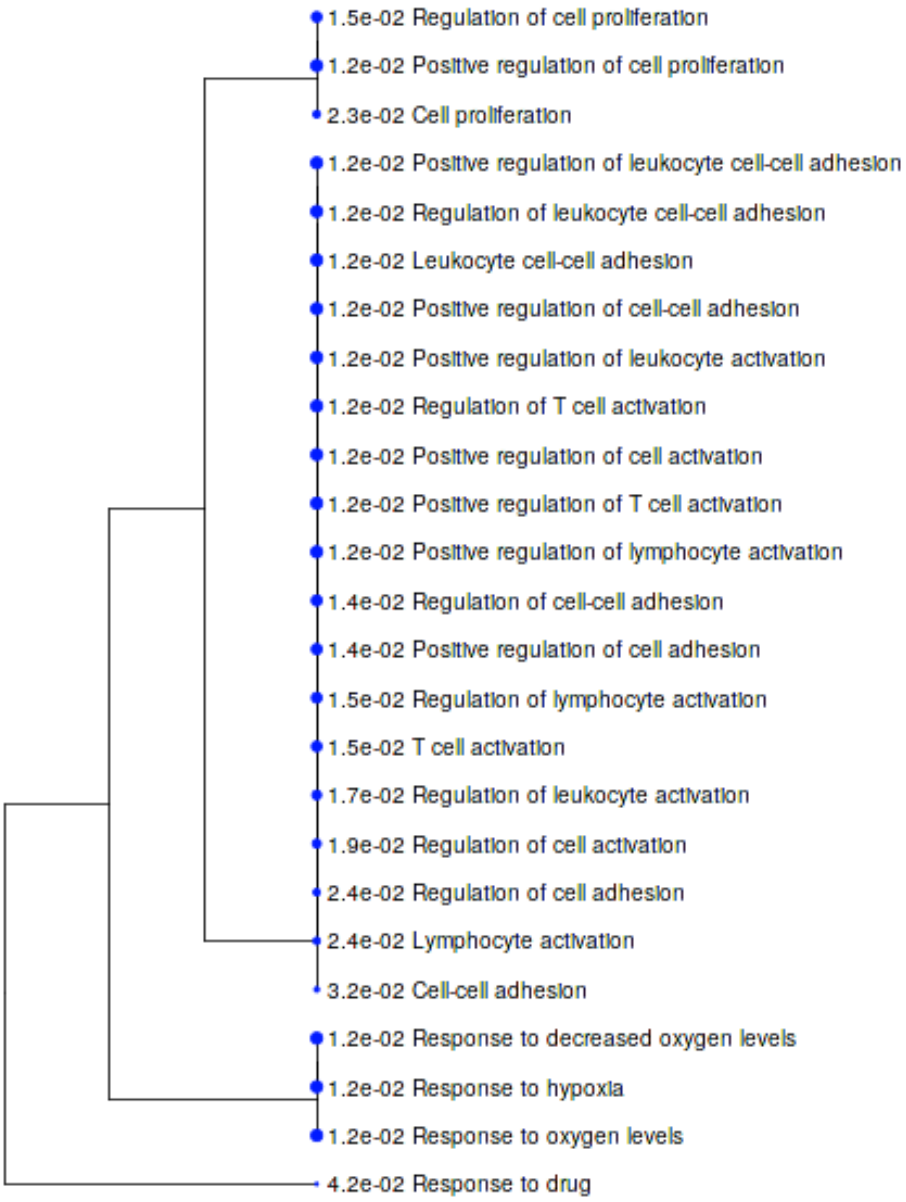

Fig. 4.55 Hierarchical clustering tree showing the correlation among enriched pathways that are significantly downregulated when platelets are added to ovarian cancer cells where PAI-1 has been silenced (http://bioinformatics.sdstate.edu/go/)

4.6 Discussion

Our initial overall analysis in iDEP92 returned a principal component analysis (PCA) which demonstrated strong clustering among the treatment types of which the 3 independent sample sets were comprised. Samples where PAI-1 had been silenced were very clearly separated from the other treatment types. Variation among the platelet-treated samples in the two treatment types that received platelets is most likely due to genetic differences among platelet donors.

Analysis through the Broad Institute's Integrated Genomics Viewer clearly showed differences in PAI-1 gene expression that occurred as a direct result of silencing PAI-1, and also showed differences that resulted from the addition of platelets to ovarian cancer cells. Of great interest is the gene expression that occurred within the intragenic regions (introns) in samples where PAI-1 had been silenced via siRNA, and also the fact that gene expression was also seen in introns in samples where PAI-1 had been silenced that had additionally been treated with platelets. Unfortunately, there was not enough time to further investigate this, but this will be addressed in future work as restriction fragment length polymorphism (RFLP) analysis along with single nucleotide polymorphisms (SNPs) could provide key insight into PAI-1's expression profile under various constraints.

Heatmaps identified many interconnected gene clades that were downregulated as a result of the loss of PAI-1, and that were upregulated in the presence of platelets. A cluster analysis gave a breakdown of how major

functional categories were affected across our 6 treatment types, and demonstrated different pathways that were either upregulated or downregulated when PAI-1 was silenced via siRNA, in the presence of platelets, or both. These pathways were mirrored in the enriched differentially-expressed gene (DEG) pathways, which included the significant downregulation of phosphorylation and regulation of response to wounding when PAI-1 was lost. Interestingly, the functional categories that were downregulated when PAI-1 was silenced were the same pathways that were upregulated when our ovarian cancer cell line was treated with platelets. These included cell proliferation, angiogenesis, positive regulation of cell migration, and type I interferon signaling pathway. This strongly suggests that SERPIN E1/PAI-1 is not only central to these molecular pathways, but also acts a molecular "switch" for these mechanisms.

4.6.1 Pathways and Genes that were significantly dysregulated in Ovarian Cancer Cells when PAI-1 was silenced

We have focused on 3 downregulated and 3 upregulated pathways that were intimately intertwined with the downregulation of PAI-1, and that were relevant to our gene of interest, SERPIN E1, to our results from chapter 3, and to cancer and potentially to ovarian cancer metastasis.

4.6.1.1 Downregulated Genes and Pathways in an Ovarian Cancer Cell PAI-1 Knockdown Model

Three significantly downregulated pathways relevant to the focus of this thesis were:

- cell migration (Fig. 4.24)
- cell motility (Fig. 4.25)
- regulation of cellular component organisation (Fig. 4.26).

The significant downregulation of 51 genes associated with cell migration and motility, 52 genes of the cell motility pathway, and 78 genes involved in the regulation of cellular component organisation as a direct result of the loss of PAI-1 was unsurprising, and again points to the SERPIN E1 as a potential master regulator of these molecular mechanisms, as shown in Fig. 4.28. Among these were CXCL1 (1.6 expression-fold change, $p = 0.00013$), which has been shown to be elevated in plasma and ascites of ovarian cancer patients (Bolitho *et al*, 2010) and CXCL3 (1.6 expression-fold change, $p = 0.00126$), which has been demonstrated to be upregulated in ovarian cancer, to mediate ascites-directed tumour cell migration in ovarian cancer, and has also been found to be an independent marker for reduced PFS in HGSOC (Windmüller *et al*, 2017). Targeting PAI-1 with a small-molecule inhibitor could potentially affect these pathways and provide better patient outcomes and longer survival. Other significantly downregulated genes in all three pathway lists included pro-inflammatory cytokine interleukin 6 (IL-6: expression-fold change = 2.23, $p = 0.0099$) and matrix metalloproteinase-1 (MMP-1: expression-fold change = 2.98, $p < 0.0001$). IL-6 has been found to stimulate cancer cell invasion through basement membrane via matrix metalloproteinase activity, to promote the cell cycle, and has been implicated in the epithelial-to-mesenchymal transition (EMT) (Browning *et al*, 2018). MMP-1 is correlated

with poor outcome in ovarian cancer, and extracellular vesicles derived from malignant ovarian cancer cells carrying MMP-1 mRNA have been shown to facilitate peritoneal dissemination (Yokoi *et al*, 2017). SH2B3, also known as lymphocyte adapter protein (LNK), has been demonstrated to be essential to ovarian cancer metastasis. Tissue staining arrays and *in vitro* assays by Ding and colleagues found that LNK was elevated in ovarian cancer, and further research revealed that silencing LNK decreased ovarian cancer cell growth both *in vitro* and *in vivo* (Ding *et al*, 2015). Significant loss of SERPIN E1/PAI-1 has also been shown to suppress tumour growth and reduce the invasiveness of glioblastoma (GBM) cells in the brain (Seker *et al*, 2019). Our results here combined with results by others suggest that SERPIN E1 is a key regulator of the metastatic process in ovarian cancer. While much more research is needed, silencing this gene and the subsequent results of our differential gene expression analysis here has provided insight into the metastatic network employed by HGSOC, and has highlighted potential therapeutic avenues.

4.6.1.2 Upregulated Genes and Pathways in an Ovarian Cancer Cell PAI-1 Knockdown Model

The list of significantly upregulated genes in our PAI-1 knockdown model returned a list of significantly affected functional categories and molecular pathways via DEGs and GSEA, and was interpreted by ShinyGO and STRING. These four results were cross-referenced, as described above for the list of significantly downregulated genes, and the three pathways chosen were:

- glycosylation (Fig. 4.30)
- homophilic cell adhesion via plasma membrane adhesion molecules (Fig. 4.31)
- cell adhesion (Fig. 4.32)

Inasmuch as transiently silencing PAI-1 expression resulted in the significant downregulation of many pathways and molecular processes, it also triggered the upregulation of many genes and subsequent pathways, including glycosylation, homophilic cell adhesion via plasma membrane adhesion molecules, and cell adhesion in general. These upregulated genes and pathways suggest that PAI-1 could potentially exert different effects that may be contingent upon its gradient within the cell (or the whole body), and this could give us insight into potential side-effects of small molecule PAI-1 inhibitors. For example, a loss of 50% of functional PAI-1 might cause the upregulation of another important protein and result in an undesirable effect for the patient, but a loss of 35% of functional PAI-1 might not have this unwanted side effect. This also would be likely to be different for every patient.

There were not any common genes shared between the glycosylation pathway and the other two pathways, but that they are all upregulated when SERPIN E1 is silenced suggests that PAI-1 protein is a master regulator of these mechanisms. Of the glycosylation pathway, many genes related to the Golgi apparatus are affected (string-db.org), which would be expected as this is where, along with the endoplasmic reticulum (ER), glycosylation occurs during protein production. Glucoside xylosyltransferase 1 (GXYLT1: expression-fold

change = 2.83, $p < 0.0001$) and glucoside xylosyltransferase 2 (GXYLT2: expression-fold change =1.69, $p = 0.00038$), for example, are responsible for the elongation of O-linked glucose molecules that are attached to the endothelial growth factor (EGF)- like repeats in the extracellular domains of Notch family proteins (Sethi *et al*, 2010). While Notch 1 and Notch 2 were not significantly differentially expressed themselves, their functions are most certainly affected by the silencing of PAI-1. This is important as the Notch pathway is a primary regulator of angiogenesis in ovarian carcinoma (Xie *et al*, 2017). RNAi Knockdown of the GXYLT homologue Shams was shown to directly increase Notch activation in *Drosophila*, while overexpression of a human influenza hemagglutinin (HA) tagged human GXYLT in *Drosophila* was shown to decrease cell surface expression of Notch and to decrease Notch activation (Lee *et al*, 2013). Taken together with our results, this suggests that reducing PAI-1 indirectly reduced notch surface expression and signaling capabilities via increased glycosylation. A Western blot would be useful to investigate this.

Homophilic cell adhesion via plasma membrane adhesion molecules was another pathway that was upregulated in conjunction with the loss of PAI-1. All of the genes of this pathway are also members of our third category, cell adhesion, and include several protocadherins, such as PCDH7 (expression-fold change = 2.83, $p < 0.0001$), and PCDH10 (expression-fold change = 2.2, $p < 0.0001$), which are both located on chromosome 4 – a frequent site of loss of heterozygosity (LOH) in cervical cancer (Narayan *et al*, 2009). PCDH7 has been shown to be overexpressed in breast cancer and in non-small cell lung cancer

(NSCLC), and is also central to the metastasis of breast cancer to the brain (Shishodia *et al*, 2017). PCDH10 is a tumour suppressor gene that has been shown to be an early target of hypermethylation in cervical cancer (Narayan *et al*, 2009). Downregulation of PCDH10 has been demonstrated to correlate with advanced stage, higher grade, recurrence, and reduced overall survival (OS) in patients with bladder cancer compared to normal controls (Ma *et al*, 2013). All of these could have implications in ovarian cancer diagnosis and prognosis. Upregulation of PCDH10 as a result of a significant loss of PAI-1 suggests that targeting PAI-1 for reduction could be beneficial if the result is an increase in tumour suppressor protocadherins.

In addition to several protocadherins, the cell adhesion pathway included many significantly upregulated genes that could have implications in the diagnosis and treatment of ovarian cancer. Among these was wingless-related integration site 4 (Wnt4), an important protein in the stabilisation of ß-catenin and female sex development. The Wnt/ ß-catenin pathway is suspected to play a role in ovarian cancer, and correlations have been shown between Wnt activity and cancer grade, EMT, chemoresistance, and poor prognosis (Teeuwssen and Fodde, 2019). While Wnt4 was significantly upregulated when the SERPIN E1 gene was silenced, the important part of this equation is that ß-catenin was not significantly differentially expressed in our RNA-Seq results. This helps to confirm that it is Wnt that stabilises ß-catenin and not the other way around. Of note is that none of the genes involved in the ß-catenin "destruction complex", which includes protein phosphatase 2A

(PP2a), glycogen synthase kinase 3 (GSK3β), casein kinase 1α (CK1α), adenomatous polyposis coli (APC), and the scaffold proteins/ tumour suppressor proteins AXIN1/2, was significantly dysregulated as a result of the loss of PAI-1. Another thing that stood out was that the Wnt ligands were not significantly altered either. Frizzled (FZD1) was not significantly altered, neither LRP5 or LRP6 was significantly altered, none of T-cell factor/lymphoid enhancer factors (TCF/LEF) were significantly altered, and the TCF/LEF called LEF1 was missing entirely from our genetic profile. It is interesting that of these two symbiotic pathways, Wnt4 alone was significantly differentially expressed. One might expect that the overexpression of Wnt4 in the absence of an upregulation of its ligands would trigger the ß-catenin proteasome, but this is not what happened, and in fact our results here support research by Pascal Bernard and his colleagues which showed that of the Wnt proteins, Wnt4 was unique in that it did not participate in the translocation of ß-catenin to the nucleus for interaction with TCF, but that it instead facilitated the translocation of ß-catenin to the cell membrane (Bernard *et al*, 2008). Bernard's research further suggested that Wnt4 acted as a molecular "switch" for ß-catenin functionality as either a transcription factor or participant in cell-cell adhesion and migration (Bernard *et al*, 2008). This switch is likely to be a phosphorylation event, and could potentially be the phosphorylation of Tyr^{142}, which has been shown to disrupt adherens junctions and to promote the transcriptional activity of ß-catenin (Bernard *et al*, 2008). As silencing PAI-1 instigates significant upregulation of Wnt4, while none of its ligands or ß-

catenin proteasomal degradation components are significantly altered, this could point to PAI-1 as a regulator of non-canonical Wnt signaling in ovarian cancer, and this warrants further investigation.

4.6.2 Differential Gene Expression when Platelets were added to Ovarian Cancer Cells

Previous investigation by our laboratory into the effects of platelets on cancer cells, their contribution to immune evasion, and their prominence in the establishment of metastatic niches revealed that PAI-1 was one of the five most commonly dysregulated genes when platelets were co-incubated with 15 cancer cell lines that spanned 7 different cancer types, including ovarian cancer (Cluxton *et al*, 2019). We have demonstrated in chapter 3 that platelets increase migration, wound-healing, and the cell cycle, and that they also increase the amount of both PAI-1 mRNA and PAI-1 protein in SK-OV-3 cells. To highlight genotypic changes with regard to specific molecular pathways that are influenced by the presence of platelets, we added platelets to ovarian cancer cells. Again, our four gene ontology lists were cross-referenced, where applicable, for each set of up or downregulated genes, and three pathways were chosen based on their relevance to research discussed in chapter 3, to cancer in general, and to ovarian cancer metastasis.

4.6.2.1 Pathways and Genes that were significantly upregulated when Ovarian Cancer Cells were treated with Platelets

Our analysis in iDEP92 yielded 59 genes that were significantly upregulated when platelets were added to our ovarian cancer cell model, 5 of which were undefined. Submitting this gene list to ShinyGO identified many

upregulated pathways that were virtually identical to those identified by submitting the list of genes we obtained as a result of adding platelets to our siNEG-treated cells. These including the following pathways, which were chosen for discussion:

- anatomical structure formation involved in morphogenesis (Fig. 4.43)
- cell migration (Fig. 4.44)
- angiogenesis (Fig 4.45)

The genes involved in all three of these pathways included SERPIN E1, which was shown to be significantly upregulated in our RNA-Seq analysis, with an expression-fold change of 2.04, and $p < 0.0001$. Previous research has demonstrated that PAI-1 is involved with the aforementioned processes of anatomical structure formation involved in morphogenesis (Ma *et al*, 2013), cell migration (Lee and Huang, 2005), and angiogenesis (Wu *et al*, 2015). In addition to PAI-1, the mesenchymal-related gene SNAI2 was also found to be significantly upregulated when platelets were added to our ovarian cell line model, and is listed in the first two of our three pathways. This supports previous research by Guo and colleagues, who found that platelets promote invasion and induce EMT in ovarian cancer cells (Cooke *et al*, 2015; Guo *et al*, 2019). Other genes of these pathways include sensory histidine protein kinase (SHPK1: expression-fold change = 1.82, $p < 0.0001$), which has recently been identified as a viable target for treatment of ovarian cancer with metformin, a drug commonly used to treat type II diabetes, gestational diabetes, metabolic syndrome, and polycystic ovarian syndrome (PCOS). It is perhaps noteworthy

that women with diabetes were not found to be at an elevated risk of ovarian carcinoma (Adler *et al*, 1996).

Neuropilin-2 (NRP2: expression fold-change = 1.5, p = 0.01495), first identified as a gene involved in axon guidance, was the first gene listed in our anatomical structure formation pathway, and has been shown to be essential to tumour metastasis (Caunt *et al*, 2008). It was also listed in our cell migration and angiogenesis pathways. NRP2 was slightly upregulated in our PAI-1 knockdown, but not significantly, suggesting that PAI-1 may be a "link" in the "chain". Blocking NRP2 disrupted VEGF-C binding, ultimately reducing endothelial cell migration in the lymphatic system as well as tumoural lymphangiogenesis in mice (Caunt *et al*, 2008). It was also demonstrated to reduce metastasis to sentinal nodes, and it is thought that this is accomplished via a "delayed departure" of cells from the primary tumour (Caunt *et al*, 2008). Additional research by Grandclement and colleagues demonstrated that the expression of NRP2 promoted EMT that was mediated by TGF- ß1 in colorectal cancer cells (Grandclement *et al*, 2011). TGF- ß1 binds the promoter of SERPIN E1 as a TF (Samarakoon and Higgins, 2008), and so could be a mediator for any potential crosstalk that may be occurring between NRP2 and SERPIN E1. In addition to neuronal and endothelial function, it has been demonstrated that NRP2-positive osteosarcoma tumours display increased vascularization (Handa *et al*, 2000), and NRPs have also been implicated in epithelial neoplasms of the gastrointestinal (GI) tract, prostate, lung, and ovary (Wild *et al*, 2012). The exact mechanism involved in the upregulation of this pathway by the platelets

requires further research. As adding platelets significantly upregulated NRP2 in our ovarian cancer cell model, this could have enormous implications for circulating tumour cells (CTCs), and the contribution of the platelet cloak to immune evasion, and metastasis.

4.6.2.2 Pathways and Genes that were significantly downregulated when Ovarian Cancer Cells were treated with Platelets

No significant gene enrichment was found in ShinyGO with regard to the list of genes that are downregulated when platelets are added to ovarian cancer cells, and this suggests that platelets contribute an additive effect only on ovarian cancer cells and do not detract from the functionality of these cells. Gene set enrichment analysis (GSEA) in iDEP92 did yield downregulated pathways that included the type I interferon signaling pathway and cholesterol biosynthesis and metabolism, but did not return a usable gene list. Our analysis in STRING yielded downregulated pathways related to membrane plasma membrane, but no gene ontology related to biological process was found.

4.6.3 Differentially Expressed Genes when Platelets were added to an Ovarian Cancer PAI-1 Knockdown Model

What was clear from the very basic analyses that we were able to perform with the few genes that were affected when platelets were added to our PAI-1 knockdown is that PAI-1 is essential to the overall functionality of ovarian cancer cells in general. When PAI-1 is lost, platelets alone are not able to recover the genotype necessary for a functional phenotype. The pathways that were downregulated in our analysis of siRNA+P v siRNA were not the

same pathways that were downregulated in our knockdown where platelets were not added. This supports the results of our research in chapter 3, and suggests that when PAI-1 is lost, an entirely different set of molecular pathways comes into play as frantic yet unsuccessful attempts at recovery of function by the SK-OV-3 cells are made. These pathways are listed in the appendix, and include regulation of T-cell activation, response to hypoxia, and leukocyte activation - all biological processes which can have profound implications for ovarian cancer and cancer in general. However, only 2 of our significantly downregulated genes were involved in the majority of these pathways, and these were DPP4 and HLA-DMB. DPP4 is a surface glycoprotein that is regulated by hypoxia in ovarian cancer (Moffitt *et al*, 2020), so it not surprising that this gene is prominently featured here. HLA-DMB is a class II histocompatibility antigen that interacts with MHC-II on B-cells in humans, and while this was significantly downregulated here, it was significantly upregulated when PAI-1 was silenced without the addition of platelets. It was not significantly affected by adding platelets to otherwise untreated ovarian cancer cells, however its alpha chain HLA-DMA was significantly upregulated when platelets were added to ovarian cancer cells. HLA-DMB has been identified as a potential susceptibility gene for risk of developing HHV-8-induced Kaposi's sarcoma in HIV-1+ men (Aissani *et al*, 2014). Overexpression of HLA-DMB in the tumour epithelium has been associated with improved prognosis in advanced serous ovarian cancer due to increased cytotoxic T-lymphocyte (CD8+) infiltration, which is also associated with improved

survival in serous ovarian cancer (Callahan *et al*, 2008). These important discoveries by Aissani and by Callahan taken together with the downregulation of the HLA-DMB gene in the context of both a significant loss of PAI-1 and the presence of platelets, and also with the significant upregulation of HLA-DMB when PAI-1 is silenced with no platelets added, suggests that platelets and PAI-1 function in tandem in immune regulation. It also suggests that the loss of too much PAI-1 coupled with an increase in platelets could have disastrous effects for patient outcomes, but that keeping a balance between PAI-1 and platelets could potentially provide a benefit if infiltration of CD8+ T-cells into the tumour microenvironment can be achieved.

Enriched pathways (appendix) from our iDEP92 analysis showed a significantly downregulated response to hypoxia when platelets were added to an ovarian cancer cell PAI-1 knockdown model. Exactly what that response is requires further investigation, and leaves the door open to many questions that warrant further investigation, not the least of which is that when PAI-1 is not functional, could platelets assist in suppressing angiogenesis rather than encouraging it? Do the platelets somehow "switch teams" in response to a PAI-1 gradient? This is a crucial question that could have significant implications for the future treatment of ovarian cancer with small-molecule inhibitors that could perhaps target some of the PAI-1 but not all of it. As platelets have been shown to assist in immune evasion, as well as drive EMT and the formation of metastatic niches, gauging platelet response in any cancer treatment is of the utmost importance (Egan *et al*, 2011; Labelle *et al*, 2011; Cooke *et al*, 2013). The

only gene that was significantly downregulated in our siRNA+P v siRNA analysis that was also significantly downregulated in our siRNA v siNEG analysis was KRT17. This further supports that it is not only the loss of PAI-1, but the added presence of platelets that is key in the dysregulation of the other ten genes that were significantly downregulated in the siRNA+P v siRNA analysis.

Table 4.5 KRT17 is the sole significantly downregulated gene not affected by platelets

Symbol	siRNAP-siRNA___log2FoldChange	Expression-fold Change	siRNAP-siRNA___padj
CSF3;CSF3	2.381327916	5.210160863	0.001863342
CGB5;CGB3	1.831341908	3.558679255	0.004274264
CGB8;CGB3	1.431449027	2.697174806	0.015219634
NKAIN4;NKAIN4	1.31383331	2.486012086	0.002592665
P2RY6;P2RY6	1.296260193	2.455914257	0.004274264
TAGLN;DKFZp686P11128	0.831570765	1.779621909	1.23312E-05
SMOC1;SMOC1	0.807959891	1.750733986	0.031297509
KRT17;KRT17	0.806037453	1.74840263	0.004274264
TGFBI;TGFBI	0.739530118	1.669631955	0.004274264
PMEPA1;TMEPAI	0.691672855	1.615155262	0.001863342
TFPI2;TFPI2	0.6080966	1.524246887	0.009089654

4.7 Study Limitations

The goal of this chapter was to interrogate differential gene expression using RNA sequencing (RNA-Seq) in an ovarian cancer cell line model where PAI-1 had been silenced, co-incubation with platelets had occurred, or both. RNA-Seq is a valuable high-throughput sequencing (HTS) tool in the fields of genomics, proteomics, and transcriptomics. It can, however, be limited in some respects due to the low number of replicates typically processed, and its reliance on inferences that do not treat each gene as a separate entity (Love *et al*, 2014). In order to tame this, RNA-Seq analysis methods such as DESeq2 typically pool information about genes, and thereby assume similarities in variances among those genes, and this provides a robust gene-level analysis for downstream investigations (Love *et al*, 2014).

Despite this, there can be drawbacks from what is known as the "batch effect" stemming from the fact that untransformed count matrices must be input into DESeq2, and not the normalised data (Zhang *et al*, 2020). "Batch effect" is a relatively normal occurrence in RNA-Seq that is often simply a technical variation between sample sets. However, these slight variations can cause undesirable downstream issues, such as differences in sample read count distribution. These differences cannot be fully corrected via normalisation, but can often be corrected using a negative binomial regression such as ComBat or ComBat-Seq (Zhang *et al*, 2020), as was done here.

We live in a great age of bioinformatics and computational power, but it is important to remember that biology, chemistry, and physics are the true underpinnings of those processes that are delineated by the bioinformatics, and that while they sometimes conform to our manmade ideas of how they should function, sometimes they do not. This is not to say that these tools do not give us great advantage in shedding light on the path ahead, but rather that we would be wise to remember that it is only a light, and not the path itself.

4.8 Conclusion

This chapter has presented RNA-Seq data pertaining to the differential expression of SERPIN E1 in an ovarian cancer cell line model as the result of transfection with SERPIN E1 siRNA, co-incubation of ovarian cancer cells with donor platelets, and both of these treatments combined. Our results here provide evidence for the SERPIN E1 gene and its product, PAI-1, as genetic and molecular regulators of many of the hallmarks of ovarian cancer metastasis,

including cell migration, cell adhesion, glycosylation, and angiogenesis. These results also suggest that PAI-1 is a master mediator of platelet-cancer cell interactions, and this has enormous implications for future research into CTCs, platelet-facilitated immune evasion, and the hematogenous metastasis of ovarian cancer and other cancers.

CHAPTER 5

ASSESSMENT OF PAI-1 IN CLINICAL SAMPLES

5.1 Introduction

Performing research in vitro is important for establishing proof of concept for those elements of assay design that may prove useful in a clinical context. It enables us to define and fine-tune those aspects of that research which may be clinically relevant, the goal of research ultimately being to benefit the patient.

Overexpression of PAI-1 in tumour cells and associated stromal tissue has been implicated in many cancer types, including those of the breast, bladder, colon, cervix, kidney, prostate, skin, and ovary (Chambers *et al*, 1998; Kuhn *et al*, 1999; Pappot *et al*, 1995; McMahon *et al*, 2001; Nakatsuka *et al*, 2017). A study by Pappot and colleagues noted that elevated plasma PAI-1 levels have been associated with cancers of the pancreas, ovary, and urinary tract (Pappot *et al*, 1995). Two studies have investigated plasma PAI-1 in ovarian cancer (Ho *et al,* 1999; Teliga-Czajkowska *et al*, 2019), however the study by Ho and colleagues was a very small study, and both studies were performed on subtypes of mixed histology. Results of Ho's study demonstrated that plasma PAI-1 was significantly higher in malignancy than in healthy controls (Ho *et al*, 1999), and that plasma PAI-1 correlated with higher disease stage (Ho *et al*, 1999). In Teliga-Czajkowska's study, high plasma PAI-1 pre-neoadjuvant chemotherapy correlated with a significantly lower probability of 5-year survival (Teliga-Czajkowska *et al*, 2019), suggesting that plasma PAI-1 is an independent adverse predictor of survival. Neither study focused solely on the high-grade serous subtype (HGSOC), which accounts for 70-80% of all ovarian

cancer deaths, and is what our study aims to do.

Having previously established the importance of PAI-1 in ovarian cancer metastasis via cell migration, wound-healing, and invasion assays in which PAI-1 was transiently silenced (chapter 3), and having also established that platelets are an important source of PAI-1 that contribute to ovarian cancer cell migration, wound-healing, and proliferation (chapter 3), the next logical step is to interrogate circulating PAI-1 levels in ovarian cancer to determine its role in metastasis. While ovarian cancer typically metastasises across the peritoneal cavity, there is well-documented evidence for hematogenous dissemination (Pradeep *et al*, 2014; Masuda *et al*, 2016; van Berckelaer *et al*, 2016; Kim *et al*, 2019;) thus making investigation into potentially associated molecules in the circulation essential. Patients with stage IV ovarian carcinoma, where there is metastasis to the liver or the lungs, could be more likely to have hematogenous involvement. Based on findings in both breast and ovarian cancers (Ho *et al*, 1999; Teliga-Czajkowska *et al*, 2019; Ferroni *et al*, 2014; Iacoviello *et al*, 2013), here we analysed plasma PAI-1 in patients with metastatic disease to gain insight into the prognostic value of these data.

5.2 Hypothesis

PAI-1 plays a central role in ovarian cancer metastasis.

5.3 Specific Aims

1. To assess if plasma PAI-1 is associated with metastatic disease in ovarian cancer patients.

2. To assess the effect of neoadjuvant chemotherapy on plasma PAI-1 levels.

3. To assess any relationship that may exist between platelet counts and plasma PAI-1 levels.

4. To assess any correlation that may exist between plasma PAI-1 levels and circulating tumour cell (CTC) counts in an additional cohort of 5 breast cancer (BC) patients.

5.4 Materials and Methods

5.4.1 Ethics and Recruitment

Women with a diagnosis of HGSOC who had undergone surgical staging over the 8-year period between 2012 and 2020 were included in this study if they had consented to participate in the Discovary biobank, and if a citrated plasma sample was available. The biobank invites patients undergoing treatment for gynaecological cancer in St. James's Hospital (SJH) Gynaecology-oncology unit (a tertiary referral center) in Dublin to donate blood, tissue and medical data for research. The study was approved by the joint research ethics committee of SJH and the Adelaide Meath and National Children's Hospital (AMNCH).

5.4.2 Patient Cohorts

Banked patient plasma samples have been collected in the Discovary biobank since 2011. For this study 5 cohorts of patients were included.

- Cohort 1 (n = 72) was composed of treatment-naïve HGSOC patients undergoing primary surgery for whom pre-operative citrated plasma samples were biobanked. This included a small number of preneoadjuvant patients who had blood samples taken just prior to commencing neoadjuvant chemotherapy.
- Cohort 2 (n = 79) consisted of patients who had undergone neoadjuvant chemotherapy and had blood and plasma sample biobanked prior to their interval debulking surgery (IDS).
- Cohort 3 (n = 15) was composed of patients with recurrent disease.

- Cohort 4 (n = 35) consisted of patients with benign serous histology and were included for plasma PAI-1 comparison.
- Cohort 5 (n = 5) was a smaller but extremely relevant set of breast cancer patients in which PAI-1 levels were examined in the context of CTC isolation, enumeration, and characterisation. Due to complications stemming from the Covid19 pandemic, ovarian patients were moved off-site for surgeries, preventing samples from being collected.

Patients who had experienced a venous thrombotic event (VTE) were excluded. For some analyses, patients from cohorts 1 and 2 were grouped into "early-stage", which was defined as stages I and II combined, and "late-stage", which was defined as stages III and IV combined.

5.4.3 Plasma PAI-1 Blood Collection Procedure

4.5mL of whole blood were collected from the antecubital fossa with minimum venous stasis using 3.13% sodium citrate as anticoagulant. Blood samples were centrifuged at 4°C for 20min at 2000 x g. The resulting platelet-free plasma (PFP) was carefully removed, aliquoted into cryotubes, snap frozen in liquid nitrogen, and stored at – 80°C until assay. All samples were processed and stored within 1 hour of phlebotomy.

5.4.4 PAI-1 ELISA of Patient Samples

All samples were tested for plasma PAI-1 by ELISA using the R&D Human Serpin E1/PAI-1 DuoSet and its companion ancillary kit (R&D) as described in Chapter 2, section 2.14. All reagents were prepared with strict adherence to the protocol provided with the ELISA kit. The plate was read at

450nm with a correction λ of 540nm. Standard curves for each individual plate were created using a sigmoidal 4PL curve in GraphPad Prism 8, and the data were interpolated to give PAI-1 values for each individual sample in ng/mL.

5.4.5 Additional Patient Data

Patient haematology, biochemistry, and metric data presented here were collected by the biobank, and had been processed by the Central Pathology Laboratory (CPL) at SJH according to their protocols (reference ranges for haematology and biochemistry are listed in Table 6.1). Reported blood results that have been previously shown to have an impact on ovarian cancer patient outcomes and overall survival (OS) were included for those patients for whom such data were available, such as haemoglobin (Macciò *et al*, 2005), serum albumin (Asher *et al*, 2011), carcinoembryonic antigen (CEA) (Moro *et al,* 2018*)*, cancer antigen 125 (CA-125) (Lee *et al*, 2016), platelets (Miao *et al*, 2016), neutrophils (Fridlender *et al*, 2012; Uribe-Querol and Rosales, 2015), lymphocytes (Hwang and Nguyen, 2015; Miao *et al*, 2016), fibrinogen (Hefler-Frischmuth *et al*, 2015), and D-dimer (Table 6.3). Neutrophil-to-lymphocyte ratio (NLR) and platelet-to-lymphocyte ratio (PLR) were calculated as they are not routinely reported in this center. Reference ranges for the neutrophil-to-lymphocyte ratio (NLR) and the platelet-to-lymphocyte ratio (PLR) were also calculated as they are not routinely reported, and were therefore not available on the hospital system. It should be noted that what constitutes a normal NLR is generally considered to be from 1.76-2.89, and that normal PLR for women ranges anywhere from 120-284 according to the literature. In light of this, the

reference ranges used for analyses of these two measures in this thesis were calculated by taking an average of mean NLR and PLR from the available literature, which encompassed several different ethnic regions as well as ROC curve analysis cutoff guidelines for cancer patients (Alexander, 2016; Fest *et al*, 2018; Hirahara *et al*, 2019; Moosazadeh *et al*, 2019; Wu *et al,* 2019; Fang *et al*, 2020). These calculated reference ranges are shown in Table 5.1.

Patient age, body mass index (BMI), menopausal status, and tumour stage were also included (Table 5.6). Overall survival was calculated for patients in the treatment-naïve cohort from date of diagnosis to either date of death or last recorded follow-up date. Histology and radiology for all patients are routinely reviewed and updated at our multidisciplinary team (MDT) meetings and by our tumour board, both prior to and after surgical staging.

Table 5.1 Haematology and biochemistry reference ranges

Factor	*range*	*unit*
Fibrinogen	1.9-3.5	g/L
D-dimer	<500	ng/mL
CEA	0-5.2	ng/mL
CA-125	35	U/mL
Haemoglobin	11.5-16.4	g/dL
Albumin	35-50	g/dL
Platelets	140-450	10^9/L
Neutrophils	2-7.5	10^9/L
Lymphocytes	1.5-3.5	10^9/L
NLR	< 2.8	
PLR	< 160	

5.4.6 Statistical Analysis

GraphPad Prism 8 was used to perform one-way ANOVA and t-tests. Odds ratios (OR) and risk ratios (RR) were calculated using MedCalc (MedCalc Software LTD, Belgium). Cumulative Overall Survival (OS) was calculated using the Kaplan-Meier estimator with the Mantel-Cox log rank test in SPSS

v26 (IBM). Log10 transformations were used for those analyses where data were not normally distributed (Fig. 5.1), and the Kruskal-Wallis non-parametric ANOVA was used for those data that continued to demonstrate non-normal residuals even after log-transformation. Odds ratios (OR) and risk ratios/relative risk (RR) are presented for those factors whose mean values are significant and fall outside of normal clinicopathological parameters. For all tests, a p-value less than or equal to 0.05 was considered significant. Data are presented as mean ± SD or mean ± SEM.

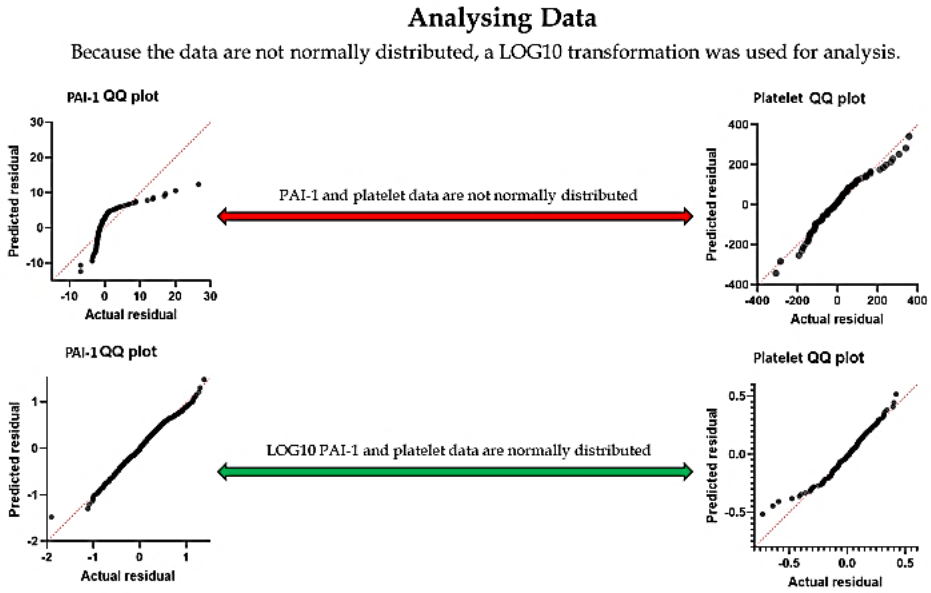

Fig. 5.1 Residual plots before (upper) and after (lower) log10 transformation of data.

5.5 Results

The results in the first part of this section (5.4.1) include patient cohort demographics, and results of haemotology and biochemistry parameters which have previously been shown to have prognostic value in ovarian cancer. These results were processed by the Central Pathology Laboratory (CPL) at St. James' Hospital (SJH) and were added to anonymised patient records in the Discovary Biobank. Plasma PAI-1 levels were assessed by ELISA, and those results are reported in the second part of this results section (5.4.2).

5.5.1 Cohort Demographics, Haematology, and Biochemistry

A treatment-naïve cohort was composed of 72 women with a mean age of 63.4. Of those women for whom menopausal status were available, 89.2% were postmenopausal. 79 women who underwent neoadjuvant chemotherapy prior to interval debulking surgery (IDS) comprised a second cohort, and had a mean age of 62.9. 95.6% of those women were postmenopausal. Patients diagnosed with recurrent disease had a mean age of 57.9, and 71.4% of those women were postmenopausal. 35 women comprised a fourth cohort of benign serous histology. 67.7% of women in this cohort were of postmenopausal status, with a mean age of 59.6. These results are outlined in Table 5.2.

Table 5.2 Demographics and cohort details as mean *(SD)*

	n	Mean Age (*SD*)	Postmenopausal %	Mean BMI (*SD*)
Treatment-naïve	72	63.4 *(11)*	89.2	27.4 *(6.0)*
Neoadjuvant	79	62.9 *(11.3)*	95.6	26.6 *(5.0)*
Recurrent	15	57.9 *(12.8)*	71.4	30.6 *(6.5)*
Benign	35	59.6 *(13.1)*	67.7	29.3 *(7.4)*

5.5.1.1 Body Mass Index

Mean body mass index values were reported for treatment-naïve, neoadjuvant, benign, and recurrent cohorts by stage in Tables 5.2, 5.4, and 5.5. Normal BMI was defined as being between 18.5 and 24.9 (Lukanova and Kaaks, 2004). Although no significant difference was seen among cohorts, mean BMI was higher in late-stage treatment-naïve patients (27.5) than in early-stage treatment-naïve patients (25.9), and was lower in late-stage patients who had undergone neoadjuvant chemotherapy (26.6) compared to late-stage treatment-naïve patients. Women in the benign cohort had a mean BMI of 29.3. It is of note that mean BMI was highest in those patients with recurrent disease (30.6).

Table 5.3 Haematology, biochemistry, and plasma PAI-1 of treatment-naïve, neoadjuvant, recurrent and benign cohorts, shown as mean (*SD*) values

Stage	n	D-dimer	Fibrinogen	CA-125	CEA	Hgb	Albumin	Platelets	Neutrophils	Lymphocytes	PLR	NLR	PAI-1
Treatment-naive	72	4146.5 *(2998.5)*	4.1 *(1.1)*	958.2 *(1712.2)*	5.5 *(21.3)*	12.4 *(1.5)*	39.5 *(6.1)*	348.7 *(130.6)*	6.2 *(2.6)*	1.6 *(0.7)*	259.5 *(184.3)*	4.6 *(3.3)*	3.3 *(4.0)*
Neoadjuvant	79	1454.3 *(2042.8)*	3.5 *(0.8)*	180.5 *(368.7)*	12.3 *(57.4)*	11.3 *(1.5)*	43.9 *(5.5)*	279.5 *(109.2)*	3.5 *(2.1)*	1.7 *(0.6)*	182.5 *(93.6)*	2.3 *(2.0)*	2.8 *(5.2)*
Recurrent	15	913.2 *(684.4)*	3.8 *(0.6)*	79.07 *(150.5)*	2.6 *(2.0)*	13.3 *(1.2)*	43.6 *(3.1)*	261.8 *(75.2)*	4.0 *(1.3)*	1.95 *(0.6)*	149.8 *(64.4)*	2.2 *(0.9)*	2.1 *(2.9)*
Benign	35	589.4 *(600.6)*	3.2 *(0.5)*	53.2 *(81.1)*	3.0 *(3.7)*	13.4 *(1.3)*	45.6 *(4.4)*	307.3 *(70.6)*	4.7 *(1.3)*	3.1 *(4.1)*	146.2 *(59.6)*	2.2 *(1.0)*	2.6 *(2.7)*

Table 5.4 Demographics, haematology, biochemistry and plasma PAI-1 of the treatment-naïve cohort by early-stage and late-stage, shown as mean (*SD*) values

Stage	n	Age	BMI	D-dimer	Fibrinogen	CA-125	CEA	Hgb	Albumin	Platelets	Neutrophils	Lymphocytes	PLR	NLR	PAI-1
Early (I and II)	10	61.8 *(11.8)*	26.5 *(7.2)*	3361.2 *(3095.7)*	3.8 *(0.5)*	303.5 *(440.8)*	4.4 *(7.3)*	13.6 *(1.6)*	41.1 *(6.8)*	255.3 *(107.1)*	5.9 *(1.8)*	2.0 *(1.0)*	155.7 *(85.3)*	3.9 *(2.1)*	2.4 *(3.6)*
Late (III and IV)	62	63.7 *(11.0)*	27.5 *(5.9)*	4268.7 *(3000.2)*	4.2 *(1.2)*	1067.3 *(1820.5)*	5.7 *(22.9)*	12.2 *(1.5)*	39.2 *(6.0)*	363.8 *(128.4)*	6.2 *(2.7)*	1.6 *(0.6)*	276.2 *(187.5)*	4.7 *(3.4)*	3.5 *(4.1)*

Table 5.5 Demographics, haematology, biochemistry and plasma PAI-1 of the neoadjuvant chemotherapy cohort by early-stage and late-stage, shown as mean (*SD*) values

Stage	n	Age	BMI	D-dimer	Fibrinogen	CA-125	CEA	Hgb	Albumin	Platelets	Neutrophils	Lymphocytes	PLR	NLR	PAI-1
Early (I and II)	10	62.4 *(9.6)*	25.5 *(4.2)*	741.8 *(490.8)*	3.3 *(0.4)*	63.3 *(94.6)*	68.2 *(150.3)*	11.8 *(1.7)*	45.4 *(4.0)*	260.5 *(54.6)*	2.6 *(1.4)*	2.0 *(0.5)*	139.9 *(55.2)*	1.3 *(1.3)*	4.5 *(7.1)*
Late (III and IV)	69	63.0 *(11.6)*	26.6 *(5.1)*	1616.2 *(2224.5)*	3.6 *(0.8)*	196.4 *(389.3)*	2.7 *(2.0)*	11.2 *(1.4)*	43.7 *(5.7)*	282.3 *(115.0)*	3.7 *(2.1)*	1.6 *(0.6)*	188.7 *(96.6)*	2.5 *(2.1)*	2.5 *(4.8)*

Table 5.6 Demographics, haematology, biochemistry and plasma PAI-1 of the treatment-naïve and neoadjuvant chemotherapy cohorts by stage, shown as mean (*SD*) values

Stage/ Cohort	n	Age	BMI	D-dimer	Fibrinogen	CA-125	CEA	Hgb	Albumin	Platelets	Neutrophils	Lymphocytes	PLR	NLR	PAI-1
I/Naïve	4	59.3 *(8.2)*	22.9 *(1.2)*	5250.8 *(4173.7)*	4.1 *(0.47)*	600. *(579.1)*	8.7 *(13.0)*	12.6 *(0.8)*	36 *(8.0)*	233.3 *(143.9)*	6.1 *(2.7)*	1.5 *(1.9)*	149.6 (121.9)	4.4 *(2.9)*	2.3 *(3.6)*
I/Neo$_y$	7	61.3 *(11.5)*	26.6 *(3.1)*	608.3 *(350.6)*	3.3 *(0.2)*	86.8 *(110.7)*	113 *(193.9)*	12.2 *(1.7)*	46.3 *(4.3)*	264.1 *(60.8)*	2.6 *(1.7)*	1.9 *(0.4)*	144.4 *(60.7)*	1.3 *(0.6)*	2.8 *(3.9)*
II/Naïve	6	63.5 *(14.2)*	28.3 *(8.5)*	1944.1 *(1142.3)*	3.6 *(0.5)*	105.7 *(176.5)*	2.3 *(1.4)*	14.3 *(1.7)*	44.5 *(3.2)*	270 *(86.9)*	5.7 *(1.3)*	1.9 *(0.9)*	159.8 *(64.2)*	3.5 *(1.5)*	2.5 *(3.9)*
II/Neo$_y$	3	65.0 *(2.0)*	22.9 *(6.9)*	1053.4 *(712.3)*	3.4 *(0.6)*	16.3 *(12.7)*	<1	10.9 *(1.5)*	43.3 *(2.5)*	252 *(46.7)*	2.6 *(0.6)*	2.1 *(0.7)*	129.3 *(49.4)*	1.3 *(0.4)*	8.6 *(11.9)*
III/Naïve	40	63.4 *(11.4)*	27.9 *(6.5)*	3830.6 *(2730.3)*	3.9 *(0.9)*	793.5 *(1695.6)*	3.1 *(6.5)*	12.7 *(1.2)*	40.8 *(5.9)*	347.8 *(113.2)*	6.0 *(2.5)*	1.8 *(0.6)*	224.5 *(114.9)*	3.8 *(2.1)*	3.5 *(4.2)*
III/Neo$_y$	63	63.2 *(11.5)*	26.4 *(4.9)*	1693.4 *(2319.9)*	3.5 *(0.7)*	195.1 *(397.4)*	2.7 *(2.1)*	11.2 *(1.5)*	44.0 *(5.6)*	280.4 *(117.2)*	3.8 *(2.2)*	1.7 *(0.6)*	185.3 *(100.4)*	2.6 *(2.2)*	2.6 *(5.0)*
IV/Naïve	22	64.4 *(10.5)*	26.8 *(4.5)*	5062.6 *(3382.9)*	4.7 *(1.4)*	1575.7 *(1973.9)*	11 *(38.7)*	11.2 *(1.4)*	36.4 *(4.9)*	392.9 *(150.8)*	6.7 *(3.1)*	1.2 *(0.4)*	370.1 *(251.5)*	6.4 *(4.6)*	3.4 *(3.9)*
IV/Neo$_y$	6	60.5 *(13.9)*	28.6 *(7.2)*	844.6 *(297.1)*	4.3 *(1.7)*	209.8 *(325.8)*	2.5 *(0.6)*	11.1 *(1.3)*	40.8 *(7.2)*	302.5 *(96.2)*	2.8 *(1.4)*	1.4 *(0.4)*	223.6 *(20.7)*	1.9 *(0.6)*	1.6 *(2.2)*

A "y" subscript denotes the pathological stage of patients who have received neoadjuvant chemotherapy, which may have differed from initial clinical staging.

5.5.1.2 D-dimer

In the treatment-naïve cohort, elevated D-dimer (> 500ng/mL) was observed in all early-stage patients, and in 93.3% of late-stage patients. In the neoadjuvant cohort elevated D-dimer was observed in 60% of patients with pathological early-stage disease and in 71% of patients with late-stage disease. 69.2% of patients with recurrent disease exhibited elevated D-dimer, as did 32% of patients in the benign cohort. No significance was noted in mean d-dimer values among stages within the treatment-naïve cohort. A one-way ANOVA of late-stage treatment-naïve, late-stage neoadjuvant chemotherapy, benign, and recurrent cohorts was significant, with $p < 0.0001$, however no post hoc significance was noted between any two cohorts. Mean D-dimer was significantly higher in patients with late-stage disease in the treatment-naïve cohort than for those in the neoadjuvant cohort (Fig. 5.2, $p < 0.0001$), and was also significantly higher in patients with late-stage disease in the treatment-naïve cohort than for those with recurrent disease ($p < 0.0001$). Additionally, mean D-dimer was significantly higher in late-stage treatment-naïve patients than in the benign cohort (Fig. 5.3, $p < 0.0001$), and mean D-dimer in late-stage neoadjuvant patients was higher than that of the benign cohort ($p = 0.0075$).

The OR for having elevated D-dimer in late-stage disease in the treatment-naïve cohort versus late-stage in the neoadjuvant chemotherapy cohort was 5.87 (95%CI: 1.5397 - 22.3866, $p = 0.0095$), with a RR of 1.33 (95%CI: 1.0774- 1.6289, $p = 0.0077$). The OR for having elevated D-dimer with late-stage disease in the treatment-naïve cohort versus the benign cohort was 45.4 (95%

CI: 8.9416 to 230.4009, p < 0.0001), with a RR of 2.9 (95% CI: 1.7292 to 5.1109, p = 0.0001). The OR for having elevated D-dimer with late-stage disease in the neoadjuvant cohort versus the benign cohort was 5.6 (95% CI: 2.0017 to 15.8326, p = 0.0011), with a RR of 2.3 (95% CI: 1.2824 to 3.9921, p = 0.0048).

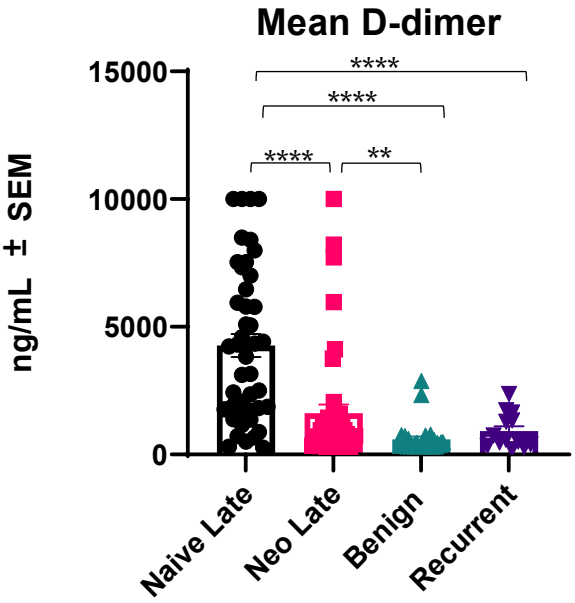

Fig. 5.2 Mean D-dimer ± SEM in late-stage naïve (n=62), late-stage neoadjuvant (n=69), benign (n=35) and recurrent (n=15) cohorts, ** p ≤ 0.01, ****p ≤ 0.0001

5.5.1.3 Fibrinogen

In the treatment-naïve cohort, fibrinogen was elevated in 63.8% of patients, as compared with 34.7% of patients who had undergone neoadjuvant chemotherapy. This percentage was 66.7% for the recurrent cohort, and 23.1% for the benign cohort. Mean fibrinogen values were not significantly different in a one-way ANOVA among stages in the treatment-naïve cohort, or in a two-tailed t-test when grouped into early-stage and late-stage. A one-way ANOVA of late-stage treatment-naïve patients, late-stage neoadjuvant chemotherapy

patients, a benign cohort, and a recurrent cohort was significant, with a p-value of 0.0002. Mean fibrinogen was significantly lower in late-stage patients receiving neoadjuvant chemotherapy versus patients in the treatment-naïve cohort with late-stage disease (Fig. 5.3, p = 0.0078). Mean fibrinogen in late-stage treatment-naïve patients was also significantly higher than in the benign cohort (p = 0.0001). The OR for having clinically elevated (> 3.5g/dL) fibrinogen with late-stage disease in the treatment-naïve cohort versus the neoadjuvant chemotherapy cohort was 2.37 (95%CI: 1.0109 to 5.5532, p = 0.0472), with a RR of 1.56 (95%CI: 1.0149 to 2.3903, p = 0.0426). The OR for having elevated fibrinogen with late-stage disease in the treatment-naïve cohort versus the benign cohort was 5.9 (95% CI: 1.9793 to 17.4819, p = 0.0014), with a RR of 2.8 (95% CI: 1.3276 to 5.7629, p = 0.0066).

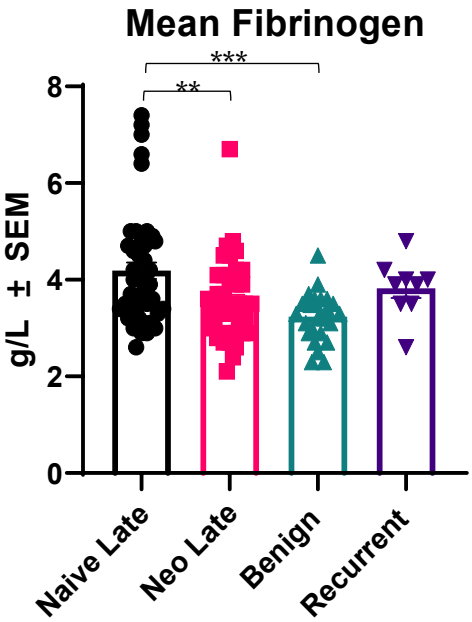

Fig. 5.3 Mean fibrinogen ± SEM in late-stage naïve (n=62), late-stage neoadjuvant (n=69), benign (n=35) and recurrent (n=15) cohorts, **p ≤ 0.01,*** p ≤ 0.001

5.5.1.4 Haemoglobin

Anaemia was not present in any early-stage patients in the treatment-naïve cohort, and was present in 30.7% of patients with late-stage disease in this same cohort. In the neoadjuvant chemotherapy cohort, 30% of early-stage patients and 56.5% of late-stage patients were anaemic. 8.5% and 6.7% of patients in the benign and recurrent cohorts were anaemic, respectively. Mean haemoglobin (Hg) for the treatment-naïve, neoadjuvant, benign, and recurrent cohorts and any details of any subdivisions within those cohorts are reported in Tables 5.3, 5.4, 5.5, and 5.6. Mean values were slightly below normal (< 11.5g/dL) for stages II – IV in the neoadjuvant cohort, and also for stage IV in the treatment-naïve cohort. All other mean Hg in both cohorts was within an accepted normal range (11.5 - 16.4g/dL), as was mean Hg in early-stage and late-stage groups in the treatment-naïve cohort. Patients with late-stage disease in the neoadjuvant cohort had mean Hg of 11.2g/dL, which is slightly below normal, and patients with early-stage disease in this same cohort had a normal mean Hg (11.8g/dL). A one-way ANOVA showed that mean Hg among stages in the treatment-naïve cohort was significantly different, with $p < 0.0001$. Significance occurred between stage II and stage III ($p = 0.0417$), between stage II and stage IV ($p < 0.0001$) and between stage III and stage IV ($p = 0.0003$) (Fig. 5.4). A two-tailed t-test showed significantly lower Hg in patients with late-stage versus early-stage disease in this cohort. (Fig. 5.5, $p = 0.0069$), but this did not fall outside of an accepted normal range. Results of a one-way ANOVA of late-stage patients in both the treatment-naïve and neoadjuvant chemotherapy

cohorts together with the benign and recurrent cohorts was significant, with $p < 0.0001$ (Fig. 5.6). Mean Hg in late-stage neoadjuvant patients was significantly lower than that of the treatment-naïve cohort ($p = 0.0024$), the benign cohort ($p < 0.0001$), and that of the recurrent cohort ($p < 0.0001$). Mean Hg in late-stage treatment-naïve patients was significantly lower that of the benign cohort ($p = 0.0103$). The OR for having anaemia with late-stage disease in the neoadjuvant cohort versus late-stage disease in the treatment-naïve cohort was 3.2 (95% CI: 1.5373 to 6.5688, $p = 0.0018$), with a RR of 1.9 (95% CI: 1.2529 to 3.0253, $p = 0.0031$). The OR for having anaemia with late-stage disease in the neoadjuvant cohort versus patients in the benign cohort was 13.9 (95% CI: 3.8725 to 49.6541, $p = 0.0001$), with a RR of 6.6 (95% CI: 2.1914 to 19.8425, $p = 0.0008$).

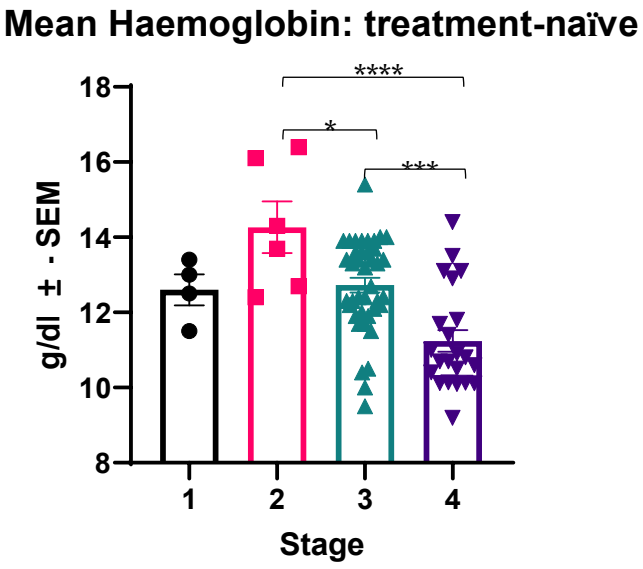

Fig. 5.4 Mean haemoglobin ± SEM across stages in the treatment-naïve cohort: stage 1 n = 4, stage 2 n = 6, stage 3 n = 40, stage 4 n = 22, * $p \leq 0.05$, ***$p \leq 0.001$, ****$p \leq 0.0001$

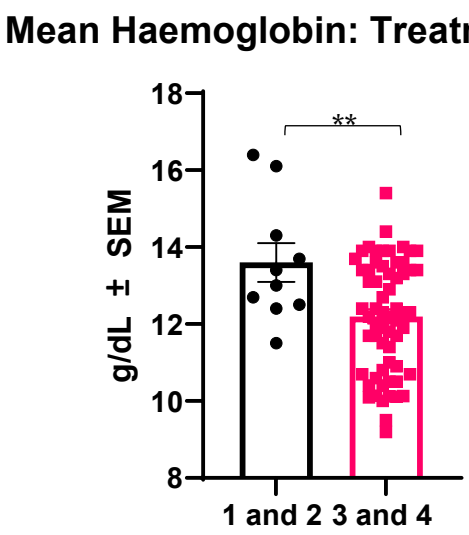

Fig. 5.5 Mean haemoglobin ± SEM, early-stage (n = 10) versus late-stage (n = 62) treatment-naive, **p ≤ 0.01

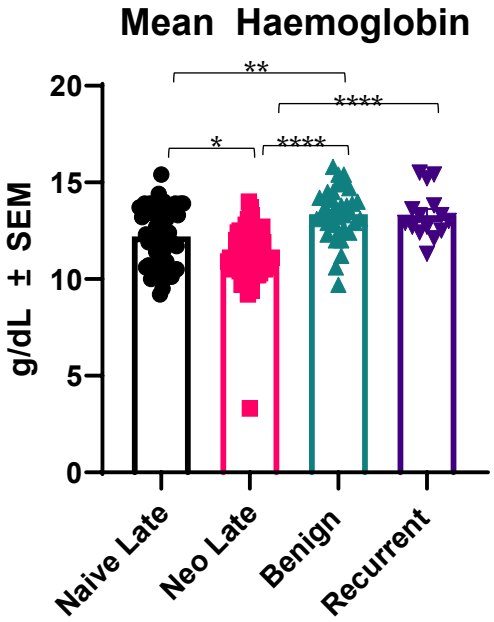

Fig. 5.6 Mean haemoglobin ± SEM in late-stage naïve (n=62), late-stage neoadjuvant (n=69), benign (n=35) and recurrent (n=15) cohorts * p ≤ 0.05, **p ≤ 0.01, ****p ≤ 0.0001

5.5.1.5 Tumour Markers: Cancer Antigen 125 and Carcinoembryonic Antigen

5.5.1.5.1 Cancer Antigen 125 (CA-125)

A one-way ANOVA of mean cancer antigen 125 (CA-125) levels among stages in the treatment-naïve cohort was significant (Fig. 5.7, p = 0.0002). Mean

CA-125 was significantly lower in stage II than in stage III ($p = 0.0064$), and was also significantly lower in stage II than in stage IV ($p < 0.0001$). Additionally, mean CA-125 was significantly lower in early-stage disease versus late-stage disease in the treatment-naïve cohort (Fig. 5.8), with $p = 0.0022$. Results of a one-way ANOVA of late-stage disease in both the treatment-naïve and neoadjuvant chemotherapy cohorts together with the benign and recurrent cohorts were significant (Fig. 5.9, $p < 0.0001$). Mean CA-125 was significantly lower in late-stage pathological disease in the neoadjuvant cohort than in late-stage disease in the treatment-naïve cohort ($p < 0.0001$). Mean CA-125 was also significantly lower in both the benign cohort and the recurrent cohort than in patients with late-stage disease in the treatment-naïve cohort, with $p < 0.0001$ in both instances.

The OR for having clinically elevated (> 35U/mL) CA-125 in late-stage disease in the treatment-naïve cohort versus the neoadjuvant chemotherapy cohort was 12.67 (95%CI: 2.2746 to 70.5359, $p = 0.0038$), with no significant RR. The OR for having elevated CA-125 for patients with late-stage disease in the treatment-naïve cohort as compared with the benign cohort was 36.4 (95% CI: 9.3968 to 141.1300, $p < 0.0001$), with a RR of 2.8 (%CI: 1.7451 to 4.3994, $p < 0.0001$). The OR for having elevated CA-125 for patients with late-stage disease in the treatment-naïve cohort as compared with the recurrent cohort was 16.6 (95% CI: 3.5579 to 77.6830, $p = 0.0004$), with a RR of 1.8 (95% CI: 1.1056 to 2.8698, $p = 0.0177$).

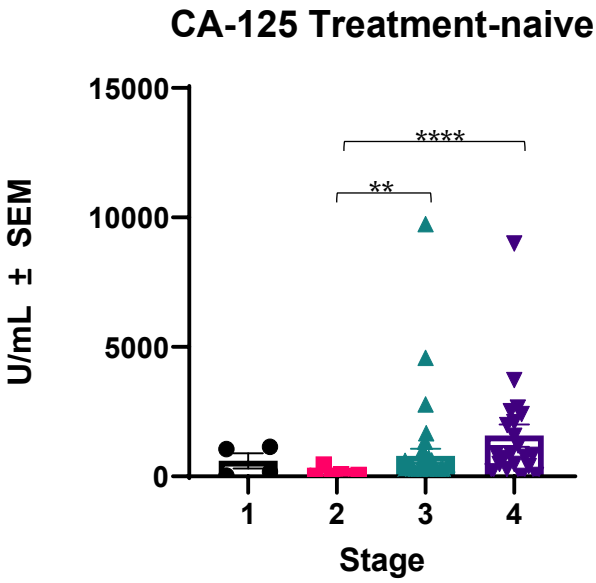

Fig. 5.7 Mean CA-125 ± SEM across stages in the treatment-naïve cohort: : stage 1 n = 4, stage 2 n = 6, stage 3 n = 40, stage 4 n = 22 **p ≤ 0.01, ****p ≤ 0.0001

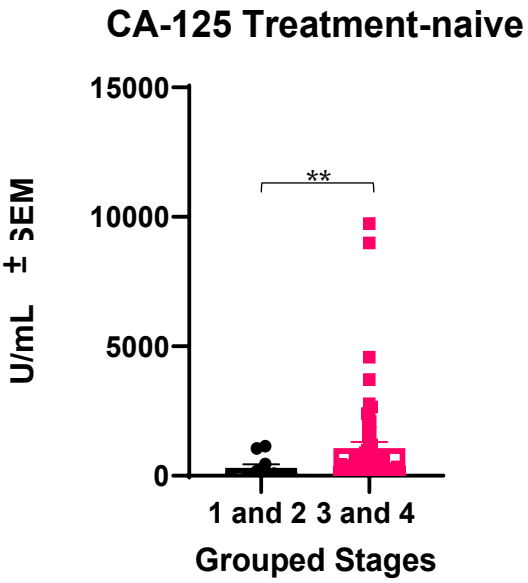

Fig. 5.8 Mean CA-125 ± SEM in early (n = 10) and late-stage (n = 62) in the treatment-naïve cohort, **p ≤ 0.01

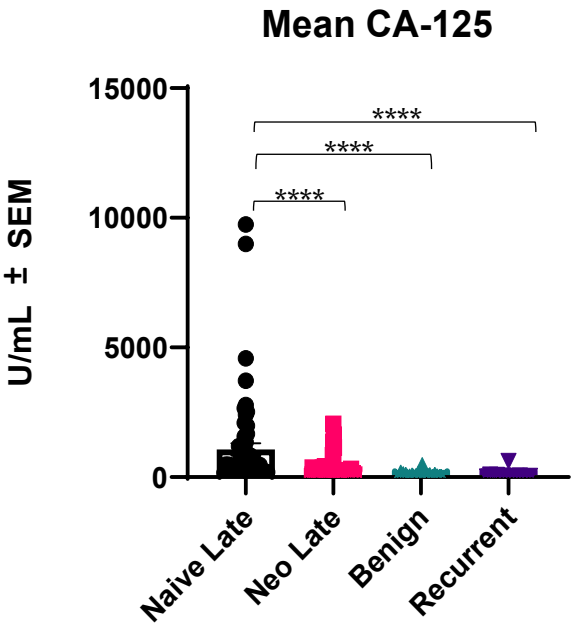

Fig. 5.9 Mean CA-125 ± SEM in late-stage naïve (n=62), late-stage neoadjuvant (n=69), benign (n=35) and recurrent (n=15) cohorts, ****p ≤ 0.0001

5.5.1.5.2 Carcinoembryonic Antigen (CEA)

Mean Carcinoembryonic Antigen (CEA) was not significantly different among stages in the treatment-naïve cohort, among late-stage treatment-naïve, neoadjuvant chemotherapy, benign, and recurrent cohorts, or between the treatment-naïve and neoadjuvant chemotherapy cohorts for patients with late-stage disease.

5.5.1.6 Serum Albumin

Mean serum albumin values for the treatment-naïve, neoadjuvant, and recurrent cohorts are reported in Tables 5.3, 5.4, 5.5, and 5.6 with none being outside the accepted normal range. A one-way ANOVA of serum albumin among stages in the treatment-naïve cohort was significant, with $p = 0.0034$. Means are illustrated in Fig. 5.10, and were significantly lower in stage IV than in stage II ($p = 0.0135$) and also lower in stage IV than in stage III ($p = 0.0234$). A two-tailed t-test of early versus late-stage disease in the treatment-naïve

cohort was not significant, however results of a two-tailed t-test showed that serum albumin was significantly higher in patients with late-stage disease in the neoadjuvant cohort than in patients with late-stage disease in the treatment-naïve cohort, with $p < 0.0001$ (Fig. 5.11).

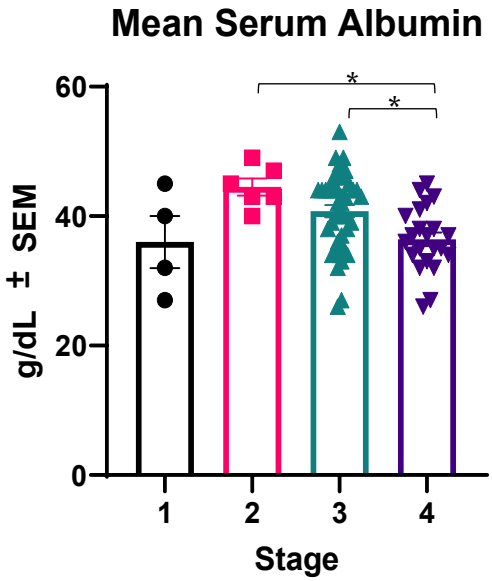

Fig. 5.10 Mean serum albumin ± SEM across stages in the treatment-naïve cohort: stage 1 n = 4, stage 2 n = 6, stage 3 n = 40, stage 4 n = 22, *p ≤ 0.05

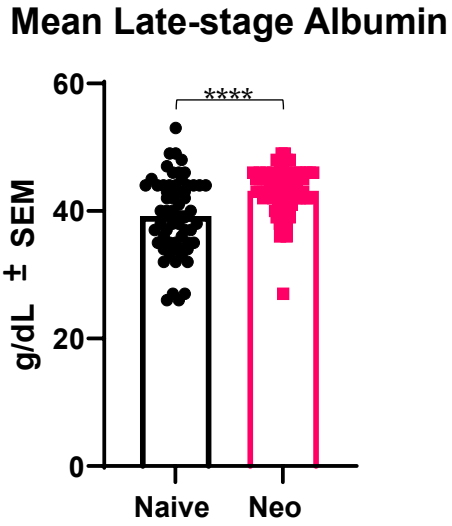

Fig. 5.11 Mean serum albumin ± SEM in late-stage treatment-naïve patients (n = 62) compared with late-stage neoadjuvant chemotherapy patients (n = 69) , ****p ≤ 0.0001

5.5.1.7 Platelets in Treatment-naïve and Neoadjuvant Chemotherapy Cohorts

Mean platelet counts for patients in the treatment-naïve, neoadjuvant, and recurrent cohorts are shown in Table 5.3. A one-way ANOVA comparing platelet counts for all stages in the treatment-naïve cohort was significant (Fig. 5.12 A, $p = 0.0265$), with significance between stages I and IV ($p = 0.0276$). Results of an additional analysis between early (grouped stages I and II) and late (grouped stages III and IV) stage disease were significant (Fig. 5.12 B, $p = 0.0068$).

A positive linear relationship was noted between both mean and median platelets and stage in the treatment-naïve cohort (Fig. 5.13).

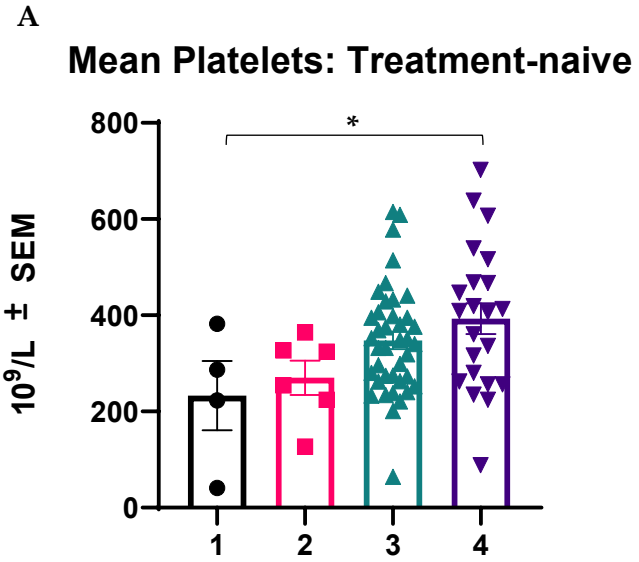

B

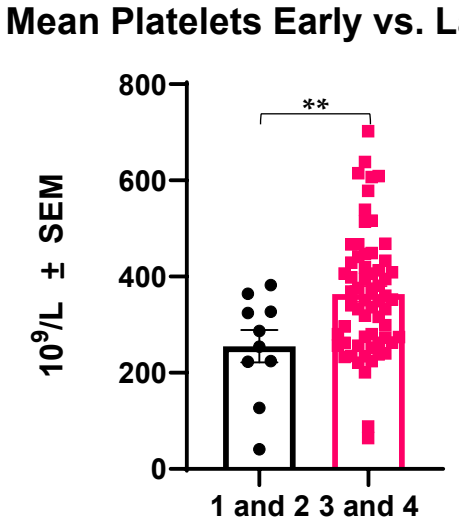

Fig. 5.12 A A one-way ANOVA of mean treatment-naïve platelets ± SEM by stage (stage 1 n = 4, stage 2 n = 6, stage 3 n = 40, stage 4 n = 22) was significant, **B** A two-tailed t-test of treatment-naïve mean early-stage (n= 10) versus late-stage (n = 62)) platelet counts ±SEM was significant *p ≤ 0.05, **p ≤ 0.01

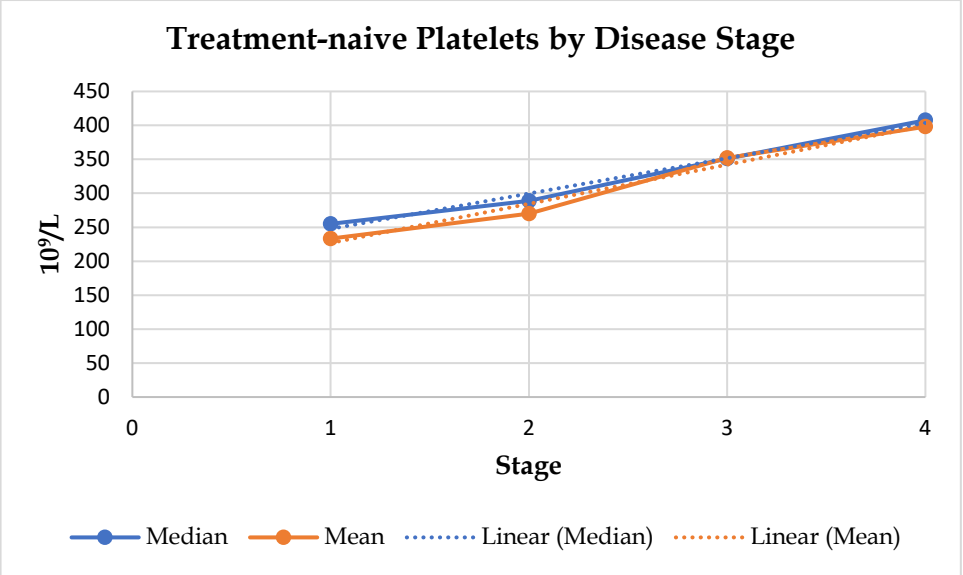

Fig. 5.13 Mean and median platelets increase with stage in the treatment-naïve cohort.

A two-tailed t-test highlighted significantly lower mean platelets in the neoadjuvant cohort than in the treatment-naïve cohort in patients experiencing pathologically late-stage disease, with a p-value of 0.0004 (Fig. 5.14).

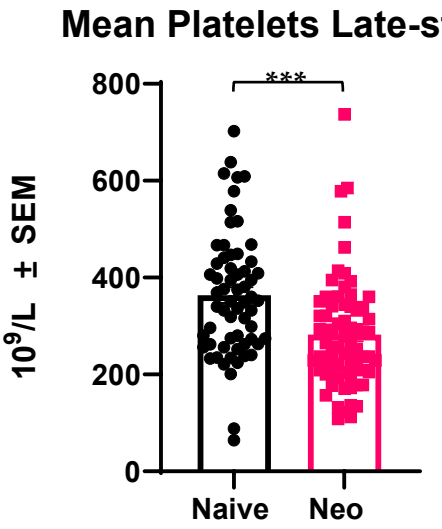

Fig. 5.14 Platelet counts ± SEM in late-stage treatment-naïve patients (n=62) versus late-stage neoadjuvant chemotherapy patients (n = 69),***p ≤ 0.001

19% of late-stage treatment-naive patients exhibited thrombocytosis (≥ 450 x 10^9 platelets/L) versus none of the early-stage patients and 7% of late-stage patients in the neoadjuvant cohort. No patients in either the benign or the recurrent cohort exhibited thrombocytosis. The OR of thrombocytosis for late-stage treatment-naïve patients versus late-stage patients who had undergone neoadjuvant chemotherapy prior to IDS was 3.0720 (95%CI: 1.015510507-9.293044172, p = 0.0469), with a RR of 2.67 (95%CI: 0. 0.997144641 - 7.154497333, p = 0.05028).

5.5.1.8 Lymphocytes and Neutrophils: Platelet-to-Lymphocyte and Neutrophil-to-Lymphocyte Ratios

Mean neutrophils and lymphocytes for each cohort and its respective subdivisions are listed in Tables 5.3-5.6. Mean neutrophils were within the normal range for all cohorts, and neutrophils among stages in the treatment-naive cohort were not significantly different. Results of a one-way ANOVA

comparing mean late-stage naïve and late-stage neoadjuvant neutrophils with those of the benign and recurrent cohorts were significant (Fig. 5.15, $p < 0.0001$). Mean neutrophils were significantly higher in late-stage treatment-naïve patients than in both late-stage neoadjuvant chemotherapy patients ($p < 0.0001$) and patients with recurrent disease ($p = 0.0222$), while mean neutrophils in late-stage neoadjuvant chemotherapy patients were significantly lower than in the benign cohort ($p = 0.0039$).

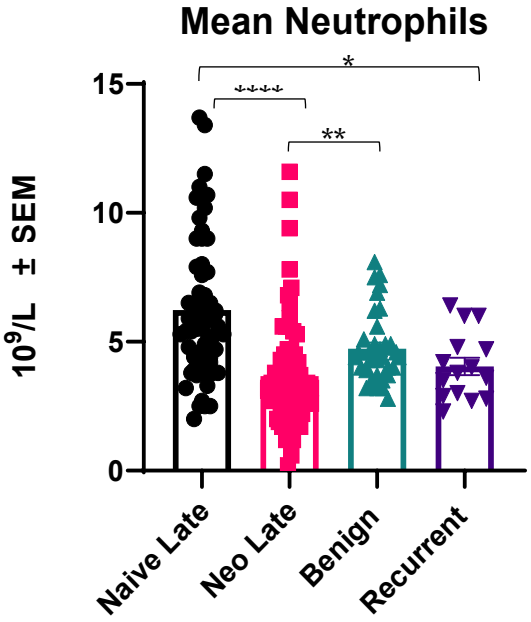

Fig. 5.15 Mean neutrophils ±SEM in late-stage naïve (n=62), late-stage neoadjuvant (n=69), benign (n=35) and recurrent (n=15) cohorts *p ≤ 0.05, **p ≤ 0.01, ****p ≤ 0.0001

Mean lymphocytes were below normal (< 2 x 10^9/L) for stage IV patients in both the treatment-naïve and the neoadjuvant chemotherapy cohorts. A one-way ANOVA of lymphocytes among stages in the treatment-naïve cohort was significant (Fig. 5.16, $p = 0.0089$), with stage IV being significantly lower than stage III ($p = 0.0079$). There was no significant difference in lymphocytes between early and late-stage disease in this same cohort. A one-way ANOVA

comparing lymphocytes of patients with late-stage disease in the treatment-naïve and neoadjuvant chemotherapy cohorts with those of the benign and recurrent cohorts was significant, with $p < 0.0001$ (Fig. 5.17). Mean lymphocytes were significantly lower in late-stage treatment-naïve patients than in the benign cohort ($p < 0.0001$) and were also significantly lower in late-stage neoadjuvant chemotherapy patients than in the benign cohort ($p = 0.0003$).

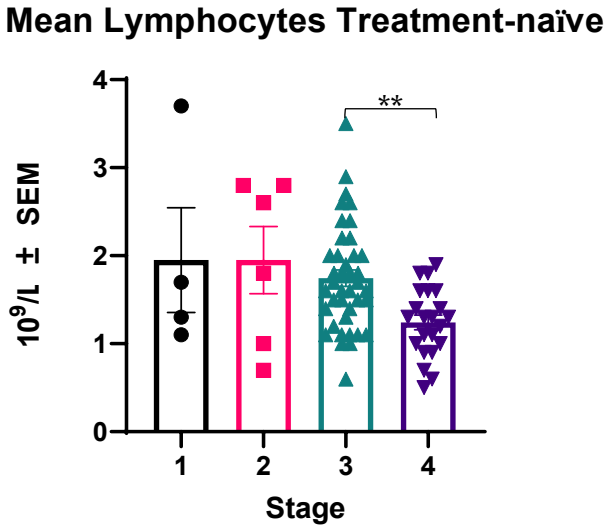

Fig. 5.16 A one-way ANOVA of mean lymphocytes ± SEM by stage in the treatment-naïve cohort was significant: stage 1 n = 4, stage 2 n = 6, stage 3 n = 40, stage 4 n = 22, **p ≤ 0.01

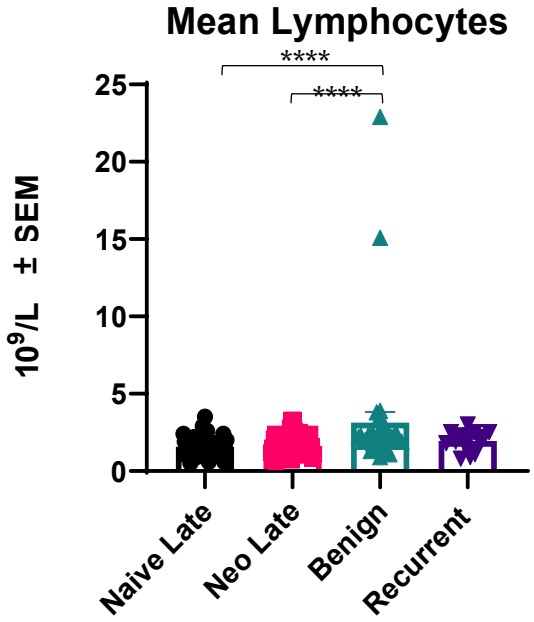

Fig. 5.17 Mean lymphocytes ± SEM in late-stage naïve (n=62), late-stage neoadjuvant (n=69), benign (n=35) and recurrent (n=15) cohorts, ****p ≤ 0.0001

A one-way ANOVA of platelet-to-lymphocyte ratios (PLR) among stages in the treatment-naïve cohort was significant (Fig 5.18A, $p < 0.0001$). Mean PLR for stage IV in this cohort was significantly higher than all other stages: between stages I and IV ($p = 0.0062$), stages II and IV ($p = 0.0479$), and stages III and IV ($p = 0.0359$). A two-tailed t-test demonstrated a significantly higher PLR for patients with late-stage disease versus those with early-stage disease in the treatment-naïve cohort, with $p = 0.0067$ (Fig. 5.18B). Mean PLR was significantly higher in patients with late-stage disease in the treatment-naïve cohort than in late-stage patients in the neoadjuvant chemotherapy cohort ($p < 0.0001$), patients in the benign cohort ($p < 0.0001$), and patients with recurrent disease ($p < 0.0001$) (Fig. 5.19).

A calculated OR for having an elevated PLR (>160) with late-stage disease in the treatment-naïve cohort versus late-stage disease in the

neoadjuvant cohort was 2.56 (95% CI: 1.2071 to 5.4126, p = 0.0142), with a corresponding RR of 1.38 (95% CI: 1.0663 to 1.7769, p = 0.0142). The OR for elevated PLR in late-stage treatment-naïve versus benign was 4.7 (95% CI: 1.9268 to 11.4649, p = 0.0007), with a RR of 1.89 (95% CI: 1.2335 to 2.9117, p = 0.0035). The OR for elevated PLR with late-stage disease in the treatment-naïve cohort versus the recurrent cohort was 6.89 (95% CI: 2.0630 to 23.0336, p = 0.0017), with a RR of 2.15 (95% CI: 1.1114 to 4.1508, p = 0.023).

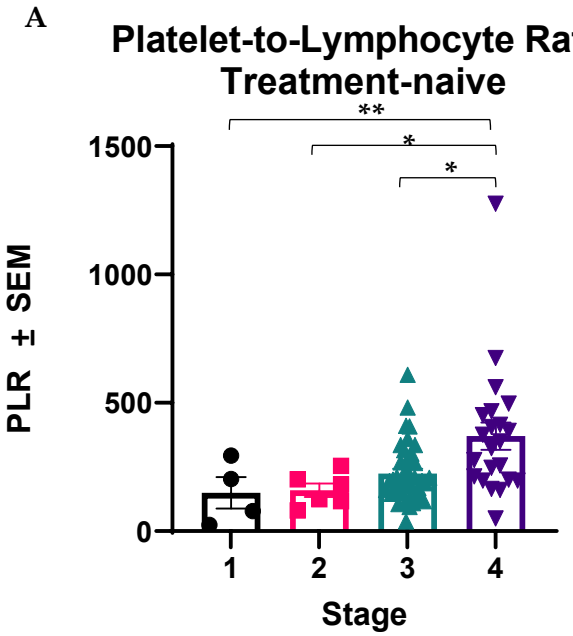

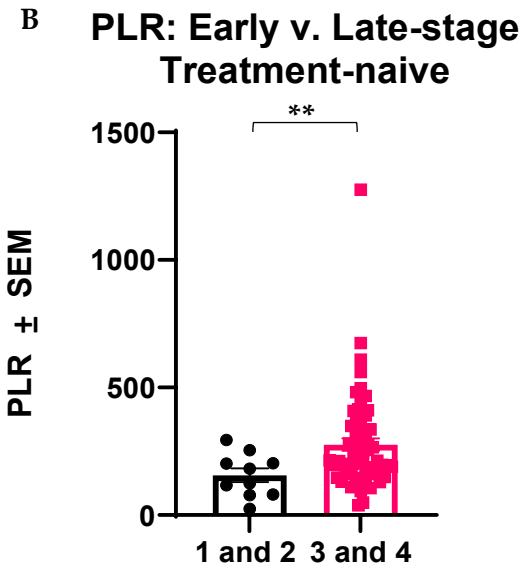

Fig. 5.18 Mean PLR ± SEM in the treatment-naïve cohort : stage 1 n = 4, stage 2 n = 6, stage 3 n = 40, stage 4 n = 22 **A** by individual stage, **B** grouped into early (n = 10) and late stage (n = 62), * p ≤ 0.05, ** p ≤ 0.01

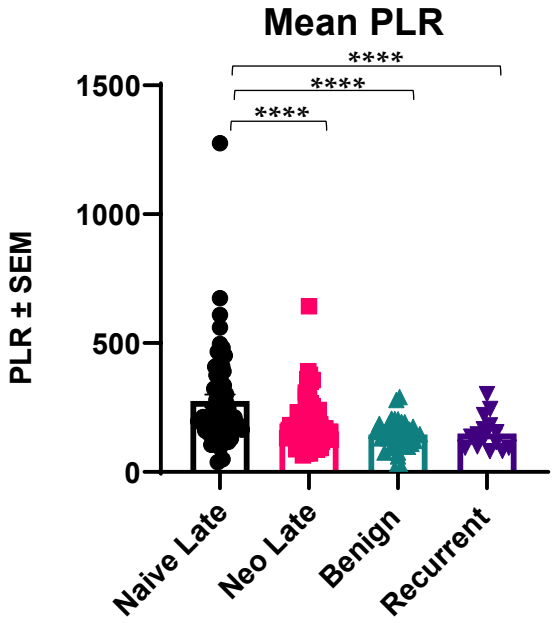

Fig. 5.19 Mean PLR ± SEM in late-stage naïve (n=62), late-stage neoadjuvant (n=69), benign (n=35) and recurrent (n=15) cohorts, ****p ≤ 0.0001

A one-way ANOVA of neutrophil-to-lymphocyte ratios (NLR) in the treatment-naïve cohort was significant (Fig. 5.20), with an overall p-value of

0.0459, and stage IV being significantly higher than stage III with a p-value of 0.0368. Results of a second one-way ANOVA comparing mean NLR in patients with late-stage disease in the treatment-naïve and neoadjuvant chemotherapy cohorts with those of the benign and recurrent cohorts was also significant (Fig. 5.21, $p < 0.0001$). Mean NLR was significantly higher in the treatment-naïve cohort than in the neoadjuvant cohort, with $p < 0.0001$, and in both the benign and recurrent cohorts, with $p < 0.0001$ and $p = 0.0047$, respectively. Mean neutrophil to lymphocyte ratios (NLR) were elevated (> 2.8) in all stages of the treatment-naïve cohort, and were normal (≤ 2.8) in all stages of the neoadjuvant cohort, and were also normal in both the benign and recurrent cohorts.

The OR for having an elevated NLR in conjunction with late-stage disease in the treatment-naïve cohort versus late-stage in neoadjuvant cohort was 5.95 (95%CI: 2.7924 to 12.6783, $p < 0.0001$), with a RR of 2.6 (95%CI: 1.6846 to 4.0028, $p < 0.0001$). The OR for this versus benign histology was 10.15 (95% CI: 3.6318 to 28.3671, $p< 0.0001$), with a RR of 3.95 (95%CI: 1.8697 to 8.3517, $p = 0.0003$). The OR for having an elevated NLR with late-stage disease in the treatment-naïve cohort versus the recurrent cohort was 8.4 (95%CI: 2.1288 to 33.1452, $p = 0.0024$), with a RR of 3.38 (95% CI: 1.2133 to 9.4554, $p = 0.0199$).

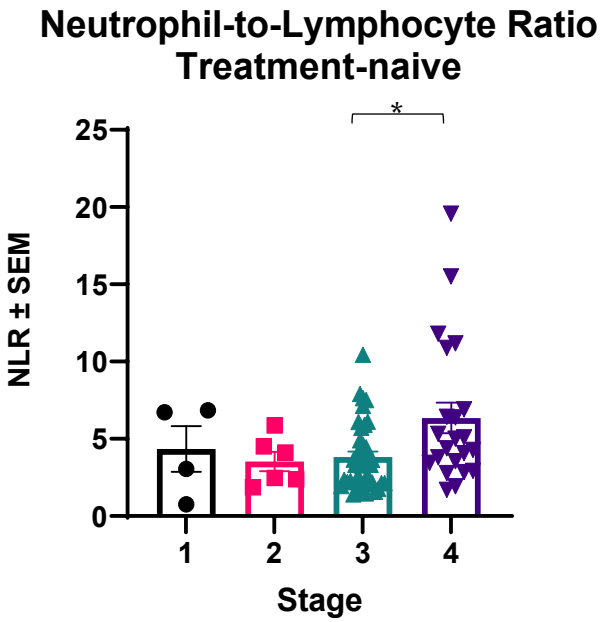

Fig. 5.20 Mean neutrophil-to-lymphocyte ratios ± SEM by stage in the treatment-naïve cohort: stage 1 n = 4, stage 2 n = 6, stage 3 n = 40, stage 4 n = 22, *p ≤ 0.05

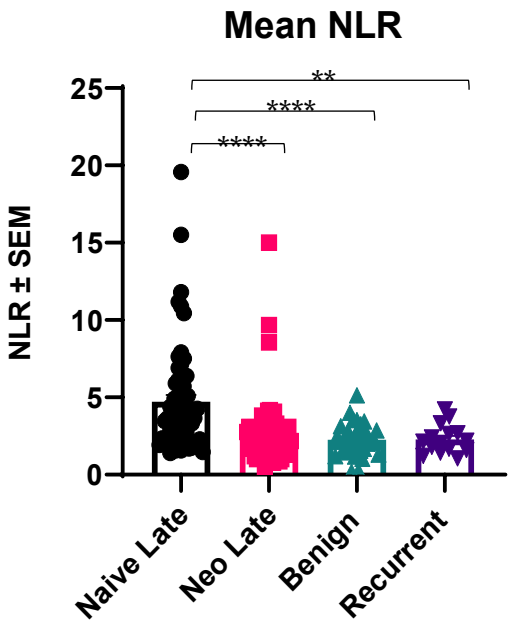

Fig. 5.21 Mean neutrophil-to-lymphocyte ratios ± SEM in late-stage naïve (n=62), late-stage neoadjuvant (n=69), benign (n=35) and recurrent (n=15) cohorts, **p≤ 0.01, ****p ≤ 0.0001

5.5.2 Plasma PAI-1

Plasma PAI-1 values for treatment-naïve, neoadjuvant, recurrent, and benign cohorts are shown in Fig. 5.22. Results of a one-way ANOVA were significant, with p = 0.0352. Mean values were in ng/mL: 3.328 in the treatment-naïve cohort, 2.756 in the neoadjuvant chemotherapy cohort, 2.133 in the recurrent cohort, and 2.642 in the benign cohort.

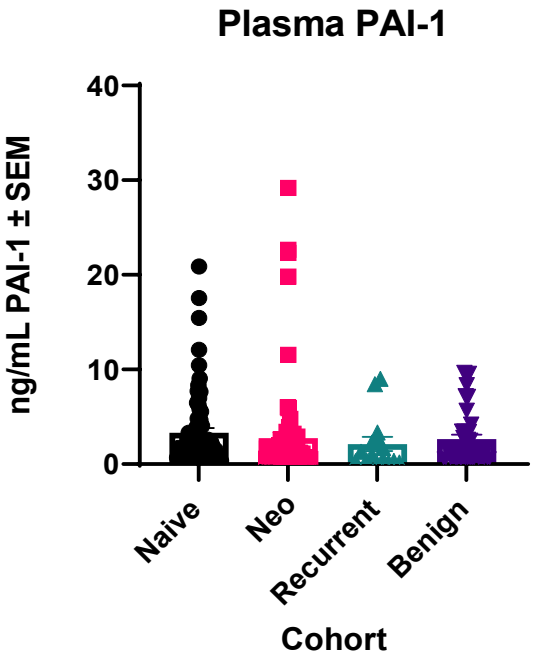

Fig. 5.22 Mean plasma PAI-1 ± SEM in naïve (n=72), neoadjuvant (n=79), benign (n=35) and recurrent (n=15) cohorts, p = 0.0352 in an overall ANOVA with no post hoc significance.

5.5.2.1 Plasma PAI-1 in a Treatment-naïve Cohort

Mean plasma PAI-1 values for each cohort and its corresponding subgroups are outlined in Tables 5.3, 5.4, 5.5, and 5.6. A one-way ANOVA comparing plasma PAI-1 among stages in the treatment-naïve cohort was not significant (Fig. 5.23A, p = 0.2387). However, a two-tailed t-test demonstrated significantly higher mean plasma PAI-1 of 3.3 ng/mL in treatment-naïve

patients with late-stage disease (grouped stages III and IV) versus 2.4ng/mL for those in the same cohort with early-stage disease (grouped stages I and II) (Fig. 5.23 B, p = 0.039). Median and mean plasma PAI-1 were noted to follow a positive linear trend by stage in the treatment-naïve cohort (Fig. 5.24).

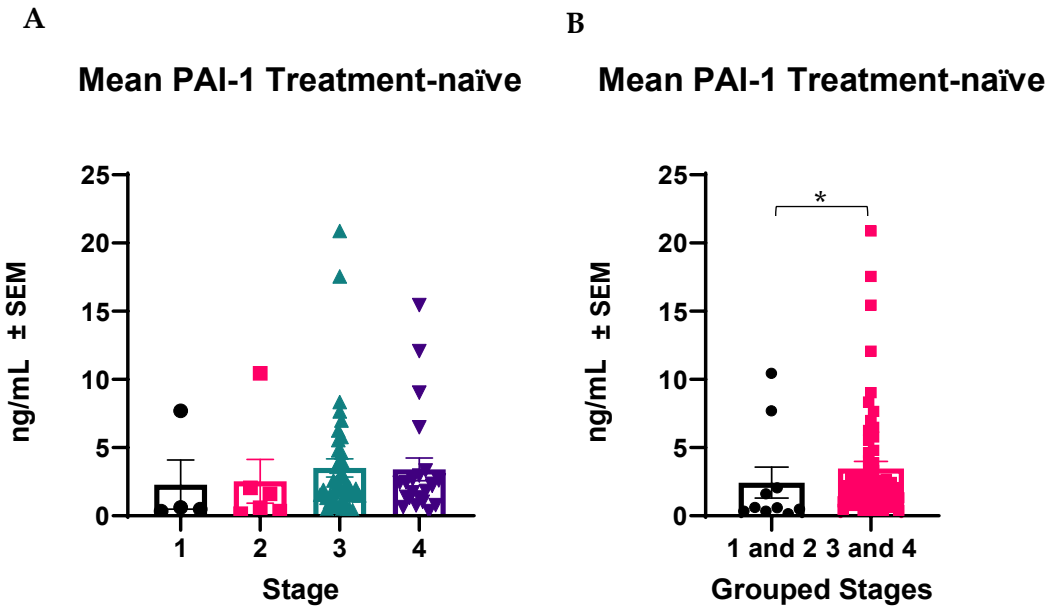

Fig. 5.23 Mean plasma PAI-1 ± SEM in the treatment-naïve cohort **A** by stage: stage 1 n = 4, stage 2 n = 6, stage 3 n = 40, stage 4 n = 22, and **B** grouped into early (n = 10) and late-stages (n = 62) *p ≤ 0.05

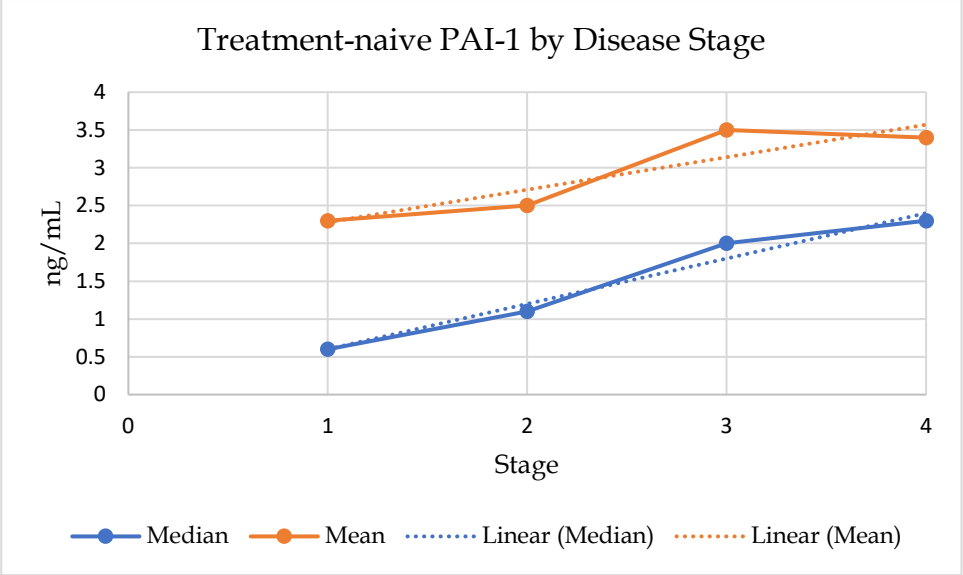

Fig. 5.24 PAI-1 follows a positive linear trend by disease stage in the treatment-naïve cohort.

5.5.2.2 Plasma PAI-1 Comparisons among Late-stage Patients in the Treatment-naïve and Neoadjuvant Chemotherapy Cohorts, Patients in the Benign Cohort, and Patients in the Recurrent Cohort

When Stages III and IV were grouped together into a single late-stage disease group, mean plasma PAI-1 in the neoadjuvant chemotherapy cohort (n = 69) was significantly lower than that of the treatment-naïve cohort (n = 62) (Fig. 5.25, p = 0.0089), and was also significantly lower than that of the recurrent cohort (p = 0.0129). Mean plasma PAI-1 for late-stage disease in the treatment-naïve cohort was 3.3ng/mL, 2.5ng/mL in the neoadjuvant cohort, 2.64 in the benign cohort, and 2.13 in the recurrent cohort.

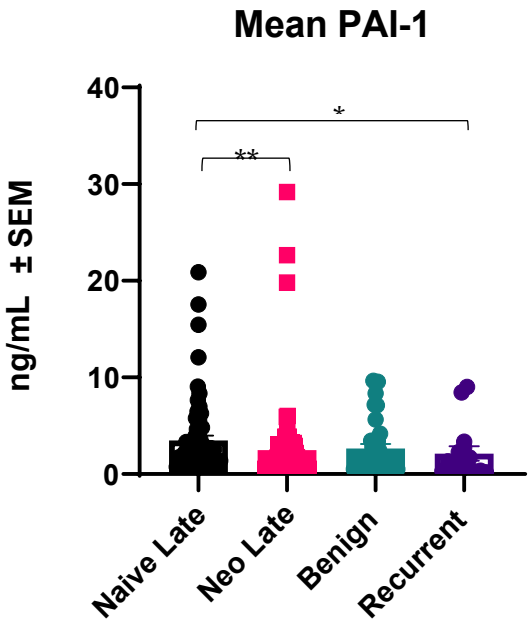

Fig. 5.25 Mean plasma PAI-1 ± SEM in naïve (n=72), neoadjuvant (n=79), benign (n=35) and recurrent (n=15) cohorts * p≤ 0.05, ** p ≤ 0.01

5.5.2.3 Plasma PAI-1 did not correlate with Platelets in a Treatment-naïve Cohort

No correlation was noted in the treatment-naïve cohort between plasma PAI-1 and platelets (Fig. 5.26); however, a positive linear relationship was observed (Fig. 5.27) between them for both the means and the medians.

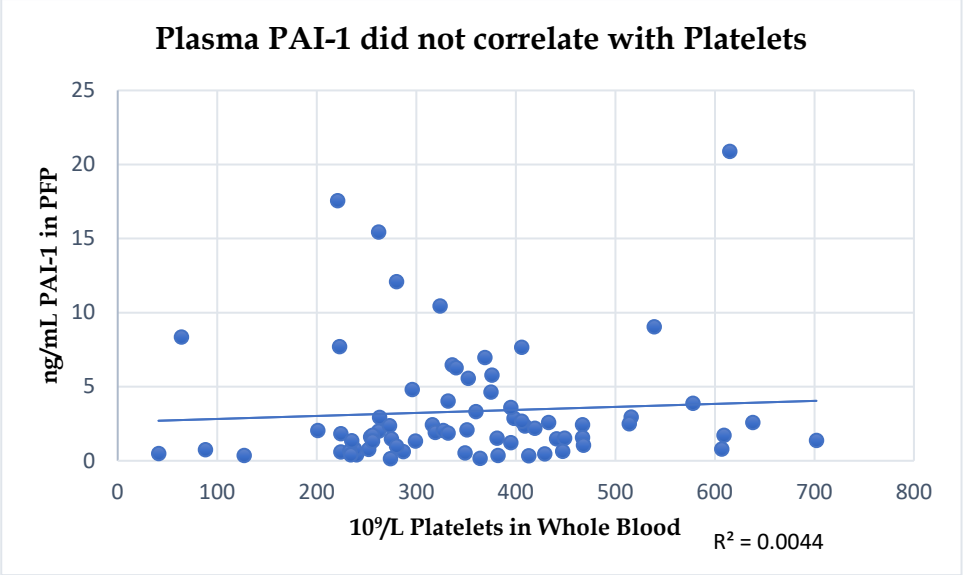

Fig. 5.26 No correlation exists between PFP-derived PAI-1 and platelet counts from whole blood.

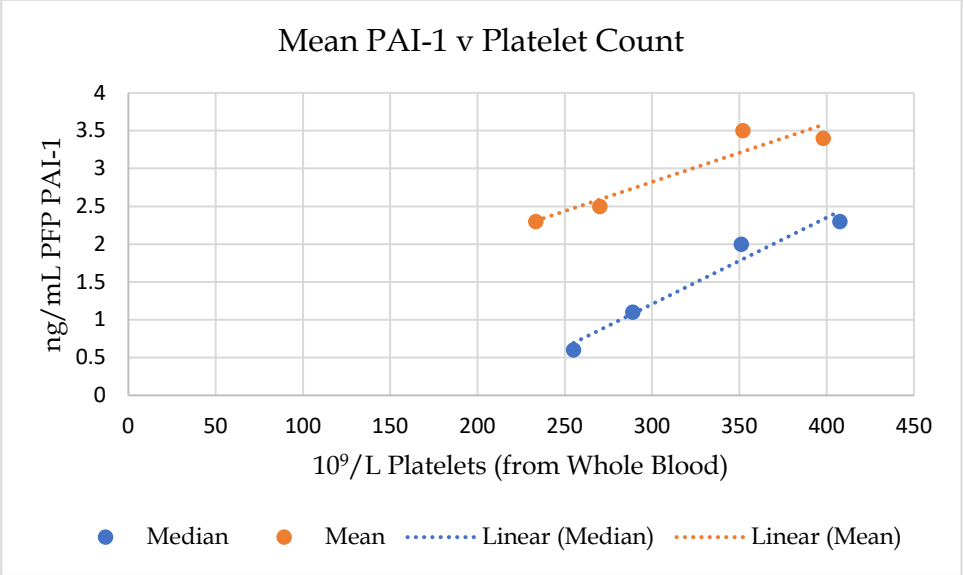

Fig. 5.27 Platelets versus plasma PAI-1 in the treatment-naïve cohort.

5.5.2.4 Plasma PAI-1 correlated with Neutrophils in a Treatment-naïve Cohort

A positive Pearson correlation was observed between plasma PAI-1 and neutrophil counts in the treatment-naïve cohort, with R = 0.2821 and a p-value of 0.031919 (Fig. 5.28).

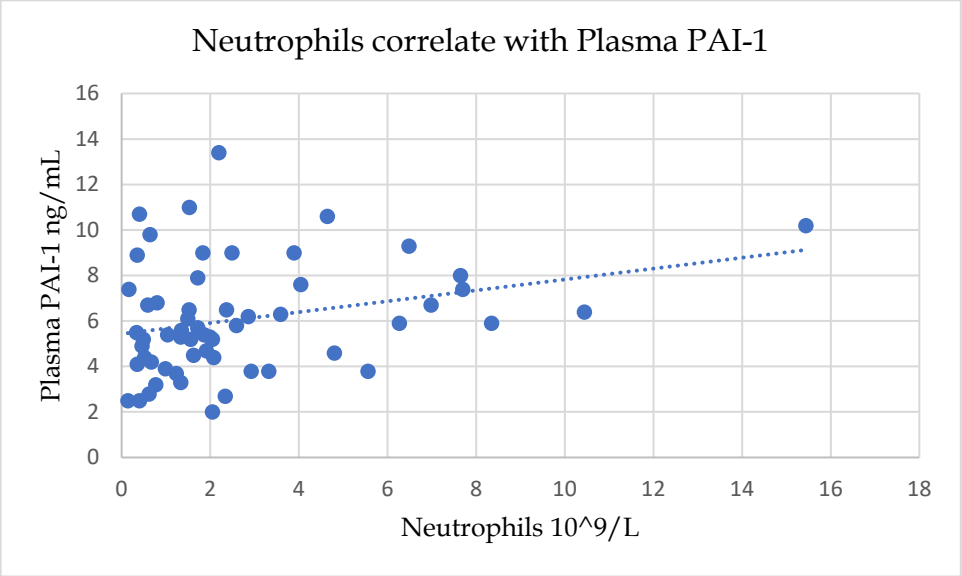

Fig. 5.28 Neutrophils versus plasma PAI-1 in the treatment-naïve cohort.

No correlation was observed between PAI-1 and any of the other blood factors examined.

5.5.2.5 Plasma PAI-1 and Overall Survival in a Treatment-naïve Cohort

Results of a Kaplan-Meier overall survival (OS) analysis of the treatment-naïve cohort were not significant when median PAI-1 for the treatment-naïve cohort (1.775) was set as the determining factor. Pre-neoadjuvant cases that were included in the treatment-naïve cohort were not included in this analysis as their treatment pathway was different from that of those who underwent primary surgery. Overall mean survival time for the treatment-naïve cohort was 59.8 months (Table 5.7), and patients with plasma

PAI-1 less than 1.775ng/mL had a mean survival time of 63.7 months compared with 51.4 months for those patients with plasma PAI-1 greater than 1.775ng/mL, with p = 0.172 and χ^2 = 1.870 (Fig. 5.29; Table 5.7). When this analysis was confined to late-stage patients, overall mean survival time in the treatment-naïve cohort was 54.2 months (Table 5.8), and patients with plasma PAI-1 less than 1.775ng/mL had a mean survival time of 64.4 months compared to 43.3 months for patients with plasma PAI-1 greater than 1.775ng/mL, with p = 0.093 and χ^2 = 2.817 (Fig. 5.30; Table 5.8). This suggests a trend towards significance for plasma PAI-1 as a prognostic indicator of survival in treatment-naïve patients, particularly for those with late-stage disease.

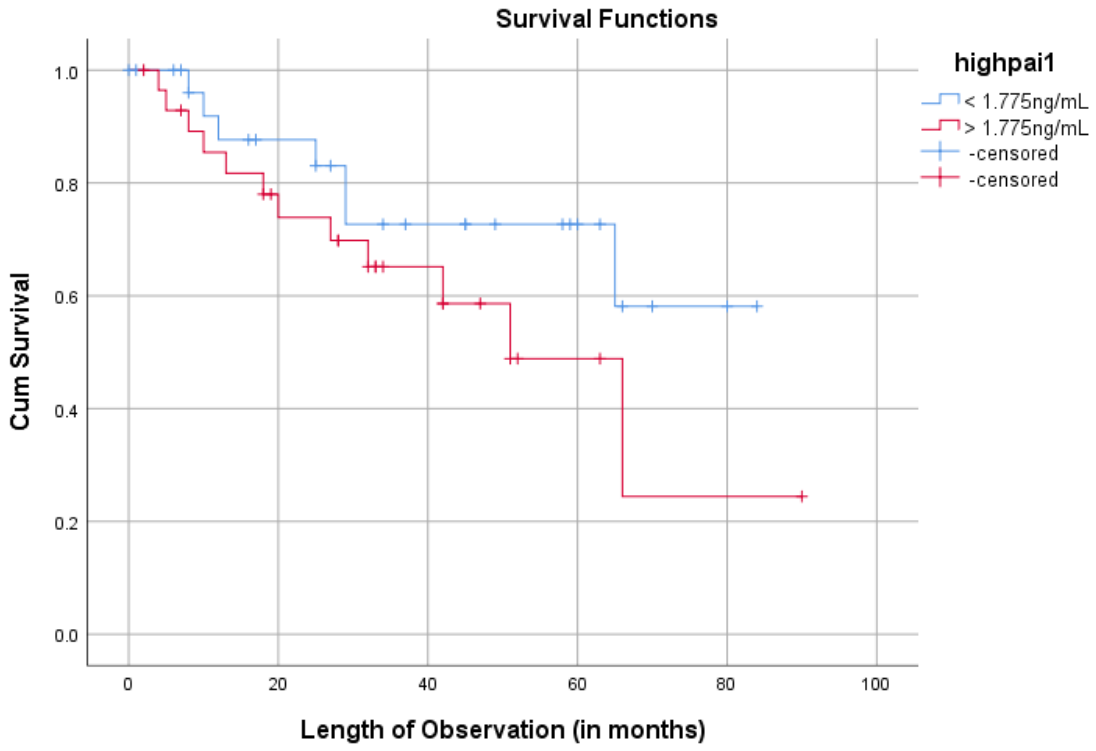

Fig. 5.29 Overall survival in all stages of the treatment-naïve cohort (n = 58) with PAI-1 as the factor, p = 0.172

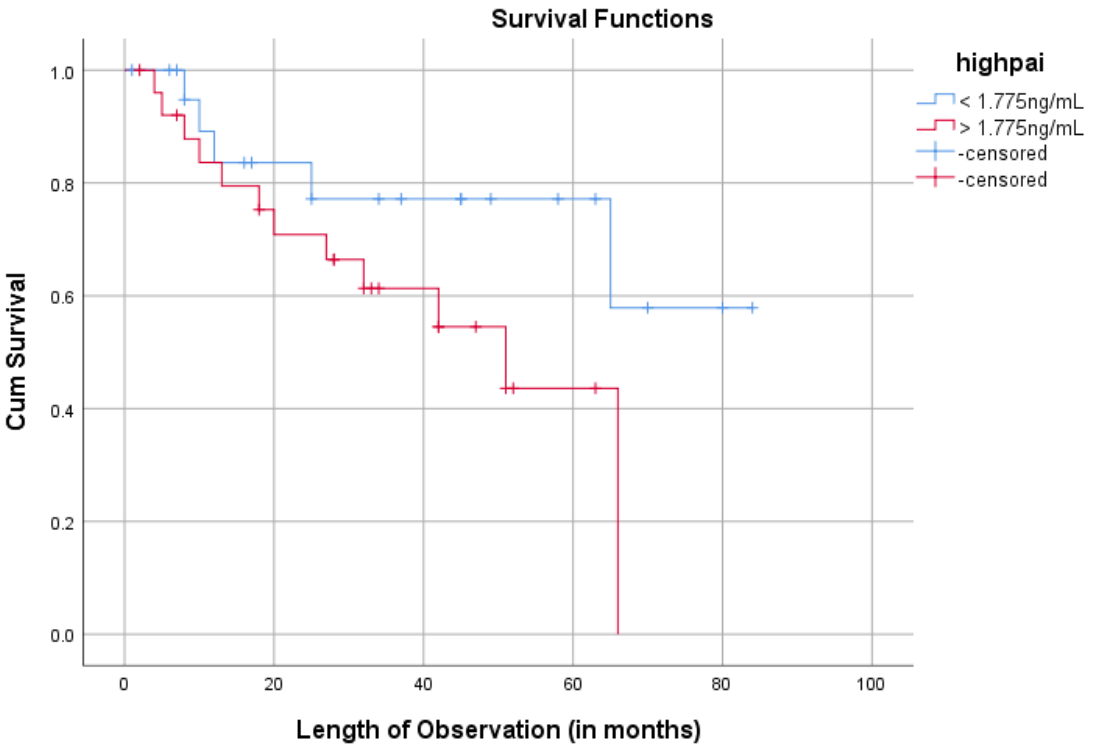

Fig. 5.30 Overall survival in late-stage treatment-naïve patients (n = 48) with PAI-1 as the factor, p = 0.093

Table 5.7 Survival Time: treatment-naïve cohort

Means and Medians for Survival Time

	Mean[a]				Median			
			95% Confidence Interval				95% Confidence Interval	
PAI-1 ng/mL	Estimate	Std. Error	Lower Bound	Upper Bound	Estimate	Std. Error	Lower Bound	Upper Bound
<1.775	63.674	6.322	51.283	76.065	.	.	.	.
>1.775	51.384	7.336	37.005	65.762	51.000	8.792	33.767	68.233
Overall	59.808	5.225	49.567	70.050	66.000	10.197	46.014	85.986

a. Estimation is limited to the largest survival time if it is censored.

Table 5.8 Survival Time: late-stage treatment-naïve patients

Means and Medians for Survival Time

	Mean[a]				Median			
			95% Confidence Interval				95% Confidence Interval	
PAI-1 ng/mL	Estimate	Std. Error	Lower Bound	Upper Bound	Estimate	Std. Error	Lower Bound	Upper Bound
<1.775	64.405	7.288	50.120	78.690	.	.	.	.
>1.775	43.319	5.295	32.941	53.696	51.000	14.164	23.238	78.762
Overall	54.202	5.196	44.019	64.386	65.000	8.178	48.970	81.030

a. Estimation is limited to the largest survival time if it is censored.

5.5.2.6 Plasma PAI-1 correlated with CTC Counts in a Breast Cancer Patient Cohort

Plasma samples from 5 breast cancer patients were analysed by ELISA, and corresponding whole blood samples were screened for CTCs using Angle PLC's (Surrey, UK) Parsortix® System (Appendix B). Patients with high plasma PAI-1 values were also found to have a greater number of CTCs, resulting in a significantly positive linear correlation with R = 0.9679 (Fig. 5.31,Tables 5.9, 5.10).

Table 5.9 Plasma PAI-1 values as measured by ELISA and corresponding Parsortix® CTC counts

ID	Plasma PAI-1 ng/mL	Partsortix® CTCs
CTC BR39	7.663755884	17
CTC BR41	2.434819288	5
CTC BR42	2.10970054	3
CTC BR43	1.852116774	4
CTC BR44	>20	25

Table 5.10 Plasma PAI-1 significantly correlated with Parsortix® CTC counts in a small (n=5) breast cancer patient cohort

Correlations

		Plasma PAI-1	CTC Count
Plasma PAI-1	Pearson Correlation	1	.968**
	Sig. (2-tailed)		.007
	N	5	5
CTC Count	Pearson Correlation	.968**	1
	Sig. (2-tailed)	.007	
	N	5	5

**. Correlation is significant at the 0.01 level (2-tailed).

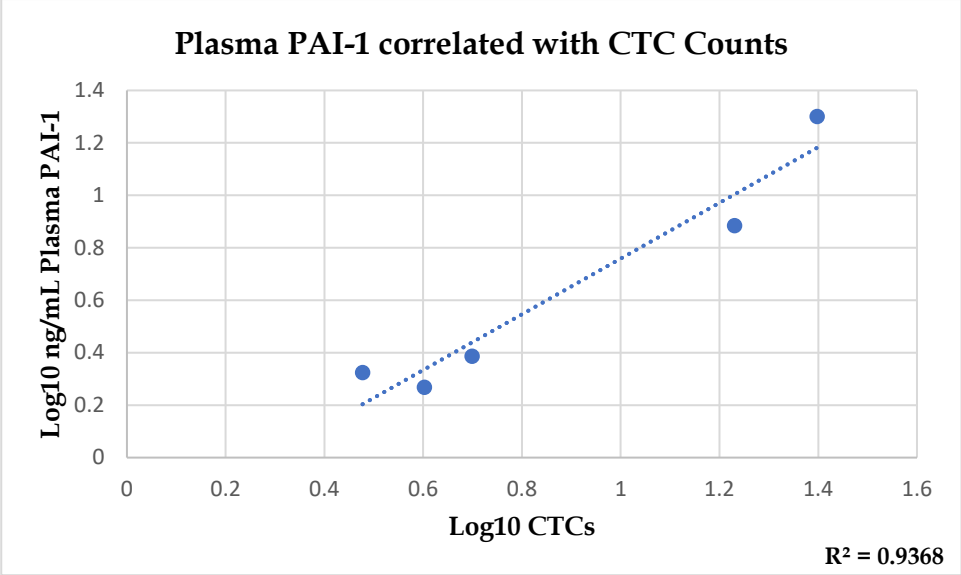

Fig. 5.31 Plasma PAI-1 correlated with CTC counts in a BC cohort.

5.5.3 Other Blood Factors affecting Overall Survival in a Treatment-naïve Cohort

5.5.3.1 Serum Albumin

A serum albumin higher than 40g/L had a significant positive association with overall survival (OS) in the treatment-naïve cohort (Fig. 5.31). Mean survival time for patients with serum albumin greater than 40g/L was 69.6 months, versus 48.9 months for those patients having serum albumin less than 40g/L, with $p = 0.02$ and $\chi^2 = 4.326$ (Table 5.11).

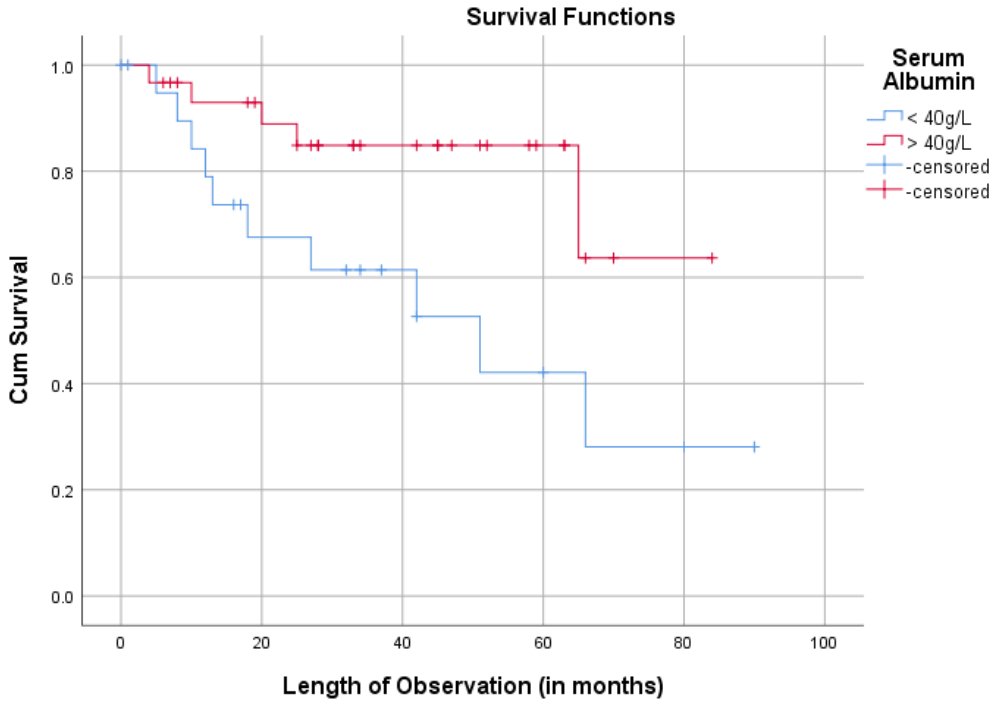

Fig. 5.32 Overall survival in treatment-naïve patients (n = 58) with serum albumin > 40g/L as the factor, p = 0.02

5.5.3.2 Lymphocytes

Lymphocyte counts below 1.5 x10^9/L were associated with a worse survival time in the treatment-naïve cohort (Fig. 5.32). Mean overall survival time for patients with low lymphocytes was 49.9 months versus 62.8 months for patients with normal lymphocyte counts. This was trending towards significance, with p = 0.056 and $\chi^2 = 3.637$ (Table 5.12).

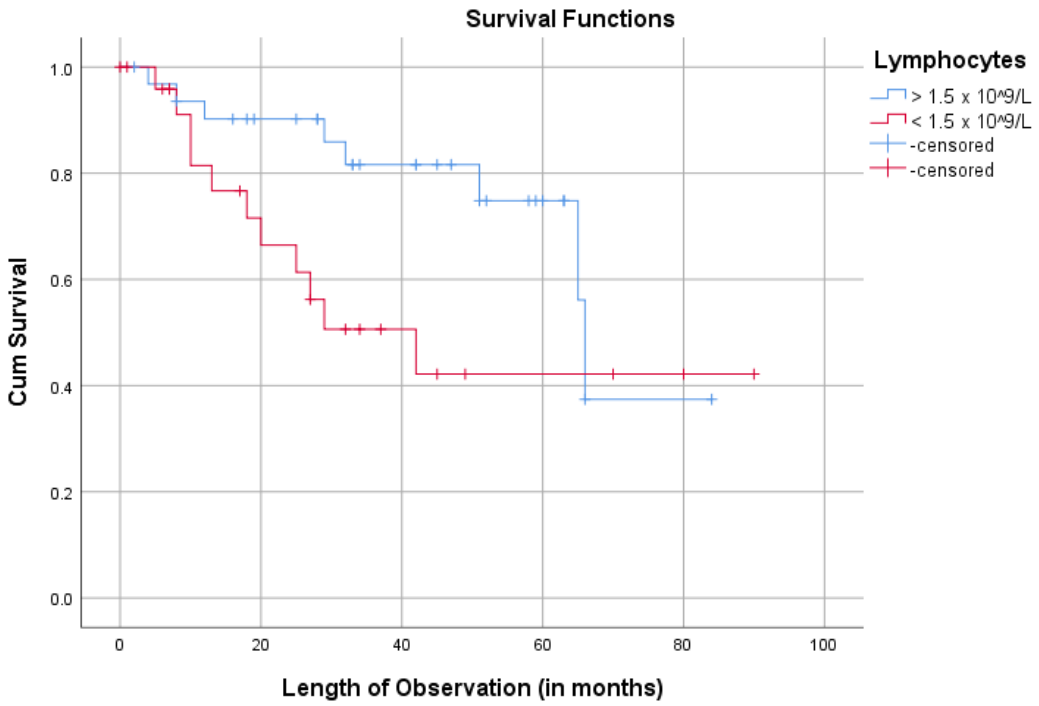

Fig. 5.33 Overall survival in treatment-naïve patients (n = 58) with lymphocytes < 1.5 x 10^9/L as the factor, p = 0.056

5.5.3.3 Platelet-to-lymphocyte Ratio

A platelet-to-lymphocyte ratio (PLR) of less than 250 was found to be significantly associated with increased overall survival in the treatment-naïve cohort (Fig. 5.33). Mean overall survival for patients with a PLR less than 250 was 65.4 months versus 40.8 months for patients with a PLR greater than 250, with p = 0.028 and $\chi^2 = 4.827$ (Table 5.13).

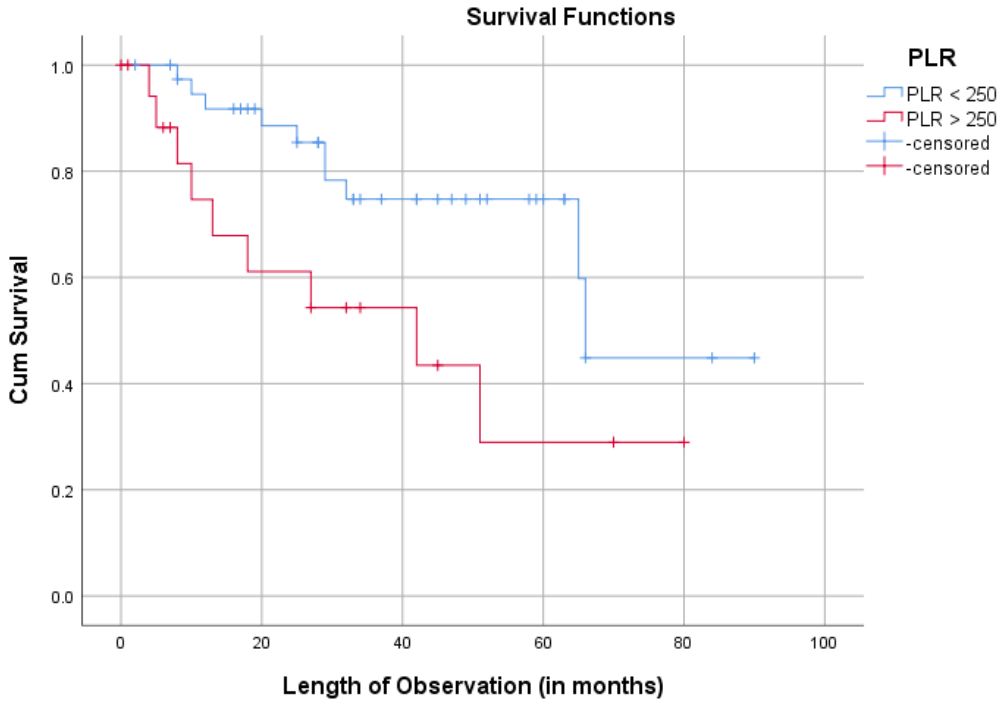

Fig. 5.34 Overall survival in treatment-naïve patients (n = 58) with PLR as the factor, p = 0.028

5.5.3.4 D-dimer, Fibrinogen, Neutrophils, Lymphocytes, and Haemoglobin

D-dimer, fibrinogen, haemoglobin (Hg), neutrophils, and lymphocytes were investigated in the treatment-naïve cohort using the cut-off values defined as normal by SJH pathology, however none of these were found to be significantly associated with either positive or negative survival outcomes. Low Hg did show a trend towards negative association with overall survival, with p = 0.117 and $\chi^2 = 2.459$.

Table 5.11 Survival time: serum albumin in treatment-naïve patients

Means and Medians for Survival Time

	Mean[a]				Median			
			95% Confidence Interval				95% Confidence Interval	
Albumin g/L	Estimate	Std. Error	Lower Bound	Upper Bound	Estimate	Std. Error	Lower Bound	Upper Bound
< 40	48.868	8.224	32.749	64.987	51.000	17.310	17.073	84.927
> 40	69.580	5.679	58.449	80.712	.	.	.	.
Overall	63.087	5.437	52.431	73.743	66.000	.	.	.

a. Estimation is limited to the largest survival time if it is censored.

Table 5.12 Survival time: lymphocytes in treatment-naïve patients

Means and Medians for Survival Time

	Mean[a]				Median			
			95% Confidence Interval				95% Confidence Interval	
lymphocytes	Estimate	Std. Error	Lower Bound	Upper Bound	Estimate	Std. Error	Lower Bound	Upper Bound
> 1.5x10^9/L	62.801	5.569	51.887	73.715	66.000	1.032	63.978	68.022
< 1.5x10^9/L	49.895	8.237	33.752	66.039	42.000	12.964	16.590	67.410
Overall	59.808	5.225	49.567	70.050	66.000	10.197	46.014	85.986

a. Estimation is limited to the largest survival time if it is censored.

Table 5.13 Survival time: PLR in treatment-naïve patients

Means and Medians for Survival Time

	Mean[a]				Median			
			95% Confidence Interval				95% Confidence Interval	
PLR	Estimate	Std. Error	Lower Bound	Upper Bound	Estimate	Std. Error	Lower Bound	Upper Bound
< 250	65.391	6.086	53.462	77.320	66.000	1.140	63.766	68.234
> 250	40.801	8.088	24.949	56.653	42.000	19.227	4.315	79.685
Overall	59.808	5.225	49.567	70.050	66.000	10.197	46.014	85.986

a. Estimation is limited to the largest survival time if it is censored.

5.6 Discussion

The goal of this chapter was to interrogate banked clinical samples for PAI-1, and to use those data obtained in conjunction with relevant demographic, clinicopathological, and surgical patient data to gain insight into the potential role of plasma PAI-1 in HGSOC metastasis.

5.6.1 Plasma PAI-1 is a potential Indicator, Predictor, and Prognosticator in Ovarian Carcinoma

Significantly higher mean plasma PAI-1 in late-stage versus early-stage treatment-naïve patients (Fig. 5.23) suggests a role for plasma PAI-1 as a prognostic indicator of metastatic ovarian disease. This is consistent with previous research correlating plasma PAI-1 with higher disease stage in ovarian cancer (Ho *et* al, 1999). Our results also indicated a trend towards significance for PAI-1 as an independent factor for overall survival, and indeed PAI-1 has been shown to be an independent prognostic indicator of five-year survival in patients with ovarian cancer (Teliga-Czajkowska *et al*, 2019). PAI-1 has also been shown to be an adverse prognostic indicator of both relapse-free and overall survival (Ferroni *et al*, 2014) in ovarian cancer patients.

Research to date regarding PAI-1 in epithelial ovarian cancer has been conducted mainly in tumour and stromal tissue, and also has been conducted in combined histological subtypes, but these studies have not considered HGSOC on its own. The most notable of these studies is that by Chambers and colleagues, which performed IHC on both primary and metastatic tissues. Their research found that 50% of both primary and metastatic tumours expressed PAI-1, and that in patients with late-stage disease for whom PAI-1 expression

was detected in the primary tumour, overall survival was shorter than for patients whose primary tumours were negative for PAI-1 staining (Chambers *et al*, 1998). Thus, high PAI-1 expression in the primary tumour epithelium was determined to be an independent prognostic factor for poor survival outcome (Chambers *et al*, 1998). Another study by Peng highlighted a correlation between PAI-1 and peritoneal dissemination and metastasis in ovarian cancer, also linking PAI-1 to poor prognosis in ovarian cancer patients (Peng *et al*, 2019). PAI-1 was found to activate mesothelial cells, transforming them into cancer-associated mesothelial (CAMs) cells, and both *in vivo* and *ex vivo* studies demonstrated a significant decrease in metastasis when PAI-1 was "knocked down", leading to a blockage of CAM formation (Peng *et al*, 2019). This, too, suggests a prognostic role for PAI-1 in ovarian cancer tumour cells.

Plasma PAI-1 research has been conducted in other cancer types, including breast and colorectal cancers (Palmirotta *et al*, 2009; Ferroni *et al*, 2014; Bal *et al*, 2019). Palmirotta and colleagues found that plasma PAI-1 was higher in patients with breast cancer than in controls, and that pre-surgical plasma PAI-1 could have prognostic value for relapse (Palmirotta *et al*, 2009). Ferroni and colleagues investigated coagulation and fibrinolytic factors as prognostic indicators of outcome in breast cancer. It was determined that elevated plasma PAI-1 was an indicator of relapse (Ferroni *et al*, 2014). As breast cancer and ovarian cancer share some risk factors, such as BRCA1/2 mutations in hereditary breast and ovarian cancer (HBOC), indicators for breast cancer could potentially impact ovarian cancer. Research by Bal and colleagues showed that

treatment-naïve patients with metastatic colorectal cancer (mCRC) had a significant decrease in plasma PAI-1, from 46.3 to 27.1pg/mL, with p = 0.033, after 3 cycles of bevacizumab-containing chemotherapy (CB) (Bal *et al*, 2019). Bal's results also demonstrated that patients who responded positively to CB were those with lower baseline plasma PAI-1 (29.9pg/mL [range 15.5–126.5pg/mL] vs. 57.9pg/mL [range 19.2–202.1pg/mL], P = 0.036), and that patients with a higher baseline plasma PAI-1 tended to not respond as well to CB (Bal *et al*, 2019). It was also noted that those patients who responded with a 46% or greater decrease in plasma PAI-1 after CB were more likely to have a clinical benefit from the therapy. Despite their findings of predictive significance for treatment outcome, plasma PAI-1 did not appear to be a significant prognostic factor for mCRC (Bal *et al*, 2019). Discrepancies in the value of PAI-1 as a marker for treatment, survival, or both across various cancer types serves to highlight the dual nature of PAI-1, whose function could be dose-dependent. This highlights both the importance of this molecule, as well as the need for further research into it. Research into plasma PAI-1 by others as discussed here, coupled with our own observations that a significant decrease in mean plasma PAI-1 in patients in our neoadjuvant chemotherapy cohort suggests that plasma PAI-1 may be a valuable predictive factor in HGSOC treatment.

While mean plasma PAI-1 in our late-stage treatment-naïve patients (3.5ng/mL) was found to be significantly higher than in our neoadjuvant chemotherapy (2.5ng/mL) and recurrent cohorts (2.1ng/mL), it was not

significantly higher than that of our benign cohort (2.6ng/mL). Evaluation of a cohort of healthy controls would be advantageous for comparison in future studies. It is also noteworthy that mean plasma PAI-1 in the benign cohort was close to that of late-stage patients in the neoadjuvant chemotherapy cohort. This is not surprising, and suggests that those in the neoadjuvant chemotherapy cohort have had their PAI-1 levels reduced to a level comparable to tumours with benign histology, and therefore warrants further investigation. A 2002 study by Boss and colleagues compared PAI-1 in ovarian cyst fluid from malignant, borderline, and benign tumours, and found that the highest levels were in malignant tumours (Boss *et al*, 2002). Another study by Casslén in 1994 examined PAI-1 and other factors in blood, PAF, and tumour fluids from patients with malignant and benign ovarian tumours, as well as blood from healthy controls, and 16 of these were of the benign serous subtype (Casslén *et al*, 1994). Results from the analysis of plasma PAI-1 in peripheral blood showed no significant difference between benign and malignant tumours in the pre-menopausal group (Casslén *et al*, 1994). Plasma PAI-1 was higher in both benign and malignant than in healthy controls. In the post-menopausal group, women with both malignant tumours and ascites had significantly higher plasma PAI-1 than women with malignant tumours and no ascites, women with benign tumours, and healthy controls (Casslén *et al*, 1994). However, these results were not stratified by histological subtype, and are therefore difficult to interpret and align with our data. It is suggested that the elevated plasma PAI-1 in patients with benign ovarian tumours may be due to increased

concentrations of tPA present in the vascular endothelium, and indeed investigation into this would be beneficial.

Additionally, PAI-1 4G/5G promoter polymorphism has been the subject of many investigations, and those bearing a homozygous 4G allelotype have been found to be more susceptible to colorectal and endometrial cancers (Wang et al, 2013), as well as hypertension (Jeng *et al,* 2003). Interestingly, it was a heterozygous 5G/4G allelotype that increased susceptibility to occlusion of the coronary artery during myocardial infarction (Parpugga *et al*, 2015). The 4G allele is characterised by the deletion of a G nucleotide in the promotor, and has been shown to exhibit higher PAI-1 transcriptional activity, resulting in higher plasma PAI-1 levels in people homozygous for the 4G allele (Wiklund *et al*, 2005). The 5G polymorphism is characterised by the insertion of a G nucleotide in the promoter region of PAI-1, and has been shown to decrease transcription of PAI-1, and indeed people homozygous for the 5G allele have been found to have the lowest levels of plasma PAI-1 (Wiklund *et al*, 2005). The implications of this are unclear relative to ovarian cancer, however two studies to date have not shown this polymorphism to be a risk factor in ovarian cancer (Türkmen *et al*, 1997; Bentov *et al,* 2009). Regardless, these are older studies, and continuing investigation into the various genetic factors directly affecting PAI-1 transcription, translation, and post-translational modification is of the utmost importance as polymorphism in the PAI-1 promoter may play a role in baseline plasma PAI-1 levels.

Mean plasma PAI-1 in pathological early-stage neoadjuvant

chemotherapy/interval debulk patients was actually the highest of all of the groups at 4.5ng/mL, however this was not significant when compared to late-stage neoadjuvant chemotherapy patients, which is likely due to the small number of patients in the pathological early-stage neoadjuvant chemotherapy group. It is important to remember that this is a pathological stage, and that all neoadjuvant patients had advanced disease at the time of their diagnoses. This could be a contributing factor in high plasma PAI-1.

5.6.2 Plasma PAI-1 did not correlate with Platelet Counts in a Treatment-naïve Cohort

PAI-1 did not correlate with platelet counts in our treatment-naïve cohort (Fig. 5.25), and while these two factors shared a positive linear relationship (Fig. 5.26), lack of correlation demonstrated that PAI-1 from PFP was independent of platelet PAI-1. This is consistent with research by Booth and colleagues who demonstrated that while 93% of total circulating PAI-1 did in fact come from platelets, there was no correlation between platelet count in PRP and PAI-1 antigen from PFP (Booth *et al*, 1988). Furthermore, Booth confirmed that plasma PAI-1 antigen in a patient with grey platelet syndrome was close to normal (Booth *et al*, 1988), and this also suggests that the PAI-1 antigen in our PFP was not from the platelets. Similar *in vitro* results were observed in previous studies in our laboratory (Spillane *et al*, submitted). The linear relationship that exists between PFP-derived PAI-1 and platelet counts from patient whole blood samples is likely due to the increased risk of thrombocytosis and thrombosis often seen in cancer patients with late-stage

and metastatic disease.

5.6.3 Plasma PAI-1 demonstrated a significant positive Correlation with CTCs in a Breast Cancer Patient Cohort

A significant correlation was found to exist between plasma PAI-1 and CTCs in whole blood in a small cohort of breast cancer patients. Ovarian patients undergoing surgery had been moved to another facility due to the Covid19 pandemic, and so we were not able to collect samples from these patients. However, our cohort of breast cancer patients for whom we were able to obtain samples yielded promising preliminary results that demonstrate the potential positive impact of plasma PAI-1 analysis coupled with current CTC technologies on the future of patient care.

5.6.4 Cohort Demographics

Ovarian cancer diagnosis is most common after menopause, with the median age of diagnosis being 63. The cohorts included in this study reflect this. Higher mean BMI was observed in our late-stage treatment-naïve (27.5), recurrent patients (30.6), and benign patients (29.3) than in early-stage treatment-naïve (26.5), early-stage neoadjuvant (25.6) and late-stage neoadjuvant patients (26.6). While this is consistent with research showing that women with OC were more likely to have a high BMI (Adler *et al*, 1996), this may be a result of disease rather than a causative factor (Adler *et al,* 1996; Lukanova and Kaaks, 2004). This does not explain high BMI in the benign cohort, which may be random, or may be due to other health-related factors. The mass of fluid accumulation in benign tumours may also contribute to an increased BMI. Some studies have shown that BMI does not appear to be a risk

factor for ovarian cancer, while others have shown a correlation between the two (Lukanova and Kaaks, 2004), and indeed many women present with large pelvic masses which may contribute to higher BMI in these patients. Lower BMI in patients receiving neoadjuvant chemotherapy may be the result of the resolution of ascitic fluid (Cohen and Petignat, 2014), or may be due to the loss of appetite associated with some chemotherapeutics.

5.6.5 Haematology and Biochemistry

D-dimer, a by-product of fibrinolysis, has been shown to be a negative prognostic marker in terms of 5-year survival and overall survival (OS) in ovarian, cervical, and endometrial cancers (Xu *et al*, 2017), and has been also been shown to have potential use as a preoperative evaluation of post-chemotherapeutic progress for patients with high-grade musculoskeletal carcinoma (Morii *et al*, 2015). Our results here, which demonstrated that D-dimer is significantly lower in late-stage patients who have received neoadjuvant chemotherapy than in late-stage treatment-naïve patients, support this. A retrospective analysis by Ge and colleagues created a new risk index for potential use in differentiating abnormal vaginal bleeding from endometrial cancer. This index found that both D-dimer and fibrinogen were significantly associated with the risk of endometrial cancer when combined with HE4 and CA199 (Ge *et al*, 2020). This may have potential use in ovarian cancer screening as well. A meta-analysis of 15 studies on D-dimer in ovarian carcinoma found that plasma D-dimer was significantly higher in malignancy than in benign controls, and that D-dimer could be used to predict disease progression and

risk of venous thrombotic events (VTEs), but that the association was significantly sample-size dependent (Wu *et al,* 2017).

Fibrinogen levels in our cohorts were consistent with the findings of a meta-analysis showing that elevated plasma fibrinogen may be related to poor prognosis in EOC (Luo *et al*, 2017). Our results were also consistent with research by Lu and colleagues in which mean fibrinogen was 4.5g/L in female patients with cancers of the lung, stomach, liver, colon, and breast (Lu *et al*, 2000). Lu's research showed that mean fibrinogen actually increased after chemotherapy in those patients who did not undergo primary tumour debulking surgery (Lu *et al*, 2000), further suggesting that plasma fibrinogen may be related to tumour growth. However, fibrinogen response to chemotherapy may be specific to cancer type. While mean fibrinogen in our late-stage neoadjuvant chemotherapy patients was significantly lower than that of our late-stage treatment-naïve patients, it was still higher than normal, and this may be consistent with findings by Lu were we to more closely analyse neoadjuvant chemotherapy patients before and after primary debulking surgery. Another set of findings by Zhu showed that fibrinogen, along with D-dimer, was predictive of response to chemotherapy in small-cell lung carcinoma (SCLC) patients (Zhu *et al*, 2015). Significantly lower fibrinogen post-neoadjuvant chemotherapy may also be due in part to the effects of chemotherapy on the liver (Ward *et al*, submitted for publication).

30.6% of late-stage patients in the treatment-naïve cohort were anaemic, compared with 56.5% in the neoadjuvant cohort, and this is fairly consistent

with results of the European Cancer Anaemia Survey (ECAS), which found that 39% of patients were anaemic upon enrollment in the study, with 67% experiencing anaemia related to chemotherapy (Ludwig *et al*, 2004). Anaemia can be a result of having cancer, or a side-effect of the chemotherapy or radiation used to treat it. In cases of chemotherapy or radiation-induced anaemia, this can potentially correct itself after cessation of the therapy. However, if the patient is quite anaemic prior to onset of therapy, or becomes very anaemic during therapy, hypoxic conditions in body tissues can result in a poor clinical result as both ionising radiation therapies and some chemotherapies rely on oxygenation for clinical benefit (Aldoss *et al*, 2008). This can be treated with red blood cell transfusion, iron, or erythropoietin stimulating agent (ESA), depending on disease stage and severity of anaemia (Bryer and Henry, 2018), however peri-operative allogeneic blood transfusions have been linked to worse survival in OC patients (Connor *et al*, 2018).

Results of tests for tumour markers CA-125 and CEA were also considered to see if there was any significance among stages within cohorts or between cohorts. CA-125 is often used as an indicator of both metastasis and successful chemotherapeutic treatment, and indeed our results support this. Mean CA-125 was significantly lower in late-stage patients who had undergone neoadjuvant chemotherapy, and was significantly higher in patients in the treatment-naïve cohort who had metastatic disease. CEA was not shown to be a significant factor in any cohort or between any cohorts, and this supports research showing that while it may be a relevant factor in differentiating

mucinous from serous ovarian cancer (Marchand *et al*, 1975), and has been shown to be present in 35% of low-grade serous ovarian cancers (Bashizadeh-Fakhar *et al*, 2018), it has not been demonstrated to be a relevant marker for the high-grade serous histotype.

Serum albumin is a useful gauge of nutritional status in ovarian cancer patients, particularly as cachexia and ascites accumulation are often associated with malnutrition in advanced disease (Asher *et al*, 2011). Asher's study found that treatment-naïve ovarian cancer patients with pre-operative serum albumin that was greater 35g/L had a median survival that was 9 times that of patients whose serum albumin was less than 25g/L (Asher *et al*, 2011). While mean serum albumin for all cohorts in our study were within normal range, late-stage patients who received neoadjuvant chemotherapy had significantly higher serum albumin than patients in the treatment-naïve cohort who had late-stage disease. This is also consistent with our OS survival analysis showing that patients with serum albumin > 40g/L had significantly longer OS than those with < 40g/L (69.2 months versus 50.9 months, $p = 0.038$).

Findings of this study regarding the platelet-to lymphocyte ratio (PLR), a marker of inflammation, were such that a significantly higher PLR was found in patients with late-stage disease in our treatment-naïve cohort than in any patients with late-stage disease in our neoadjuvant chemotherapy cohort, our benign cohort, or our recurrent cohort. PLR was also significantly higher in stage IV treatment-naïve patients than in any other stage of that cohort. Previous research has demonstrated prognostic value for PLR ≥ 200 in patients

with epithelial ovarian carcinoma (EOC) (Raungkaewmanee *et al*, 2012). PLR was also found to have better predictive value for both advanced stage and suboptimal cytoreductive surgery than either thrombocytosis or the neutrophil-to-lymphocyte ratio (NLR) alone (Raungkaewmanee *et al*, 2012). It was not possible to assess the predictive ability for suboptimal cytoreductive surgery as the majority of our patients are optimally debulked due to the improvements in patient triage for surgery assisted by multidisciplinary team discussion. A meta-analysis by Zhao also showed that a high PLR was significantly associated with poor OS and PFS in ovarian cancer (Zhao *et al*, 2018). A second meta-analysis by Templeton showed that a high PLR was associated with poor OS for cancers with solid tumours, including colorectal, liver, esophageal, ovarian, and pancreatic carcinomas (Templeton *et al*, 2014). Despite these and other findings, PLR in our treatment-naïve cohort was not found to be of prognostic value when adjusted to the cut-off value of 200 used in Raungkaewmanee's study, however we did see significance when a cut off of 250 (slightly higher than the mean of the cohort) was assessed. There are several factors that could affect PLR. Elevated lymphocytes in patients with higher platelet counts, which did occur in several of our patients, could have the effect of decreasing the PLR. PLR may also vary by ethnic group, and this should be elucidated and taken under consideration if found to be relevant.

The neutrophil-to-lymphocyte ratio (NLR) can be an important marker of inflammation in cancer, particularly as neutrophils can affect both arms of the immune system, and affect both CD4+ and CD8+ T-cell function.

Neutrophils are the most abundant leukocyte in the human body, accounting for 40-60% of white blood cell (WBC) composition in peripheral blood. Elevated neutrophil levels are common in patients with advanced cancers (Uribe-Querol and Rosales, 2015); however, how tumours recruit neutrophils remains largely unknown (Uribe-Querol and Rosales, 2015). Peripheral blood lymphocytes account for 20-40% of WBCs, and are important in both innate and adaptive immune response. Neutrophils are recruited into tissue by IL-8, which is stored in Weibel-Palade bodies in endothelial cells (EC) along with the platelet-activator CD62P (Romani de Wit *et al,* 2002). It has been shown that PAI-1 is necessary for the stabilisation of IL-8 that induces transendothelial migration of circulating neutrophils to sites of inflammation, and that platelet PAI-1 is not a factor in this (Marshall *et al*, 2003). PAI-1 did significantly correlate with neutrophil counts in our treatment-naïve cohort, and this does suggest a potential role for PAI-1 in the inflammatory response and in immune regulation in ovarian cancer as tumour PAI-1 may be contributing to endothelial IL-8 stabilisation and subsequent neutrophil recruitment.

5.7 Study Limitations

Early-stage high-grade serous cancers are a much rarer entity than late-stage ones, and while some do exist in the biobank and were analysed, we did not have sufficient power for statistical analyses of all markers mentioned in this chapter. We do feel that PAI-1 showed a trend towards significance as a prognostic marker or treatment management marker, and that it will gain significance with an increase in the number of clinical samples.

The SARS-CoV-2 pandemic presented a special challenge, and created an unforeseen and unwelcome obstacle to our research. We were not able to collect consented patient plasma and blood samples, and as a result, we lost valuable and irreplaceable patient data. Limited laboratory access has also impeded our ability to process any consented samples that we were able to collect, and has unfortunately severely impacted our CTC study, which is still underway.

5.8 Conclusion

The analyses performed here on plasma PAI-1 and other blood factors in patient samples provide insight into the value of PAI-1, both separately and in conjunction with other factors, as a prognostic indicator of treatment outcome in patients with HGSOC. Our results indicate a trend towards significance for PAI-1 as an indicator of overall survival in treatment-naïve HGSOC patients, suggesting that this could become significant with a larger number of patients. Preliminary results of our CTC study suggest that PAI-1 could be indicative of CTC status.

CHAPTER 6

GENERAL DISCUSSION

6.1 Introduction

The novel research conducted in this thesis had its basis in the Affymetrix array results previously obtained by our team, which showed that incubating platelets with several cancer cell lines formed a platelet cloak, and subsequently resulted in the consistent and significant differential expression of several genes across those lines, including serine protease inhibitor E1 (SERPIN E1), which codes for the plasminogen activator inhibitor 1 (PAI-1) protein (Egan *et al*, 2011; Cluxton et *al*, 2019). PAI-1 is heavily involved in wound-healing (Wilkins-Port *et al*, 2010), coagulation (Kwaan *et al*, 2019), maintenance and restructuring of the extracellular matrix (ECM) (Lee *et al*, 2005), in cancer cell migration and invasion (Czekay *et al*, 2011), and in angiogenesis (Isogai *et al,* 2001). We therefore hypothesized that PAI-1 could be central to the metastasis of high grade serous ovarian cancer (HGSOC), and the research conducted and reported in this thesis supports this.

6.2 Chapter 3 Results: PAI-1 and Platelet Assays

Chapter 3 results provided evidence that platelets induced both the transcription of PAI-1 mRNA, and the translation of PAI-1 mRNA into protein in SK-OV-3 cells, as demonstrated by significant results in RT-qPCR and ELISA, respectively. This supports previous research in which it has been demonstrated that platelets drive PAI-1 production in cloaked ovarian cancer cells (Cooke *et al*, 2015), and could have implications in the context of circulating tumour cells (CTCs) for which it has been demonstrated that platelets not only provide a protective effect (Egan *et al*, 2011; Egan *et al*, 2014), but potentially contribute to immune evasion in the circulation (Cluxton *et al*,

2019). An increase in intracellular PAI-1 protein as a direct result of the incubation of platelets with SK-OV-3 cells was observed via antibody staining and fluorescence microscopy, which further supports that platelets drive both transcription and translation of PAI-1 in ovarian cancer cells. Platelets were not able to bring PAI-1 mRNA levels back to normal when PAI-1 had been silenced via siRNA, and RT-qPCR assays performed by our lab have clarified that although platelets *induce* PAI-1 mRNA transcription, the number of platelets incubated with the cells were alone insufficient to provide the number of PAI-1 mRNA transcripts measured in our co-incubations by RT-qPCR (Spillane *et al*, unpublished data). This strongly suggests that the platelet-cancer cell interaction is responsible for triggering PAI-1 transcription. The precise mechanisms involved in this process are still under investigation. Previous research by others has demonstrated the role of TGF-ß in increased PAI-1 transcription (Placencio and DeClerck, 2015; Dennler *et al*, 1998), and that has been taken under consideration here; however, our results suggest that in addition to TGF-ß, horizontal transfer of platelet PAI-1 to cancer cells during cloaking may also serve as a TF for itself in a tumour microenvironment (Kirschbaum *et al*, 2015).

Results of chapter 3 additionally demonstrated a significant decrease in invasion when PAI-1 has been transiently silenced via siRNA, as well as a significant decrease in the rate and totality of wound closure, regardless of the presence of platelets or their releasate, whereas platelets and their releasate significantly increased the rate and totality of wound closure when added to

cells treated with a negative control. This demonstrated that when PAI-1 has been lost, the PAI-1 contained in platelets is insufficient to resurrect functionality. Furthermore, the addition of platelets and their releasate to SK-OV-3 cells resulted in an increase in cell proliferation, as demonstrated via FACS analysis, and this is consistent with previous research (Giacoia *et al*, 2014). Additionally, novel findings here that wound edge velocity – that is to say the *rate* at which the cells are migrating - is significantly increased in the presence of platelets and their releasate demonstrate that platelets play a role in expediting cellular migration in ovarian cancer cells *in vitro*, and all results here combined suggest that this could be due to increased PAI-1.

6.3 Chapter 4 Results: RNA-Sequencing

The results of research in chapter 3 provided a strong basis for performing a transcriptomic analysis of HGSOC cells - both when PAI-1 has been silenced, and when platelets are co-incubated with these cells. The results of this novel RNA sequencing and subsequent analyses did indeed demonstrate that the SERPIN E1 gene is central to a great number of the biological processes and molecular pathways that underpin ovarian cancer metastasis, and also showed that platelets significantly increase the number of SERPIN E1 transcripts in SK-OV-3 cells. This provided further evidence that platelet-cancer cell interactions are central to ovarian cancer metastasis.

In our sample sets where PAI-1 had been silenced via siRNA, differential gene expression analysis demonstrated significant downregulation of those molecular pathways associated with the regulation of cellular migration,

phosphorylation, anatomical structure morphogenesis, intracellular signal transduction, cellular protein modification, and the stress-activated protein kinase signaling cascade, all of which are important within the scope of cancer and the metastatic process. Also significantly downregulated was the biosynthetic process responsible for Acetyl-CoA production, which is glycolysis. This strongly suggests that PAI-1 is involved in cancer cell metabolism. Previous research has demonstrated that increased PAI-1 in triple-negative breast cancer (TNBC) cells not only enhanced migration, but also promoted glycolysis and activated ERK signaling, which in turn promoted mitochondrial fragmentation (Humphries *er al*, 2019). The association between TNBC and BRCA1/2 mutations has been reported in many clinical investigations (Couch *et al*, 2015), and as a BRCA1/2 mutation also carries an increased risk of ovarian cancer, the potential effects of PAI-1 on ovarian cancer metabolism is a critical area of research that warrants further investigation. The significant inhibition of cellular migration via the silencing of PAI-1 as seen in chapter 3 wound-healing assays aligns with the downregulation of mRNA seen as the result of transcriptomic analysis – in other words, the genotype matches the phenotype. Significant downregulation of phosphorylation has massive implications across many, many cellular processes including protein function and signal transduction, inflammation, apoptosis, molecule transport across cell membranes, not the least of which is oxidative phosphorylation. Also significantly downregulated were the pathways involving coagulation, which was expected, cell adhesion, and homologous recombination. This last category

suggests that PAI-1 could play a role in monitoring response to chemotherapy or potentially provide some answers regarding the development of chemoresistance, but more research is needed to determine precisely how homologous recombination is affected by the loss of PAI-1. This could perhaps affect treatment options with Poly-ADP-ribose polymerase (PARP) inhibitors, which affect base-excision repair (BER) pathways in patients with BRCA mutations by forcing non-homologous end joining NHEJ, ultimately leading to apoptosis (Mittica *et al*, 2018).

Significant differential expression of genes included many that have been implicated in ovarian cancer metastasis and reduced PFS, including CXCL1, CXCL3, IL-6, and MMP-1. Silencing PAI-1 simultaneously resulted in the significant upregulation of molecular pathways and biological processes such as glycosylation via increased expression of GXYLT, which when silenced has been shown to increase Notch expression and activity (Lee *et al*, 2013). This suggests that silencing PAI-1 decreases Notch activity which could decrease angiogenesis. Additionally, it has been demonstrated that hypoxia, which results in angiogenesis and subsequent platelet recruitment as a result of leaky basement membrane in the tumour vasculature, contributes to PAI-1 transcription and translation in the human lung cancer cell line EBC-1 (Kimura *et al*, 2002). This may also be occurring in ovarian cancer cells, and warrants further investigation. PAI-1 was also shown to be a target gene of HIF-2α in hepatocellular carcinoma, whereby plasmin was decreased by the upregulation of PAI-1 and supported angiogenesis (Geis *et al*, 2014). While much more

research is required in this area, this provides evidence that the increase in PAI-1 resulting from platelet-cancer cell interactions is essential to angiogenesis, cancer metastasis, including HGSOC metastasis, and supports our hypothesis. Co-incubating platelets with our ovarian cancer cell line model significantly upregulated SERPIN E1 transcripts and the molecular pathways and biological processes related to angiogenesis, and suggests that targeting PAI-1 has the potential to suppress angiogenesis. Also significantly upregulated in conjunction with a loss of PAI-1 are several protocadherins, including the tumour suppressor gene PCDH10, which is an early methylation target in cervical cancer (Narayan *et al*, 2009) and is downregulated in advanced stage bladder cancer (Ma *et al*, 2013). This suggests that reducing PAI-1 could result in a potentially beneficial increase in some tumour suppressor genes. Further supporting our hypothesis that PAI-1 is central to ovarian cancer metastasis is the significant upregulation of Wnt4 when PAI-1 is silenced, which suggests that PAI-1 could be a regulator of non-canonical signaling in ovarian cancer (Teeuwssen and Fodde, 2019; Bernard *et al*, 2008).

Adding platelets to otherwise untreated SK-OV-3 cells resulted in the significant upregulation of SERPIN E1 transcription, and this aligns with the RT-qPCR results seen in chapter 3. As a result of this upregulation, significant upregulation of the pathways involving cell migration, angiogenesis, regulation of response to wounding, extracellular matrix organization, cell cycle DNA replication, negative regulation of interferon-gamma production, and interstrand crosslink repair was found to exist. Increased migration, response

to wounding, and cell-cycle DNA replication are all consistent with the results in chapter 3. Upregulation in interstrand crosslink repair in ovarian cancer cells in the presence of platelets demonstrates a "see-saw" effect corresponding to the significant downregulation of homologous recombination we noted when PAI-1 was silenced, and could provide insight into chemotherapeutic strategies, cancer cell mutation that occurs via expedited proliferation when cell-cycle checkpoints are dysfunctional, and the genesis of chemoresistance. Further analysis of our 6 treatment types could assist in determining exactly where in the genome changes are occurring both when PAI-1 is silenced and when platelets are added, particularly in the highly-conserved intronic regions seen to be dysregulated in the IGV graph (Fig. 4.13).

6.4 Chapter 5 Results: PAI-1 in HGSOC Patient Cohorts

The goal of any research is ultimately to help the patient, and through the gracious and selfless donations of so many people affected by HGSOC, we have been able to examine plasma PAI-1 levels in five patient cohorts. The results of our novel analysis demonstrated that plasma PAI-1 is highest in treatment-naïve patients, and lowest in patients with recurrent disease, with patients who had neoadjuvant chemotherapy and those with benign histology ranking in second and third place, respectively. Patients in the treatment-naïve cohort with late-stage disease had significantly higher plasma PAI-1 than those with early-stage disease in the same cohort. Patients with late-stage disease in the neoadjuvant chemotherapy cohort had significantly lower plasma PAI-1 levels than patients with late-stage disease in the treatment-naïve cohort. These

results support our hypothesis that PAI-1 plays a central role in metastasis, and suggests a potential role for PAI-1 in the diagnosis of HGSOC, as well as chemotherapy monitoring in patients with tumours that do not express CA-125; however, further evaluation is required here, particularly with respect to 4G and 5G allelotypes that can create differences in base plasma PAI-1 levels (Wiklund *et al*, 2005).

The CTC study was severely impacted by the Covid19 pandemic. In light of this, the patient samples that were able to be analysed demonstrated a significant positive correlation between plasma PAI-1 and the number of CTCs a patient has. This preliminary yet potentially pivotal analysis also provides support for our hypothesis, and together with the results from the other 4 cohorts, further suggests that plasma PAI-1 is an indicator of metastatic disease.

6.5 Conclusion

It has been demonstrated here that PAI-1 is crucial to the progression and metastasis of ovarian cancer, that platelets play an important role in these, and that platelet-cancer cell interactions increase PAI-1. We have demonstrated in chapter 3 that platelets significantly increase PAI-1 in an ovarian cancer cell line model, and we have also demonstrated via RT-qPCR of platelets only that this increase is not coming from the platelets themselves. RT-qPCR and immunofluorescence suggest that PAI-1 released from the platelets during adhesion and degranulation may be an indirect cause of PAI-1 in ovarian cancer cells as well as in the ovarian tumour microenvironment through potential action as a TF. Previous research by our group demonstrated that

platelet cloaking of cancer cells occurs across multiple cancer cell lineages, and that the platelet cloak induces a mesenchymal phenotype in cancer cells which may lend itself to invasion and subsequent haematogenous metastasis (Cooke *et al*, 2015; Guo *et al*, 2019). Research by others has shown that cancer cells undergoing EMT experience an increase in PAI-1 expression (Bydoun *et al*, 2018; Xu *et al*, 2018) that can aid in angiogenesis and the intravasation of tumour cells into the circulation during pre-metastatic events, and that once they are in the circulation the platelets further assist in haematogenous metastasis (Egan *et al*, 2011; Labelle *et al*, 2011; Labelle *et al*, 2014; Cluxton *et al*, 2019). As there are many parallels that can be drawn between cancer and embryogenesis, and as it has been demonstrated that PAI-1 expression is induced during EMT, tissue repair, and cancer cell dissemination (Kalluri and Weinberg, 2009), it is not out of the question to suggest that PAI-1 could be considered a morphogen within the scope of the genesis, progression, and metastasis of cancer, including HGSOC; however, much more research is required to support this.

Silencing PAI-1 resulted in the significant inhibition of invasion, migration, and wound-healing phenotypically, which corresponded to the significant downregulation of many crucial pathways and biological processes integral to the functionality of both healthy cells and cancerous ones, such as coagulation, haemostasis, stress responses and their associated signaling cascades, inflammation, regulation of cellular metabolic processes, homologous recombination, and histone ubiquitination. All of these results, taken together

with our novel findings in chapter 5 that plasma PAI-1 was significantly lower in patients with early-stage disease than in those with late-stage disease in our treatment-naïve cohort, and was also significantly lower in patients with late-stage disease in our neoadjuvant chemotherapy cohort than in our treatment-naïve cohort, support our hypothesis that PAI-1 is central to ovarian cancer metastasis. Results here also support previous findings that PAI-1 could be a targetable molecule by a small-molecule inhibitor, as seen with IMD-4482 (Nakatsuka *et al*, 2017) and TM5275 (Mashiko *et al,* 2015), and they suggest that PAI-1 could be utilised in ovarian cancer diagnostics and in the monitoring of response to chemotherapy in instances where CA-125 may not be useful. IMD-4482 was found to block PAI-1 function in OC cells, and was observed to suppress proliferation by upregulating p27kip1 and downregulating CDK2 and cyclin D3 (Nakatsuka *et al*, 2017). Importantly, this was not observed in ovarian cancer cells that did not express PAI-1, however as PAI-1 is integral to the coagulation cascade, research into how molecules targeting PAI-1 affect the body overall is paramount. Dose-dependent effects blocking PAI-1 adhesion to vitronectin were also noted in this particular study, but other studies have found that blocking PAI-1 increased this (Nakatsuka *et al*, 2017), which suggests a co-dependent factor or interdependence of many other network factors. Our RNA-sequencing results certainly demonstrate the latter, and in working with inhibitors of this kind, it is crucial to view through a wide scope. All results here together provide evidence that PAI-1 is central to ovarian cancer metastasis, and that it has great potential in the diagnosis, monitoring, and

treatment of HGSOC.

6.6 Study Limitations

There were several limitations to this study, which have been duly noted in their respective sections. Furthermore, while we possess several ovarian cell lines in storage, two were negative for PAI-1, and others were not deemed to be a suitable model of HGSOC by virtue of previous work in our laboratory. For the purposes of publication, additional suitable cell lines will be determined, and some of our PAI-1 assays will be repeated in those lines.

6.7 Future Work

In light of the many novel findings here and their relevance to ovarian cancer research, it would be beneficial to OC patients to continue research in these directions, including exploration into the potential of PAI-1 as both a mitogen and a potential morphogen, with specific attention to PAI-1 as a gradient in individual cells or groups of cells. Acknowledging the "see-saw" effect morphogens have in cells, and treating PAI-1 accordingly by targeting PAI-1 at various concentrations could produce effects that are indeed concentration-dependent, and could also be variable based on both individual PAI-1 genotype and disease stage.

Findings by Humphries and colleagues have indicated that PAI-1 directly inhibits mitochondrial function and facilitates the subsequent switch from oxidative phosphorylation to glycolytic metabolism in TNBC (Humphries *et al*, 2019). As our research found that silencing PAI-1 inhibits phosphorylation, and given that TNBC and HGSOC may share BRCA1/2 mutation genotypes, it

would be prudent to examine this within the context of ovarian cancer, and could prove beneficial for both germline and somatic mutations. BRCA information should become more readily available as treatment with olaparib has recently been expanded to include use in combination with bevacizumab for maintenance of patients with high-grade epithelial ovarian, fallopian tube, or peritoneal cancer who responded to platinum-based chemotherapy combined with bevacizumab, and whose cancer was defined by BRCA1/2 mutation and/or genomic instability (European Society for Medical Oncology, 17 September 2020).

Future work will also include validation studies of data regarding the genes and pathways affected by platelet-cancer cell interactions obtained via RNA-Seq. As previously mention in chapter 5, the BC patient CTC study is currently being expanded to include ovarian cancer patients, and this will examine any correlation between CTCs and plasma PAI-1 in ovarian cancer patients. In light of findings in patient cohorts which revealed that plasma PAI-1 is significantly affected by neoadjuvant chemotherapy, consideration of PAI-1 as a marker of treatment management should be considered. Additionally, future research should include a closer investigation of the non-coding regions within the SERPIN E1 gene, which may play a role in alternative splicing, or could contain important markers such as SNPs or microsatellites (STRs). This type of genetic fingerprinting may be useful in identifying those patients who may become platinum-resistant, as well as those who might potentially benefit from therapy with a PAI-1 small-molecule inhibitor in

addition to treatment with chemotherapy and PARP-inhibitors.

Recently, a study of chronic myeloid leukaemia (CML) and leukaemic stem cells (LSCs) involving the selective targeting of PAI-1 with the small molecule inhibitors TM5275, TM5509 and TM5614 was performed (Yahata *et al*, 2021). TM5614 is also currently in phase 1 and 2 clinical trials for the treatment of Covid-19 (Sillen and Declerck 2021; ClinicalTrials.gov:NCT04634799). Selectively blocking PAI-1 was found to increase the susceptibility of CML-LSCs to the tyrosine-kinase inhibitor (TKI) imatinib in a murine model (Yahata *et al*, 2021) . This led to the eradication of CML-LSCs in the bone marrow and sustained remission without interference in other serine protease systems, whereas TGF-ß-induced intracellular PAI-1 (iPAI-1) was found to have a protective effect on CML-LSCs. (Yahata *et al*, 2021). This is an important study that places emphasis on the potential of PAI-1 as a cancer treatment target, particularly in combination with other therapies. Coupled with genetic fingerprinting for appropriately-tailored dosage concentrations, this could have massive implications for the treatment of many cancer types, including EOC.

REFERENCES

1. Adler, Amanda I., Noel S. Weiss, Mary L. Kamb, and Joseph L. Lyon. "Is diabetes mellitus a risk factor for ovarian cancer? A case-control study in Utah and Washington (United States)." Cancer Causes and Control. 1996.

2. Aissani, B, A K Boehme, H W Wiener, S Shrestha, L P Jacobson and R A Kaslow. "SNP screening of central MHC-identified HLA-DMB as a candidate susceptibility gene for HIV-related Kaposi's sarcoma." Genes and Immunity. Volume 15, pp424–429. 2014.

3. Aldoss, Ibrahim T., Sue Wilson, and Peter T. Silberstein. "Chemotherapy-induced Anaemia." Asia-Pacific Oncology & Haematology. 2008.

4. Alexander, N.I. "Reference Values of Neutrophil-Lymphocyte Ratio, Platelet-Lymphocyte Ratio and Mean Platelet Volume in Healthy Adults in North Central Nigeria." Journal of Blood and Lymph. 2016.

5. Anderson JP, Ross JA, and Folsom AR. "Anthropometric variables, physical activity, and incidence of ovarian cancer: the Iowa Women's Health Study. " Cancer. 2004.

6. Antoniou, A, P D P Pharoah, S Narod, H A Risch, J E Eyfjord, J L Hopper, N Loman, H Olsson, O Johannsson, A Borg, B Pasini, P Radice, S Manoukian, D M Eccles, N Tang, E Olah, H Anton-Culver, E Warner, J Lubinski, J Gronwald, B Gorski, H Tulinius, S Thorlacius, H Eerola, H Nevanlinna, K Syrjäkoski, O-P Kallioniemi, D Thompson, C Evans, J Peto, F Lalloo, D G Evans, and D F Easton. "Average risks of breast and ovarian cancer associated with BRCA1 or BRCA2 mutations detected in case Series unselected for family history: a combined analysis of 22 studies." American Journal of Human Genetics. 2003.

7. Applied Biosystems. "Real-time PCR: understanding C_t." 2016.

8. Asher, V. J. Lee, and A. Bali. "Preoperative serum albumin is an independent prognostic predictor of survival in ovarian cancer." Medical Oncology. 2011.

9. Åstedt, Birger. "Adjuvant treatment of ovarian carcinoma with tranexamic acid." Journal of Clinical Pathology. 1980.

10. Aune, Guro, Astrid Kamilla Stunes, Aina-Mari Lian, Janne Elin Reseland, Solveig Tingulstad, Sverre H. Torp, and Unni Syversen. "Circulating interleukin-8 and plasminogen activator inhibitor-1 are increased in women with ovarian carcinoma." Results in Immunology. 2012.

11. Bal, Oznur, Ahmet Siyar Ekinci, Mutlu Dogan, Cigdem Atay, Ayse Demirci, Berna Oksuzoglu, and Selim Kilic. "The prognostic and predictive significance of plasma type 1 plasminogen activator inhibitor and endoglin in metastatic colorectal cancer patients treated with bevacizumab-containing chemotherapy." Journal of Cancer Research and Therapeutics. 2019.

12. Balsara, Rashna D., and Victoria A. Ploplis. "Plasminogen Activator Inhibitor-1: The Double-Edged Sword in Apoptosis." Thrombosis and Haemostasis. 100(6): 1029-1036. 2008.

13. Barriere, Guislane, Pietro Fici, Giulia Gallerani, Francesco Fabbri, Wainer Zoli, and Michel Rigaud. "Circulating tumor cells and epithelial, mesenchymal and stemness markers: characterization of cell subpopulations." Annals of Translational Medicine. 2014.

14. Bashizadeh-Fakhar, Haniyeh, Mostafa Rezaie-Tavirani,1, Hakimeh Zali, Roya Faraji, Ehsan Kazem Nejad, and Mohamadhossein Aghazadeh. "The Diagnostic Value of Serum CEA, CA-125, and ROMA Index in Low-Grade Serous Ovarian Cancer." International Journal of Cancer Management. 2018.

15. Bast, Robert, Maryellen Feeney, Herbert Lazarus, Lee M. Nadler, Robert B. Colvin, and Robert C. Knapp. "Reactivity of a Monoclonal Antibody with Human Ovarian Carcinoma." Journal of Clinical Investigation. Vol.68, pp 1331-1337. 1981.

16. BD Biosciences 2350 Qume Drive San Jose, CA. "Introduction to Flow Cytometry: A Learning Guide". Manual Part Number: 11-11032-01. April, 2000. (retrieved from http://www.stemcell.umn.edu/prod/groups/med/@pub/@med/docu

ments/asset/med_80691.pdf)

17. Bentov, Yaakov, Theodore J. Brown, Mohammad R. Akbari, Robert Royer, Harvey Risch, Barry Rosen, John McLaughlin, Ping Sun, Shiyu Zhang, Steven A. Narod, and Robert F. Casper." Polymorphic Variation of Genes in the Fibrinolytic System and the Risk of Ovarian Cancer." PLoS ONE. 2009.

18. Berek, Jonathan S., Sean T. Kehoe, Lalit Kumar, and Michael Friedlander, "Cancer of the ovary, fallopian tube, and peritoneum." International Journal of Gynecology & Obstetrics. John T. Wiley and Sons, Ltd. on behalf of the International Federation of Gynecology and Obstetrics. 2018.

19. Bernard, Pascal, Alice Fleming, Arnaud Lacomb, Vincent R. Harley and Eric Vilain. "Wnt4 inhibits β-catenin/TCF signalling by redirecting β-catenin to the cell membrane." Biology of the Cell. 2008.

20. Bhatla, Neerja and Lynette Denny."FIGO Cancer Report 2018." International Journal of Gynecology and Obstetrics. 2018.

21. Binaschi, Monica, Franco Zunino and Giovanni Capranico. "Mechanism of action of DNA topoisomerase inhibitors." Stem Cells Journal. 1995.

22. Biskind, MS and Biskind, GR. "Development of tumors in the rat ovary after transplantation into the spleen." Proceedings of the Society for Experimental Biology and Medicine. Society for Experimental Biology and Medicine 55176–179. (doi:10.3181/00379727-55-14507). 1944.

23. Bleaken, Brigid M., A. Sue Menko, and Janice L.Walker. "Cells activated for wound repair have the potential to direct collective invasion of an epithelium."Molecular Biology of the Cell. 2016.

24. Bolitho, Christine, Michael A Hahn, Robert C Baxter and Deborah J Marsh. "The chemokine CXCL1 induces proliferation in epithelial ovarian cancer cells by transactivation of the epidermal growth factor receptor." Endocrine-Related Cancer. 2010.

25. Booth, N A, A J Simpson, A Croll, B Bennett, and I R MacGregor. "Plasminogen activator inhibitor (PAI-1) in plasma and platelets."

British Journal of Haematology. 1988.

26. Bosma, Piter J., Eva A. van den Berg, Teake Kooistra, David R. Siemieniak, and Jerry L. Slighton. "Human Plasminogen Activator Inhibitor-1 Gene." The Journal of Biological Chemistry. The American Society for Biochemistry and Molecular Biology. 1988.

27. Boss, EA, LFAG Massuger, CMG Thomas, A Geurts-Moespot, JHM van Schaik, H Boonstra, and CGJ Sweep. "Clinical value of components of the plasminogen activation system in ovarian cyst fluid." Anticancer Research. 2002.

28. Bottoni, Patrizia and Roberto Scatena. "The Role of CA 125 as Tumor Marker: Biochemical and Clinical Aspects." *Advances in Cancer Biomarkers*, Advances in Experimental Medicine and Biology. 2015.

29. Bowtell, David D, Steffen Böhm, Ahmed A Ahmed, Paul-Joseph Aspuria, Robert C Bast Jr, Valerie Beral, Jonathan S Berek, Michael J Birrer, Sarah Blagden, Michael A Bookman, James D Brenton, Katherine B Chiappinelli, Filipe Correia Martins, George Coukos, Ronny Drapkin, Richard Edmondson, Christina Fotopoulou, Hani Gabra, Jérôme Galon, Charlie Gourley, Valerie Heong, David G Huntsman, Marcin Iwanicki, Beth Y Karlan, Allyson Kaye, Ernst Lengyel, Douglas A Levine, Karen H Lu, Iain A McNeish, Usha Menon, Steven A Narod, Brad H Nelson, Kenneth P Nephew, Paul Pharoah, Daniel J Powell Jr, Pilar Ramos, Iris L Romero, Clare L Scott, Anil K Sood, Euan A Stronach, and Frances R Balkwill. "Rethinking Ovarian Cancer II: Reducing Mortality from High-Grade Serous Ovarian Cancer." Nature Reviews Cancer. 2015.

30. Brogren, Helén, Lena Karlsson, Maria Andersson, Lingwei Wang, David Erlinge and Sverker Jern. "Platelets synthesize large amounts of active plasminogen activator inhibitor 1." Blood. 2004.

31. Brogren, Helén, Karin Wallmark, Johanna Deinum, Lena Karlsson, and Sverker Jern. "Platelets Retain High Levels of Active Plasminogen Activator Inhibitor 1." PLOS One. 2011.

32. Browning, Landon, Megha R Patel, Eli Bring Horvath, Ken Tawara, and Cheryl L Jorcyk. "IL-6 and ovarian cancer: inflammatory cytokines in

promotion of metastasis." Cancer Management and Research. 2018.

33. Bryer, Emily and David Henry. "Chemotherapy-induced anemia: etiology, pathophysiology, and implications for contemporary practice." International Journal of Clinical Transfusion Medicine. 2018.

34. Bourguignon, Lilly Y. W., Hongbo Zhu, Arthur Chu, Naoko Iida, Lisha Zhang, and Mien-Chie Hung. "Interaction between the Adhesion Receptor, CD44, and the Oncogene Product, p185HER2, promotes Human Ovarian Tumor Cell Activation." The Journal of Biological Chemistry. Vol. 272, No. 44, Issue of October 31, pp. 27913–27918. 1997.

35. Bydoun, Maomen, Andra Sterea, Ian C. G. Weaver, Alamelu G. Bharadwaj and David M. Waisman. "A novel mechanism of plasminogen activation in epithelial and mesenchymal cells." Scientific Reports. 2018.

36. Callahan, Michael J., Zoltan Nagymanyoki, Tomas Bonome, Michael E. Johnson, Babak Litkouhi, Elizabeth H. Sullivan, Michelle S. Hirsch, Ursula A. Matulonis, Joyce Liu, Michael J. Birrer, Ross S. Berkowitz and Samuel C. Mok. "Increased HLA-DMB Expression in the Tumor Epithelium Is Associated with Increased CTL Infiltration and Improved Prognosis in Advanced-Stage Serous Ovarian Cancer." Human Cancer Biology. 2008.

37. Campos, Susana M. and Sue Ghosh. "A Current Review of Targeted Therapeutics for Ovarian Cancer." Journal of Oncology. 2010.

38. Cannistra, Stephen A., Geoffrey S. Kansas, Jonathan Niloff, Brenda DeFranzo, Young Kim, and Christian Ottensmeier. "Binding of Ovarian Cancer Cells to Peritoneal Mesothelium in Vitro Is Partly Mediated by CD44H." Cancer Research. 1993.

39. Cao, Chunzhang, Daniel A. Lawrence, Yang Li, Christine AF Von Arnim, Joachim Herz, Enming J Su, Alexandra Makarova, Bradley T. Hyman, Dudley K. Strickland, and Li Zhang. "Endocytic receptor LRP together with tPA and PAI-1 coordinates Mac-1-dependent macrophage migration." The EMBO Journal. 2006.

40. Casslén, B., T. Bossmar, I. Lecander, and B. Åstedt. "Plasminogen Activators and Plasminogen Activator Inhibitors in Blood and Tumour Fluids of Patients with Ovarian Cancer." European Journal of Cancer.

Vol.30A, No.9, pp.1302-1309. 1994.

41. Caunt, Maresa, Judy Mak, Wei-Ching Liang, Scott Stawicki, Qi Pan, Raymond K. Tong, Joe Kowalski, Calvin Ho, Hani Bou Reslan, Jed Ross, Leanne Berry, Ian Kasman, Constance Zlot, Zhiyong Cheng, Jennifer Le Couter, Ellen H. Filvaroff, Greg Plowman, Franklin Peale, Dorothy French, Richard Carano, Alexander W. Koch, Yan Wu, Ryan J. Watts, Marc Tessier-Lavigne and Anil Bagri1. "Blocking Neuropilin-2 Function Inhibits Tumor Cell Metastasis." Cancer Cell. 2008.

42. Chambers SK, Ivins CM, and Carcangiu ML. "Plasminogen activator inhibitor-1 is an independent poor prognostic factor for survival in advanced stage epithelial ovarian cancer patients." International Journal of Cancer. 79(5):449-54. October 23, 1998.

43. Chapin, John C. and Katherine A. Hajjar. "Fibrinolysis and the control of blood coagulation." Blood Reviews. 2015.

44. Chaudhry, Raheel and Hani M. Babiker. "Physiology, Coagulation Pathways." StatPearls Publishing, Treasure Island (FL). 2020.

45. Chornokur ,Ganna, Ernest K. Amankwaha, Joellen M. Schildkrautc, and Catherine M. Phelana. "Global ovarian cancer health disparities." Gynecology Oncology. 2013 April; 129(1): 258–264.doi: 10.1016/j.ygyno.2012.12.016.

46. Clancy, Lauren, Lea M. Beaulieu, Kahraman Tanriverdi, and Jane E. Freedman. "The role of RNA uptake in platelet heterogeneity." Thrombosis and Haemostasis. 2017.

47. Cloonan, N., A.R. Forrest, G. Kolle, B.B. Gardiner, G.J. Faulkne, M.K. Brown, D.F. Taylor, A.L. Steptoe, S. Wani, G. Bethel, A.J. Robertson, A.C. Perkins, S.J. Bruce, C.C. Lee, S.S. Ranade, H.E. Peckham, J.M. Manning, K.J. McKernan, and S.M. Grimmond. "Stem cell transcriptome profiling via massive-scale mRNA sequencing." Nature Methods. Jul;5(7):613-9. 2008.

48. Cluxton, Christopher D., Cathy Spillane, Sharon A. O'Toole, Orla Sheils, Clair M. Gardiner, and John J. O'Leary. "Suppression of Natural Killer cell NKG2D and CD226 anti-tumour cascades by platelet cloaked cancer cells: Implications for the metastatic cascade." PLOS One. 2019.

49. Cohen, Marie and Patrick Petignat. "The bright side of ascites in ovarian cancer." Cell Cycle. 2014.

50. Connor, Joseph P., Andrea O'Shea, Kevin McCool, Emmanuel Sampene, and Lisa M. Barroilhet. "Peri-operative allogeneic blood transfusion is associated with poor overall survival in advanced epithelial ovarian Cancer; potential impact of patient blood management on Cancer outcomes." Gynecologic Oncology. 2018.

51. Cooke, Niamh M., Karl Egan, Siobhan McFadden, Liam Grogan, Oscar S Breathnach, John O'Leary, Bryan T Hennessy, and Dermot Kenny. "Increased platelet reactivity in patients with late-stage metastatic cancer." Cancer Medicine. 2013.

52. Cooke, Niamh M., Cathy D. Spillane, Orla Sheils, John O'Leary, and Dermot Kenney. "Aspirin and $P2Y_{12}$ inhibition attenuate platelet-induced ovarian cancer cell invasion." BioMed Central Cancer. 2015.

53. Cooley, Brian C., Jose Nevado, Jason Meliad, Dan Yang, Cynthia St. Hilaire, Alejandro Negro, Fang Fang, Guibin Chen, Hong San, Avram D. Walts, Robin L. Schwartzbeck, Brandi Taylor, Jan D. Lanzer, Andrew Wragg, Abdalla Elagha, Leilani E. Beltran, Colin Berry, Robert Feil, Renu Virmani, Elena Ladich, Jason C. Kovacic, and Manfred Boehm. "TGF-β Signaling mediates endothelial to mesenchymal transition (EndMT) during vein graft remodeling." Science Translational Medicine. 2014.

54. Couch, Fergus J., Steven N. Hart, Priyanka Sharma, Amanda Ewart Toland, Xianshu Wang, Penelope Miron, Janet E. Olson, Andrew K. Godwin, V. Shane Pankratz, Curtis Olswold, Seth Slettedahl, Emily Hallberg, Lucia Guidugli, Jaime I. Davila, Matthias W. Beckmann, Wolfgang Janni, Brigitte Rack, Arif B. Ekici, Dennis J. Slamon, Irene Konstantopoulou, Florentia Fostira, Athanassios Vratimos, George Fountzilas, Liisa M. Pelttari, William J. Tapper, Lorraine Durcan, Simon S. Cross, Robert Pilarski, Charles L. Shapiro, Jennifer Klemp, Song Yao, Judy Garber, Angela Cox, Hiltrud Brauch, Christine Ambrosone, Heli Nevanlinna, Drakoulis Yannoukakos, Susan L. Slager, Celine M. Vachon, Diana M. Eccles, and Peter A. Fasching. "Inherited Mutations in 17 Breast Cancer Susceptibility Genes Among a Large Triple-Negative Breast Cancer Cohort Unselected for Family History of Breast Cancer."

Journal of Clinical Oncology. 2015.

55. Cristofanilli, Massimo, G. Thomas Budd, Matthew J. Ellis, Alison Stopeck, Jeri Matera, M. Craig Miller, James M. Reuben, Gerald V. Doyle, W. Jeffrey Allard, Leon W.M.M. Terstappen, and Daniel F. Hayes. "Circulating Tumor Cells, Disease Progression, and Survival in Metastatic Breast Cancer." The New England Journal of Medicine. 2004.

56. Czekay, Ralf-Peter, Cynthia Wilkins-Port, Stephen P.Higgins, Jennifer Freytag, Jessica M. Overstreet, R. Matthew Klein, Craig E. Higgins, Rohan Samarakoon, and Paul J. Higgins. "PAI-1: An Integrator of Cell Signaling and Migration." International Journal of Cell Biology. 2011.

57. Dal Maso L, Franceschi S, Negri E, et al. "Body size indices at different ages and epithelial ovarian cancer risk. " Eur J Cancer 2002; 38:1769 – 74.

58. Dasari, Shaloam and Paul Bernard Tchounwou. "Cisplatin in cancer therapy: molecular mechanisms of action." European Journal of Pharmacology. 2014.

59. Davis, Alison, Anna V Tinker, and Michael Friedlander. " "Platinum resistant" ovarian cancer: what is it, who to treat and how to measure benefit?" Gynecological Oncology. 2014.

60. Dawson, Sally, Anders Hamsten, Bjorn Wiman, Adriano Henney, and Steve Humphries. "Genetic Variation at the Plasminogen Activator Inhibitor-1 Locus Is Associated With Altered Levels of Plasma Plasminogen Activator Inhibitor-1 Activity." Arteriosclerosis and Thrombosis. 1991.

61. Declerck, P J, M C Alessi, M Verstreken, E K Kruithof, I Juhan-Vague, and D Collen. "Measurement of plasminogen activator inhibitor 1 in biologic fluids with a murine monoclonal antibody-based enzyme-linked immunosorbent assay." Blood. 1988.

62. Declerck, Paul J., Maria De Mol, Douglas E. Vaughan, and Desire Collen. "Identifcation of a Conformationally Distinct Form of Plasminogen Activator Inhibitor-1, Acting as a Non-inhibitory Substrate for Tissue-type Plasminogen Activator." The Journal of Biological Chemistry. Vol.

267, No. 17, pp11693-11696. 1992.

63. Degryse, Bernard, Jaap G. Neels, Ralf-Peter Czekay, Kathleen Aertgeerts, Yu-ichi Kamikubo, and David J. Loskutoffs. "The Low-Density Lipoprotein Receptor-related Protein is a Motogenic Receptor for Plasminogen Activator Inhibitor-1." The Journal of Biological Chemistry. The American Society for Biochemistry and Molecular Biology. 2004.

64. Deng, Gary, Scott A. Curriden, Geng Hu, Ralf-Peter Czekay, and David J. Lokutoff. "Plasminogen Activator Inhibitor -1 Regulates Cell Adhesion by Binding to the Somatomedin B Domain of Vitronection." Journal of Cellular Physiology. 2001.

65. Deng, Kui, Chunyan Yang, QilongTan, Wei Song, Mingliang Lu, Weiwei Zhao, Ge Lou, Zhenzi Li, Kang Li, and Yan Hou. "Sites of distant metastases and overall survival in ovarian cancer: A study of 1481 patients." Gynecologic Oncology. 2018.

66. Dennler, Sylviane, Susumu Ito, Denis Vivien, Peter ten Dijke, Stéphane Huet, and Jean-Michel Gauthier. "Direct binding of Smad3 and Smad4 to critical TGFß-inducible elements in the promoter of human plasminogen activator inhibitor-type 1 gene." The EMBO Journal. Vol.17, No.11, pp3091-3100. 1998.

67. Denny, Lynette, "Staging of ovarian cancer: time to subdivide more?" Journal of Gynecological Oncology. 2013.

68. Ding, L-W, Q-Y Sun, D-C Lin, W Chien, N Hattori, X-M Dong, S Gery, M Garg, N B Doan, J W Said, J-F Xiao, H Yang, L-Z Liu, X Meng, R Y-J Huang, K Tang and H P Koeffler. "LNK (SH2B3): paradoxical effects in ovarian cancer." Oncogene. 2015.

69. Dorn, J., N. Harbeck, R. Kates, A. Gkazepis, A. Scorilas, A. Soosaipillai, E. Diamandis, M. Kiechle, B. Schmalfeldt, and M. Schmitt. "Impact of expression differences of kallikrein-related peptidases and of uPA and PAI-1 between primary tumor and omentum metastasis in advanced ovarian cancer." Original Articles Gynecologic Tumors. 2011.

70. Dvorak, Harold F. "Tumors: wounds that do not heal. Similarities between tumor stroma generation and wound healing." The New England Journal of Medicine. 1986.

71. Ebisch, Inge M.W., Chris M. G. Thomas, Alex M. M. Wetzels, Wim N. P. Willemsen, Fred C. G. J. Sweep, and Regine P. M. Steegers-Theunissen.

"Review of the role of the plasminogen activator system and vascular endothelial growth factor in subfertility." Fertility and Sterility. Volume 90, Issue 6, Pages 2340–2350. December 2008.

72. Egan, Karl, Darragh Crowley, Paul Smyth, Sharon O'Toole, Cathy Spillane, Cara Martin, Michael Gallagher, Aoife Canney, Lucy Norris, Niamh Conlon, Lynda McEvoy, Brendan Ffrench, Britta Stordal, Helen Keegan, Stephen Finn, Victoria McEneaney, Alex Laios, Jens Ducrée, Eimear Dunne, Leila Smith, Michael Berndt, Orla Sheils, Dermot Kenny, and John O'Leary. "Platelet Adhesion and Degranulation induce Pro-survival and Pro-angiogenic Signaling in Ovarian Cancer Cells." PLOS One. 2011.

73. Egan, Karl, Niamh Cooke, and Dermot Kenney. "Living in shear: platelets protect cancer cells from shear induced damage." Clinical and Experimental Metastasis. 2014. "

74. Elies, A, Rivière S, Pouget N, Becette V, Dubot C, Donnadieu A, Rouzier R, and Bonneau C. "The role of neoadjuvant chemotherapy in ovarian cancer." Expert Review of Anticancer Therapies. 2018.

75. Elices, Mariano J., Laurelee Osborn, Yoshikazu Takada, Carol Grouse, Stefan Luhowskyj, Martin E. Hemler, and Roy R. Lobb. "VCAM-1 on Activated Endothelium Interacts with the Leukocyte lntegrin VLA-4 at a Site Distinct fromthe VLA-4/Fibronectin Binding Site." Cell. 1990.

76. Erlich, Hartmut J., Raymond Klein Gebbink, Klaus T. Preissner, Jaap Keijer, Naomi L. Esmon, Koen Mertens, and Hans Pannekoek. "Thrombin Neutralizes Plasminogen Activator Inhibitor 1(PAI-1) that is Complexed with Vitronectin in the Endothelial Cell Matrix." Journal of Cell Biology. The Rockefeller University Press. 1991.

77. Fairfield, KM, WC Willett, BA Rosner, JE Manson, FE Speizer, and SE Hankinson. "Obesity, weight gain, and ovarian cancer. " Obstet Gynecol 2002;100:288 – 96.

78. Fang, Tianyi, Yimin Wang, Xin Yin, Zhao Zhai, Yu Zhang, Yongheng Yang, Qi You, Zhiguo Li, Yan Ma, Chunfeng Li, Haibin Song, Huawen Shi, Yongle Zhang, Xuefeng Yu, Hongyu Gao, Yihua Sun, Rui Xie, and Yingwei Xue. "Diagnostic Sensitivity of NLR and PLR in Early Diagnosis

of Gastric Cancer." Journal of Immunology Research. 2020.

79. Fathalla, M.F. "Incessant Ovulation – A Factor in Ovarian Neoplasia?" The Lancet. 17 July, 1971.

80. Fay, William P., Amy D. Shapiro, Judy L. Shih, Raymond R. Schleef, and David Ginsburg. "Complete Deficiency of Plasminogen-Activator Inhibitor Type 1 Due to a Frame-Shift Mutation." The New England Journal of Medicine. 1992.

81. Ferroni, Patrizia, Mario Roselli, Ilaria Portarena, Vincenzo Formica, SSilvia Riondino, Francesca La Farina, Leopoldo Costarelli, Antonio Melino, Gioia Massimiani, Francesco Cavaliere, Raffaele Palmirotta, and Fiorella Guadagni. "Plasma Plasminogen Activator Inhibitor-1 (PAI-1) Levels in Breast Cancer – Relationship with Clinical Outcome." Anticancer Research. 2014.

82. Fest, Jesse, Rikje Ruiter, M. Arfan Ikram, Trudy Voortman, Casper H. J. van Eijck and Bruno H. Stricker. "Reference values for white blood cell-based inflammatory markers in the Rotterdam Study: a population based prospective cohort study." Scientific Reports. 2018.

83. French, Sarah L., Martha L. Sikes, Robert D. Hontz, Yvonne N. Osheim, Tashima E. Lambert, Aziz El Hage, Mitchell M. Smith, David Tollervey, Jeffrey S. Smith, and Ann L. Beyer. "Distinguishing the Roles of Topoisomerases I and II in Relief of Transcription-Induced Torsional Stress in Yeast rRNA Genes." Molecular and Cellular Biology. 2011.

84. Fridlender, Ziv.G., Jing Sun, Samuel Kim, Veena Kapoor, Guanjun Cheng, Leona Ling, G. Scott Worthen, and Steven M. Albelda. "Polarization of Tumor-Associated Neutrophil (TAN) Phenotyped by TGF-ß: "N1" versus "N2" TAN." Cancer Cell. 2009.

85. Fridlender, Zvi G., Jing Sun, Inbal Mishalian, Sunil Singhal, Guanjun Cheng, Veena Kapoor, Wenhwai Horng, Gil Fridlender, Rachel Bayuh, G. Scott Worthen, and Steven M. Albelda. "Transcriptomic Analysis Comparing Tumor-Associated Neutrophils with Granulocytic Myeloid-Derived Suppressor Cells and Normal Neutrophils." PLos ONE. 2012.

86. Fields, Emma C., William P. McGuire, Lilie Lin, and Sarah M. Temkin. "Radiation Treatment in Women with Ovarian Cancer: Past, Present, and Future." Frontiers in Oncology. 2017.

87. Ge, Lili, Guangquan Liu, Kai Hu, Ke Huang, Mi Zhang, Juan Zhou, Fang Teng, Jian Cao, Chencheng Dai, and Xuemei Jia. "A New Risk Index

combining D-Dimer, Fibrinogen, HE4, and CA199 differentiates Suspecting Endometrial Cancer from Patients with Abnormal Vaginal Bleeding or Discharge." Technology in Cancer Research and Treatment. 2020.

88. Ge SX, Son EW, and Yao R. "iDEP: an integrated web application for differential expression and pathway analysis of RNA-Seq data." BMC Bioinformatics. 2018.

89. Ge, Steven Xijin, Dongmin Jung and Runan Yao. "ShinyGO: a graphical gene-set enrichment tool for animals and plants." Bioinformatics. Volume 36, Issue 8. pp 2628–2629. 15 April 2020.

90. George, Angela, Jennifer McLachlan, Nina Tunariu, Chiara Della Pepa, Cristina Migali, Martin Gore, Stan Kaye, and Susana Banerjee. "The role of hormonal therapy in patients with relapsed high-grade ovarian carcinoma: a retrospective series of tamoxifen and letrozole." BMC Cancer. 2017.

91. Geis, Theresa, Claudia Döring, Rüdiger Popp, Nina Grossmann, Ingrid Fleming, Martin-Leo Hansmann, Nathalie Dehne and Bernhard Brüne. "HIF-2alpha-dependent PAI-1 induction contributes to angiogenesis in hepatocellular carcinoma." Experimental Cell Research. Vol 331, pp46-57. 2015.

92. Giacoia, Evan Gomes, Makito Miyake, Adrienne Lawton, Steve Goodison, and Charles J. Rosser. "PAI-1 Leads to G1-phase Cell Cycle Progression through Cyclin D3/DK4/6 Up-regulation." Molecular Cancer Research. 2014.

93. Grada, Ayman, Marta Otero-Vinas, Francisco Prieto-Castrillo, Zaidal Obagi, and Vincent Falanga. "Research Techniques Made Simple: Analysis of Collective Cell Migration Using the Wound Healing Assay." Journal of Investigative Dermatology. 2016.

94. Grandclement, Camille, Jean René Pallandre, Séverine Valmary Degano, Erika Viel, Adeline Bouard, Jérémy Balland, Jean-Paul Rémy-Martin, Benoit Simon, Alain Rouleau,Wilfrid Boireau, Michael Klagsbrun, Christophe Ferrand and Christophe Borg. "Neuropilin-2 Expression Promotes TGF-β1-Mediated Epithelial to Mesenchymal Transition in Colorectal Cancer Cells." PLOS ONE. 2011.

95. Guastalla, J.P., D. Allouache, M. Combe, B. Weber, J. Cretin, H. Curé, M. Mousseau, D. Paraiso, S. Camilleri-Broët, and E. Pujade-Lauraine. "

HER2 overexpression and amplification in advanced ovarian cancer (AOC): Treatment with trastuzumab—A GINECO study." Journal of Clinical Oncology. 2007.

96. Guo, Yi, Wei Cui, Yuqing Pei, and Danfei Xu. "Platelets promote invasion and induce epithelial to mesenchymal transition in ovarian cancer cells by TGF-β signaling pathway." Gynecologic Oncology. 2019.

97. Handa, A, T Tokunaga, T Tsuchida, Y H Lee, H Kijima, H Yamazaki, Y Ueyama, H Fukuda and M Nakamura. "Neuropilin-2 expression affects the increased vascularization and is a prognostic factor in osteosarcoma." International Journal of Oncology. 2000.

98. Hefler-Frischmuth, Katrin, Judith Lafleur, Lukas Hefler, Stephan Polterauer, Veronika Seebacher, Alexander Reinthaller, and Christoph Grimm. "Plasma fibrinogen levels in patients with benign and malignant ovarian tumors." Gynecologic Oncology. 2015.

99. Hempel, George. "Handbook of Analytical Separations." Drug Monitoring and Clinical Chemistry. Vol.5, pp 1-360. 2004.

100. Higashi M, Kajiyama H, Shibata K, Mizuno M, Mizuno K, Hosono S, Kawai M, Nakanishi T, Nagasaka T, and Kikkawa F. "Survival impact of capsule rupture in stage I clear cell carcinoma of the ovary in comparison with other histological types." Gynecologic Oncology. 2011.

101. Hildenbrand, Ralf, Antonela Schaaf, Alexandra Dorn-Beineke, Heike Allgayer, Marc Sütterlin, Alexander Marx, and Philipp Stroebel. "Tumor stroma is the predominant uPA-, uPAR-, PAI-1-expressing tissue in human breast cancer: prognostic impact." Cellular and Molecular Biology. 2009.

102. Hirahara, Tetsushi, Takaaki Arigami, Shigehiro Yanagita, Daisuke Matsushita, Yasuto Uchikado,Yoshiaki Kita, Shinichiro Mori, Ken Sasaki, Itaru Omoto, Hiroshi Kurahara, Kosei Maemura, Keishi Okubo, Yoshikazu Uenosono, Sumiya Ishigami and Shoji Natsugoe. "Combined neutrophil-lymphocyte ratio and platelet-lymphocyte ratio predicts chemotherapy response and prognosis in patients with advanced gastric

cancer." BMC Cancer. 2019.

103. Ho, Chao-Hung, Chiou-Chung Yuan, and Shian-Min Liu. "Diagnostic and Prognostic Values of Plasma Levels of Fibrinolytic Markers in Ovarian Cancer." Gynecologic Oncology. 75, 397–400 (1999).

104. Horwitz, SB. "Taxol (paclitaxel): mechanisms of action." Annals of Oncology. 1994.

105. Hu, Hanqing, Meng Wang, Hongwei Wang, Zheng Liu, Xu Guan, Runkun Yang, Rui Huang, Qingchao Tang, Chaoxia Zou, Guiyu Wang, Xu Gao, and Xishan Wang. "MEGF6 Promotes the Epithelial-to-Mesenchymal Transition via the TGFβ/SMAD Signaling Pathway in Colorectal Cancer Metastasis." Cellular Physiology and Biochemistry. 2018.

106. Hu, Rong, Leena Hilakivi-Clarke, and Robert Clarke. "Molecular mechanisms of tamoxifen-associated endometrial cancer (Review)." Oncology Letters. 2015.

107. Humphries, Brock A., Johanna M. Buschhaus, Yu-Chih Chen, Henry R. Haley, Tonela Qyli, Benjamin Chiang, Nathan Shen, Shrila Rajendran, Alyssa Cutter, Yu-Heng Cheng, Yu-Ting Chen, Jason Cong, Phillip C. Spinosa, Euisik Yoon, Kathryn E. Luker and Gary D. Luker. "Plasminogen Activator Inhibitor 1 (PAI1) Promotes Actin Cytoskeleton Reorganization and Glycolytic Metabolism in Triple-Negative Breast Cancer." Molecular Cancer Research. 2019.

108. Hwang, Inkyu and Nguyet Nguyen. "Mechanisms of tumor-induced T cell immune suppression and therapeutics to counter those effects." Archives of Pharmacological Research. 2015.

109. Iacoviello, Licia, Claudia Agnoli, Amalia De Curtis, Augusto di Castelnuovo, Maria Concetta Giurdanella, Vittorio Krogh, Amalia Mattiello, Giuseppe Matullo, Carlotta Sacerdote, Rosario Tumino, Paolo Vineis, Giovanni de Gaetano, Salvatore Panico, and Maria Benedetta Donati. "Type 1 plasminogen activator inhibitor as a common risk factor for cancer and ischaemic vascular disease: the EPICOR study." BMJ Open. 2013.

110. Isogai C, Laug WE, Shimada H, Declerck PJ, Stins MF, Durden DL, Erdreich-Epstein A, DeClerck YA. "Plasminogen activator inhibitor-1 promotes angiogenesis by stimulating endothelial cell migration toward fibronectin." Cancer Research. 61(14):5587-94. July 15, 2001.

111. Iversen, Lisa, Shona Fielding, Øjvind Lidegaard, Lina S. Mørch, Charlotte W. Skovlund, and Philip C. Hannaford. "Association between contemporary hormonal contraception and ovarian cancer in women of reproductive age in Denmark: prospective, nationwide cohort study." BMJ. 2018.

112. Jacobs, Ian J, Usha Menon, Andy Ryan, Aleksandra Gentry-Maharaj, Matthew Burnell, Jatinderpal K Kalsi, Nazar N Amso, Sophia Apostolidou, Elizabeth Benjamin, Derek Cruickshank, Danielle N Crump, Susan K Davies, Anne Dawnay, Stephen Dobbs, Gwendolen Fletcher, Jeremy Ford, Keith Godfrey, Richard Gunu, Mariam Habib, Rachel Hallett, Jonathan Herod, Howard Jenkins, Chloe Karpinskyj, Simon Leeson, Sara J Lewis, William R Liston, Alberto Lopes, Tim Mould, John Murdoch, David Oram, Dustin J Rabideau, Karina Reynolds, Ian Scott, Mourad W Seif, Aarti Sharma, Naveena Singh, Julie Taylor, Fiona Warburton, Martin Widschwendter, Karin Williamson, Robert Woolas, Lesley Fallowfield, Alistair J McGuire, Stuart Campbell, Mahesh Parmar, and Steven J Skates. "Ovarian cancer screening and mortality in the UK Collaborative Trial of Ovarian Cancer Screening (UKCTOCS): a randomised controlled trial." The Lancet. 2015.

113. Javadi, Sanaz, Dakshina M. Ganeshan, Aliya Qayyum, Ravathy B. Iyer, and Priya Bhosale. "Ovarian Cancer, the Revised FIGO Staging System, and the Role of Imaging." American Journal of Roentgenology. 2016.

114. Jeng, Jing-Ren. "Association of PAI-1 gene promoter 4g/5g polymorphism with plasma PAI-1 activity in Chinese patients with and without hypertension." American Journal of Hypertension. 2003.

115. Johnstone, Tinothy C., Ga Young Park, and Stephen J. Lippard. "Understanding and Improving Platinum Anticancer Drugs – Phenanthriplatin". Anticancer Research. 2014.

116. Kajiyama, H, K Shibata, M Mizuno, T Umezu, S Suzuki, A Nawa, M Kawai, T Nagasaka and F Kikkawa. "Long-term survival of young women receiving fertility-sparing surgery for ovarian cancer in comparison with those undergoing radical surgery." British Journal of Cancer. 2011.

117. Kalluri, R. and R.A. Weinberg. "The basics of epithelial-mesenchymal transition." Journal of Clinical Investigation. Vol.119, pp1420–1428. 2009.

118. Kalluri, R. and M. Zeisberg. "Fibroblasts in cancer." Nature Reviews Cancer. 2006.

119. Kim HS, Ahn JH, Chung HH, Kim JW, Park NH, Song YS, Lee HP, and Kim YB. "Impact of intraoperative rupture of the ovarian capsule on prognosis in patients with early-stage epithelial ovarian cancer: a meta-analysis." European Journal of Surgical Oncology. 2012.

120. Kim, Miseon, Dong Hoon Suh, Jin Young Choi, Jiyoon Bu , Yoon-Tae Kang, Kidong Kim, Jae Hong No, Yong Beom Kim, and Young-Ho Cho. "Post-debulking circulating tumor cell as a poor prognostic marker in advanced stage ovarian cancer." Medicine. 2019.

121. Kimura, Daisuke, Tadaatsu Imaizumi, Wakako Tamo, Takehiro Sakai, Kazuo Ito, Ryo Hatanaka, Hidemi Yoshida, Takao Tsushima, Kei Satoh, and Ikuo Fukuda. "Hypoxia enhances the expression of plasminogen activator inhibitor-1 in human lung cancer cells, EBC-1." The Tohoku Journal of Experimental Medicine. 2002.

122. Kirschbaum, M., G. Karimian, J. Adelmeijer, B. N. Giepmans, R. J. Porte, and T. Lisman. "Horizontal RNA transfer mediates platelet-induced hepatocyte proliferation." Blood. 2015.

123. Koensgen, D., A.Mustea, C. Denkert, P.M.Sun, W.Lichtenegger, and J. Sehouli. "Overexpression of the Plasminogen Activator Inhibitor Type-1 in Epithelial Ovarian Cancer." Anticancer Research. 2006.

124. Kramer, MD, Reinartz J, Brunner G, and Schirrmacher V. "Plasmin in pericellular proteolysis and cellular invasion." Invasion and Metastasis. 1994.

125. Kroeger, Paul T. Jr. and Ronny Drapkin. "Pathogenesis and heterogeneity of ovarian cancer". Current Opinion in Obstetrics & Gynecology. 2016.

126. Kubala, Marta Helena, and Yves Albert DeClerck. "The plasminogen activator inhibitor-1 paradox in cancer: a mechanistic understanding." Cancer and Metastasis Reviews. 2019.

127. Kuhn, W., B. Schmalfeldt, U. Reuning, L. Pache, U. Berger, K. Ulm, N. Harbeck, K. Späthe, P. Dettmar, H. Höfler, F. Jänicke, M. Schmitt, and H. Graeff. " Prognostic significance of urokinase (uPA) and its inhibitor PAI-1 for survival in advanced ovarian carcinoma stage FIGO IIIc." British Journal of Cancer. 1999.

128. Kunz, Christina, Stefanie Pebler, Jürgen Otte, and Dietmar von der Ahe. "Differential regulation of plasminogen activator inhibitor gene transcription by the tunor suppressor p53." Nucleic Acids Research. 1995.

129. Kwaan, Hau C. and Paul F. Lindholm. "Fibrin and Fibrinolysis in Cancer." Seminars in Thrombosis and Hemostasis.Vol 45, No.9, pp413-422. 2019.

130. Labelle, Myriam, Shahinoor Begum, and Richard O. Hynes. "Platelets guide the formation of early metastatic niches." PNAS. 2014.

131. Labelle, M, S. Begum, and R.O. Hynes. "Direct signaling between platelets and cancer cells induces an epithelial-mesenchymal-like transition and promotes metastasis." Cancer Cell. 2011.

132. Labidi-Galy, S Intidhar, Eniko Papp, Dorothy Hallberg, Noushin Niknafs, Vilmos Adleff, Michael Noe, Rohit Bhattacharya, Marian Novak, Siân Jones, Jillian Phallen, Carolyn A Hruban, Michelle S Hirsch, Douglas I Lin, Lauren Schwartz, Cecile L Maire, Jean-Christophe Tille, Michaela Bowden, Ayse Ayhan, Laura D Wood, Robert B Scharpf, Robert Kurman, Tian-Li Wang, Ie-Ming Shih, Rachel Karchin, Ronny Drapkin, and Victor E Velculescu. "High grade serous ovarian carcinomas originate in the fallopian tube." Nature Communications. 2017.

133. Lang, Irene M. and Raymond R. Schleef. "Calcium–dependent Stabilization of Type I Plasminogen Activator Inhibitor within Platelet α-Granules." The Journal of Biological Chemistry. The American Society for Biochemistry and Molecular Biology, Inc. 1995.

134. Law, Ruby H.P.,Tom Caradoc-Davies, Nathan Cowieson, Anita J. Horvath, Adam J. Quek, Joanna Amarante Encarnacao, David Steer, Angus Cowan, Qingwei Zhang, Bernadine G.C. Lu, Robert N. Pike, A. Ian Smith, Paul B. Coughlin, and James C. Whisstock. "The X-ray Crystal Structure of Full-Length Human Plasminogen. "Cell Reports. Volume 1, Issue 3, pp185-190, March 29, 2012.

135. Lee, Alice W. *et al*. "Evaluating the ovarian cancer gonadotropin hypothesis: A candidate gene study." Gynecologic Oncology. Vol. 136, Issue 3, pp 542-548. March 2015.

136. Lee, Chun-Chung and Tze-Sing Huang. "Plasminogen Activator Inhibitor-1: The Expression, Biological Functions, and Effects on Tumorigenesis and Tumor Cell Adhesion and Migration." Journal of

Cancer Molecules. 1(1):25-36. 2005.

137. Lee, Maria, Min Young Chang, Hanna Yoo, Kyung Eun Lee, Doo Byung Chay,Hanbyoul Cho, Sunghoon Kim, Young Tae Kim, and Jae-Hoon Kim. "Clinical Significance of CA125 Level after the First Cycle of Chemotherapy on Survival of Patients with Advanced Ovarian Cancer." Yonsei Medical Journal. 2016.

138. Lee, Tom V., Maya K. Sethi., Jessica Leonardi1., Nadia A. Rana, Falk F. R. Buettner, Robert S. Haltiwanger, Hans Bakker and Hamed Jafar-Nejad. "Regulation of Notch Signaling by Xylose." PLOS Genetics. 2013.

139. Lengyel, Ernest. "Ovarian cancer development and metastasis." The American Journal of Pathology. 2010.

140. Liao, Tsai-Tsen and Muh-Hwa Yang. "Revisiting Epithelial-Mesenchymal Transition in Cancer Metastasis: The Connection Between Epithelial Plasticity and Stemness." Molecular Oncology. 2017.

141. Lijnen, H. Roger, Begona Arza, Berthe Van Hoef, De´sire´ Collen, and Paul J. Declerck. "Inactivation of Plasminogen Activator Inhibitor-1 by Specific Proteolysis with Stromelysin-1 (MMP-3)". The Journal of Biological Chemistry. 2000.

142. Lisio, Michael-Antony, Lili Fu, Alicia Goyeneche, Zu-Hua Gao, and Carlos Telleria. "High-Grade Serous Ovarian Cancer: Basic Sciences, Clinical and Therapeutic Standpoints." International Journal of Molecular Sciences. 2019.

143. Livak, Kenneth J. and Thomas D. Schmittgen. "Analysis of Relative Gene Expression Data Using Real-Time Quantitative PCR and the $2^{-\Delta\Delta Ct}$ Method." Methods. 2001.

144. Lou, Xiao-Liang, Jian Sun, Shu-Qi Gong, Xue-Feng Yu, Rui Gong, and Huan Deng. "Interaction between circulating cancer cells and platelets: clinical implication." Chinese Journal of Cancer Research. Vol. 27, No. 5. 2015.

145. Lu, D.-Y., X.-L. Chen, J.-Y. Cal, Z. Li, H.-W. Xue, L.-J. LUO, and B Xu. "Effects of Cancer Chemotherapy on the Blood Fibrinogen Concentrations of Cancer Patients." The Journal of International Medical Research. 2000.

146. Ludwig, Heinz, Simon Van Belle, Peter Barrett-Lee, Gunnar Birgegård, Carsten Bokemeyer, Pere Gascón, Paris Kosmidis, Maciej Krzakowski, Johan Nortier, Patrizia Olmi, Maurice Schneider, and Dirk Schrijvers. "The European Cancer Anaemia Survey (ECAS): a large, multinational, prospective survey defining the prevalence, incidence, and treatment of anaemia in cancer patients." European Journal of Cancer. 2004.

147. Lukanova, A, E Lundin, A Zeleniuch-Jacquotte, P Muti, A Mure, S Rinaldi, L Dossus, A Micheli, A Arslan, P Lenner, R E Shore, V Krogh, K L Koenig, E Riboli, F Berrino, G Hallmans, P Stattin, P Toniolo, and R Kaaks. "Body mass index, circulating levels of sex-steroid hormones, IGF-I and IGF-binding protein-3: a cross-sectional study in healthy women." European Journal of Endocrinology. 2004.

148. Lukanova, Annekatrin and Rudolf Kaaks. "Endogenous Hormones and Ovarian Cancer: Epidemiology and Current Hypotheses." Cancer Epidemiology, Biomarkers & Prevention. 2005.

149. Luo, Yanlin, Hee Seung Kim, Miseon Kim, Maria Lee, Yong Sang Song. "Elevated plasma fibrinogen levels and prognosis of epithelial ovarian cancer: a cohort study and meta-analysis." Journal of Gynecologic Oncology. 2017.

150. Ma, Jian-Guo, Zheng-Kai He, Jian-Hua Ma, Wen-Ping Li and Guang Sun. "Downregulation of protocadherin-10 expression correlates with malignant behaviour and poor prognosis in human bladder cancer." Journal of International Medical Research. 2013.

151. Ma, Xiao, Markus Wehland, Herbert Schulz, Katrin Saar, Norbert Hübner, Manfred Infanger, Johann Bauer and Daniela Grimm. "Genomic Approach to Identify Factors That Drive the Formation of Three-Dimensional Structures by EA.hy926 Endothelial Cells." PLoS One. 2013.

152. Maccio, Antonio, Clelia Madeddu, Daniela Massa, Maria C. Mudu, Maria R. Lusso, Giulia Gramignano, Roberto Serpe, Gian Benedetto Melis, and Giovanni Mantovani. "Hemoglobin levels correlate with interleukin-6 levels in patients with advanced untreated epithelial ovarian cancer: role of inflammation in cancer-related anemia." Blood. 2005.

153. Marchand, Anthony, Cecilia M. Fenoglio, Robert Pascal, Ralph M. Richart, and Sidney Bennett. "Carcinoembryonic Antigen in Human

Ovarian Neoplasms." Cancer Research. 1975.

154. Marsh, Sharon, Jim Paul, Cristi R. King, Gillian Gifford, Howard L. McLeod, and Robert Brown. "Pharmacogenetic Assessment of Toxicity and Outcome After Platinum Plus Taxane Chemotherapy in Ovarian
155. Cancer: The Scottish Randomised Trial in Ovarian Cancer." Journal of Clinical Oncology. Vol.25, No.29, pp4528-4535. 2007.

156. Marshall, Lindsay J., Lara S.P. Ramdin, Teresa Brooks, Peter Charlton, and Janis K. Shute. "Plasminogen Activator Inhibitor-1 Supports IL-8-Mediated Neutrophil Transendothelial Migration by Inhibition of the Constitutive Shedding of Endothelial IL-8/Heparan Sulfate/Syndecan-1 Complexes." The Journal of Immunology. 2003.

157. Mashiko, Satsuki, Kazuyuki Kitatani, Masafumi Toyoshima, Atsuhiko Ichimura, Takashi Dan, Toshinori Usui, Masumi Ishibashi, Shogo Shigeta, Satoru Nagase, Toshio Miyata, and Nobuo Yaegashi. "Inhibition of plasminogen activator inhibitor-1 is a potential therapeutic strategy in ovarian cancer." Cancer Biology & Therapy. 16:2,253-260. 2015.

158. Masuda, Takaaki, Naoki Hayashi, Tomohiro Iguchi, Shuhei Ito, Hidetoshi Eguchi, and Koshi Mimori. "Clinical and biological significance of circulating tumor cells in Cancer." Molecular Oncology. 2016.

159. McCann, James V., Lin Xiao, Dae Joong Kim, Omar F. Khan, Piotr S. Kowalski, Daniel G. Anderson, Chad V. Pecot, Salma H. Azam, Joel S. Parker, Yihsuan S. Tsai, Alisa S. Wolberg, Stephen D. Turner, Kohei Tatsumi, Nigel Mackman, and Andrew C. Dudley. "Endothelial miR-30c suppresses tumor growth via inhibition of TGF-β–induced Serpin E1." The Journal of Clinical Investigation. 2019.

160. McMahon, Grainne A., Eric Petitclerc, Steingrimur Stefansson, Elizabeth Smith, Michael K. K. Wong, Randal J. Westrick, David Ginsburg, Peter C. Brooks, and Daniel A. Lawrence. "Plasminogen Activator Inhibitor-1 Regulates Tumor Growth and Angiogenesis." The Journal of Biological Chemistry. Vol.279, No.36, pp 33964–33968.The American Society for Biochemistry and Molecular Biology, Inc. 2001.

161. Mehta, R, and AD Shapiro. "Plasminogen activator inhibitor type 1 deficiency." Haemophilia. Vol.14, No.6. pp1255-60. 2008.

162. Menon, Usha, Aleksandra Gentry-Maharaj, Rachel Hallett, Andy Ryan, Matthew Burnell, Aarti Sharma, Sara Lewis, Susan Davies, Susan Philpott, Alberto Lopes, Keith Godfrey, David Oram, Jonathan Herod, Karin Williamson, Mourad W Seif, Ian Scott, Tim Mould, Robert Woolas, John Murdoch, Stephen Dobbs, Nazar N Amso, Simon Leeson, Derek Cruickshank, Alistair McGuire, Stuart Campbell, Lesley Fallowfield, Naveena Singh, Anne Dawnay, Steven J Skates, Mahesh Parmar, and Ian Jacobs. "Sensitivity and specificity of multimodal and ultrasound screening for ovarian cancer, and stage distribution of detected cancers: results of the prevalence screen of the UK Collaborative Trial of Ovarian Cancer Screening (UKCTOCS)." The Lancet Oncology. 2009.

163. Miao, Yi, Qin Yan, Shuangdi Li, Bilan Li, and Youji Feng. "Neutrophil to lymphocyte ratio and platelet to lymphocyte ratio are predictive of chemotherapeutic response and prognosis in epithelial ovarian cancer patients treated with platinum-based chemotherapy." Cancer Biomarkers. 2016.

164. Miller, M. Craig, Peggy S. Robinson, Christopher Wagner, and Daniel J. O'Shannessy. "The Parsortix™ Cell Separation System – A Versatile Liquid Biopsy Platform." Cytometry Part A. 2018.

165. Mittica, Gloria, Eleonora Ghisoni, Gaia Giannone, Sofia Genta, Massimo Aglietta, Anna Sapino, and Giorgio Valabrega. "PARP Inhibitors in Ovarian Cancer." Recent Patents on Anti-Cancer Drug Discovery. 2018.

166. Moffitt, Laura R., Maree Bilandzic, Amy L. Wilson,Yiqian Chen, Mark D. Gorrell ,Martin K. Oehler, Magdalena Plebanski, andAndrew N. Stephens. "Hypoxia Regulates DPP4 Expression, Proteolytic Inactivation, and Shedding from Ovarian Cancer Cells." International Journal of Molecular Sciences. 2020.

167. Moosazadeh, Mahmood, Iradj Maleki, Reza Alizadeh-Navaei, Motahareh Kheradmand, Akbar Hedayatizadeh-Omran, Amir Shamshirian and Agil Barzegar. "Normal values of neutrophil-to-lymphocyte ratio, lymphocyte-to-monocyte ratio and platelet-to-lymphocyte ratio among Iranian population: Results of Tabari cohort." Caspian Journal of Internal Medicine. 2019.

168. Morii,Takeshi, Takashi Tajima, Takayuki Aoyagi, and Shoichi Ichimura. "D-dimer Level Changes During Systemic Chemotherapy Can Predict Prognosis of High-grade Musculoskeletal Sarcoma Patients." Anticancer Research. 2015.

169. Moro, F, T. Pasciuto, D. Djokovic, A. Di Legge, V. Granato, M. C. Moruzzi, R. Mancari, G. F. Zannoni, D. Fischerova, D. Franchi, G. Scambia, and A. C. Testa. "Role of CA125/CEA ratio and ultrasound parameters in identifying metastases to the ovaries in patients with multilocular and multilocular-solid ovarian masses." Ultrasound in Obstetrics and Gynecology. 2018.

170. Murphy, Mark and Britta Stordal. "Erlotinib or Gefitinib for the Treatment of Relapsed Platinum Pretreated Non-Small Cell Lung Cancer and Ovarian Cancer: A Systematic Review." Drug Resistance Updates. 2011.

171. Nagalakshmi, U., Z. Wang, K. Waern, C. Shou, D. Raha, M. Gerstein, and M. Snyder. "The transcriptional landscape of the yeast genome defined by RNA sequencing." Science. Jun 6;320(5881):1344-9. 2008.

172. Nakatsuka, Erika, Kenjiro Sawada, Koji Makamura, Akihito Yoshimura, Yasuto Kinose, Michiko Kodama, Kae Hashimoto, Seiji Mabuchi, Hiroshi Makino, Eiichi Morii, Yoichi Yamaguchi, Takeshi Yanese, Akiko Itai, Ken-ichirou Morishige, and Tadashi Kimura. " Plasminogen activator inhibitor-1 is an independent prognostic indicator of ovarian cancer and IMD-4482, a novel plasminogen activator inhibitor-1 inhibitor, inhibits ovarian cancer peritoneal dissemination." Oncotarget. 2017.

173. Narayan, Gopeshwar, Luigi Scotto, Vijayalakshmi Neelakantan, Sherine H Kottoor, Ada Ho Yan Wong, Shee-Loong Loke, Mahesh Mansukhani, Bhavana Pothuri, Jason D. Wright, Andreas M. Kaufmann, Achim Schneider, Hugo Arias-Pulido, Qian Tao and Vundavalli V. Murty."Protocadherin PCDH10, Involved in Tumor Progression, is a Frequent and Early Target of Promoter Hypermethylation in Cervical Cancer." Genes, Chromosomes and Cancer. 2009.

174. Ness, Roberta B., Jeanne Ann Grisso, Jennifer Klapper, and Ron Vergona. "Racial Differences in Ovarian Cancer risk." Journal of the National Medical Association. 2000.

175. Noman, Muhammad Zaeem, Yosra Messai, Jane Muret, Meriem Hasmim, and Salem Chouaib. "Crosstalk between CTC, Immune System, and Hypoxic Tumor Microenvironment." Cancer Microenvironment. 2014.

176. Nunes, N., G. Ambler, X.Foo, M. Widschwendter, and D. Jurkovic. "Prospective evaluation of IOTA logistic regression models LR1 and LR2 in comparison with subjective pattern recognition for diagnosis of ovarian cancer in an outpatient setting." Ultrasound in Obstetrics and

Gynecology. 2018.

177. Osborn L, Hession C, Tizard R, Vassallo C, Luhowskyj S, Chi-Rosso G, and Lobb R. "Direct expression cloning of vascular cell adhesion molecule 1, a cytokine-induced endothelial protein that binds to lymphocytes." Cell. 1989.

178. Ose, Jennifer, Elizabeth M. Poole, Helena Schock, Matti Lehtinen, Alan A. Arslan, Anne Zeleniuch-Jacquotte, Kala Visvanathan, Kathy Helzlsouer, Julie E. Buring, I-Min Lee, Anne Tjønneland, Laure Dossus, Antonia Trichopoulou, Giovanna Masala, N. Charlotte Onland-Moret, Elisabete Weiderpass, Eric J. Duell, Annika Idahl, Ruth C. Travis, Sabina Rinaldi, Melissa A. Merritt, Britton Trabert, Nicolas Wentzensen, Shelley S. Tworoger, Rudolf Kaaks, and Renée T. Fortner. "Androgens are differentially associated with ovarian cancer subtypes in the Ovarian Cancer Cohort Consortium." Cancer Research. 2017 Jul 15; 77(14): 3951–3960.

179. Palmirotta, Raffaele, Patrizia Ferroni, Annalisa Savonarola, Francesca Martini, Filippo Ciatti, Anastasia Laudisi, Valentina Sini, Girolamo Del Monte, Fiorella Guadagni, and Mario Roselli." Prognostic value of pre-surgical plasma PAI-1 (plasminogen activator inhibitor-1) levels in breast cancer." Thrombosis Research. 2009.

180. Pan, Jie-Xue, Fan Qu, Fang-Fang Wang, Jian Xu, Liang-Shan Mu, Long-Yun Ye, and Jun-Jian Li. "Aberrant SERPIN E1 DNA methylation is involved in carboplatin-induced epithelial-mesenchymal transition in epithelial ovarian Cancer." Archives of Gynecology and Obstetrics. 2017.

181. Pappot, H., H. Gårdsvoll, J. Rømer , A. N. Pedersen, J. Grøndahl-Hansen, C. Pyke, and N. Brünner. "Plasminogen Activator Inhibitor Type 1 in Cancer: Therapeutic and Prognostic Implications." The Journal of Biological Chemistry. 1995.

182. Parpugga, Tajinder Kumar, Vacis Tatarunas, Vilius Skipskis, Nora Kupstyte, Diana Zaliaduonyte-Peksiene, and Vaiva Lesauskaite. "The Effect of PAI-1 4G/5G Polymorphism and Clinical Factors on Coronary Artery Occlusion in Myocardial Infarction." Disease Markers. 2015.

183. Pasquier, Eddy, Manon Carré, Bertrand Pourroy, Laurence Camoin, Ouafa Rebaï, Claudette Briand and Diane Braguer. "Antiangiogenic activity of paclitaxel is associated with its cytostatic effect, mediated by the initiation but not completion of a mitochondrial apoptotic signaling

pathway." Molecular Cancer Therapeutics. 2004.

184. Peng, Yang, Hiroaki Kajiyama, Hong Yuan, Kae Nakamura, Masato Yoshihara, Akira Yokoi, Kayo Fujikake, Hiroaki Yasui, Nobuhisa Yoshikawa, Shiro Suzuki, Takeshi Senga,Kiyosumi Shibata, and Fumitaka Kikkawa. "PAI-1 secreted from metastatic ovarian cancer cells triggers the tumor-promoting role of the mesothelium in a feedback loop to accelerate peritoneal dissemination." Cancer Letters. Volume 442, pp181-192. 1 February 2019.

185. Petersen, Michael, Jeppe B. Madsen, Thomas J. D. Jørgensen, and Morten B. Trelle. "Conformational preludes to the latency transition in PAI-1 as determined by atomistic computer simulations and hydrogen/deuterium-exchange mass spectrometry." Scientific Reports. Vol. 7, No. 6636. 2017.

186. Placencio, Veronica R. and Yves A DeClerck . "Plasminogen Activator Inhibitor-1 in Cancer: Rationale and Insight for Future Therapeutic Testing." Cancer Research. 2015.

187. Placencio, Veronica R., Atsuhiko Ichimura, Toshio Miyata, and Yves A. DeClerck. " Small Molecule Inhibitors of Plasminogen Activator Inhibitor-1 Elicit Anti-Tumorigenic and Anti-Angiogenic Activity." PLOS One. 2015.

188. Placke, Theresa, Melanie Örgel, Martin Schaller, Gundram Jung, Hans-Georg Rammensee, Hans-Georg Kopp, and Helmut Rainer Salih. "Platelet-Derived MHC Class I Confers a Pseudonomal Phenotype to Cancer Cells that Subverts the Antitumor Reactivity of Natural Killer Immune Cells." Cancer Research. American Association for Cancer Research. 2012.

189. Pradeep, S., S.W. Kim , S.Y. Wu, M. Nishimura, P. Chaluvally-Raghavan, T. Miyake , C.V. Pecot , S.J.Kim, H.J. Choy, F.Z. Bischoff, J.A. Mayer, L. Huang, A.M. Nick, C.S. Hall, C. Rodriguez-Aguay, B. Zand, H.J. Dalton, T. Arumugam, H.J. Lee, H.D. Han, M.S. Cho, R. Rupaimoole, L.S. Mangala,V. Sehgal, S.C. Oh, J. Liu, J.S. Lee, R.L. Coleman, P. Ram, G. Lopez-Berestein, I.J. Fidler, A.K. Sood. "Hematogenous metastasis of ovarian cancer: rethinking mode of spread." Cancer Cell. 2014.

190. Pyke, C., P.Kristensen, E. Ralfkiaer, J. Erikson, and K. Danø. "The Plasminogen Activation System in Human Colon Cancer: Messenger RNA for the Inhibitor PAI-1 is Located in Endothelial Cells in the Tumor Stroma." Cancer Research. 1991.

191. Qi, Cuiling, Bin Li, Simei Guo, Bo Wei, Chunkui Shao, Jialin Li, Yang Yang, Qianqian Zhang, Jiangchao Li, Xiaodong He, Lijing Wang, and Yajie Zhang. "P-Selectin-Mediated Adhesion between Platelets and Tumor Cells Promotes Intestinal Tumorigenesis in $APC^{Min/+}$ Mice." International Journal of Biological Sciences. 2015.

192. Rauh-Hain, Jose A., Thomas C. Krivak, Marcela G. del Carmen, and Alexander B. Olawaiye. "Ovarian Cancer Screening and Early Detection in the General Population." Reviews in Obstetrics & Gynecology. Vol.4, No,11. 2011.

193. Raungkaewmanee, Supachai, Siriwan Tangjitgamol, Sumonmal Manusirivithaya, Sunamchok Srijaipracharoen, and Thaovalai Thavaramara. "Platelet to lymphocyte ratio as a prognostic factor for epithelial ovarian cancer." Journal of Gynecologic Oncology. 2012.

194. Ray-Coquard, Isabelle,Patricia Pautier, Sandro Pignata, David Pérol, Antonio González-Martín, Regina Berger, Keiichi Fujiwara, Ignace Vergote, Nicoletta Colombo, Johanna Mäenpää, Frédéric Selle, Jalid Sehouli, Domenica Lorusso, Eva M. Guerra Alía, Alexander Reinthaller, Shoji Nagao, Claudia Lefeuvre-Plesse, Ulrich Canzler, Giovanni Scambia, Alain Lortholary, Frederik Marmé, Pierre Combe, Nikolaus de Gregorio, Manuel Rodrigues, Paul Buderath, Coraline Dubot, Alexander Burges, Benoît You, Eric Pujade-Lauraine, and Philipp Harter. "Olaparib plus Bevacizumab as First-Line Maintenance in Ovarian Cancer." The New England Journal of Medicine. 2019.

195. Reid, Brett M., Jennifer B. Permuth, and Thomas A Sellers. "Epidemiology of ovarian cancer: a review." Cancer Biology and Medicine. 2017.

196. Reid, Frances, Neerja Bhatla, and Annwen Jones. The World Ovarian Cancer Coalition Atlas - Global Trends in Incidence, Mortality and Survival. World Ovarian Cancer Coalition. 2018.

197. Romani de Wit, Thalia, Hubert P.J.C. de Leeuw, Mariska G. Rondaij, Rozalia T.M. de Laaf, Erica Sellink, Herm-Jan Brinkman, Jan Voorberg, and Jan A. van Mourik. "Von Willebrand factor targets IL-8 to Weibel-Palade bodies in an endothelial cell line." Experimental Cell Research. 2002.

198. Rosenberg, Barnett, Loretta vanCamp, James E. Trosko, and Virginia H. Mansour. "Platinum Compounds: a New Class of Potent Antitumour Agents." Nature. 1969.

199. Rowley, Jesse W., Hansjörg Schwertz, and Andrew S. Weyrich. "Platelet mRNA: the meaning behind the message." Current Opinion in Hematology. 2012.

200. Samarakoon, Rohan, and Paul J. Higgins. "Integration of non-SMAD and SMAD signaling in TGF-β1-induced plasminogen activator inhibitor type-1 gene expression in vascular smooth muscle cells." Thrombosis and Haemostasis. 2008.

201. Santoiemma, Phillip P. and Daniel J.Powell, Jr. "Tumor infiltrating lymphocytes in ovarian cancer." Cancer Biology and Therapy. 2015.

202. Sato, Masakazu, Kei Kawana, Katsuyuki Adachi, Asaha, Fujimoto, Mitsuyo Yoshida, Hiroe Nakamura, Haruka Nishida, Tomoko Inoue, Ayumi Taguchi, Juri Takahashi, Satoko Kojima, Aki Yamashita, Kensuke Tomio, Takeshi Nagamatsu, Osamu Wada-Hiraike, Katsutoshi Oda, Yutaka Osuga, and Tomoyuki Fujii. "Decreased expression of the plasminogen activator inhibitor type 1 is involved in degradation of extracellular matrix surrounding cervical cancer stem cells." International Journal of Oncology. 2016.

203. Sato, Seiya and Hiroaki Itamochi. "Neoadjuvant chemotherapy in advanced ovarian cancer: latest results and place in therapy." Therapeutic Advances in Medical Oncology. Vol. 6(6) 293–304. 2014.

204. Sato, Shigemi, Yoshihito Yokoyama, Tomomi Sakamoto, Masayuki Futagami, and Yoshiharu Saito. "Usefulness of mass screening for ovarian carcinoma using transvaginal ultrasonography." Cancer. Vol.89, Issue 3, pp582-588. 1 August 2000.

205. Schmalfeldt, B., W. Kuhn, U. Reuning, L. Pache, P. Dettmar, M. Schmitt, F. Jänicke, H. Höfler, and H. Graeff. "Primary Tumor Metastasis and Ovarian Cancer differ in their Content of Urokinase-type Plasminogen Activator, its Receptor, and Inhibitors Types 1 and 2." Cancer Research. 1995.

206. Schneider, David J, Yabing Chen and Burton E Sobel. "The effect of plasminogen activator inhibitor type 1 on apoptosis." Thrombosis and Haemostasis. 2008.

207. Schwab, Carlton L., Diana P. English, Dana M. Roque, and Alessandro D. Santin. "Taxanes: Their Impact on Gynecologic Malignancy." Anticancer Drugs. 2014.

208. Schwab M. (eds). "Cisplatin". Encyclopedia of Cancer. Springer, Berlin, Heidelberg. 2011.

209. Schwarzenbach, Heidi, and Peter B. Gahan. "Resistance to cis- and carboplatin initiated by epigenetic changes in ovarian cancer patients." Cancer Drug Resistance. 2019.

210. Seker, Fidan, Ahmet Cingoz, İlknur Sur-Erdem, Nazli Erguder, Alp Erkent, Fırat Uyulur, Myvizhi Esai Selvan, Zeynep Hülya Gümüş, Mehmet Gönen, Halil Bayraktar, Hiroaki Wakimoto, and Tugba Bagci-Onder. "Identification of SERPINE1 as a Regulator of Glioblastoma Cell Dispersal with Transcriptome Profiling." Cancers. 2019.

211. Selvakumaran, Muthu, Debra A. Pisarcik, Rudi Bao, Anthony T. Yeung, and Thomas C. Hamilton. "Enhanced Cisplatin Cytotoxicity by Disturbing the Nucleotide Excision Repair Pathway in Ovarian Cancer Cell Lines." Cancer Research. Vol. 63, pp1311–1316. 2003.

212. Sethi, Maya K., Falk F. R. Buettner, Vadim B. Krylov, Hideyuki Takeuchi, Nikolay E. Nifantiev, Robert S. Haltiwanger, Rita Gerardy-Schahn and Hans Bakker. "Identification of Glycosyltransferase 8 Family Members as Xylosyltransferases Acting on O-Glucosylated Notch Epidermal Growth Factor Repeats." Journal of Biological Chemistry. 2010.

213. Seubert, Bastian, Haissi Cui, Nicole Simonavicius, Katja Honert, Sandra Schäfer, Ute Reuning, Mathias Heikenwalder, Bernard Mari, and Achim

Krüger. "Tetraspanin CD63 acts as a pro-metastatic factor *via* β-catenin stabilization." International Journal of Cancer. 2014.

214. Shanker, Savita, Ariel Paulson,Howard J. Edenberg, Allison Peak, Anoja Perera, Yuriy O. Alekseyev, Nicholas Beckloff, Nathan J. Bivens, Robert Donnelly, Allison F. Gillaspy, Deborah Grove, Weikuan Gu, Nadereh Jafari, Joanna S. Kerley-Hamilton, Robert H. Lyons, Clifford Tepper, and Charles M. Nicolet. "Evaluation of Commercially Available RNA Amplification Kits for RNA Sequencing Using Very Low Input Amounts of Total RNA." Journal of Biomolecular Techniques. 2015.

215. Shetty, Sreerama, Praveenkumar Shetty, Steven Idell, Thirunavukkarasu Velusamy, Yashodhar P. Bhandary, and Rashmi S. Shetty." Regulation of Plasminogen Activator Inhibitor-1 Expression by Tumor Suppressor Protein p53." The Journal of Biological Chemistry. Vol. 283, No. 28, pp19570-19580. 2008.

216. Shishodia, Gauri, Sweaty Koul, Qin Dong, and Hari Koul. "Differential expression of Protocadherin-7 (PCDH7) in prostate cancer (PCa) cells: a direct association between PCDH7 and castrate resistant PCa." Cancer Research. 2017.

217. Sillen, Machteld and Paul Declerck. "A Narrative Review on Plasminogen Activator Inhibitor-1 and Its (Patho)Physiological Role: To Target or Not to Target?" International Journal of Molecular Sciences. 2021.

218. Sonnichsen, AC, U Lindlacher, WO Richter, and P Schwandt. "Obesity, body fat distribution and the incidence of breast, cervical, endometrial and ovarian carcinomas [in German]." Dtsch Med Wochenschr 1990;115:1906 – 10.

219. Sousa, Graziele Fonseca de, Samarina Rodrigues Wlodarczyk and Gisele Monteiro. "Carboplatin: molecular mechanisms of action associated with Chemoresistance." Brazilian Journal of Pharmaceutical Sciences. Vol. 50, No. 4. 2014.

220. Spillane, Cathy D., Niamh M. Cooke, Dermot Kenny, Gordon Blackshields, Mark P. Ward, Tanya E. Kelly, Mark Bates, Yanmei Huang, Cara Martin, Sinead Skehan, Aoife Canney, Michael Gallagher, Paul Smyth, Nathan Brady, Andres Clarke, Bashir Mohamed, Lucy Norris,

Doug A, Brooks, Robert D. Brooks, Jessica Heatlie, Stavros Selemidis, Sean Hanniffy, Eric Dixon, Orla Sheils, Sharon A. O'Toole1, and John J. O'Leary. *The Induction of a Mesenchymal Phenotype by Platelet Cloaking of Cancer Cells is a Universal Phenomenon*. Submitted for publication.

221. Stefansson, S and D A Lawrence. "The serpin PAI-1 inhibits cell migration by blocking integrin alpha V beta 3 binding to vitronectin." Nature. 1996.

222. Stone, Rebecca L., Alpa M. Nick, Iain A. McNeish, Frances Balkwill, Hee Dong Han, Justin Bottsford-Miller, Rajesha Rupaimoole, Guillermo N. Armaiz-Pena, Chad V. Pecot, Jermaine Coward, Michael T. Deavers, Hernan G. Vasquez, Diana Urbauer, Charles N. Landen, Wei Hu, Hannah Gershenson, Koji Matsuo, Mian M.K. Shahzad, Erin R. King, Ibrahim Tekedereli, Bulent Ozpolat, Edward H. Ahn, Virginia K. Bond, Rui Wang, Angela F. Drew, Francisca Gushiken, Donald Lamkin, Katherine Collins, Koen DeGeest, Susan K. Lutgendorf, Wah Chiu, Gabriel Lopez-Berestein, Vahid Afshar-Kharghan, and Anil K. Sood. "Paraneoplastic Thrombocytosis in Ovarian Cancer." The New England Journal of Medicine. 2012.

223. Streiff, Michael B., and Raagsudha Jhavar. Principles of Thrombolytic Agents. Chapter 21. Interventional Radiology. 2015.

224. Svanberg, Lars, and Birger Åstedt. "Coagulative and Fibrinolytic Properties of Ascitic Fluid Associated with Ovarian Tumors." Cancer. 1975.

225. Swisher, E.M., M. Wollan, S.M. Mahtani, J.B. Willner , R. Garcia, B.A. Goff , and M.C. King. "Tumor-specific p53 sequences in blood and peritoneal fluid of women with epithelial ovarian cancer."American Journal of Obstetrics and Gynecology. 2005.

226. Takeuchi, Hideyuki, and Robert S. Haltiwanger. "Significance of glycosylation in Notch signaling." Biochemical and Biophysical Research Communications. 2015.

227. Tang, Linlin, and Xiuzhen Han. "The urokinase plasminogen activator system in breast cancer invasion and metastasis." Biomedicine and Pharmacology. 2013.

228. Teeuwssen, Miriam and Riccardo Fodde. "Wnt Signaling in Ovarian Cancer Stemness, EMT, and Therapy Resistance." Journal of Clinical

Medicine. 2019.

229. Teliga-Czajkowska, Justyna, Jacek Sienko, Katarzyna Jalinik, Paweł Derlatka, Anna Danska-Bidzinska, and Krzysztof Czajkowski. "Plasminogen Activator Inhibitor Type 1 in Blood at Onset of Chemotherapy Unfavorably Affects Survival in Primary Ovarian Cancer." Advances in Experimental Medicine and Biology. 2019.

230. Templeton, Arnoud J, Olga Ace, Mairéad G McNamara, Mustafa Al-Mubarak, Francisco E Vera-Badillo, Thomas Hermanns, Boštjan Seruga, Alberto Ocaña, Ian F Tannock, and Eitan Amir. "Prognostic role of platelet to lymphocyte ratio in solid tumors: a systematic review and meta-analysis." Cancer Epidemiology, Biomarkers & Prevention. 2014.

231. Tewari, Krishnansu S., Robert A. Burger, Danielle Enserro, Barbara M. Norquist, Elizabeth M. Swisher, Mark F. Brady, Michael A. Bookman, Gini F. Fleming, Helen Huang, Howard D. Homesley, Jeffrey M. Fowler, Benjamin E. Greer, Matthew Boente, Sharon X. Liang, Chenglin Ye, Carlos Bais, Leslie M. Randall, John K. Chan, J. Stuart Ferriss, Robert L. Coleman, Carol Aghajanian, Thomas J. Herzog, Philip J. DiSaia, Larry J. Copeland, Robert S. Mannel, Michael J. Birrer, and Bradley J. Monk. "Final Overall Survival of a Randomized Trial of Bevacizumab for Primary Treatment of Ovarian Cancer." Journal of Clinical Oncology. 2019.

232. Thiyagarajan DK, Basit H, Jeanmonod R. Physiology, Menstrual Cycle. [Updated 2019 Apr 24]. In: StatPearls [Internet]. Treasure Island (FL): StatPearls Publishing; 2019 Jan-. Available from: https://www.ncbi.nlm.nih.gov/books/NBK500020/

233. Tothill, Richard W., Anna V. Tinker, Joshy George, Robert Brown, Stephen B. Fox, Stephen Lade, Daryl S. Johnsoon, Melanie K. Trivett, Dariush Etemadmoghadam, Biance Locandro, Ndia Triaficante, Sian Fereday, Jillian A. Hung, Yoke-Eng Chiew, Izhak Haviv, Australian Ovarian Cancer Study Group, Dorota Gertig, Anna DeFazio, and David D.L. Bowtell. "Novel Molecular Subtypes of Serous and Endometriod Ovarian Cancer Linked to Clinical Outcomes." Clinical Cancer Research. 2008.

234. Trabert, Britton, Louise A. Brinton, Garnet L. Anderson, Ruth M. Pfeiffer, Roni T. Falk, Howard D. Strickler, Sarunas, Sliesoraitis, Lewis H. Kuller, Margery L. Gass, Barbara J. Fuhrman, Xia Xu, and Nicolas Wentzensen. "Circulating estrogens and postmenopausal ovarian cancer risk in the Women's Health Initiative Observational Study". Cancer Epidemiology, Biomarkers & Prevention. February 5, 2016.

235. Türkmen, Beyhan, Manfred Schmitt, Barbara Schmalfeldt, Paul Trommle, Wolfgang Hell, Sabine Creutzburg, Henner Graeff, and Viktor Magdolen. "Mutational analysis of the genes encoding urokinase type plasminogen activator (uPA) and its inhibitor PAI-1 in advanced ovarian cancer." Electrophoresis. 1997.

236. Uccella, Stefano, Camilla Nero, Enrico Vizza, Virginia Vargiu, Giacomo Corrado, Nicolò Bizzarri, Fabio Ghezzi, Francesco Cosentino, Luigi Carlo Turco, Anna Fagotti, and Giovanni Scambia. "Sentinel-node biopsy in early-stage ovarian cancer: preliminary results of a prospective multicentre study (SELLY)." American Journal of Obstetrics and Gynecology. 2019.

237. Uribe-Querol, Eileen and Carlos Rosales. "Neutrophils in Cancer: Two Sides of the Same Coin." Journal of Immunology Research. 2015.

238. Ushijima, Kimio. "Treatment for Recurrent Ovarian Cancer—At First Relapse." Journal of Oncology. Volume 2010. 2010.

239. van Berckelaer, C., A.J. Brouwers, D.J.E. Peeters, W. Tjalma, X.B. Trinh, and P.A. van Dam. "Current and future role of circulating tumor cells in patients with epithelial ovarian cancer." The Journal of Cancer Surgery. 2016.

240. van Meijer, M. and H. Pannekoek. "Structure of plasminogen activator inhibitor 1 (PAI-1) and its function in fibrinolysis: an update." Fibrinolysis.Vol.9, No. 5, pp 263-276. 1995.

241. van Nagell, John R. Jr., Paul D. DePriest, Frederick R. Ueland, Christopher P. DeSimone, Amy L. Cooper, J. Matt McDonald, Edward J. Pavlik, and Richard J. Kryscio. "Ovarian cancer screening with annual transvaginal sonography." Cancer. Vol.109, Issue 9, pp 1887-1896. 1 May 2007.

242. Vergote, I, A du Bois, A Floquet, J Rau, J-W Kim, J M Del Campo, M Friedlander, S Pignata, K Fujiwara, N Colombo, M R Mirza, B J Monk, I Tsibulak, P M Calvert, T J Herzog, L C Hanker, J Meunier, J-Y Lee, A Bologna, M J Carrasco-Alfonso, and P Harter. "Overall Survival Results of AGO-OVAR16: A Phase 3 Study of Maintenance Pazopanib Versus Placebo in Women Who Have Not Progressed After First-Line Chemotherapy for Advanced Ovarian Cancer." Gynecologic Oncology.

2019.

243. Walker, J.M. "The Bicinchoninic Acid (BCA) Assay for Protein Quantitation." The Protein Protocols Handbook. Humana Press. 1996.

244. Wang, Guangli , Wenhe Huang, Wei Li, Shaoying Chen, Weibin Chen, Yanchun Zhou, Pei Peng and Wei Gu. "TFPI-2 suppresses breast cancer cell proliferation and invasion through regulation of ERK signaling and interaction with actinin-4 and myosin-9." Scientific Reports. Volume 8, Article number: 14402. 2018.

245. Wang, Shangqian , Qiang Cao ,Xiaoxiang Wang ,Bingjie Li,Min Tang,Wanqing Yuan,Jianzheng Fang,Jian Qian,Chao Qin ,and Wei Zhang. "PAI-1 4G/5G Polymorphism Contributes to Cancer Susceptibility: Evidence from Meta-Analysis." PLoS One. 2013.

246. Wang, Zhong, Mark Gerstein, and Michael Snyder. "RNA-Seq: a revolutionary tool for transcriptomics." Nature Review Genetics. 10(1): 57–63. 2009.

247. Ward, Mark P., Feras Abu Saadeh, Sharon A. O'Toole, John J. O'Leary, Dearbhaile M. O'Donnell, Noreen Gleeson, and Lucy A. Norris. *Procoagulant Activity in Ovarian Cancer Patients following Neoadjuvant Chemotherapy – The Role of the Activated Protein C Pathway.* Submitted for Publication. Trinity College Dublin. Dublin, Ireland.

248. Watanabe, Atai, Hiroyoshi Kanai, Masashi Arai, Kenichi Sekiguchi, Tsuyoshi Uchiyama, Ryozo Nagai and Masahiko Kurabayashi. "Retinoids induce the PAI-1 gene expression through tyrosine kinase-dependent pathways in vascular smooth muscle cells." Journal of Cardiovascular Pharmacology. 2002.

249. Whitman, Steven, Jennifer Orsi and Marc Hurlbert. "The racial disparity in breast cancer mortality in the 25 largest cities in the United States." Cancer Epidemiology. 2007.

250. Wiklund, Per-Gunnar, Lennart Nilsson, Sofie Nilsson Ardnor, Per Eriksson, Lars Johansson, Birgitta Stegmayr, Anders Hamsten, Dan Holmberg, and Kjell Asplund. "Plasminogen activator inhibitor-1 4G/5G polymorphism and risk of stroke: replicated findings in two nested case-control studies based on independent cohorts." Stroke. 2005.

251. Wild, Jonathan R. L., Carolyn A. Staton, Keith Chapple and Bernard M. Corfe. "Neuropilins: expression and roles in the epithelium." International

Journal of Experimental Pathology. 2012.

252. Wilkins-Port, Cynthia E., Jennifer Freytag, Stephen P. Higgins and Paul J. Higgins. "PAI-1: A Multifunctional SERPIN with Complex Roles in Cell Signaling and Migration." Cell Communication Insights. August 2010.

253. Williams, David R. and Chiquita Collins. "Racial Residential Segregation: A Fundamental Cause of Racial Disparities in Health." Public Health Reports. Volume 116, pp 404-416. September–October 2001.

254. Windmüller C, D Zech, S Avril, M Boxberg, T Dawidek, B Schmalfeldt, M Schmitt, M Kiechle and H Bronger. "CXCR3 mediates ascites-directed tumor cell migration and predicts poor outcome in ovarian cancer patients." Oncogenesis. 2017.

255. Wu, Jiacong, Ziyi Fu, Guangquan Liu, Pengfei Xu, Juan Xu, and Xuemei Jia. "Clinical significance of plasma D-dimer in ovarian cancer." Medicine. 2017.

256. Wu, Jianbo, Tammy L. Strawn, Mao Luo, Liqun Wang, Rong Li, Meiping Ren, Jiyi Xia, Zhuo Zhang, Weizhong Ma, Tingting Luo, Daniel A. Lawrence, and William P. Fay. "Plasminogen Activator Inhibitor-1 Inhibits Angiogenic Signaling by Uncoupling VEGF Receptor-2-αVβ3 Integrin Cross-talk." Arteriosclerosis, Thrombosis, and Vascular Biology. 2015.

257. Wu, Lishan, Shan Zou, Cantian Wang, Xuerui Tan and Min Yu. "Neutrophil-to-lymphocyte and platelet-to lymphocyte ratio in Chinese Han population from Chaoshan region in South China." BMC Cardiovasular Disorders. 2019.

258. Xie, Qi, Zuowang Cheng, Xiaocui Chen, Corrinne G. Lobe and Ju Liu. "The role of Notch signalling in ovarian Angiogenesis." Journal of Ovarian Research. 2017.

259. Xu, Jing, Wenwen Zhang, Lin Tang, Weiwei Chen, and Xiaoxiang Guan. "Epithelial-mesenchymal transition induced PAI-1 is associated with prognosis of triple-negative breast cancer patients." Gene. 2018.

260. Xu, Lei, Fan He, Hongcai Wang, Bei Gao, Huini Wu, and Shuping Zhao. "A high plasma D-dimer level predicts poor prognosis in gynecological tumors in East Asia area: a systematic review and meta-analysis." Oncotarget. 2017.

261. Yahata, Takashi, Abd Aziz Ibrahim, Ken-ichi Hirano, Yukari Muguruma, Kazuhito Naka, Katsuto Hozumi, Douglas E. Vaughan, Toshio Miyata

and Kiyoshi Ando. "Targeting of plasminogen activator inhibitor-1 activity promotes elimination of chronic myeloid leukemia stem cells." Haematologica. 2021.

262. Ye, Yao, Aurelia Vattai, Xi Zhnad, Junyan Zhu, Christian J. Thaler, Sven Mahner, Udo Jeschke, and Viktoria von Schönfeldt. "Role of Plasminogen Activator Inhibitor Type 1 in Pathologies of Female Reproductive Diseases." International Journal of Molecular Sciences. 2017.

263. Yokoi, Akira, Yusuke Yoshioka, Yusuke Yamamoto, Mitsuya Ishikawa, Shun-ichi Ikeda, Tomoyasu Kato, Tohru Kiyono, Fumitaka Takeshita, Hiroaki Kajiyama, Fumitaka Kikkawa, and Takahiro Ochiya. "Malignant extracellular vesicles carrying MMP1 mRNA facilitate peritoneal dissemination in ovarian cancer." Nature Communications. Volume 8. 2017.

264. Yun, Seong-Hoon, Eun-Hye Sim, Ri-Young Goh, Joo-In Park, and Jin-Yeong Han. "Platelet Activation: The Mechanisms and Potential Biomarkers." Biomed Research International. Hindawi. 2016.

265. Zhang, Jitao David, Markus Ruschaupt, and Rudolf Biczok. "ddCt Method for qRT-PCR data analysis." Open-source Bioconductor software package, 2017. (retrieved from: https://bioc.ism.ac.jp/packages/3.5/bioc/vignettes/ddCt/inst/doc/rtPCR.pdf).

266. Zhang, Yuqing, Giovanni Parmigiani, and W. Evan Johnson. "ComBat-Seq: batch effect adjustment for RNA-Seq count data." NAR Genomics and Bioinformatics. Vol.2, No.3. 2020.

267. Zhou, Yongping, Sijin Cheng, Abdel Hamid Fathy, Haixin Qian, and Yongzhao Zhao. "Prognostic value of platelet-to-lymphocyte ratio in pancreatic cancer: a comprehensive meta-analysis of 17 cohort studies." Onco Targets and Therapy. 2018.

268. Zhu, L.-R., J. Li, P. Chen, Q. Jiang, and X.-P. Tang. "Clinical significance of plasma fibrinogen and D-dimer in predicting the chemotherapy efficacy and prognosis for small cell lung cancer patients." Clinical and Translational Oncology. 2015.

WEBSITE REFERENCES

1. http://ovarian.org/about-ovarian-cancer/what-is-ovarian-cancer/types-a-stages

2. http://ovarian.org/component/content/article/33/385

3. https://www.cancer.org/cancer/ovarian-cancer/causes-risks-prevention/risk-factors.html

4. https://www.ncri.ie/atlas/171-summary

5. http://www.genecards.org/cgi-bin/carddisp.pl?gene=SERPINE1

6. https://www.wcrf.org/int/cancer-facts-figures/data-specific-cancers/ovarian-cancer-statistics

7. https://www.ctu.mrc.ac.uk/studies/all-studies/u/ukctocs/

8. https://www.cancer.org/cancer/ovarian-cancer/detection-diagnosis-staging/staging.html

9. https://www.figo.org/news/staging-ovftp-malignancies-0016123

10. https://www.cancerresearchuk.org/about-cancer/ovarian-cancer/stages-grades/stage-1

11. https://www.cancer.org/cancer/ovarian-cancer/treating/by-stage.html

APPENDIX A: CHAPTER 4 TABLES

siRNA vs. siNEG

Table A4-1 Enriched pathways for clusters in Fig. 4.13

Cluster	adj.Pval	nGenes	Pathways
A	9.3e-16	15	Sterol biosynthetic process
	3.3e-15	14	Cholesterol biosynthetic process
	4.1e-14	22	Steroid metabolic process
	8.9e-14	17	Sterol metabolic process
	9.8e-14	14	Regulation of steroid biosynthetic process
	1.2e-13	18	Steroid biosynthetic process
	1.2e-13	16	Cholesterol metabolic process
	1.2e-13	15	Regulation of steroid metabolic process
	4.0e-12	11	Regulation of cholesterol metabolic process
	5.7e-12	16	Regulation of lipid biosynthetic process
	8.7e-12	10	Regulation of cholesterol biosynthetic process
	7.3e-11	17	Organic hydroxy compound biosynthetic process
B	3.9e-03	5	Acute-phase response
	4.0e-03	8	Regulation of leukocyte migration
	9.0e-03	14	Inflammatory response
C	3.1e-03	8	Protein glycosylation
	3.1e-03	9	Glycoprotein biosynthetic process
	3.1e-03	2	Trans-synaptic signaling by soluble gas, modulating synaptic transmission
D	1.8e-13	16	Cellular response to molecule of bacterial origin
	7.2e-11	22	Cytokine-mediated signaling pathway

Table A4-1 Enriched pathways for clusters in Fig. 4.13

	1.3e-10	19	Cellular response to lipid
	2.2e-10	25	Response to cytokine
	3.2e-10	24	Cellular response to cytokine stimulus
	4.1e-10	35	Cellular response to organic substance
	4.6e-10	19	Response to bacterium
	5.6e-10	38	Cellular response to chemical stimulus
	6.2e-10	38	Response to organic substance
	8.2e-10	23	Cellular response to oxygen-containing compound
	1.5e-09	32	Immune response
E	2.2e-05	29	Tissue development
	6.4e-05	38	Animal organ development
	1.6e-04	7	Molting cycle
	3.1e-04	30	Anatomical structure morphogenesis
	3.8e-04	18	Anatomical structure formation involved in morphogenesis
	5.7e-04	17	Circulatory system development
	6.1e-04	24	Cell proliferation
	7.5e-04	19	Epithelium development
	1.6e-03	11	Angiogenesis
	1.6e-03	6	Sprouting angiogenesis
	1.9e-03	16	Animal organ morphogenesis
	1.9e-03	11	Positive regulation of cell migration
	2.4e-03	10	Extracellular structure organization
	2.4e-03	18	Cellular response to endogenous stimulus
F	6.1e-08	19	Response to virus

Table A4-1 Enriched pathways for clusters in Fig. 4.13

	2.5e-07	30	Response to external biotic stimulus
	5.1e-07	11	Type I interferon signaling pathway
	5.1e-07	11	Cellular response to type I interferon
	5.5e-07	11	Response to type I interferon
	5.5e-07	15	Defense response to virus
	9.4e-06	45	Response to external stimulus
	2.0e-05	19	Defense response to other organisms
	7.7e-05	23	Cytokine-mediated signaling pathway
	9.4e-05	52	Immune system process
	9.4e-05	7	Negative regulation of viral genome replication
	9.4e-05	27	Cellular response to cytokine stimulus
	1.1e-04	28	Response to cytokine

Table A4-2 Enriched pathways in DEGs for the selected comparison: siRNA v siNEG

Direction	adj.Pval	nGenes	Pathways
Down regulated	2.4e-03	79	Regulation of cellular component organization
	5.9e-03	106	Organelle organization
	5.9e-03	51	Cell migration
	5.9e-03	84	Intracellular signal transduction
	6.0e-03	46	Regulation of organelle organization
	7.2e-03	59	Locomotion
	8.0e-03	34	Regulation of cell migration
	8.3e-03	59	Regulation of intracellular signal transduction
	9.0e-03	5	Acetyl-CoA biosynthetic process

Table A4-2 Enriched pathways in DEGs for the selected comparison: siRNA v siNEG

	9.0e-03	91	Phosphorus metabolic process
	9.0e-03	20	Negative regulation of organelle organization
	9.0e-03	70	Phosphorylation
	9.0e-03	17	Stress-activated protein kinase signaling cascade
	9.0e-03	52	Cell motility
Up regulated	2.9e-06	17	Protein glycosylation
	2.9e-06	19	Glycoprotein biosynthetic process
	2.9e-06	17	Glycosylation
	1.1e-05	20	Glycoprotein metabolic process
	2.4e-05	11	Protein O-linked glycosylation
	1.1e-03	24	Carbohydrate derivative biosynthetic process
	1.5e-03	36	Cell adhesion
	2.3e-03	10	Homophilic cell adhesion via plasma membrane adhesion molecules
	4.4e-03	25	Cell-cell adhesion

Table A4-3 Top genes for selected comparison in DEGs: siRNA v siNEG

Ensembl ID	log2 Fold Change	Adj.Pval	Symbol	Chr	Type
ENSG00000185621	2.63	9.08e-12	LMLN;LMLN	3q29	protein_coding
ENSG00000116489	-2.59	7.17e-51	CAPZA1;CAPZA1	1p13.2	protein_coding
ENSG00000152661	-2.47	4.53e-38	GJA1;GJA1	6q22.31	protein_coding
ENSG00000180776	-2.22	3.36e-56	ZDHHC20;ZDHHC20	13q12.11	protein_coding
ENSG00000159871	-2.16	6.64e-07	LYPD5;LYPD5	19q13.31	protein_coding
ENSG00000106366	-2.04	3.72e-09	SERPINE1;SERPINE1	7q22.1	protein_coding
ENSG00000075461	2.00	6.96e-10	CACNG4;CACNG4	17q24.2	protein_coding

Table A4-3 Top genes for selected comparison in DEGs: siRNA v siNEG

ENSG00000152127	-1.85	5.70e-49	MGAT5;MGAT5	2q21.2	protein_coding
ENSG00000124767	-1.85	4.27e-35	GLO1;GLO1	6p21.2	protein_coding
ENSG00000050438	1.83	2.01e-35	SLC4A8;SLC4A8	12q13.13	protein_coding
ENSG00000204392	-1.81	1.01e-30	LSM2;LSM2	6p21.33	protein_coding
ENSG00000143845	-1.81	5.17e-27	ETNK2;ETNK2	1q32.1	protein_coding
ENSG00000171055	-1.81	4.37e-53	FEZ2;FEZ2	2p22.2	protein_coding
ENSG00000231298	-1.78	1.05e-07	MANCR;	10p15.1	lncRNA
ENSG00000250696	-1.78	1.17e-03	;	4q13.2	lncRNA
ENSG00000160201	-1.75	1.81e-03	U2AF1;U2AF1L5	21q22.3	protein_coding
ENSG00000160201	-1.75	1.81e-03	U2AF1;U2AF1	21q22.3	protein_coding
ENSG00000204604	-1.74	2.86e-46	ZNF468;ZNF468	19q13.41	protein_coding
ENSG00000157851	-1.66	1.37e-18	DPYSL5;DPYSL5	2p23.3	protein_coding
ENSG00000149474	-1.66	3.21e-19	KAT14;KAT14	20p11.23	protein_coding
ENSG00000009844	-1.61	4.06e-48	VTA1;VTA1	6q24.1	protein_coding
ENSG00000224531	-1.60	1.64e-28	SMIM13;SMIM13	6p24.2	protein_coding
ENSG00000215182	1.60	6.30e-03	MUC5AC;MUC5AC	11p15.5	protein_coding
ENSG00000144893	1.59	7.48e-06	MED12L;MED12L	3q25.1	protein_coding
ENSG00000145781	-1.58	7.39e-26	COMMD10;COMMD10	5q23.1	protein_coding
ENSG00000111252	-1.58	6.15e-06	SH2B3;SH2B3	12q24.12	protein_coding
ENSG00000196611	-1.57	2.89e-22	MMP1;MMP1	11q22.2	protein_coding
ENSG00000054392	-1.57	9.33e-11	HHAT;HHAT	1q32.2	protein_coding
ENSG00000186198	1.57	2.08e-03	SLC51B;SLC51B	15q22.31	protein_coding
ENSG00000138744	1.54	3.53e-10	NAAA;NAAA	4q21.1	protein_coding
ENSG00000267106	-1.52	1.51e-07	ZNF561-AS1;	19p13.2	lncRNA
ENSG00000169851	1.50	1.03e-11	PCDH7;PCDH7	4p15.1	protein_coding
ENSG00000151233	1.50	1.01e-55	GXYLT1;GXYLT1	12q12	protein_coding

Table A4-3 Top genes for selected comparison in DEGs: siRNA v siNEG

ENSG00000052723	-1.49	1.63e-19	SIKE1;SIKE1	1p13.2	protein_coding
ENSG00000148248	-1.48	2.98e-49	SURF4;SURF4	9q34.2	protein_coding
ENSG00000170915	-1.47	1.84e-10	PAQR8;PAQR8	6p12.2	protein_coding
ENSG00000170439	1.46	5.68e-03	METTL7B;METTL7B	12q13.2	protein_coding
ENSG00000105323	-1.45	4.89e-68	HNRNPUL1;HNRNPUL1	19q13.2	protein_coding
ENSG00000105323	-1.45	4.89e-68	HNRNPUL1;HNRPUL1	19q13.2	protein_coding
ENSG00000131242	-1.45	2.36e-15	RAB11FIP4;RAB11FIP4	17q11.2	protein_coding
ENSG00000103429	-1.45	3.50e-34	BFAR;BFAR	16p13.12	protein_coding
ENSG00000143502	-1.43	7.05e-07	SUSD4;SUSD4	1q41	protein_coding
ENSG00000105974	-1.42	1.91e-38	CAV1;CAV1	7q31.2	protein_coding
ENSG00000089250	-1.41	1.40e-12	NOS1;NOS1	12q24.22	protein_coding
ENSG00000186862	1.39	1.32e-03	PDZD7;PDZD7	10q24.31	protein_coding
ENSG00000179841	-1.38	2.42e-09	AKAP5;AKAP5	14q23.3	protein_coding
ENSG00000008083	-1.37	2.04e-32	JARID2;JARID2	6p22.3	protein_coding
ENSG00000197903	1.37	6.02e-07	H2BC12;H2BC12	6p22.1	protein_coding
ENSG00000197903	1.37	6.02e-07	H2BC12;HIST1H2BK	6p22.1	protein_coding
ENSG00000126821	-1.37	1.46e-31	SGPP1;SGPP1	14q23.2	protein_coding

Table A4-4 Gene set enrichment analysis GSEA: siRNA vs siNEG

Direction	GSEA analysis: siRNA vs siNEG	NES	Genes	adj.Pval
Down	Protein monoubiquitination	-2.0784	67	2.4e-03
	Reciprocal meiotic recombination	-2.0111	37	6.6e-03
	Homologous recombination	-2.0093	38	8.5e-03
	Regulation of coagulation	-2.0033	46	3.4e-03
	Cellular response to lipopolysaccharide	-1.9904	115	2.4e-03

Table A4-4 Gene set enrichment analysis GSEA: siRNA vs siNEG

	Regulation of blood coagulation	-1.9881	41	9.0e-03
	Regulation of hemostasis	-1.9881	41	9.0e-03
	Negative regulation of coagulation	-1.9865	27	1.3e-02
	Histone ubiquitination	-1.9654	45	6.6e-03
	Negative regulation of blood coagulation	-1.962	23	1.4e-02
	Negative regulation of hemostasis	-1.962	23	1.4e-02
	Negative regulation of wound healing	-1.9553	42	9.2e-03
Up	Glycosylation	2.0683	196	2.4e-03
	Protein glycosylation	2.0537	186	2.4e-03
	Macromolecule glycosylation	2.0537	186	2.4e-03
	Protein O-linked glycosylation	2.0393	82	2.4e-03
	Glycoprotein metabolic process	2.0173	294	2.4e-03
	O-glycan processing	1.9821	33	1.1e-02
	Homophilic cell adhesion via plasma membrane adhesion molecules	1.9749	91	2.4e-03
	Glycoprotein biosynthetic process	1.9666	241	2.4e-03
	Aminoglycan metabolic process	1.9661	109	2.4e-03
	Aminoglycan biosynthetic process	1.9654	77	4.1e-03
	Protein mannosylation	1.9536	21	2.0e-02
	Keratan sulfate metabolic process	1.9531	24	1.8e-02
	Glycosaminoglycan metabolic process	1.9458	104	2.4e-03
	Peptidyl-proline hydroxylation	1.9433	16	1.9e-02
	Glycosaminoglycan biosynthetic process	1.9416	74	3.0e-03
	Protein transport within lipid bilayer	1.9251	24	2.2e-02
	Glycolipid metabolic process	1.9155	85	4.1e-03
	Liposaccharide metabolic process	1.9155	85	4.1e-03

Table A4-5 Enriched pathways for clusters in Fig. 4.20

Cluster	adj.Pval	nGenes	
A	1.2e-03	12	Protein glycosylation
	1.2e-03	14	Glycoprotein biosynthetic process
B	1.8e-17	12	Cholesterol biosynthetic process
	2.6e-17	14	Cholesterol metabolic process
	2.6e-17	12	Sterol biosynthetic process
	1.2e-16	14	Sterol metabolic process
	4.0e-13	9	Regulation of cholesterol metabolic process
	3.0e-12	8	Regulation of cholesterol biosynthetic process
	6.2e-12	10	Regulation of steroid metabolic process
	2.5e-11	9	Regulation of steroid biosynthetic process
C	8.5e-10	15	Response to lipopolysaccharide
	8.5e-10	13	Cellular response to lipopolysaccharide
	1.2e-08	20	Response to lipid
	4.0e-08	17	Response to bacterium
	4.2e-08	26	Positive regulation of multicellular organismal process
	6.8e-08	16	Cellular response to lipid
	1.2e-07	31	Cellular response to organic substance
	1.4e-07	34	Cellular response to chemical stimulus
	1.4e-07	34	Response to organic substance
	1.4e-07	19	Response to external biotic stimulus
D	7.5e-03	2	Response to jasmonic acid
E	1.4e-12	15	Response to virus
	1.4e-12	14	Defense response to virus

Table A4-5 Enriched pathways for clusters in Fig. 4.20

	1.4e-12	11	Type I interferon signaling pathway
	1.4e-12	11	Cellular response to type I interferon
	1.5e-12	11	Response to type I interferon
	1.2e-09	15	Defense response to other organism
	4.7e-09	18	Response to external biotic stimulus
	2.3e-08	7	Negative regulation of viral genome replication
	2.2e-07	17	Innate immune response
	5.5e-07	8	Regulation of viral life cycle
	7.4e-07	23	Response to external stimulus
F	5.2e-03	34	Cell migration
	5.2e-03	40	Locomotion
	5.7e-03	24	Regulation of cell migration
	6.0e-03	4	Acetyl-CoA biosynthetic process from pyruvate
	6.0e-03	35	Cell motility

Table A4-6 Gene enrichment in ShinyGOv0.61 for significantly downregulated genes: siRNA vs siNEG

Enrichment FDR	Genes in list	Total genes	Functional Category
3.4E-02	5	21	Acetyl-CoA biosynthetic process
3.4E-02	51	1506	Cell migration
3.4E-02	78	2653	Regulation of cellular component organization
4.0E-02	46	1347	Regulation of organelle organization
4.1E-02	4	16	Acetyl-CoA biosynthetic process from pyruvate
4.1E-02	3	6	Detection of virus
4.1E-02	23	521	Positive regulation of cell migration
4.1E-02	17	326	Stress-activated protein kinase signaling cascade
4.1E-02	59	1921	Locomotion
4.1E-02	52	1670	Cell motility
4.1E-02	24	558	Positive regulation of cellular component movement
4.1E-02	16	298	Stress-activated MAPK cascade
4.1E-02	52	1670	Localization of cell

Table A4-7 Gene enrichment for downregulated pathways: siRNA v siNEG

GENE ENRICHMENT FOR DOWNREGULATED PATHWAYS: siRNA v siNEG														Matches
	ALL GENES IN iDEP92						SIGNIFICANTLY DOWNREGULATED GENE LIST IN ShinyGOv0.61							4
Pathway	# of genes	DEGs	p adj	Total Genes	GSEA	padj	# of Our Genes	Total Genes	ShinyGO	FDR	# of Genes	STRING	padj	3
Regulation of cellular component organization	79	Y	0.0024	N/A	N	N/A	78	2653	Y	0.034	N/A	N	N/A	2
Organelle organization	106	Y	0.0059	N/A	N	N/A	N/A	N/A	N	N/A	N/A	N	N/A	
Cell migration	51	Y	0.0059	N/A	N	N/A	51	1506	Y	0.034	28	Y	0.0036	
Intracellular signal transduction	84	Y	0.0059	N/A	N	N/A	N/A	N/A	N	N/A	N/A	N	N/A	
Regulation of organelle organization	46	Y	0.006	N/A	N	N/A	46	1347	Y	0.04	N/A	N	N/A	
Locomotion	59	Y	0.0072	N/A	N	N/A	59	1921	Y	0.041	41	Y	0.00051	
Regulation of cell migration	34	Y	0.008	N/A	N	N/A	N/A	N/A	N	N/A	N/A	N	N/A	
Regulation of intracellular signal transduction	59	Y	0.0083	N/A	N	N/A	N/A	N/A	N	N/A	45	Y	0.00051	
Acetyl-CoA biosynthetic process	5	Y	0.009	N/A	N	N/A	5	21	Y	0.034	N/A	N	N/A	
Phosphorus metabolic process	91	Y	0.009	N/A	N	N/A	N/A	N/A	N	N/A	N/A	N	N/A	
Negative regulation of organelle organization	20	Y	0.009	N/A	N	N/A	N/A	N/A	N	N/A	N/A	N	N/A	
Phosphorylation	70	Y	0.009	N/A	N	N/A	N/A	N/A	N	N/A	N/A	N	N/A	
Stress-activated protein kinase signaling cascade	17	Y	0.009	N/A	N	N/A	17	326	Y	0.041	N/A	N	N/A	
Cell motility	52	Y	0.009	N/A	N	N/A	52	1670	Y	0.041	29	Y	0.0042	
Protein monoubiquitination	N/A	N	N/A	67	Y	0.0024	N/A	N/A	N	N/A	N/A	N	N/A	
Reciprocal meiotic recombination	N/A	N	N/A	37	Y	0.0066	N/A	N/A	N	N/A	N/A	N	N/A	
Homologous recombination	N/A	N	N/A	38	Y	0.0085	N/A	N/A	N	N/A	N/A	N	N/A	
Regulation of coagulation	N/A	N	N/A	46	Y	0.0034	N/A	N/A	N	N/A	N/A	N	N/A	
Cellular response to lipopolysaccharide	N/A	N	N/A	115	Y	0.0024	N/A	N/A	N	N/A	N/A	N	N/A	
Regulation of blood coagulation	N/A	N	N/A	41	Y	0.009	N/A	N/A	N	N/A	N/A	N	N/A	
Regulation of hemostasis	N/A	N	N/A	41	Y	0.009	N/A	N/A	N	N/A	N/A	N	N/A	
Negative regulation of coagulation	N/A	N	N/A	27	Y	0.013	N/A	N/A	N	N/A	N/A	N	N/A	
Histone ubiquitination	N/A	N	N/A	45	Y	0.0066	N/A	N/A	N	N/A	N/A	N	N/A	
Negative regulation of blood coagulation	N/A	N	N/A	23	Y	0.014	N/A	N/A	N	N/A	N/A	N	N/A	
Negative regulation of hemostasis	N/A	N	N/A	23	Y	0.014	N/A	N/A	N	N/A	N/A	N	N/A	
Negative regulation of wound healing	N/A	N	N/A	42	Y	0.0092	N/A	N/A	N	N/A	N/A	N	N/A	
Detection of virus	N/A	N	N/A	N/A	N	N/A	3	6	Y	0.041	N/A	N	N/A	
Acetyl-CoA biosynthetic process from pyruvate	N/A	N	N/A	N/A	N	N/A	4	16	Y	0.041	N/A	N	N/A	
Positive regulation of cell migration	N/A	N	N/A	N/A	N	N/A	23	521	Y	0.041	N/A	N	N/A	
Positive regulation of cellular component movement	N/A	N	N/A	N/A	N	N/A	24	558	Y	0.041	N/A	N	N/A	
Stress-activated MAPK cascade	N/A	N	N/A	N/A	N	N/A	16	298	Y	0.041	N/A	N	N/A	
Localization of cell	N/A	N	N/A	N/A	N	N/A	52	1670	Y	0.041	29	Y	0.0042	
regulation of response to stress	N/A	N	N/A	N/A	N	N/A	N/A	N/A	N	N/A	49	Y	0.000084	
regulation of cellular response to stress	N/A	N	N/A	N/A	N	N/A	N/A	N/A	N	N/A	32	Y	0.000094	
response to mechanical stimulus	N/A	N	N/A	N/A	N	N/A	N/A	N/A	N	N/A	14	Y	0.0022	
response to other organism	N/A	N	N/A	N/A	N	N/A	N/A	N/A	N	N/A	27	Y	0.0023	
positive regulation of protein metabolic process	N/A	N	N/A	N/A	N	N/A	N/A	N/A	N	N/A	42	Y	0.0035	
response to biotic stimulus	N/A	N	N/A	N/A	N	N/A	N/A	N/A	N	N/A	27	Y	0.0035	
regulation of cytoskeleton organization	N/A	N	N/A	N/A	N	N/A	N/A	N/A	N	N/A	19	Y	0.0035	
cellular response to abiotic stimulus	N/A	N	N/A	N/A	N	N/A	N/A	N/A	N	N/A	15	Y	0.0042	
regulation of protein transport	N/A	N	N/A	N/A	N	N/A	N/A	N/A	N	N/A	27	Y	0.0042	
regulation of cytoplasmic transport	N/A	N	N/A	N/A	N	N/A	N/A	N/A	N	N/A	20	Y	0.0042	
transmembrane receptor protein tyrosine kinase signaling pathway	N/A	N	N/A	N/A	N	N/A	N/A	N/A	N	N/A	26	Y	0.0045	
regulation of actin filament-based process	N/A	N	N/A	N/A	N	N/A	N/A	N/A	N	N/A	16	Y	0.0049	
response to lipopolysaccharide	N/A	N	N/A	N/A	N	N/A	N/A	N/A	N	N/A	15	Y	0.0049	
regulation of establishment of protein localization	N/A	N	N/A	N/A	N	N/A	N/A	N/A	N	N/A	28	Y	0.0052	
inflammatory response	N/A	N	N/A	N/A	N	N/A	N/A	N/A	N	N/A	19	Y	0.0054	
regulation of cellular localization	N/A	N	N/A	N/A	N	N/A	N/A	N/A	N	N/A	36	Y	0.0065	
response to molecule of bacterial origin	N/A	N	N/A	N/A	N	N/A	N/A	N/A	N	N/A	15	Y	0.0066	
positive regulation of intracellular signal transduction	N/A	N	N/A	N/A	N	N/A	N/A	N/A	N	N/A	28	Y	0.007	
regulation of intracellular protein transport	N/A	N	N/A	N/A	N	N/A	N/A	N/A	N	N/A	17	Y	0.007	
response to endogenous stimulus	N/A	N	N/A	N/A	N	N/A	N/A	N/A	N	N/A	40	Y	0.007	
regulation of protein localization	N/A	N	N/A	N/A	N	N/A	N/A	N/A	N	N/A	30	Y	0.007	
cellular response to external stimulus	N/A	N	N/A	N/A	N	N/A	N/A	N/A	N	N/A	15	Y	0.007	

Table A4-8 Significantly downregulated genes of the cell migration pathway

User ID	Ensembl Gene ID	Symbol	Gene Type	Species	Chr	Position (Mbp)
ENSG00000171608	ENSG00000171608	PIK3CD	protein_coding	Human	1	9.6517
ENSG00000117525	ENSG00000117525	F3	protein_coding	Human	1	94.5292
ENSG00000155380	ENSG00000155380	SLC16A1	protein_coding	Human	1	112.9118
ENSG00000196754	ENSG00000196754	S100A2	protein_coding	Human	1	153.5611
ENSG00000162738	ENSG00000162738	VANGL2	protein_coding	Human	1	160.4006
ENSG00000158769	ENSG00000158769	F11R	protein_coding	Human	1	160.9952
ENSG00000174059	ENSG00000174059	CD34	protein_coding	Human	1	207.8810
ENSG00000152127	ENSG00000152127	MGAT5	protein_coding	Human	2	134.1200
ENSG00000115221	ENSG00000115221	ITGB6	protein_coding	Human	2	160.0997
ENSG00000196220	ENSG00000196220	SRGAP3	protein_coding	Human	3	8.9806
ENSG00000163993	ENSG00000163993	S100P	protein_coding	Human	4	6.6939
ENSG00000157404	ENSG00000157404	KIT	protein_coding	Human	4	54.6579
ENSG00000163739	ENSG00000163739	CXCL1	protein_coding	Human	4	73.8694
ENSG00000163734	ENSG00000163734	CXCL3	protein_coding	Human	4	74.0366
ENSG00000145675	ENSG00000145675	PIK3R1	protein_coding	Human	5	68.2158
ENSG00000111863	ENSG00000111863	ADTRP	protein_coding	Human	6	11.7121
ENSG00000078401	ENSG00000078401	EDN1	protein_coding	Human	6	12.2904
ENSG00000112769	ENSG00000112769	LAMA4	protein_coding	Human	6	112.1088
ENSG00000152661	ENSG00000152661	GJA1	protein_coding	Human	6	121.4356
ENSG00000136244	ENSG00000136244	IL6	protein_coding	Human	7	22.7259
ENSG00000075213	ENSG00000075213	SEMA3A	protein_coding	Human	7	83.9558
ENSG00000106366	ENSG00000106366	SERPINE1	protein_coding	Human	7	101.1271
ENSG00000105974	ENSG00000105974	CAV1	protein_coding	Human	7	116.5250
ENSG00000008853	ENSG00000008853	RHOBTB2	protein_coding	Human	8	22.9874
ENSG00000156735	ENSG00000156735	BAG4	protein_coding	Human	8	38.1765

Table A4-8 Significantly downregulated genes of the cell migration pathway

ENSG00000185900	ENSG00000185900	POMK	protein_coding	Human	8	43.0935
ENSG00000019549	ENSG00000019549	SNAI2	protein_coding	Human	8	48.9176
ENSG00000107201	ENSG00000107201	DDX58	protein_coding	Human	9	32.4553
ENSG00000155827	ENSG00000155827	RNF20	protein_coding	Human	9	101.5339
ENSG00000133818	ENSG00000133818	RRAS2	protein_coding	Human	11	14.2779
ENSG00000011405	ENSG00000011405	PIK3C2A	protein_coding	Human	11	17.0777
ENSG00000149177	ENSG00000149177	PTPRJ	protein_coding	Human	11	47.9806
ENSG00000196611	ENSG00000196611	MMP1	protein_coding	Human	11	102.7899
ENSG00000151491	ENSG00000151491	EPS8	protein_coding	Human	12	15.6201
ENSG00000181852	ENSG00000181852	RNF41	protein_coding	Human	12	56.2022
ENSG00000135679	ENSG00000135679	MDM2	protein_coding	Human	12	68.8082
ENSG00000090612	ENSG00000090612	ZNF268	protein_coding	Human	12	133.1814
ENSG00000140575	ENSG00000140575	IQGAP1	protein_coding	Human	15	90.3882
ENSG00000140443	ENSG00000140443	IGF1R	protein_coding	Human	15	98.6485
ENSG00000167193	ENSG00000167193	CRK	protein_coding	Human	17	1.4207
ENSG00000168961	ENSG00000168961	LGALS9	protein_coding	Human	17	27.6298
ENSG00000176749	ENSG00000176749	CDK5R1	protein_coding	Human	17	32.4870
ENSG00000186832	ENSG00000186832	KRT16	protein_coding	Human	17	41.6098
ENSG00000170558	ENSG00000170558	CDH2	protein_coding	Human	18	27.9510
ENSG00000183287	ENSG00000183287	CCBE1	protein_coding	Human	18	59.4309
ENSG00000167601	ENSG00000167601	AXL	protein_coding	Human	19	41.2192
ENSG00000101311	ENSG00000101311	FERMT1	protein_coding	Human	20	6.0748
ENSG00000124145	ENSG00000124145	SDC4	protein_coding	Human	20	45.3253
ENSG00000147010	ENSG00000147010	SH3KBP1	protein_coding	Human	X	19.5340
ENSG00000165240	ENSG00000165240	ATP7A	protein_coding	Human	X	77.9107
ENSG00000077264	ENSG00000077264	PAK3	protein_coding	Human	X	110.9443

Table A4-9 Significantly downregulated genes of the cell motility pathway

User ID	Ensembl Gene ID	Symbol	Gene type	Species	Chr	Position (Mbp)
ENSG00000171608	ENSG00000171608	PIK3CD	protein_coding	Human	1	9.6517
ENSG00000117525	ENSG00000117525	F3	protein_coding	Human	1	94.5292
ENSG00000155380	ENSG00000155380	SLC16A1	protein_coding	Human	1	112.9118
ENSG00000196754	ENSG00000196754	S100A2	protein_coding	Human	1	153.5611
ENSG00000162738	ENSG00000162738	VANGL2	protein_coding	Human	1	160.4006
ENSG00000158769	ENSG00000158769	F11R	protein_coding	Human	1	160.9952
ENSG00000174059	ENSG00000174059	CD34	protein_coding	Human	1	207.8810
ENSG00000152127	ENSG00000152127	MGAT5	protein_coding	Human	2	134.1200
ENSG00000115221	ENSG00000115221	ITGB6	protein_coding	Human	2	160.0997
ENSG00000196220	ENSG00000196220	SRGAP3	protein_coding	Human	3	8.9806
ENSG00000163993	ENSG00000163993	S100P	protein_coding	Human	4	6.6939
ENSG00000157404	ENSG00000157404	KIT	protein_coding	Human	4	54.6579
ENSG00000163739	ENSG00000163739	CXCL1	protein_coding	Human	4	73.8694
ENSG00000163734	ENSG00000163734	CXCL3	protein_coding	Human	4	74.0366
ENSG00000145675	ENSG00000145675	PIK3R1	protein_coding	Human	5	68.2158
ENSG00000119048	ENSG00000119048	UBE2B	protein_coding	Human	5	134.3712
ENSG00000111863	ENSG00000111863	ADTRP	protein_coding	Human	6	11.7121
ENSG00000078401	ENSG00000078401	EDN1	protein_coding	Human	6	12.2904
ENSG00000112769	ENSG00000112769	LAMA4	protein_coding	Human	6	112.1088
ENSG00000152661	ENSG00000152661	GJA1	protein_coding	Human	6	121.4356
ENSG00000136244	ENSG00000136244	IL6	protein_coding	Human	7	22.7259
ENSG00000075213	ENSG00000075213	SEMA3A	protein_coding	Human	7	83.9558
ENSG00000106366	ENSG00000106366	SERPINE1	protein_coding	Human	7	101.1271
ENSG00000105974	ENSG00000105974	CAV1	protein_coding	Human	7	116.5250

Table A4-9 Significantly downregulated genes of the cell motility pathway

ENSG00000008853	ENSG00000008853	RHOBTB2	protein_coding	Human	8	22.9874
ENSG00000156735	ENSG00000156735	BAG4	protein_coding	Human	8	38.1765
ENSG00000185900	ENSG00000185900	POMK	protein_coding	Human	8	43.0935
ENSG00000019549	ENSG00000019549	SNAI2	protein_coding	Human	8	48.9176
ENSG00000107201	ENSG00000107201	DDX58	protein_coding	Human	9	32.4553
ENSG00000155827	ENSG00000155827	RNF20	protein_coding	Human	9	101.5339
ENSG00000133818	ENSG00000133818	RRAS2	protein_coding	Human	11	14.2779
ENSG00000011405	ENSG00000011405	PIK3C2A	protein_coding	Human	11	17.0777
ENSG00000149177	ENSG00000149177	PTPRJ	protein_coding	Human	11	47.9806
ENSG00000196611	ENSG00000196611	MMP1	protein_coding	Human	11	102.7899
ENSG00000151491	ENSG00000151491	EPS8	protein_coding	Human	12	15.6201
ENSG00000181852	ENSG00000181852	RNF41	protein_coding	Human	12	56.2022
ENSG00000135679	ENSG00000135679	MDM2	protein_coding	Human	12	68.8082
ENSG00000090612	ENSG00000090612	ZNF268	protein_coding	Human	12	133.1814
ENSG00000140575	ENSG00000140575	IQGAP1	protein_coding	Human	15	90.3882
ENSG00000140443	ENSG00000140443	IGF1R	protein_coding	Human	15	98.6485
ENSG00000167193	ENSG00000167193	CRK	protein_coding	Human	17	1.4207
ENSG00000168961	ENSG00000168961	LGALS9	protein_coding	Human	17	27.6298
ENSG00000176749	ENSG00000176749	CDK5R1	protein_coding	Human	17	32.4870
ENSG00000186832	ENSG00000186832	KRT16	protein_coding	Human	17	41.6098
ENSG00000170558	ENSG00000170558	CDH2	protein_coding	Human	18	27.9510
ENSG00000183287	ENSG00000183287	CCBE1	protein_coding	Human	18	59.4309
ENSG00000167601	ENSG00000167601	AXL	protein_coding	Human	19	41.2192
ENSG00000101311	ENSG00000101311	FERMT1	protein_coding	Human	20	6.0748
ENSG00000124145	ENSG00000124145	SDC4	protein_coding	Human	20	45.3253
ENSG00000147010	ENSG00000147010	SH3KBP1	protein_coding	Human	X	19.5340

Table A4-9 Significantly downregulated genes of the cell motility pathway

ENSG00000165240	ENSG00000165240	ATP7A	protein_coding	Human	X	77.9107
ENSG00000077264	ENSG00000077264	PAK3	protein_coding	Human	X	110.9443

Table A4-10 Significantly downregulated genes of regulation of cellular component organization pathway

User ID	Ensembl Gene ID	Symbol	Gene Type	Species	Chr	Position (Mbp)
ENSG00000116213	ENSG00000116213	WRAP73	protein_coding	Human	1	3.6308
ENSG00000171612	ENSG00000171612	SLC25A33	protein_coding	Human	1	9.5395
ENSG00000117676	ENSG00000117676	RPS6KA1	protein_coding	Human	1	26.5298
ENSG00000116489	ENSG00000116489	CAPZA1	protein_coding	Human	1	112.6198
ENSG00000162738	ENSG00000162738	VANGL2	protein_coding	Human	1	160.4006
ENSG00000158769	ENSG00000158769	F11R	protein_coding	Human	1	160.9952
ENSG00000171055	ENSG00000171055	FEZ2	protein_coding	Human	2	36.5318
ENSG00000078018	ENSG00000078018	MAP2	protein_coding	Human	2	209.4241
ENSG00000197548	ENSG00000197548	ATG7	protein_coding	Human	3	11.2723
ENSG00000047849	ENSG00000047849	MAP4	protein_coding	Human	3	47.8507
ENSG00000163946	ENSG00000163946	TASOR	protein_coding	Human	3	56.6201
ENSG00000283154	ENSG00000283154	IQCJ-SCHIP1	protein_coding	Human	3	158.9622
ENSG00000121864	ENSG00000121864	ZNF639	protein_coding	Human	3	179.3230
ENSG00000175193	ENSG00000175193	PARL	protein_coding	Human	3	183.8293
ENSG00000109171	ENSG00000109171	SLAIN2	protein_coding	Human	4	48.3415
ENSG00000157404	ENSG00000157404	KIT	protein_coding	Human	4	54.6579
ENSG00000071539	ENSG00000071539	TRIP13	protein_coding	Human	5	0.8929
ENSG00000145675	ENSG00000145675	PIK3R1	protein_coding	Human	5	68.2158
ENSG00000172795	ENSG00000172795	DCP2	protein_coding	Human	5	112.9767
ENSG00000119048	ENSG00000119048	UBE2B	protein_coding	Human	5	134.3712

Table A4-10 Significantly downregulated genes of regulation of cellular component organization pathway

ENSG00000135083	ENSG00000135083	CCNJL	protein_coding	Human	5	160.2491
ENSG00000111863	ENSG00000111863	ADTRP	protein_coding	Human	6	11.7121
ENSG00000078401	ENSG00000078401	EDN1	protein_coding	Human	6	12.2904
ENSG00000008083	ENSG00000008083	JARID2	protein_coding	Human	6	15.2461
ENSG00000030110	ENSG00000030110	BAK1	protein_coding	Human	6	33.5725
ENSG00000112697	ENSG00000112697	TMEM30A	protein_coding	Human	6	75.2529
ENSG00000152661	ENSG00000152661	GJA1	protein_coding	Human	6	121.4356
ENSG00000146425	ENSG00000146425	DYNLT1	protein_coding	Human	6	158.6365
ENSG00000136244	ENSG00000136244	IL6	protein_coding	Human	7	22.7259
ENSG00000006451	ENSG00000006451	RALA	protein_coding	Human	7	39.6236
ENSG00000075213	ENSG00000075213	SEMA3A	protein_coding	Human	7	83.9558
ENSG00000106366	ENSG00000106366	SERPINE1	protein_coding	Human	7	101.1271
ENSG00000105974	ENSG00000105974	CAV1	protein_coding	Human	7	116.5250
ENSG00000008853	ENSG00000008853	RHOBTB2	protein_coding	Human	8	22.9874
ENSG00000156735	ENSG00000156735	BAG4	protein_coding	Human	8	38.1765
ENSG00000104365	ENSG00000104365	IKBKB	protein_coding	Human	8	42.2713
ENSG00000019549	ENSG00000019549	SNAI2	protein_coding	Human	8	48.9176
ENSG00000164754	ENSG00000164754	RAD21	protein_coding	Human	8	116.8459
ENSG00000155827	ENSG00000155827	RNF20	protein_coding	Human	9	101.5339
ENSG00000119392	ENSG00000119392	GLE1	protein_coding	Human	9	128.5047
ENSG00000148248	ENSG00000148248	SURF4	protein_coding	Human	9	133.3614
ENSG00000107643	ENSG00000107643	MAPK8	protein_coding	Human	10	48.3066
ENSG00000148677	ENSG00000148677	ANKRD1	protein_coding	Human	10	90.9121
ENSG00000107960	ENSG00000107960	STN1	protein_coding	Human	10	103.8776
ENSG00000165650	ENSG00000165650	PDZD8	protein_coding	Human	10	117.2773
ENSG00000135387	ENSG00000135387	CAPRIN1	protein_coding	Human	11	34.0517

Table A4-10 Significantly downregulated genes of regulation of cellular component organization pathway

ENSG00000134574	ENSG00000134574	DDB2	protein_coding	Human	11	47.2145
ENSG00000149177	ENSG00000149177	PTPRJ	protein_coding	Human	11	47.9806
ENSG00000184743	ENSG00000184743	ATL3	protein_coding	Human	11	63.6241
ENSG00000196611	ENSG00000196611	MMP1	protein_coding	Human	11	102.7899
ENSG00000110395	ENSG00000110395	CBL	protein_coding	Human	11	119.2063
ENSG00000151491	ENSG00000151491	EPS8	protein_coding	Human	12	15.6201
ENSG00000151239	ENSG00000151239	TWF1	protein_coding	Human	12	43.7937
ENSG00000181852	ENSG00000181852	RNF41	protein_coding	Human	12	56.2022
ENSG00000135679	ENSG00000135679	MDM2	protein_coding	Human	12	68.8082
ENSG00000089250	ENSG00000089250	NOS1	protein_coding	Human	12	117.2081
ENSG00000140575	ENSG00000140575	IQGAP1	protein_coding	Human	15	90.3882
ENSG00000140443	ENSG00000140443	IGF1R	protein_coding	Human	15	98.6485
ENSG00000102967	ENSG00000102967	DHODH	protein_coding	Human	16	72.0086
ENSG00000167193	ENSG00000167193	CRK	protein_coding	Human	17	1.4207
ENSG00000072849	ENSG00000072849	DERL2	protein_coding	Human	17	5.4713
ENSG00000176749	ENSG00000176749	CDK5R1	protein_coding	Human	17	32.4870
ENSG00000276293	ENSG00000276293	PIP4K2B	protein_coding	Human	17	38.7657
ENSG00000128422	ENSG00000128422	KRT17	protein_coding	Human	17	41.6194
ENSG00000108395	ENSG00000108395	TRIM37	protein_coding	Human	17	58.9826
ENSG00000168461	ENSG00000168461	RAB31	protein_coding	Human	18	9.7083
ENSG00000170558	ENSG00000170558	CDH2	protein_coding	Human	18	27.9510
ENSG00000197046	ENSG00000197046	SIGLEC15	protein_coding	Human	18	45.8255
ENSG00000167601	ENSG00000167601	AXL	protein_coding	Human	19	41.2192
ENSG00000078747	ENSG00000078747	ITCH	protein_coding	Human	20	34.3632
ENSG00000124145	ENSG00000124145	SDC4	protein_coding	Human	20	45.3253
ENSG00000197457	ENSG00000197457	STMN3	protein_coding	Human	20	63.6397

Table A4-10 Significantly downregulated genes of regulation of cellular component organization pathway

ENSG00000185721	ENSG00000185721	DRG1	protein_coding	Human	22	31.3995
ENSG00000101871	ENSG00000101871	MID1	protein_coding	Human	X	10.4453
ENSG00000147010	ENSG00000147010	SH3KBP1	protein_coding	Human	X	19.5340
ENSG00000165240	ENSG00000165240	ATP7A	protein_coding	Human	X	77.9107
ENSG00000077264	ENSG00000077264	PAK3	protein_coding	Human	X	110.9443
ENSG00000158290	ENSG00000158290	CUL4B	protein_coding	Human	X	120.5246

Table A4-11 Gene enrichment in ShinyGOv0.61 for significantly upregulated genes: siRNA vs siNEG

Enrichment FDR	Genes in list	Total genes	Functional Category
1.1E-05	17	268	Protein glycosylation
1.1E-05	17	268	Macromolecule glycosylation
1.3E-05	19	357	Glycoprotein biosynthetic process
1.3E-05	17	280	Glycosylation
2.0E-04	19	432	Glycoprotein metabolic process
1.6E-03	9	112	Protein O-linked glycosylation
3.9E-03	24	800	Carbohydrate derivative biosynthetic process
6.4E-03	10	172	Homophilic cell adhesion via plasma membrane adhesion molecules
2.3E-02	2	2	Trans-synaptic signaling by soluble gas, modulating synaptic transmission
2.3E-02	2	2	Trans-synaptic signaling by nitric oxide, modulating synaptic transmission
2.4E-02	34	1541	Cell adhesion
2.4E-02	34	1548	Biological adhesion
3.4E-02	6	77	Glycosphingolipid metabolic process
3.7E-02	23	922	Cell-cell adhesion

Table A4-11 Gene enrichment in ShinyGOv0.61 for significantly upregulated genes: siRNA vs siNEG

3.7E-02	2	3	Synaptic signaling by nitric oxide
3.7E-02	2	3	Trans-synaptic signaling by soluble gas
3.7E-02	2	3	Trans-synaptic signaling by nitric oxide
3.7E-02	3	13	Axo-dendritic protein transport
3.7E-02	3	13	Regulation of metallopeptidase activity
4.9E-02	29	1327	Carbohydrate derivative metabolic process

Table A4-12 Gene enrichment for upregulated pathways: siRNA v siNEG

GENE ENRICHMENT FOR UPREGULATED PATHWAYS: siRNA v siNEG														
	ENTIRE GENE LIST IN iDEP92						SIGNIFICANTLY UPREGULATED GENE LIST in ShinyGOv0.61							Matches
Pathway	# of Genes	DEGs	p adj	Total Genes	GSEA	padj	# of Our Genes	Total Genes	ShinyGO	FDR	# of Genes	STRING*	padj	4
Protein glycosylation	17	Y	2.9E-06	186	Y	0.0024	17	268	Y	0.000011	16	Y	0.000019	3
Glycoprotein biosynthetic process	19	Y	2.9E-06	241	Y	0.0024	19	357	Y	0.000013	16	Y	0.00011	2
Glycosylation	17	Y	2.9E-06	196	Y	0.0024	17	280	Y	0.000013	16	Y	0.000019	
Glycoprotein metabolic process	20	Y	0.000011	294	Y	0.0024	19	432	Y	0.0002	15	Y	0.0011	
Protein O-linked glycosylation	11	Y	0.000024	82	Y	0.0024	9	112	Y	0.0016	7	Y	0.0071	
Carbohydrate derivative biosynthetic process	24	Y	0.0011	N/A	N	N/A	24	800	Y	0.0039	19	Y	0.00096	
Cell adhesion	36	Y	0.0015	N/A	N	N/A	34	1541	Y	0.024	25	Y	0.00064	
Homophilic cell adhesion via plasma membrane adhesion molecules	10	Y	0.0023	91	Y	0.0024	10	172	Y	0.0064	10	Y	0.00056	
Cell-cell adhesion	25	Y	0.0044	N/A	N	N/A	23	922	Y	0.037	N/A	N	N/A	
Macromolecule glycosylation	N/A	N	N/A	186	Y	0.0024	N/A	N/A	N	N/A	N/A	N	N/A	
O-glycan processing	N/A	N	N/A	33	Y	0.011	N/A	N/A	N	N/A	N/A	N	N/A	
Aminoglycan metabolic process	N/A	N	N/A	109	Y	0.0024	N/A	N/A	N	N/A	N/A	N	N/A	
Aminoglycan biosynthetic process	N/A	N	N/A	77	Y	0.0041	N/A	N/A	N	N/A	N/A	N	N/A	
Protein mannosylation	N/A	N	N/A	21	Y	0.02	N/A	N/A	N	N/A	N/A	N	N/A	
Keratan sulfate metabolic process	N/A	N	N/A	24	Y	0.018	N/A	N/A	N	N/A	N/A	N	N/A	
Glycosaminoglycan metabolic process	N/A	N	N/A	104	Y	0.0024	N/A	N/A	N	N/A	N/A	N	N/A	
Peptidyl-proline hydroxylation	N/A	N	N/A	16	Y	0.019	N/A	N/A	N	N/A	N/A	N	N/A	
Glycosaminoglycan biosynthetic process	N/A	N	N/A	74	Y	0.003	N/A	N/A	N	N/A	N/A	N	N/A	
Protein transport within lipid bilayer	N/A	N	N/A	24	Y	0.022	N/A	N/A	N	N/A	N/A	N	N/A	
Glycolipid metabolic process	N/A	N	N/A	85	Y	0.0041	N/A	N/A	N	N/A	N/A	N	N/A	
Liposaccharide metabolic process	N/A	N	N/A	85	Y	0.0041	N/A	N/A	N	N/A	N/A	N	N/A	
Trans-synaptic signaling by soluble gas, modulating synaptic transmission	N/A	N	N/A	N/A	N	N/A	2	2	Y	0.023	N/A	N	N/A	
Trans-synaptic signaling by nitric oxide, modulating synaptic transmission	N/A	N	N/A	N/A	N	N/A	2	2	Y	0.023	N/A	N	N/A	
Glycosphingolipid metabolic process	N/A	N	N/A	N/A	N	N/A	6	77	Y	0.034	6	Y	0.0032	
Synaptic signaling by nitric oxide	N/A	N	N/A	N/A	N	N/A	2	3	Y	0.037	N/A	N	N/A	
Trans-synaptic signaling by soluble gas	N/A	N	N/A	N/A	N	N/A	2	3	Y	0.037	N/A	N	N/A	
Trans-synaptic signaling by nitric oxide	N/A	N	N/A	N/A	N	N/A	2	3	Y	0.037	N/A	N	N/A	
Axo-dendritic protein transport	N/A	N	N/A	N/A	N	N/A	3	13	Y	0.037	N/A	N	N/A	
Regulation of metallopeptidase activity	N/A	N	N/A	N/A	N	N/A	3	13	Y	0.037	N/A	N	N/A	
Carbohydrate derivative metabolic process	N/A	N	N/A	N/A	N	N/A	29	1327	Y	0.049	25	Y	0.00096	
biological adhesion	N/A	N	N/A	N/A	N	N/A	34	1548	Y	0.024	25	Y	0.00064	
single-organism carbohydrate metabolic process	N/A	N	N/A	N/A	N	N/A	N/A	N/A	N	N/A	18	Y	0.0018	
glycosphingolipid metabolic process	N/A	N	N/A	N/A	N	N/A	6	77	Y	0.034	6	Y	0.0032	
interaction with host	N/A	N	N/A	N/A	N	N/A	N/A	N/A	N	N/A	8	Y	0.0049	
cell-cell adhesion via plasma-membrane adhesion molecules	N/A	N	N/A	N/A	N	N/A	N/A	N/A	N	N/A	9	Y	0.0083	

Table A4-13 Significantly upregulated genes of the glycosylation pathway

User ID	Ensembl Gene ID	Symbol	Gene Type	Species	Chr	Position (Mbp)
ENSG00000176022	ENSG00000176022	B3GALT6	protein_coding	Human	1	1.2322
ENSG00000115525	ENSG00000115525	ST3GAL5	protein_coding	Human	2	85.8371
ENSG00000172986	ENSG00000172986	GXYLT2	protein_coding	Human	3	72.8881
ENSG00000172461	ENSG00000172461	FUT9	protein_coding	Human	6	96.0160
ENSG00000106392	ENSG00000106392	C1GALT1	protein_coding	Human	7	7.1569
ENSG00000215182	ENSG00000215182	MUC5AC	protein_coding	Human	11	1.1580
ENSG00000151348	ENSG00000151348	EXT2	protein_coding	Human	11	44.0955
ENSG00000165905	ENSG00000165905	LARGE2	protein_coding	Human	11	45.9216
ENSG00000174684	ENSG00000174684	B4GAT1	protein_coding	Human	11	66.3454
ENSG00000151233	ENSG00000151233	GXYLT1	protein_coding	Human	12	42.0818
ENSG00000179104	ENSG00000179104	TMTC2	protein_coding	Human	12	82.6869
ENSG00000100626	ENSG00000100626	GALNT16	protein_coding	Human	14	69.2593
ENSG00000186198	ENSG00000186198	SLC51B	protein_coding	Human	15	65.0454
ENSG00000196547	ENSG00000196547	MAN2A2	protein_coding	Human	15	90.9022
ENSG00000179913	ENSG00000179913	B3GNT3	protein_coding	Human	19	17.7948
ENSG00000183778	ENSG00000183778	B3GALT5	protein_coding	Human	21	39.5564
ENSG00000128242	ENSG00000128242	GAL3ST1	protein_coding	Human	22	30.5546

Table A4-14 Significantly upregulated genes of the homophilic cell adhesion via plasma membrane adhesion pathway

User ID	Ensembl Gene ID	Symbol	Gene Type	Species	Chr	Position (Mbp)
ENSG00000169851	ENSG00000169851	PCDH7	protein_coding	Human	4	30.7204
ENSG00000138650	ENSG00000138650	PCDH10	protein_coding	Human	4	133.1493
ENSG00000113209	ENSG00000113209	PCDHB5	protein_coding	Human	5	141.1352
ENSG00000113211	ENSG00000113211	PCDHB6	protein_coding	Human	5	141.1500
ENSG00000120322	ENSG00000120322	PCDHB8	protein_coding	Human	5	141.1778

Table A4-14 Significantly upregulated genes of the homophilic cell adhesion via plasma membrane adhesion pathway

ENSG00000204956	ENSG00000204956	PCDHGA1	protein_coding	Human	5	141.3306
ENSG00000165731	ENSG00000165731	RET	protein_coding	Human	10	43.0771
ENSG00000148600	ENSG00000148600	CDHR1	protein_coding	Human	10	84.1945
ENSG00000149573	ENSG00000149573	MPZL2	protein_coding	Human	11	118.2534
ENSG00000110400	ENSG00000110400	NECTIN1	protein_coding	Human	11	119.6234

Table A4-15 Significantly upregulated genes of the cell adhesion pathway

User ID	Ensembl Gene ID	Symbol	Gene Type	Species	Chr	Position (Mbp)
ENSG00000162552	ENSG00000162552	WNT4	protein_coding	Human	1	22.1173
ENSG00000171812	ENSG00000171812	COL8A2	protein_coding	Human	1	36.0952
ENSG00000162407	ENSG00000162407	PLPP3	protein_coding	Human	1	56.4948
ENSG00000117155	ENSG00000117155	SSX2IP	protein_coding	Human	1	84.6437
ENSG00000160712	ENSG00000160712	IL6R	protein_coding	Human	1	154.4052
ENSG00000138061	ENSG00000138061	CYP1B1	protein_coding	Human	2	38.0670
ENSG00000169604	ENSG00000169604	ANTXR1	protein_coding	Human	2	69.0132
ENSG00000153094	ENSG00000153094	BCL2L11	protein_coding	Human	2	111.1194
ENSG00000115232	ENSG00000115232	ITGA4	protein_coding	Human	2	181.4572
ENSG00000114948	ENSG00000114948	ADAM23	protein_coding	Human	2	206.4435
ENSG00000090539	ENSG00000090539	CHRD	protein_coding	Human	3	184.3801
ENSG00000185621	ENSG00000185621	LMLN	protein_coding	Human	3	197.9602
ENSG00000169851	ENSG00000169851	PCDH7	protein_coding	Human	4	30.7204
ENSG00000138650	ENSG00000138650	PCDH10	protein_coding	Human	4	133.1493
ENSG00000164171	ENSG00000164171	ITGA2	protein_coding	Human	5	52.9893
ENSG00000113209	ENSG00000113209	PCDHB5	protein_coding	Human	5	141.1352
ENSG00000113211	ENSG00000113211	PCDHB6	protein_coding	Human	5	141.1500
ENSG00000120322	ENSG00000120322	PCDHB8	protein_coding	Human	5	141.1778

Table A4-15 Significantly upregulated genes of the cell adhesion pathway

ENSG00000204956	ENSG00000204956	PCDHGA1	protein_coding	Human	5	141.3306
ENSG00000242574	ENSG00000242574	HLA-DMB	protein_coding	Human	6	32.9346
ENSG00000010810	ENSG00000010810	FYN	protein_coding	Human	6	111.6603
ENSG00000106211	ENSG00000106211	HSPB1	protein_coding	Human	7	76.3027
ENSG00000008277	ENSG00000008277	ADAM22	protein_coding	Human	7	87.9341
ENSG00000136999	ENSG00000136999	CCN3	protein_coding	Human	8	119.4164
ENSG00000153310	ENSG00000153310	FAM49B	protein_coding	Human	8	129.8396
ENSG00000165731	ENSG00000165731	RET	protein_coding	Human	10	43.0771
ENSG00000148600	ENSG00000148600	CDHR1	protein_coding	Human	10	84.1945
ENSG00000149573	ENSG00000149573	MPZL2	protein_coding	Human	11	118.2534
ENSG00000110400	ENSG00000110400	NECTIN1	protein_coding	Human	11	119.6234
ENSG00000149557	ENSG00000149557	FEZ1	protein_coding	Human	11	125.4429
ENSG00000135424	ENSG00000135424	ITGA7	protein_coding	Human	12	55.6846
ENSG00000108797	ENSG00000108797	CNTNAP1	protein_coding	Human	17	42.6825
ENSG00000146938	ENSG00000146938	NLGN4X	protein_coding	Human	X	5.8406
ENSG00000101955	ENSG00000101955	SRPX	protein_coding	Human	X	38.1493

UNT+P v UNT

Table A4-16 Enriched pathways in DEGs: UNT+P v UNT

Direction	adj.Pval	nGenes	Pathways
Up regulated	5.1e-05	19	Tissue development
	9.2e-05	24	Animal organ development
	1.2e-04	15	Cell migration
	1.2e-04	10	Positive regulation of locomotion
	2.1e-04	9	Positive regulation of cell migration

Table A4-16 Enriched pathways in DEGs: UNT+P v UNT

	2.1e-04	16	Locomotion
	2.1e-04	12	Regulation of locomotion
	2.3e-04	11	Regulation of cell migration
	2.3e-04	12	Circulatory system development
	3.3e-04	12	Anatomical structure formation involved in morphogenesis

Table A4-17 Top genes for the selected comparison: UNT+P v UNT

Ensembl ID	log2 Fold Change	Adj.Pval	Symbol	Chr	Type
ENSG00000225067	-2.55	3.85e-03	RPL23AP2;	19p13.12	processed_pseudogene
ENSG00000164283	2.51	2.70e-04	ESM1;ESM1	5q11.2	protein_coding
ENSG00000144583	2.20	1.71e-02	MARCHF4;MARCH4	2q35	protein_coding
ENSG00000141469	-2.17	5.83e-04	SLC14A1;SLC14A1JK	18q12.3	protein_coding
ENSG00000141469	-2.17	5.83e-04	SLC14A1;SLC14A1	18q12.3	protein_coding
ENSG00000101198	2.05	2.74e-02	NKAIN4;NKAIN4	20q13.33	protein_coding
ENSG00000213030	1.98	6.43e-06	CGB8;CGB3	19q13.33	protein_coding
ENSG00000123977	1.96	3.85e-03	DAW1;DAW1	2q36.3	protein_coding
ENSG00000100604	-1.94	5.99e-04	CHGA;CHGA	14q32.12	protein_coding
ENSG00000269706	1.92	3.72e-03	;	19q13.33	unprocessed_pseudogene
ENSG00000214814	-1.81	2.90e-03	FER1L6;FER1L6	8q24.13	protein_coding
ENSG00000273760	1.71	4.05e-03	;	10q11.22	lncRNA

Table A4-17 Top genes for the selected comparison: UNT+P v UNT

ENSG00000103740	-1.64	1.09e-02	ACSBG1;ACSBG1	15q25.1	protein_coding
ENSG00000189052	1.63	1.04e-02	CGB5;CGB3	19q13.33	protein_coding
ENSG00000086570	-1.50	4.47e-02	FAT2;FAT2	5q33.1	protein_coding
ENSG00000283930	-1.48	1.20e-02	;	10p11.1	protein_coding
ENSG00000015568	1.47	1.89e-02	RGPD5;RGPD8	2q13	protein_coding
ENSG00000015568	1.47	1.89e-02	RGPD5;RGPD5	2q13	protein_coding
ENSG00000015568	1.47	1.89e-02	RGPD5;RGPD6	2q13	protein_coding
ENSG00000015568	1.47	1.89e-02	RGPD5;HEL161	2q13	protein_coding
ENSG00000276850	1.43	3.45e-02	;	10q11.22	lncRNA
ENSG00000128422	1.40	4.40e-03	KRT17;KRT17	17q21.2	protein_coding
ENSG00000106541	-1.33	1.43e-02	AGR2;AGR2	7p21.1	protein_coding
ENSG00000250697	1.32	3.93e-02	;	5p13.3	lncRNA
ENSG00000134321	-1.28	4.87e-02	RSAD2;RSAD2	2p25.2	protein_coding
ENSG00000156466	1.26	2.56e-02	GDF6;GDF6	8q22.1	protein_coding
ENSG00000228158	1.25	1.32e-02	TLE1P1;	Xq12	processed_pseudogene
ENSG00000244468	-1.25	6.81e-04	;	3q25.1	lncRNA
ENSG00000148677	1.25	1.11e-02	ANKRD1;ANKRD1	10q23.31	protein_coding
ENSG00000267453	1.24	1.63e-02	CLEC4O;	19p13.12	transcribed_unprocessed_pseudogene

Table A4-17 Top genes for the selected comparison: UNT+P v UNT

ENSG00000136960	-1.21	5.61e-03	ENPP2;ENPP2	8q24.12	protein_coding
ENSG00000148344	1.19	9.91e-03	PTGES;PTGES	9q34.11	protein_coding
ENSG00000171631	1.19	1.34e-04	P2RY6;P2RY6	11q13.4	protein_coding
ENSG00000180638	-1.18	2.90e-02	SLC47A2;SLC47A2	17p11.2	protein_coding
ENSG00000149596	1.13	1.14e-02	JPH2;JPH2	20q13.12	protein_coding
ENSG00000109107	-1.12	4.14e-05	ALDOC;ALDOC	17q11.2	protein_coding
ENSG00000187800	1.11	5.83e-04	PEAR1;PEAR1	1q23.1	protein_coding
ENSG00000149591	1.11	2.61e-13	TAGLN;DKFZp686P11128	11q23.3	protein_coding
ENSG00000149591	1.11	2.61e-13	TAGLN;TAGLN	11q23.3	protein_coding
ENSG00000186897	-1.11	1.11e-02	C1QL4;ADIK	12q13.12	protein_coding
ENSG00000186897	-1.11	1.11e-02	C1QL4;C1QL4	12q13.12	protein_coding
ENSG00000124102	1.10	4.62e-02	PI3;PI3	20q13.12	protein_coding
ENSG00000108602	-1.09	1.40e-09	ALDH3A1;ALDH3A1	17p11.2	protein_coding
ENSG00000115590	-1.04	2.61e-04	IL1R2;IL1R2	2q11.2	protein_coding
ENSG00000135480	1.04	3.81e-08	KRT7;KRT7	12q13.13	protein_coding
ENSG00000103742	1.04	1.53e-02	IGDCC4;IGDCC4	15q22.31	protein_coding
ENSG00000163283	-1.03	4.71e-02	ALPP;ALPP	2q37.1	protein_coding
ENSG00000125148	1.03	3.26e-02	MT2A;MT2A	16q13	protein_coding

Table A4-17 Top genes for the selected comparison: UNT+P v UNT

ENSG00000106366	1.03	8.57e-06	SERPINE1;SERPINE1	7q22.1	protein_coding
ENSG00000197635	-1.02	4.66e-06	DPP4;DPP4	2q24.2	protein_coding

Table A4-18 Gene set enrichment analysis (GSEA): UNT+P vs UNT

Direction	GSEA analysis: UNTP vs UNT	NES	Genes	adj.Pval
Down	Cholesterol biosynthetic process	-2.1659	56	2.2e-03
	Cholesterol metabolic process	-2.1474	104	2.2e-03
	Sterol metabolic process	-2.1131	113	2.2e-03
	Triglyceride metabolic process	-2.1	58	2.2e-03
	Steroid metabolic process	-2.0861	204	2.2e-03
	Response to type I interferon	-2.0701	76	2.2e-03
	Bile acid and bile salt transport	-2.069	15	2.2e-03
	Type I interferon signaling pathway	-2.062	72	2.2e-03
	Cellular response to type I interferon	-2.062	72	2.2e-03
	Secondary alcohol metabolic process	-2.0597	108	2.2e-03
	Organic hydroxy compound transport	-2.0493	133	2.2e-03
	Secondary alcohol biosynthetic process	-2.0463	57	2.2e-03
	Sterol biosynthetic process	-2.0273	61	2.2e-03
Up	DNA-dependent DNA replication	2.2329	143	2.2e-03
	Cardiac muscle tissue morphogenesis	2.2285	36	2.2e-03
	Nucleoside biosynthetic process	2.184	37	2.2e-03

Table A4-18 Gene set enrichment analysis (GSEA): UNT+P vs UNT

	Glycosyl compound biosynthetic process	2.1726	41	2.2e-03
	SRP-dependent cotranslational protein targeting to membrane	2.168	95	2.2e-03
	Cell cycle DNA replication	2.1441	60	2.2e-03
	Nuclear DNA replication	2.1364	56	2.2e-03
	Nuclear-transcribed mRNA catabolic process, nonsense-mediated decay	2.1321	118	2.2e-03
	Pyrimidine nucleoside biosynthetic process	2.0917	25	3.7e-03
	DNA strand elongation	2.08	27	3.2e-03
	Ribonucleoside biosynthetic process	2.075	29	3.2e-03
	Interstrand cross-link repair	2.0642	52	2.7e-03
	DNA replication initiation	2.0449	39	4.5e-03
	Negative regulation of interferon-gamma production	2.0397	15	4.9e-03
	Muscle tissue morphogenesis	2.0171	43	4.5e-03
	Cotranslational protein targeting to membrane	2.0088	99	2.2e-03
	Cellular response to retinoic acid	2.0004	45	3.8e-03

Table A4-19 Enriched pathways for each cluster in Fig. 4.40

Cluster	adj.Pval	nGenes	Pathways
B	5.6e-05	19	Circulatory system process
	5.6e-05	19	Blood circulation
	1.1e-04	19	Regulation of system process
	1.1e-04	54	Regulation of multicellular organismal process
	1.1e-04	63	Regulation of biological quality
	2.6e-04	34	Ion transport
	4.0e-04	12	Heart contraction
	4.1e-04	12	Heart process
	4.1e-04	36	Regulation of transport
	4.1e-04	22	Inorganic ion transmembrane transport
	4.9e-04	11	Regulation of heart contraction
	4.9e-04	26	Ion transmembrane transport
	4.9e-04	12	Regulation of blood circulation
	5.4e-04	10	Multicellular organismal signaling
	1.3e-03	25	Chemical homeostasis
C	4.7e-21	17	Sterol biosynthetic process
	2.0e-20	16	Cholesterol biosynthetic process
	5.1e-20	20	Sterol metabolic process
	1.0e-19	19	Cholesterol metabolic process
	2.6e-19	24	Steroid metabolic process
	8.9e-19	28	Organic hydroxy compound metabolic process
	1.7e-18	17	Regulation of steroid metabolic process
	3.5e-17	19	Steroid biosynthetic process
	3.5e-17	15	Regulation of steroid biosynthetic process
	4.7e-17	23	Alcohol metabolic process

Table A4-19 Enriched pathways for each cluster in Fig. 4.40

	4.8e-17	13	ARegulation of cholesterol metabolic process
	9.7e-17	12	Regulation of cholesterol biosynthetic process
D	6.5e-05	13	Cytokine-mediated signaling pathway
	6.5e-05	15	Cellular response to cytokine stimulus
	1.2e-04	20	Immune response
	1.2e-04	13	Response to external biotic stimulus
	1.9e-04	8	Response to virus
	4.2e-04	11	Inflammatory response
	4.2e-04	22	Cellular response to chemical stimulus
	4.2e-04	5	Negative regulation of viral life cycle
	4.3e-04	21	Cell surface receptor signaling pathway
	4.8e-04	5	Neutrophil chemotaxis
	6.3e-04	8	Regulation of multi-organism process
	6.3e-04	6	Negative regulation of multi-organism process
E	1.8e-10	47	Tissue development
	6.4e-08	64	Cell differentiation
	6.4e-08	58	Animal organ development
	3.5e-07	64	Cellular developmental process
	5.2e-07	33	Cell adhesion
	2.1e-06	45	Anatomical structure morphogenesis
	2.6e-06	17	Extracellular structure organization
	8.2e-06	26	Anatomical structure formation involved in morphogenesis
	8.3e-06	25	Circulatory system development
	9.5e-06	15	Extracellular matrix organization
	9.8e-06	21	Regulation of cell adhesion
	1.2e-05	18	Positive regulation of locomotion

Table A4-19 Enriched pathways for each cluster in Fig. 4.40

	1.3e-05	28	Epithelium development
	1.3e-05	17	Positive regulation of cell migration
F	8.9e-05	5	Acute-phase response
	8.9e-05	14	Inflammatory response
	8.9e-05	27	Response to organic substance
	8.9e-05	14	Response to lipid
	8.9e-05	27	Cellular response to chemical stimulus
	8.9e-05	8	Cellular response to molecule of bacterial origin
	8.9e-05	24	Cellular response to organic substance
	1.2e-04	6	Neutrophil chemotaxis
	1.2e-04	25	Cell surface receptor signaling pathway
	1.2e-04	10	Leukocyte migration
	1.3e-04	30	Response to stress
	1.3e-04	13	Cytokine-mediated signaling pathway
	1.3e-04	15	Cellular response to cytokine stimulus

Table A4-20 Enrichment in ShinyGO for upregulated genes: UNT+P v UNT

Enrichment FDR	Genes in list	Total genes	Functional Category
8.9E-04	19	2168	Tissue development
8.9E-04	10	576	Positive regulation of locomotion
1.0E-03	9	544	Positive regulation of cell motility
1.0E-03	15	1506	Cell migration
1.0E-03	11	883	Regulation of cell migration
1.0E-03	9	521	Positive regulation of cell migration
1.0E-03	5	117	Sprouting angiogenesis
1.0E-03	5	123	Chondrocyte differentiation
1.0E-03	12	1041	Regulation of locomotion
1.0E-03	24	3779	Animal organ development
1.0E-03	15	1670	Cell motility
1.0E-03	9	558	Positive regulation of cellular component movement
1.0E-03	15	1670	Localization of cell
1.0E-03	5	125	Cornification
1.0E-03	12	1077	Circulatory system development
1.1E-03	16	1921	Locomotion
1.3E-03	6	225	Regulation of chemotaxis
1.3E-03	11	946	Regulation of cell motility
1.7E-03	12	1164	Anatomical structure formation involved in morphogenesis
1.8E-03	5	148	Positive regulation of chemotaxis
1.8E-03	3	27	Positive regulation of hemostasis
1.8E-03	3	27	Positive regulation of blood coagulation
1.8E-03	8	511	Angiogenesis
1.8E-03	4	79	Regulation of blood coagulation

Table A4-20 Enrichment in ShinyGO for upregulated genes: UNT+P v UNT

1.8E-03	3	28	Positive regulation of coagulation
1.8E-03	4	80	Regulation of hemostasis
1.8E-03	11	1028	Regulation of cellular component movement
1.9E-03	5	166	Regulation of response to wounding
1.9E-03	7	392	Extracellular matrix organization
1.9E-03	5	167	Positive regulation of angiogenesis

Table A4-21 Gene enrichment for upregulated pathways: UNT+P v UNT

GENE ENRICHMENT FOR UPREGULATED PATHWAYS: UNT+P v UNT													
	ALL GENES IN iDEP92						SIGNIFICANTLY UPREGULATED GENE LIST IN ShinyGOv0.61						
Pathway	# of genes	DEGs	p adj	Total Genes	GSEA	padj	# of Our Genes	Total Genes	ShinyGO	FDR	# of Genes	STRING	padj
Tissue development	19	Y	0.000051	N/A	N	N/A	19	2168	Y	0.00089	N/A	N	N/A
Animal organ development	24	Y	0.000092	N/A	N	N/A	24	3779	Y	0.001	N/A	N	N/A
Cell migration	15	Y	0.00012	N/A	N	N/A	15	1506	Y	0.001	N/A	N	N/A
Positive regulation of locomotion	10	Y	0.00012	N/A	N	N/A	10	576	Y	0.00089	9	Y	0.000013
Positive regulation of cell migration	9	Y	0.00021	N/A	N	N/A	9	521	Y	0.001	8	Y	0.00007
Locomotion	16	Y	0.00021	N/A	N	N/A	16	1921	Y	0.0011	N/A	N	N/A
Regulation of locomotion	12	Y	0.00021	N/A	N	N/A	12	1041	Y	0.001	10	Y	0.00007
Regulation of cell migration	11	Y	0.00023	N/A	N	N/A	11	883	Y	0.001	9	Y	0.0002
Circulatory system development	12	Y	0.00023	N/A	N	N/A	12	1077	Y	0.001	9	Y	0.00075
Anatomical structure formation involved in morphogenesis	12	Y	0.00033	N/A	N	N/A	12	1164	Y	0.0017	N/A	N	N/A
DNA-dependent DNA replication	N/A	N	N/A	143	Y	0.0022	N/A	N/A	N	N/A	N/A	N	N/A
Cardiac muscle tissue morphogenesis	N/A	N	N/A	36	Y	0.0022	N/A	N/A	N	N/A	N/A	N	N/A
Nucleoside biosynthetic process	N/A	N	N/A	37	Y	0.0022	N/A	N/A	N	N/A	N/A	N	N/A
Glycosyl compound biosynthetic process	N/A	N	N/A	41	Y	0.0022	N/A	N/A	N	N/A	N/A	N	N/A
SRP-dependent cotranslational protein targeting to membrane	N/A	N	N/A	95	Y	0.0022	N/A	N/A	N	N/A	N/A	N	N/A
Cell cycle DNA replication	N/A	N	N/A	60	Y	0.0022	N/A	N/A	N	N/A	N/A	N	N/A
Nuclear DNA replication	N/A	N	N/A	56	Y	0.0022	N/A	N/A	N	N/A	N/A	N	N/A
Nuclear-transcribed mRNA catabolic process, nonsense-mediated decay	N/A	N	N/A	118	Y	0.0022	N/A	N/A	N	N/A	N/A	N	N/A
Pyrimidine nucleoside biosynthetic process	N/A	N	N/A	25	Y	0.0037	N/A	N/A	N	N/A	N/A	N	N/A
DNA strand elongation	N/A	N	N/A	27	Y	0.0032	N/A	N/A	N	N/A	N/A	N	N/A
Ribonucleoside biosynthetic process	N/A	N	N/A	29	Y	0.0032	N/A	N/A	N	N/A	N/A	N	N/A
Interstrand cross-link repair	N/A	N	N/A	52	Y	0.0027	N/A	N/A	N	N/A	N/A	N	N/A
DNA replication initiation	N/A	N	N/A	39	Y	0.0045	N/A	N/A	N	N/A	N/A	N	N/A
Negative regulation of interferon-gamma production	N/A	N	N/A	15	Y	0.0049	N/A	N/A	N	N/A	N/A	N	N/A
Muscle tissue morphogenesis	N/A	N	N/A	43	Y	0.0045	N/A	N/A	N	N/A	N/A	N	N/A
Cotranslational protein targeting to membrane	N/A	N	N/A	99	Y	0.0022	N/A	N/A	N	N/A	N/A	N	N/A
Cellular response to retinoic acid	N/A	N	N/A	45	Y	0.0038	N/A	N/A	N	N/A	N/A	N	N/A
Positive regulation of cell motility	N/A	N	N/A	N/A	N	N/A	9	544	Y	0.001	8	Y	0.00007
Sprouting angiogenesis	N/A	N	N/A	N/A	N	N/A	5	117	Y	0.001	4	Y	0.00022
Chondrocyte differentiation	N/A	N	N/A	N/A	N	N/A	5	123	Y	0.001	N/A	N	N/A
Cell motility	N/A	N	N/A	N/A	N	N/A	15	1670	Y	0.001	N/A	N	N/A
Positive regulation of cellular component movement	N/A	N	N/A	N/A	N	N/A	9	558	Y	0.001	8	Y	0.00007
Localization of cell	N/A	N	N/A	N/A	N	N/A	15	1670	Y	0.001	N/A	N	N/A
Cornification	N/A	N	N/A	N/A	N	N/A	5	125	Y	0.001	N/A	N	N/A
Regulation of chemotaxis	N/A	N	N/A	N/A	N	N/A	6	225	Y	0.0013	5	Y	0.00063
Positive regulation of chemotaxis	N/A	N	N/A	N/A	N	N/A	5	148	Y	0.0018	5	Y	0.00027
Positive regulation of hemostasis	N/A	N	N/A	N/A	N	N/A	3	27	Y	0.0018	3	Y	0.0008
Positive regulation of blood coagulation	N/A	N	N/A	N/A	N	N/A	3	27	Y	0.0018	3	Y	0.0008
Angiogenesis	N/A	N	N/A	N/A	N	N/A	8	511	Y	0.0018	N/A	N	N/A
Regulation of blood coagulation	N/A	N	N/A	N/A	N	N/A	4	79	Y	0.0018	N/A	N	N/A
Positive regulation of coagulation	N/A	N	N/A	N/A	N	N/A	3	28	Y	0.0018	3	Y	0.00095
Regulation of hemostasis	N/A	N	N/A	N/A	N	N/A	4	80	Y	0.0018	N/A	N	N/A
Regulation of cellular component movement	N/A	N	N/A	N/A	N	N/A	11	1028	Y	0.0018	9	Y	0.00043
Regulation of response to wounding	N/A	N	N/A	N/A	N	N/A	5	166	Y	0.0019	N/A	N	N/A
Extracellular matrix organization	N/A	N	N/A	N/A	N	N/A	7	392	Y	0.0019	N/A	N	N/A
Positive regulation of angiogenesis	N/A	N	N/A	N/A	N	N/A	5	167	Y	0.0019	N/A	N	N/A
regulation of multicellular organismal development	N/A	N	N/A	N/A	N	N/A	N/A	N/A	N	N/A	16	Y	4.1E-06
positive regulation of cellular component movement	N/A	N	N/A	N/A	N	N/A	9	558	Y	0.001	8	Y	0.00007
positive regulation of developmental process	N/A	N	N/A	N/A	N	N/A	N/A	N/A	N	N/A	12	Y	0.00007
regulation of cell motility	N/A	N	N/A	N/A	N	N/A	11	946	Y	0.0013	9	Y	0.00027
positive regulation of multicellular organismal process	N/A	N	N/A	N/A	N	N/A	N/A	N/A	N	N/A	12	Y	0.00028
positive regulation of behavior	N/A	N	N/A	N/A	N	N/A	N/A	N/A	N	N/A	5	Y	0.00043
cardiovascular system development	N/A	N	N/A	N/A	N	N/A	N/A	N/A	N	N/A	9	Y	0.00075
response to inorganic substance	N/A	N	N/A	N/A	N	N/A	N/A	N/A	N	N/A	7	Y	0.0008
response to metal ion	N/A	N	N/A	N/A	N	N/A	N/A	N/A	N	N/A	6	Y	0.00095
apoptotic cell clearance	N/A	N	N/A	N/A	N	N/A	N/A	N/A	N	N/A	3	Y	0.0011
regulation of response to external stimulus	N/A	N	N/A	N/A	N	N/A	N/A	N/A	N	N/A	9	Y	0.0011
regulation of angiogenesis	N/A	N	N/A	N/A	N	N/A	N/A	N/A	N	N/A	5	Y	0.0018
regulation of behavior	N/A	N	N/A	N/A	N	N/A	N/A	N/A	N	N/A	5	Y	0.0018
negative regulation of plasminogen activation	N/A	N	N/A	N/A	N	N/A	N/A	N/A	N	N/A	2	Y	0.0019
regulation of cytokine production	N/A	N	N/A	N/A	N	N/A	N/A	N/A	N	N/A	7	Y	0.0019

Matches
4
3
2

Table A4-22 Significantly upregulated genes of the anatomical structure formation involved in morphogenesis pathway

User ID	Ensembl Gene ID	Symbol	Gene Type	Species	Chr	Position (Mbp)
User ID	Ensembl Gene ID	Symbol	Gene Type	Species	Chr	Position (Mbp)
ENSG00000117525	ENSG00000117525	F3	protein_coding	Human	1	94.5292
ENSG00000114270	ENSG00000114270	COL7A1	protein_coding	Human	3	48.5641
ENSG00000164283	ENSG00000164283	ESM1	protein_coding	Human	5	54.9779
ENSG00000111863	ENSG00000111863	ADTRP	protein_coding	Human	6	11.7121
ENSG00000106366	ENSG00000106366	SERPINE1	protein_coding	Human	7	101.1271
ENSG00000134013	ENSG00000134013	LOXL2	protein_coding	Human	8	23.2972
ENSG00000019549	ENSG00000019549	SNAI2	protein_coding	Human	8	48.9176
ENSG00000148677	ENSG00000148677	ANKRD1	protein_coding	Human	10	90.9121
ENSG00000137801	ENSG00000137801	THBS1	protein_coding	Human	15	39.5811
ENSG00000140416	ENSG00000140416	TPM1	protein_coding	Human	15	63.0426
ENSG00000176170	ENSG00000176170	SHPK1	protein_coding	Human	17	76.3766

Table A4-23 Significantly upregulated genes of the cell migration pathway

User ID	Ensembl Gene ID	Symbol	Gene Type	Species	Chr	Position (Mbp)
ENSG00000142949	ENSG00000142949	PTPRF	protein_coding	Human	1	43.5252
ENSG00000117407	ENSG00000117407	ARTN	protein_coding	Human	1	43.9333
ENSG00000117525	ENSG00000117525	F3	protein_coding	Human	1	94.5292
ENSG00000079308	ENSG00000079308	TNS1	protein_coding	Human	2	217.7996
ENSG00000111863	ENSG00000111863	ADTRP	protein_coding	Human	6	11.7121
ENSG00000106366	ENSG00000106366	SERPINE1	protein_coding	Human	7	101.1271
ENSG00000134013	ENSG00000134013	LOXL2	protein_coding	Human	8	23.2972
ENSG00000019549	ENSG00000019549	SNAI2	protein_coding	Human	8	48.9176
ENSG00000171631	ENSG00000171631	P2RY6	protein_coding	Human	11	73.2645
ENSG00000183087	ENSG00000183087	GAS6	protein_coding	Human	13	113.8205

Table A4-23 Significantly upregulated genes of the cell migration pathway

ENSG00000137801	ENSG00000137801	THBS1	protein_coding	Human	15	39.5811
ENSG00000140416	ENSG00000140416	TPM1	protein_coding	Human	15	63.0426
ENSG00000138623	ENSG00000138623	SEMA7A	protein_coding	Human	15	74.4093
ENSG00000176170	ENSG00000176170	SHPK1	protein_coding	Human	17	76.3766
ENSG00000183287	ENSG00000183287	CCBE1	protein_coding	Human	18	59.4309

Table A4-24 Significantly upregulated genes of the angiogenesis pathway

User ID	Ensembl Gene ID	Symbol	Gene Type	Species	Chr	Position (Mbp)
ENSG00000117525	ENSG00000117525	F3	protein_coding	Human	1	94.5292
ENSG00000164283	ENSG00000164283	ESM1	protein_coding	Human	5	54.9779
ENSG00000111863	ENSG00000111863	ADTRP	protein_coding	Human	6	11.7121
ENSG00000106366	ENSG00000106366	SERPINE1	protein_coding	Human	7	101.1271
ENSG00000134013	ENSG00000134013	LOXL2	protein_coding	Human	8	23.2972
ENSG00000137801	ENSG00000137801	THBS1	protein_coding	Human	15	39.5811
ENSG00000176170	ENSG00000176170	SHPK1	protein_coding	Human	17	76.3766
ENSG00000183287	ENSG00000183287	CCBE1	protein_coding	Human	18	59.4309

siRNA+P v siRNA

Table A4-25 Top Genes for selected comparison: siRNA+P v siRNA

Ensembl ID	log2 Fold Change	Adj.Pval	Symbol	Chr	Type
ENSG00000108342	2.38	1.86e-03	CSF3;CSF3	17q21.1	Protein coding
ENSG00000189052	1.83	4.27e-03	CGB5;CGB3	19q13.33	protein_coding
ENSG00000213030	1.43	1.52e-02	CGB8;CGB3	19q13.33	protein_coding
ENSG00000101198	1.31	2.59e-03	NKAIN4;NKAIN4	20q13.33	protein_coding

Table A4-25 Top Genes for selected comparison: siRNA+P v siRNA

ENSG00000171631	1.30	4.27e-03	P2RY6;P2RY6	11q13.4	protein_coding
ENSG00000242574	-1.10	3.41e-04	HLA-DMB;HLA-DMB	6p21.32	protein_coding
ENSG00000108602	-0.95	5.12e-06	ALDH3A1;ALDH3A1	17p11.2	protein_coding
ENSG00000197635	-0.91	2.82e-04	DPP4;DPP4	2q24.2	protein_coding
ENSG00000180638	-0.88	3.13e-02	SLC47A2;SLC47A2	17p11.2	protein_coding
ENSG00000149591	0.83	1.23e-05	TAGLN;TAGLN	11q23.3	protein_coding
ENSG00000149591	0.83	1.23e-05	TAGLN;DKFZp686P11128	11q23.3	protein_coding
ENSG00000162591	-0.83	3.41e-04	MEGF6;MEGF6	1p36.32	protein_coding
ENSG00000198732	0.81	3.13e-02	SMOC1;SMOC1	14q24.2	protein_coding
ENSG00000128422	0.81	4.27e-03	KRT17;KRT17	17q21.2	protein_coding
ENSG00000137648	-0.77	2.55e-02	TMPRSS4;TMPRSS4	11q23.3	protein_coding
ENSG00000120708	0.74	4.27e-03	TGFBI;TGFBI	5q31.1	protein_coding
ENSG00000124225	0.69	1.86e-03	PMEPA1;PMEPA1	20q13.31	protein_coding
ENSG00000124225	0.69	1.86e-03	PMEPA1;TMEPAI	20q13.31	protein_coding
ENSG00000105825	0.61	9.09e-03	TFPI2;TFPI2	7q21.3	protein_coding

Table A4-26 Cluster analysis: siRNA+P v siRNA

Cluster	adj.Pval	nGenes	Pathways
A	5.6e-06	5	Response to type I interferon
	5.6e-06	5	Type I interferon signaling pathway
	6.4e-06	6	Defense response to virus
	1.6e-05	4	Negative regulation of viral genome replication
	2.0e-05	7	Defense response to other organism
	5.3e-05	8	Response to external biotic stimulus
	2.3e-04	8	Immune effector process

Table A4-26 Cluster analysis: siRNA+P v siRNA

B	7.8e-03	3	Regulation of chemotaxis
	9.0e-03	4	Regulation of response to external stimulus
	9.0e-03	3	Positive regulation of response to external stimulus
	9.0e-03	4	Regulation of locomotion
	9.8e-03	2	Positive chemotaxis
D	9.6e-05	4	Acute-phase response
	2.0e-04	5	Acute inflammatory response
	4.8e-04	7	Response to bacterium
	4.8e-04	3	Positive regulation of alcohol biosynthetic process
	6.4e-04	10	Defense response
	7.0e-04	4	Response to organophosphorus
	8.1e-04	2	Positive regulation of prostaglandin biosynthetic process
	8.1e-04	4	Positive regulation of small molecule metabolic process
	1.0e-03	2	Pantothenate metabolic process

Table A4-27 GSEA Analysis: siRNA+P v siRNA

Direction	GSEA analysis: siRNAP vs siRNA	NES	Genes	adj.Pval
Down	Cellular lipid catabolic process	-1.8439	162	4.1e-02
	Fatty acid metabolic process	-1.6689	274	4.1e-02
	Cellular lipid metabolic process	-1.4872	759	4.1e-02
	Carboxylic acid metabolic process	-1.4418	804	4.1e-02
	Lipid metabolic process	-1.4393	985	4.1e-02
	Oxoacid metabolic process	-1.3839	866	4.1e-02
	Organic acid metabolic process	-1.3797	874	4.1e-02

Table A4-28 ShinyGO enrichment upregulated pathways: siRNA+P v siRNA

Enrichment FDR	Genes in list	Total genes	Functional Category
1.5E-02	3	260	Hormone-mediated signaling pathway
1.5E-02	2	39	Peptide hormone processing
1.5E-02	4	742	Cellular response to hormone stimulus
4.0E-02	4	1040	Response to hormone

Table A4-29 ShinyGO enrichment downregulated pathways: siRNA+P v siRNA

Enrichment FDR	Genes in list	Total genes	Functional Category
1.2E-02	2	363	Regulation of leukocyte cell-cell adhesion
1.2E-02	2	272	Positive regulation of leukocyte cell-cell adhesion
1.2E-02	2	399	Leukocyte cell-cell adhesion
1.2E-02	3	1022	Positive regulation of cell proliferation
1.2E-02	2	373	Response to hypoxia
1.2E-02	2	315	Positive regulation of cell-cell adhesion
1.2E-02	2	384	Response to decreased oxygen levels
1.2E-02	2	374	Positive regulation of leukocyte activation
1.2E-02	2	377	Regulation of T cell activation
1.2E-02	2	394	Positive regulation of cell activation
1.2E-02	2	253	Positive regulation of T cell activation
1.2E-02	2	329	Positive regulation of lymphocyte activation
1.2E-02	2	408	Response to oxygen levels
1.4E-02	2	471	Regulation of cell-cell adhesion
1.4E-02	2	465	Positive regulation of cell adhesion
1.5E-02	2	499	Regulation of lymphocyte activation
1.5E-02	2	534	T cell activation

Table A4-29 ShinyGO enrichment downregulated pathways: siRNA+P v siRNA

1.5E-02	3	1756	Regulation of cell proliferation
1.7E-02	2	592	Regulation of leukocyte activation
1.9E-02	2	638	Regulation of cell activation
2.3E-02	3	2165	Cell proliferation
2.4E-02	2	765	Regulation of cell adhesion
2.4E-02	2	775	Lymphocyte activation
3.2E-02	2	922	Cell-cell adhesion
4.2E-02	2	1082	Response to drug

APPENDIX B: BUFFERS AND SOLUTIONS

Acid Citrate Dextrose (ACD) Solution

Acid citrate dextrose (ACD) was made by adding 0.366 g anhydrous citric acid, 1.1 g sodium citrate, and 1.226 g dextrose to 50 mL cell culture grade H_2O (HyClone, USA). This was filter-sterilized through a syringe with a 0.22 µm filter.

Modified Tyrode's Buffer (JNL Buffer)

Modified Tyrode's Buffer (JNL Buffer) was created by first creating four separate components; A, B, D, and E. All chemicals were purchased from Sigma, USA. 10X JNL A was created by adding 0.54 g dextrose ($C_6H_{12}O_6$; 198.17 g/mol ∴ 0.0545 M) to 50 mL cell culture grade H_2O. 10X JNL B was created by adding 3.79 g sodium chloride (NaCl; 58.44 g/mol ∴ 1.297 M), 0.378 g sodium bicarbonate ($NaHCO_3$; 84 g/mol ∴ 0.09 M), 1.47 g sodium citrate tribasic, dehydrate ($C_6H_9Na_3O_9$; 294.1 g/mol ∴ 0.1 M), 0.606 g Tris-HCl ($C_4H_{11}NO_3$; 121.14 g/mol ∴ 0.1 M), 0.112 g potassium chloride (KCl) (74.55 g/mol ∴ 0.03 M) to 50mL cell culture grade H_2O. 10X JNL D was created by adding 0.055 g monobasic potassium phosphate (H_2KPO_4; 136.09 g/mol ∴ 0.008 M) to 50 mL cell culture grade H_2O. 100X JNL E was created by adding 0.183 g magnesium chloride hexahydrate ($MgCl_2$-6 H_2O; 203.3g/mol ∴ 0.09 M) to 10 mL cell culture grade H_2O. 5 mL each of JNL A, B, and D (Appendix B) were combined in a 50 mL Falcon tube. 0.5 mL of JNL E was added, and cell culture grade H_2O was filled to the 35 mL mark. The pH was adjusted to 7.4 by the addition of ACD. H_2O was added to 50 mL, and the solution was filtered through a syringe with

a 0.22 µm filter. The final molarities of the JNL buffer solution are shown in Table B1.

Propidium Iodide (PI) Staining Solution

PI staining solution was made using 0.1% v/v Triton-X, 10 µg/mL PI, and 100 µg/mL DNase-free RNase A in PBS containing $CaCl_2$ and $MgCl_2$. This was incubated in the dark at RT.

Tris-NaCl Coating Buffer

Coating buffer for the Engelbreth-Holm-Swarm (EHS) mouse sarcoma ECM gel was made per the manufacturer's protocol (Corning, USA) by adding 0.12114 g Tris-HCl (Sigma,USA) (0.1 M) and 0.07 g (0.7%) NaCl (Sigma, USA) to 10 mL cell culture grade H_2O (HyClone, USA). The pH was adjusted to 8.0, and the solution was filter-sterilized through a 0.22 µm syringe filter apparatus.

Table B1 Working concentrations of JNL buffer components

Dextrose	0.00545 M
Sodium Chloride	0.1297 M
Sodium Bicarbonate	0.009 M
Sodium Citrate Tribasic	0.01 M
Tris-HCl	0.01 M
Potassium Chloride	0.003 M
Potassium Phosphate Monobasic	0.0008 M
Magnesium Chloride Hexahydrate	0.0009 M

Table B2 cDNA synthesis components

Component	**Per Reaction (µL)**
10x RT Buffer	2
25x 100 mM dNTP Mix	1
10x RT random primers	2
MultiScribe Reverse Transcriptase	1
Nuclease Free H_2O	4
Total Volume	10

Table B3 RT-qPCR components

Component	**Per Rxn (µL)**
Primer/Probe	1
TaqMan Master Mix (Applied Biosystems, Lot #1506231)	10
Nuclease free H_2O	7
cDNA	2
Total Volume (T.V.)	20

Table B4 Blocking and staining buffer protocol

Blocking Buffer	
45 mL	DPBS
1.35 g	Fraction V BSA
40 µL	Tween-20
Primary Antibody Staining Solution	
15 mL	Blocking Buffer
30 µL	mAb -33H1F7
Secondary Antibody Staining Solution with Hoechst	
15 mL	Blocking Buffer
15 µL	goat anti-mouse Alexafluor 488 conjugate
15 µL	Höechst 33342

APPENDIX C: CTC ISOLATION

CTCs were isolated from whole patient blood samples by Dr. Mark Ward using the Parsortix® PL1 Cell Separation System (Angle PLC, Surrey, UK) as described by Miller *et al*, 2018. Using this system, whole blood is moved through a GEN3 cassette mechanism (Fig. B-1) at 99mbar pressure via a series of fluidic and pneumatic controls. GEN3 cell separation cassettes are 6.5µm single-use looped microfluidic devices that are laid out in a "step" configuration containing a critical gap that allows for the capture of whole, large cells (8µm or larger) while simultaneously maintaining the morphological integrity of those cells.

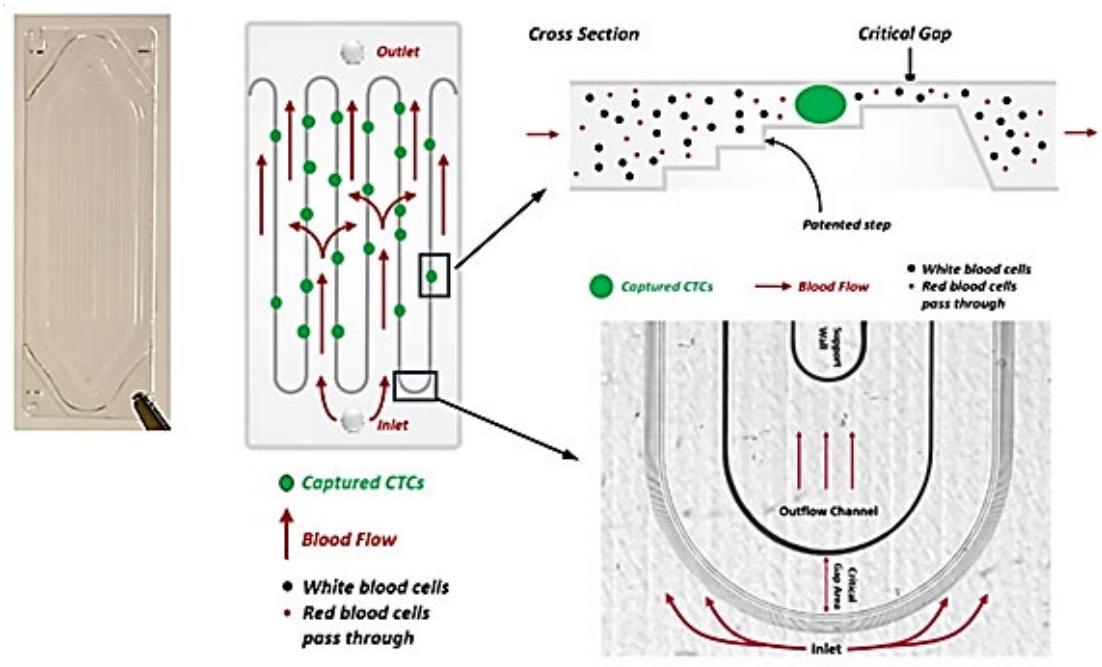

Fig. B-1 Diagram of GEN3 microfluidic cassette chamber

Once captured, cells can either be stained in the cassette, or they can be manually eluted from the cassette into a small amount of buffer by reversing

the flow direction. In this case, they were stained and counted inside the cassette. Cells were fixed and permeabilized using Miltenyi Biotech's Inside Stain Kit, and subsequently stained with 5 µL rabbit anti-human mAb CK19-488 (anti-Cytokeratin 19 Alexa Fluor® 488, Abcam), 7 µL mouse anti-human mAb CD45-PE (Miltenyi Biotec), and 5 µL 4',6-diamidino-2-phenylindole (DAPI) (ThermoFisher). Cells that were $CK45^-/DAPI^+/CD19^+$ and also displayed a round, intact morphology were considered to be CTCs (Fig. B-2). These were counted *in situ* using the EVOS fluorescence microscope (ThermoFisher, USA).

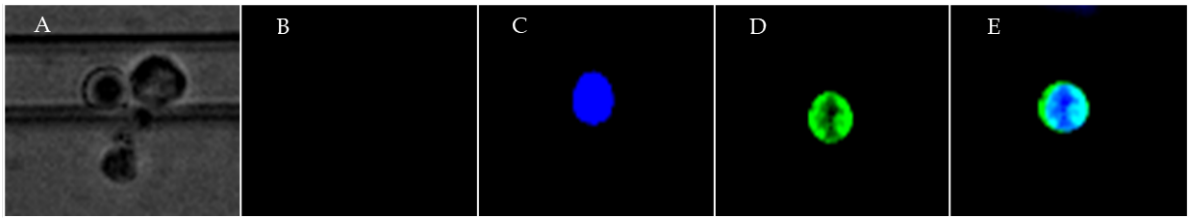

Fig. B-2 Circulating tumour cells as imaged by **A** brightfield microscopy and **B-E** fluorescence microscopy: **A** demonstration of morphology, **B** cells are $CD45^-$, **C** cells are $DAPI^+$, **D** cells are $CK19^+$, and **E** shows the overlay of all three channels.

APPENDIX D: PRESENTATIONS AND PUBLICATIONS

Journal Publications

O'Toole, Sharon A, Cathy Spillane, Yanmei Huang, Marie C Fitzgerald, Brendan Ffrench, Bashir Mohamed, Mark Ward, Michael Gallagher, **Tanya Kelly**, Cathal O'Brien, Carmel Ruttle, Anna Bogdanska, Cara Martin, Dorinda Mullen, Elizabeth Connolly, Sarah A McGarrigle, John Kennedy, and John J O'Leary. "Circulating tumour cell enumeration does not correlate with Miller-Payne grade in a cohort of breast cancer patients undergoing neoadjuvant chemotherapy." Breast Cancer Research and Treatment. Vol. 181, pp571–580. 2020.

Ward, MP, LE Kane, L Norris, BM Mohamed, **T Kelly**, M Bates, A Clarke, N Brady, CM Martin, RD Brooks, DA Brooks, S Selemidis, S Hanniffy, EP Dixon, SA O'Toole, and JJ O'Leary. "Platelets, Immune Cells and the Coagulation Cascade; Friend or Foe of the Circulating Tumour Cell?" *Submitted for publication.*

Kelly, Tanya E, Yanmei Huang, Mark Ward, Bashir Mohamed, Cara Martin, Lucy Norris, Noreen Gleason, Feras Abu Saadeh, Waseem Kamran, John O'Leary, and Sharon O'Toole. "Plasma PAI-1 is associated with Metastasis and Therapy Response in High Grade Serous Ovarian Cancer (HGSOC)." *Manuscript in progress.*

Kelly, Tanya E, Karsten Hokamp, Mark Ward, Bashir Mohamed, Cara Martin, Lucy Norris, Sharon O'Toole, and John O'Leary. "Interrogating the Role of PAI-1 and the Contribution of Platelets to Metastatic Disease in an Ovarian Cell Line Model using RNA-Sequencing." *Manuscript in progress.*

Mohamed, Bashir M., Mark P. Ward, Mark Bates, Cathy D. Spillane, **Tanya Kelly**, Cara Martin, Michael Gallagher, Sheena Heffernan, Lucy Norris, John Kennedy, Feras Abu Saadeh, Noreen Gleeson, Doug A. Brooks, Robert D. Brooks, Stavros Selemidis, Sean Hannify, Siobhan Cashman, Eric P. Dixon, Sharon O'Toole, and John J. O'Leary. "Optimising Cell Culture Conditions for Ex Vivo Expansion of Circulating Tumour Cells (CTCs)." *Manuscript in progress.*

Spillane, Cathy D., Niamh M. Cooke, Dermot Kenny, Gordon Blackshields, Mark P. Ward, **Tanya Kelly**, Mark Bates, Yanmei Huang, Cara Martin, Sinead Skehan, Aoife Canney, Michael Gallagher, Paul Smyth, Nathan Brady, Andres Clarke, Bashir Mohamed, Lucy Norris, Doug A. Brooks, Robert D. Brooks, Jessica Heatlie, Stavros Selemidis, Sean Hanniffy, Eric Dixon, Orla Sheils, Sharon A. O'Toole, and John J. O'Leary. "The Induction of a Mesenchymal Phenotype by Platelet Cloaking of Cancer Cells is a Universal Phenomenon." *Manuscript in progress.*

Published Abstracts

Ward, MP, BM Mohamed, L Kane, M Bates, J Berghoff, C Spillane, **T Kelly**, J Kennedy, FA Saadeh, K Hokamp, O Sheils, C Martin, M Gallagher, S Hannify, EP Dixon, SA O'Toole, JJ O'Leary. "Influence of platelets and neutrophils on circulating tumour cells." (2020, AACR, Accepted for publication).

Kelly, Tanya, Mark Ward, Bashir Mohamed, Cara Martin, Cathy Spillane, Sharon O'Toole, and John O'Leary. "Plasminogen Activator Inhibitor 1 (PAI-1) is a Key Driver of Ovarian Cancer Metastasis." Modern Pathology 2020; 30(3): 1079.

Kelly, Tanya, Cara Martin, Bashir Mohamed, Sharon O'Toole, Cathy Spillane, John O'Leary. "Exposure to Platelets accelerates Mitosis in SKOV3 Cells." Laboratory Investigations 2019; 99(1): 56.

Conference Proceedings

Tanya Kelly, Cathy Spillane, Sharon O'Toole, and John O'Leary "Platelets and Plasminogen-Activator Inhibitor 1 (PAI-1) contribute to Metastasis in Ovarian Cancer." Proceedings of the Irish Association of Cancer Research (IACR) Annual Conference, Dublin, Ireland, 2018.

MP Ward, BM Mohamed, L Kane, J Berghoff, C Spillane, B John, **T Kelly**, J Kennedy, FA Saadeh, K Hokamp, O Sheils, C Martin, M Gallagher, S Hanniffy, EP Dixon, SA O'Toole, JJ O'Leary. "Influence of platelets and neutrophils on Circulating Tumour Cells (CTCs)." Proceedings of the 11th TCD International Cancer Conference 2019.

Sharon O'Toole, Cathy Spillane, Yanmei Huang, Brendan Ffrench, Cathal O'Brien, Carmel Ruttle, Cara Martin, Bashir Mohamed, Mark Ward, Michael Gallagher, **Tanya Kelly**, Dorinda Mullen, John Kennedy John O'Leary. "Circulating tumour cell enumeration does not correlate with Miller-Payne grade in a cohort of breast cancer patients undergoing neoadjuvant chemotherapy." Proceedings of the Liquid Biopsy Conference, Bergamo, Italy May 2019.

Yanmei Huang, Cathy Spillane, Brendan Ffrench, Bashir Mohamed, Mark Ward, Michael Gallagher, **Tanya Kelly**, Cathal O'Brien, Cara Martin, Dorinda Mullen, Elizabeth Connolly, Sarah A McGarrigle, John Kennedy, Sharon A O'Toole*, John J O'Leary. (*Joint Senior Authors). "No correlation between Circulating Tumour Cell Enumeration and Miller-Payne Grade in a Cohort of Breast Cancer Patients undergoing Neoadjuvant Chemotherapy." Proceedings of the 11th TCD International Cancer Conference 2019.

Tanya Kelly, Mark Ward, Bashir Mohamed, Cathy Spillane, Cara Martin, Sharon O'Toole, and John O'Leary. "Platelets and PAI-1 expedite Ovarian

Cancer Metastasis." Proceedings of the Irish Association of Cancer Research (IACR) Annual Conference, Galway, Ireland, 2020.

Tanya Kelly, Yanmei Huang, Mark Ward, Bashir Mohamed, Cara Martin, Lucy Norris, Noreen Gleason, Feras Abu Saadeh, Waseem Kamran, John O'Leary, and Sharon O'Toole. "Plasma PAI-1 is associated with Metastasis and Therapy Response in High Grade Serous Ovarian Cancer (HGSOC)." Proceedings of the Irish Association of Cancer Research (IACR) Annual Conference, Online, Ireland, 2021.

Yanmei Huang, Cathy Spillane, Brendan Ffrench, Bashir Mohamed, Mark Ward, Michael Gallagher, **Tanya Kelly**, Cathal O'Brien, Cara Martin, Dorinda Mullen, Elizabeth Connolly, Sarah A McGarrigle, John Kennedy, Sharon A O'Toole, John J O'Leary. "No Correlation Between Enumeration of Circulating Tumour Cells and Miller-Payne Grade in a Cohort of Breast Cancer Patients undergoing Neoadjuvant Chemotherapy." Proceedings of the Irish Association for Cancer Research 2020, Galway, Ireland.

Tanya Kelly, Karsten Hokamp, Mark Ward, Bashir Mohamed, Cara Martin, Lucy Norris, Sharon O'Toole, and John O'Leary. "Interrogating the Role of PAI-1 and the Contribution of Platelets to Metastatic Disease in an Ovarian Cell Line Model using RNA-Sequencing." Proceedings of the Irish Association of Cancer Research (IACR) Annual Conference, Online, Ireland, 2021.

APPENDIX E: EUROPEAN CREDIT TRANSFER AND ACCUMULATION SYSTEM (ECTS)

	INSTITUTION	COURSE	CREDITS
	Trinity College Dublin, Dublin 2	Statistics: Base Module	15
	Royal College of Surgeons in Ireland, Dublin 2	Biomedical Imaging	1
TOTAL			**16**